Modelling of Strain Accumulation Due to Low Level Vibrations in Granular Soils

Christian Karg

Promotor: prof. dr. ir. W. Haegeman
Proefschrift ingediend tot het behalen van de graad van
Doctor in de Ingenieurswetenschappen: Bouwkunde

Vakgroep Civiele Techniek
Voorzitter: prof. dr. ir. J. De Rouck
Faculteit Ingenieurswetenschappen
Academiejaar 2007 - 2008

UNIVERSITEIT GENT

ISBN 978-90-8578-179-0
NUR 955, 956
Wettelijk depot: D/2007/10.500/53

Dit proefschrift is goedgekeurd door de promotor:

Prof. dr. ir. W. Haegeman	Universiteit Gent

Samenstelling promotiecomissie:

Prof. dr. ir. R. Verhoeven	Universiteit Gent
Prof. dr. ir. P. Troch	Universiteit Gent
Prof. dr. ir. R. van Impe	Universiteit Gent
Prof. dr. ir. W. van Impe	Universiteit Gent
Prof. dr. ir. G. Degrande	K.U. Leuven
Dr.-Ing. F. Wuttke	Bauhaus University Weimar
Dr. ir. P. Mengé	Dredging International N.V.

Published and distributed by:

Faculty of Engineering
Ghent University
Jozef Plateaustraat 22
B-9000 Ghent

Keywords: strain accumulation, cyclic triaxial test, bender element test, non-cohesive granular soil

Printed in Belgium

Preface

The work presented in this thesis could not have been conducted without support of many people I would like to express my acknowledgements. First of all, I wish to gratefully acknowledge Prof. Wim Haegeman, the supervisor of this thesis, for his support, encouragement and helpful comments during the course of the study.

This work is carried out within the frame of the SBO project IWT 03175 'Structural damage due to dynamic excitations: a multi-disciplinary approach'. The financial support of the Flemish Community is also gratefully acknowledged. In this regard I would like to express my gratitude to the co-workers of the research project, especially to Stijn François for stimulating and invaluable discussions and Prof. Geert Degrande from the K.U. Leuven for his numerous useful suggestions and comments.

In addition, I am indebted to the staff of the Laboratory of Geotechnics at the Ghent University and the Department of Industrial Engineering Sciences at the KHBO in Ostende for their direct and indirect support. Special thanks deserve Luc Boehme for his patient support during the installation of the testing device and Kenny Deswelgh, who performed most of the extensive laboratory works. Furthermore, I thank Dr. Lutz Karl for many helpful discussions and creative ideas and Dr. Frank Wuttke for his encouragement and inspiring discussions.

Finally, I appreciate the great support and encouragement of my family for all intents and purposes. I deeply thank my wife, for her support, patience and appreciation. The birth of our children has provided the happiness that makes life much more complete.

Christian Karg
Ghent, September 2007

Abstract

Vibrations in the ground are a matter of growing concern, especially in densely populated areas. Beside natural vibration sources as seismics and wave loading, manmade vibrations gained in importance in recent years as recent developments lead to a significant increase of the traffic volume. This comes along with higher construction activities in urban areas as the built environment needs to be adapted to new demands. Machine foundations and wind power plants are further examples for manmade vibrations sources. As a result significant higher vibration levels as in the past are observed. This increased dynamic impact may lead to a reduction of serviceability and diminish the lifetime of buildings. For this reason it is important to investigate consequences of vibrations in the ground with respect to their damage risks for buildings. Another important aspect is the consideration of permanent or long term vibrations at low strains in the design process. More detailed understanding of the mechanisms in the soil during dynamic long term impacts would allow for optimisation in dimension foundations, leading to economically advantageous design.

The understanding of mechanisms in the soil caused by low level vibrations, their consequences on the built environment, their modelling and prediction are in the focus of this work. In particular the elasto-plastic long term behaviour of non-cohesive granular soil under cyclic loading at the low strain level is studied in experimental investigations as well as in theory. The conducted literature study revealed that single dynamic events at the low strain level can be considered to be purely elastic as no plastic deformations are detectable. Accordingly, the dynamic soil behaviour can be well modelled using simple elastic constitutive laws. As a consequence, residual deformations cannot be predicted using common dynamic soil models. Both field measurements and laboratory investigations, however, have proven

non-negligible permanent deformations after application of large numbers of dynamic load applications.

This process of strain accumulation is explained as a kind of aging process of the soil, comparable to creeping due to dynamic loading in other materials. In general, the accumulation process is characterised by three main influencing aspects: the current state of the soil, the current state of stress and the characteristics of the dynamic impact. The combination of these parameters defines the intensity as well as the direction of accumulation. Theoretical considerations in combination with experimental studies on these accumulation phenomena are subject of main interest in this thesis. Constitutive models for accumulation prediction in the literature are studied and evaluated regarding their power and applicability.

Based on these cognitions a new accumulation model is proposed for prediction of accumulation problems. The essential advantages of this approach are the small number of model parameters, the simple formulation and the proper implementation in a commonly used finite element code. All model parameters can be determined from a single kind of laboratory test, namely the cyclic triaxial test. The simple formulation allows for easy comprehension, extension and general applicability for a wide range of practical problems. The implementation in the finite element code supports the use of the model in practical applications.

The validation of any accumulation model is difficult. Up to now experimental investigations considering all, current state of the soil, current state of stress and the characteristics of the cyclic loading, are quite rare both in the field and in laboratory tests. For this reason advanced cyclic triaxial and bender element test equipment is set up at the Laboratory of Geotechnics, Department of Industrial Engineering Sciences, KHBO in Ostende, Belgium in the frame of the present work. A test procedure including sample preparation, saturation, consolidation, bender element and cyclic triaxial testing of cylindrical soil samples is defined. The apparatus allows for the investigation of elastic material properties and the accumulation behaviour of soil. A wide range of test options allows for consideration of many influence parameters in laboratory tests.

In testing campaigns the influence of different parameters on the elastic material behaviour as well as on the accumulation properties of the sand of Mol is investigated. Thereafter a hyperbolic non-linear constitutive model well describes the degradation of soil stiffness with increasing cyclic

strain amplitudes. An empirical formulation, developed on the basis of resonant column tests to describe the maximum shear modulus as a function of the void ratio and the mean effective stress, is also valid for bender element test results. An influence of the cyclic loading frequency on the elastic material properties is not detected in the range of 0 to 10*Hz*.

Test results confirmed the applicability of elastic constitutive laws for description of the dynamic soil behaviour. The elastic material parameters are found to be independent from the number of load cycles already applied. During accumulation of large numbers of cycles, however, non-negligible residual deformations are observed. Increasing void ratios and cyclic strain amplitudes lead to increasing strain accumulation rates. An influence of the cyclic loading frequency on the accumulation behaviour is not detected in the range of 0 to 10*Hz*. Therewith the frequency content of a dynamic impact is of minor importance for accumulation predictions. Test results of long term cyclic triaxial tests are used for validation of the proposed accumulation model. The procedure of parameter identification is described. Good agreement of test data and the accumulation model under consideration is achieved.

Christian Karg
Ghent, September 2007

Samenvatting

Trillingen in de grond verdienen de laatste jaren vooral in dichtbevolkte gebieden een groeiende aandacht. Naast trillingen van natuurlijke oorsprong zoals seismiek en golfbelasting worden trillingen ten gevolge van industriële activiteiten belangrijker, denken we maar aan de toegenomen verkeersintensiteit in de laatste decennia. Komen daarbij een stijging van bouwactiviteiten in stedelijke omgeving, steeds grotere machinefunderingen alsook windmolenparken als mogelijke bronnen van grondtrillingen. Dit alles resulteert in steeds grotere waargenomen trillingsamplitudes. Deze belangrijke dynamische impact op naburige constructies kan leiden tot een daling van het gebruiksgemak en bijhorende levensduur van het gebouw. Daarom is het belangrijk de gevolgen van deze trillingen op het schaderisico van gebouwen grondig te bestuderen met de nodige aandacht voor lange termijneffecten bij kleine gronddeformaties bvb zettingen van funderingen. Een meer gedetailleerd begrip van de mechanismen in de grond tijdens lange termijn dynamische belastingen zal leiden tot een geoptimaliseerd en economisch ontwerp van de funderingsdimensies.

Onderwerp van dit werk is de studie, de modellering en voorspelling van de vervormingen in de grond onder trillingsniveaus van lage amplitude. Meer specifiek wordt zowel theoretisch als experimenteel het elasto-plastisch gedrag van een niet-cohesief granulair materiaal op lange termijn bestudeerd onder een cyclische belasting bij kleine amplitudes. De uitgevoerde literatuurstudie toont aan dat een éénmalige dynamische belasting bij kleine amplitude tot een pure elastische vervorming van de grond aanleiding geeft of althans zo kan worden benaderd. Aldus kan het dynamisch spannings-vervormingsgedrag van de grond via eenvoudige elastische constitutieve wetten worden gemodelleerd en worden geen blijvende vervormingen voorspeld. Zowel terreinmetingen als laboratoriumonderzoek tonen echter aan dat onder een groot aantal

"elastische" belastingscycli niet-verwaarloosbare plastische vervormingen in de grond optreden.

Dit proces van vervormingsaccumulatie wordt gerelateerd aan het verouderingsproces van de grond vergelijkbaar met het kruipeffect onder dynamische belasting in andere materialen. Over het algemeen wordt dit accumulatieproces gekarakteriseerd door drie procesparameters: de begintoestand van de grond, de beginspanning in de grond en de dynamische belastingskarakteristieken. De combinatie van deze parameters definieert de intensiteit en richting van de vervormingsaccumulatie. Theoretische beschouwingen gecombineerd met experimenteel werk inzake deze vervormingsaccumulatie onder een groot aantal belastingscycli met kleine amplitude zijn het hoofdonderwerp van dit doctoraatswerk. Bestaande constitutieve modellen voor de voorspelling van deze accumulatie worden bestudeerd en geëvalueerd inzake hun mogelijkheden en toepasbaarheid. Gebaseerd op deze ervaringen wordt een nieuw accumulatiemodel voorgesteld voor de voorspelling van permanente zettingen onder dynamische belastingen. Als belangrijkste voordelen van dit nieuwe model worden vermeld: een klein aantal modelparameters, een eenvoudige formulering en vooral de implementatie in een wijd verspreide eindige elementen code. Alle modelparameters kunnen worden afgeleid uit de cyclische triaxiaalproef en de eenvoudige formulering zorgt voor een goed begrip van het vervormingsgedrag en opent mogelijkheden tot een algemeen gebruik in een groot gebied van praktische dynamische problemen. De implementatie in een eindige elementen code zorgt voor een gebruik van dit model in vele complexe toepassingen.

De validatie van een accumulatiemodel is moeilijk. Experimentele terrein- of laboratoriumstudies die alle invloedsparameters (huidige toestand van de grond, beginspanning in de grond en belastingskarakteristieken) in beschouwing nemen zijn zeldzaam. Daarom werd beslist om in het kader van dit onderzoek een geavanceerde cyclische triaxiaalcel met bender elementen te bouwen in het labo geotechniek van het departement Industriële Wetenschappen en Technologie van de KHBO te Oostende. Een volledige testprocedure omvattende de aanmaak van het zandmonster, de verzadiging, de consolidatie en uiteindelijk de bender element en cyclische belastingsproef werden ontwikkeld. Deze proefopstelling laat uiteindelijk toe de elastische materiaalkarakteristieken alsook de vervormingsaccumulatie te bestuderen. Een groot gamma aan

testopties maakt het mogelijk alle bovenvermelde invloedsparameters in beschouwing te nemen.

Het proevenprogramma focusseert op het zand van Mol als testmateriaal waarbij de invloed van verschillende parameters op het elastisch alsook het accumulatiegedrag in beschouwing wordt genomen. Er wordt vooreerst een niet-lineair hyperbolisch constitutief model opgesteld voor de stijfheidsdegradatie in functie van de vervorming. Er wordt verder aangetoond dat een empirische relatie die vroeger voor het materiaal is opgesteld op basis van resonantiekolomproeven en die de maximale glijdingsmodulus beschrijft in functie van het poriëngetal en de spanning, eveneens geldt voor bender elementresultaten. Tot slot wordt geconstateerd dat de cyclische belastingsfrequentie geen invloed heeft op de elastische materiaalparameters althans in het frequentiegebied 0 tot 10*Hz*. Test resultaten bevestigen de bruikbaarheid van elastische constitutieve wetten voor de beschrijving van het dynamisch grondgedrag. De elastische materiaalparameters zijn tevens onafhankelijk van het aantal opgelegde belastingscycli.

Toepassing van een groot aantal cycli bevestigen inderdaad een niet-verwaarloosbare residuele vervorming van het materiaal. Toenemend initieel poriëngetal en cyclische vervormingsamplitude leiden tot hogere vervormingsaccumulatie. De belastingsfrequentie blijkt ook hier geen invloed te hebben op het accumulatiegedrag aldus kan de frequentie-inhoud van een dynamische belasting als minder belangrijk worden beschouwd bij accumulatievoorspellingen. Proefresultaten uit lange termijn cyclische triaxiaalproeven worden gebruikt voor validatie van het voorgestelde accumulatiemodel en de parameteridentificatie wordt toegelicht. Er wordt een goede overeenkomst waargenomen tussen test data en voorspellingen met het nieuwe accumulatiemodel!

Christian Karg
Gent, September 2007

Contents

Frequently used symbols

The most frequently used symbols are presented in the following. In most cases, they are also defined when introduced in the text.

Symbols and units

c	cohesion	kPa
d_0	model parameter	-
e	void ratio	-
e_{ij}	deviatoric strain component	-, %
f	model function	-
h	specimen layer height	mm
h_{t-t}	tip-to-tip distance	mm
m	mass	g, kg
m_{ij}	direction of accumulation	-
n	free parameter	-
n_e	free parameter	-
p	mean (effective) stress, hydrostatic pressure	kPa
q	deviatoric stress invariant	kPa
s_{ij}	deviatoric stress component	kPa
t	time	s
t_t	travel time	$msec$
u	pore (water) pressure	kPa
u_i	displacement	-
w	water content	%
x_1, x_2, x_3	mutually orthogonal coordinates in space	-
x, y, z	mutually orthogonal coordinates in space	-
A_{loop}	hysteresis loop area	kPa
$A_{\triangle}$	triangle area	kPa

B	Skempton factor	-
C	model parameter	-
CC	coefficient of curvature	%
C_{ijkl}	elastic compliance tensor	*MPa*
D_{ijkl}	constitutive tensor	*MPa*
D	damping ratio	-, %
D	specimen diameter	*mm*
D_r	relative density	-, %
E	Young's modulus	*MPa*
$E_0, E_{\max}$	dynamic Young's modulus	*MPa*
G	shear modulus	*MPa*
$G_0, G_{\max}$	dynamic shear modulus	*MPa*
H	specimen height	*mm*
I_1, I_2, I_3	invariants of the stress tensor	*kPa*, kPa^2, kPa^3
J_1, J_2, J_3	invariants of the deviatoric stress component	*kPa*, kPa^2, kPa^3
K	bulk modulus	*MPa*
K_0	ratio of horizontal and vertical pressure	-
N	number of load applications, load cycles	-
S	saturation degree, free parameter	-, %
U	under compaction degree	%
UC	uniformity coefficient	%
V	volume	cm^3, m^3, *ml*
V	wave velocity	*m/s*
α	model parameter	-
β	model parameter	-
δ_{ij}	Kronecker delta	-
ε	total strain	-, %
ε_{ij}	strain tensor	-, %
ε_{kk}	volumetric strain invariant	-, %
φ	angle of inner friction	-
γ	engineering deviatoric strain	-, %
γ	unit weight	kN/m^3
η	stress ratio	-
κ	deviatoric strain invariant	-, %
λ, μ	Lamé constants	*MPa*
θ	Lode angle	-

ϑ	model parameter	-
ρ	density	kg/cm^3
σ	stress	*kPa*
σ_{ij}	stress tensor	*kPa*
τ	shear stress	*kPa*
υ	Poisson's ratio	-
ω	direction of accumulation	-
ζ	cyclic stress ratio	-
Δ	increment	-
Γ	state variable	-
T	shear strength	*kPa*

Subscripts

1, 2, 3	principal axes, principal directions
a	axial, air, atmospheric
c	critical, related to volumetric compaction
d	dry
f	related to frictional sliding
max	maximum
min	minimum
p	primary
r, *ref*	reference
s	soil, shear, saturation
t	tangent
v	void
vol	volumetric
w	water

Superscripts

acc	accumulated
ampl	amplitude, cyclic value
av	average
DA	double amplitude
e	elastic
p	plastic
$\dot{}$	first derivative with respect to the time or the number of cycles

Chapter 1
Introduction

1.1 Theme and objective of this work

The all-around problem of vibrations in the ground is a matter of growing concern, especially in densely populated areas. Beside natural vibration sources as seismics and wave loading, manmade vibrations gained in importance in recent years. Increasing densities of population, the demand of mobility of people, reduction of stock and just-in-time delivery policies contribute to a significant increase of the traffic volume. This comes along with higher construction activities in urban areas as the built environment needs to be adapted to new demands. Also blasting as the controlled explosion of duds or industrial activities as looms and printing machines lead to considerable vibration levels in nearby buildings. In recent years the installation of wind power plants became more and more important, where continues vibrations in the foundation are a matter of concern.

The sum of these factors results in a significant higher vibration level as in the past. Although, in general, regular vibrations will not lead to immediate damage of structures, they are, on the one hand, reason for inconvenience of people. On the other hand they may, in the long run, lead to a reduction of serviceability and diminish the lifetime of buildings. For this reason it is important to investigate consequences of vibrations in the ground with respect to their damage risks for buildings.

Another important aspect is the consideration of permanent or long term vibrations at low strains in the design process. E.g. in the foundation design of wind power plants or machine foundations high safety

factors and conservative soil parameters are common use, founded by a lack of knowledge on the dynamic long-term behaviour of soil. More detailed understanding of the mechanisms in the soil during dynamic long term impacts would allow for optimisation in dimension foundations, leading to economically advantageous design.

The understanding of mechanisms in the soil caused by low level vibrations, their consequences on the built environment, their modelling and prediction are in the focus of this work. In particular the elasto-plastic long term behaviour of non-cohesive granular soil under cyclic loading at the low strain level is studied in experimental investigations as well as in theory.

The conducted literature study revealed that single dynamic events at the low strain level can be considered to be purely elastic as no plastic deformations are detectable. Accordingly, the dynamic soil behaviour can be well modelled using simple elastic constitutive laws. As a consequence, residual deformations cannot be predicted using common dynamic soil models. Both field measurements and laboratory investigations, however, have proven non-negligible permanent deformations after application of large numbers of dynamic load applications. That is, the assumption of purely elastic behaviour only applies for limited numbers of load repetitions, whereas plastic material behaviour is detected during long term or permanent dynamic loading.

Theoretical considerations in combination with experimental studies on these accumulation phenomena are subject of main interest in this thesis. Constitutive models for accumulation prediction in the literature are studied and evaluated regarding their power and applicability. Based on these cognitions a new accumulation model is proposed for prediction of accumulation problems. The model is implemented in a commonly used finite element code and can be applied to a wide range of practical engineering problems.

For experimental investigations on the accumulation properties of granular non-cohesive soil advanced cyclic triaxial and bender element test equipment is set up at the Laboratory of Geotechnics, Department of Industrial Engineering Sciences, KHBO in Ostende, Belgium in the frame of the present work. A test procedure including sample preparation, saturation, consolidation, bender element and cyclic triaxial testing of cylindrical soil samples is defined. The influence of different parameters on

the accumulation behaviour is studied in several testing campaigns. Test results are used for validation of the proposed accumulation model.

1.2 Outline of this thesis

As introduction, an overview on types of vibrations in the soil is presented in Chapter 2. Damage risks and reduction of living standard and serviceability resulting from vibrations in the ground are briefly discussed in connection with existing standards to take them into account in engineering practice. To sensitise to the problem of strain accumulation the accordant possible failure and damage mechanisms are explained and influencing parameters are considered.

In Chapter 3 governing equations are summarised as a basis for later discussion. The definitions of stresses and strains in the soil are given and the consideration of soil as a homogeneous isotropic elastic medium is described. Characteristic soil parameters, commonly used in soil mechanics, are introduced. The determination of strain dependent dynamic soil parameters is discussed in another section of this chapter.

The outcome of a literature study on existing accumulation models is summarised in Chapter 4. Two recently developed advanced accumulation models, the Bochum accumulation model and the Suiker model, are discussed in detail as a basis for own theoretical considerations.

A new accumulation model is introduced in Chapter 5. The elements of both the elastic and the accumulation model are discussed. The model calibration with the aid of cyclic triaxial test results is explained and all model parameters are determined for the used material. The capabilities, quality and applicability of the new model is discussed in a further section.

Chapter 6 provides information on the setup of the combined cyclic triaxial and bender element test equipment. Features and enhancements of the installed cyclic triaxial apparatus are explained, test procedure and demands on the execution of a high-quality cyclic triaxial test are defined. The chosen implementation of separate bender element test equipment is delineated. Data analysis of cyclic triaxial as well as bender element test results is briefly clarified.

The results of several testing campaigns are subject of Chapter 7. Elastic material properties are studied by means of bender element and

cyclic triaxial tests. The evolution of the elastic material parameters with the number of load applications is analysed. In a second part of this chapter the influence of strain amplitude, void ratio and cyclic loading frequency on the accumulation behaviour of the soil is investigated. The proposed accumulation model is applied to test results achieved in the frame of these testing campaigns.

Chapter 8 summarises the main findings and conclusions of the present work and provides proposals for further research.

Chapter 2
Vibrations in the soil

2.1 Introduction

Aim of this chapter is to call attention to the relevance of taking into account vibrations in the ground during the engineering design process and as potential damage risk for existing structures, respectively. For this purpose an overview is given on vibrations in the soil, their characteristics and possible consequences for the environment.

In a first step vibrations are characterised based on their origin, time of occurrence, strain level, propagation and seismic wave characteristics. Ground vibrations may lead to reduction of serviceability of buildings and living standard of people. Even serious damage can occur. The particular kinds of vibration are assessed regarding their damage potential and possible damage mechanisms. Different damage mechanisms are identified and consequences for soil and arising structures are described. The utilisation of waves in the ground for seismic soil investigations as a positive aspect of ground motions is shortly touched on.

A special phenomenon caused by ground vibrations is the so called strain accumulation. This effect is generally discussed in a further section of this chapter to provide an access to the main subject of the present work. The term *strain accumulation* is explained, influence parameters are discussed and possible damage risks are emphasised. Existing methods for laboratory investigations on strain accumulation are mentioned. The difficulties of in-situ observation of strain accumulation and the estimation

of strain accumulation potential of in-situ soil are discussed briefly at the end of this chapter.

2.2 Kinds of vibrations in the soil

The subgrade is subjected to many different vibrations at any time. Many sources of vibrations can be identified. Depending on their origin, duration, strain level and properties differentiation in vibrations is possible. This specification is to be done in the early stages of the planning and necessary to allow clear analysis of the consequences of the respective vibration. Effects to be expected can be derived from the respective kind of vibration. Therewith it becomes clear which effects need to be considered in the planning stage and described with an appropriate geotechnical model. That is, the kind of vibration defines the model to be used in analysis and prediction. As well in planning and design of new constructions as for estimation of consequences on existing structures detailed knowledge of existing vibrations and vibrations to be expected is of high importance for geotechnical engineering.

2.2.1 Natural versus manmade vibrations

A first distinction can be made between natural and manmade vibrations. The most obvious natural source for vibrations in the soil is, of course, seismic activity. Earthquakes and volcanism cause permanent movements of the ground. Singular events with large amplitudes (earthquakes) can lead to heavy damage in constructions. Also breakers at the sea generate waves propagating through the soil. Wind loading on e.g. high rise buildings or windmills generates vibrations in foundations and therewith functions as a source of vibrations in the soil, too.

Manmade vibrations in the ground are a matter of growing interest and importance especially in densely populated areas. Growing population and the need of modernisation in urban areas require more and more construction works in built environment. Further on increasing traffic calls for more roads, railways and subways, respectively. All these activities generate non-negligible vibrations in the soil. Also industrial activities can cause noteworthy vibration levels, e.g. due to machine foundations.

Natural vibrations are hard to describe accurately. The strain level varies strongly, durations and characteristics can be different for every event. This makes it difficult to define clear threshold values; design parameters are mostly based on statistics. Manmade vibrations are easier to evaluate since the vibration source is clearly defined. Duration and characteristics of the impact in general are known already before it emerges. This makes it easier to predict related effects and to take them into account in the design process.

2.2.2 Temporary versus permanent vibrations

Further specification of vibrations can be related to the duration of the impact. Certain effects as accumulation of strain and fatigue will mainly occur due to long term or permanent impacts, whereas immediate damage is a problem related to temporary or singular impacts as earthquakes, construction works or explosions. Construction works as pile driving, blasting or tunnel excavation will generate temporary higher vibration levels, whereas increased traffic, additional subways or new railway tracks will generate permanent higher vibration levels in future.

Temporary vibrations that cause settlements will probably not reach the maximum settlement, which could be achieved due to a permanent impact with similar characteristics. That is, an accurate prediction of the settlement related to a certain number of events (e.g. number of piles, number of blasts) is necessary.

On the other hand a new applied permanent vibration causing settlements of existing structures (possibly a new road, railway track or windmill in the neighbourhood) will reach a level of stabilisation after a certain time. A new built structure subjected to existing vibrations will behave similar. Thus, in this case, it is of bigger interest to predict the maximum settlement to be expected due to this impact, rather than the settlement related to a certain number of events.

A distinction of vibrations based on their number of appearance is also proposed in the Swiss standard SN 640312 a (1992). Therein classes of incidence are defined, talking about occasional (<< 1000 events), frequent and permanent (>> 100,000 events) impacts.

2.2.3 Small strain versus large strain vibrations

Natural soils exhibit elasto-plastic material behaviour. Nevertheless, the soil behaviour at small strain levels can be considered to be elastic in very good approximation. The threshold up to which the elastic theory is acceptable depends on the state of stress and the specific soil characteristics. Meanwhile the assumption of an elastic threshold at strains of about 10^{-3}% is commonly accepted, though. This suggests a distinction of vibrations according to their maximum strain. Vibrations below the elastic threshold, hereafter also referred to as low level vibrations, can be treated with simple constitutive laws, whereas large amplitudes call for more complex ones. Especially for modelling of wave propagation it is important to keep the constitutive laws as simple as possible (though as accurate as necessary) to minimize the anyway enormous calculation effort.

The strain level of natural vibrations may vary strongly for different events. Thus it needs to be evaluated as the case arises whether elastic constitutive laws are a sufficient approximation. In sufficient distance from the source most manmade vibrations, however, can be modelled in good approach using elastic laws, though. Since significant immediate effects of vibrations on a structure are mostly related to large strain amplitudes, complex constitutive laws are often linked to singular or temporary impacts, whereas long term or permanent vibrations mostly show small amplitudes and thus can be treated with simple constitutive models.

2.2.4 Seismic waves in the ground

Vibrations in the soil in general are seismic waves, caused by time variable internal or external impacts on the soil. A further general distinction can be made between *body waves*, propagating in all directions in the quasi-infinite continuum, and *surface waves*, propagating at the surface of a body. Body waves appear either as longitudinal (compression) waves or transversal (shear) waves, whereat shear waves may show horizontal and vertical polarisation, respectively. If body waves meet the surface they are partly reflected and partly refracted. The refracted part runs as a direct two-dimensional wave at the surface and accordingly is called surface wave. In theory, i.e. under ideal conditions, certain types of waves are identified as discussed in the following. In reality, however, such clear modes are rarely to be observed; mixed modes are more probable.

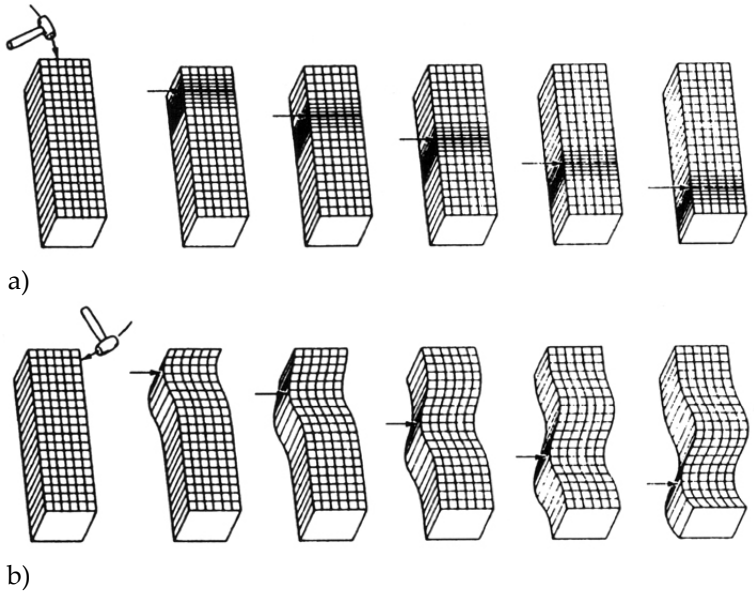

Figure 2.2-1: a) Compression (p-) wave and b) shear (s-) wave (from Knödel et al., 1997*)*

Body waves

Compression waves, illustrated in Figure 2.2-1a), are characterised by a lengthwise amplitude parallel to the axis of propagation, leading to periodic volume changes in the soil, i.e. compression and dilatation, without creating deformation. Compression waves exhibit the largest propagation velocity, i.e. they arrive first at a sensor and thus are also called *primary* or *p-waves*.

Shear waves (also *s-waves*, see Figure 2.2-1b)) possess an amplitude orthogonal to the direction of propagation. Depending on the underlying coordinate system one can further distinguish horizontal (SH) and vertical (SV) shear waves. Shear waves with inclined amplitude accordingly can be split in their SH- and SV-components. Shear waves are also called *secondary waves* since they arrive as second at a sensor.

Surface waves

Surface waves transport the biggest part of energy. Their amplitude, however, decreases exponential with the distance from the surface. The influence of surface waves thus can be neglected at a distance of about one

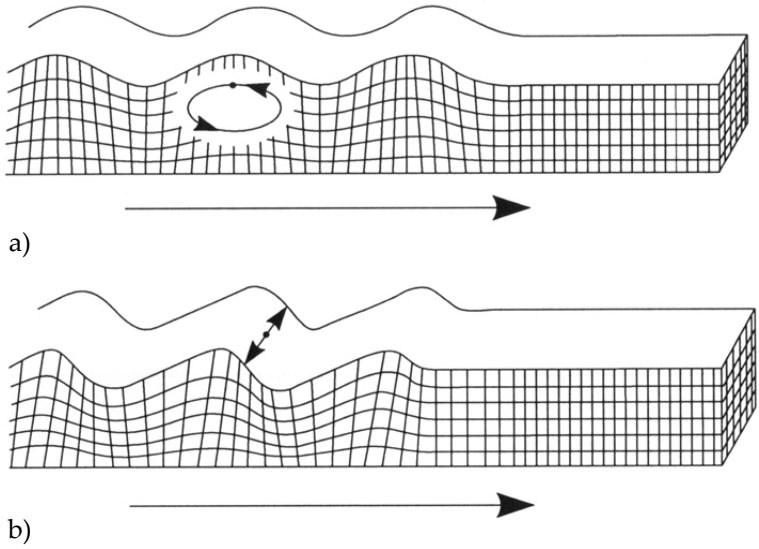

Figure 2.2-2: a) Rayleigh- and b) Love-wave (from Knödel et al., 1997*)*

wavelength from the surface. Two different kinds of surface waves are observed.

The first kind originates from a superposition of the refracted portions of p- and SV-waves and was first described by Rayleigh (1885). Accordingly these waves are also called *Rayleigh-waves*. They are characterised by retrograde, elliptic movements in the vertical plane as shown in Figure 2.2-2a) and are responsible for the typical rolling of the subgrade during an earthquake.

The second kind of surface waves was described first by Love (1903) and consequently is called *Love-wave*. Love-waves, illustrated in Figure 2.2-2b), result from an interference of two SH-waves, several times reflected in the top layer of a multi-layer system. According to their origin Love-waves are shear-waves. They exhibit large amplitudes and, as a consequence, are responsible for huge damages during earthquakes.

Another special kind of waves, although not a surface wave, is shortly introduced here since their characteristics are quite similar. So called *Stoneley-waves* (Stoneley, 1924) occur at the interface of two media as sketched in Figure 2.2-3. Whether such a wave develops depends on the properties of the conjoined media. If it develops then only one certain

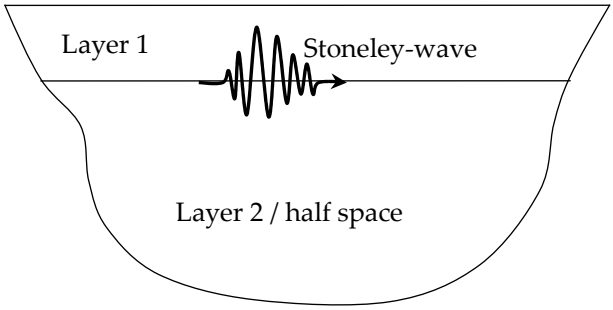

Figure 2.2-3: Stoneley-wave

Stoneley-wave is possible (Barnett, 2000). Stoneley-waves propagate with the Stoneley-wave speed along the interface, exhibiting an amplitude perpendicular to it. They are neither refracted nor reflected and are only relevant up to a depth of about one wavelength in each of the two media. Rayleigh-waves can be considered as Stoneley-waves, propagating at the interface between soil and air. Since the density of air is very small compared to the soil's density, though, the approximation as a surface wave is sufficient in that case.

Close to the vibration source body waves (mostly compression waves) are the dominant wave type. In a distance surface waves become dominant since the energy transport is higher. To initially estimate the amplitudes and therewith possible consequences of propagating waves in the ground, in general two border cases are investigated: the unimpeded propagation through the half space and propagation at the surface alone. The propagation behaviour in reality usually is in between these two border cases. E.g. the development of surface waves is supported due to a clear layer interface between layers with significant different densities close to the surface (DIN 1045-1).

2.3 Damage risks and reduction of living standard and serviceability

Depending on the kind of vibration a structure is exposed to, diverse damage mechanisms can be observed. Even if no damage occurs due to the dynamic impact, a reduction of living standard and serviceability may complicate life.

2.3.1 Reduction of living standard

The German standard DIN 1045-2 contains proposals to evaluate the effect of vibrations in a frequency range from 1 to 80 *Hz* effecting people in buildings. Arbitrary vibrations can be assessed with this procedure.

Long term or permanent vibrations come along with a reduction of living standard as they lead to annoyance, concentration disorder and deterioration of performance, i.e. general inconvenience of people. In general, a reduction of living standard due to vibrations depends on certain influence factors as the magnitude of vibration, frequency, duration, frequency of occurrence and time of day, conspicuity (surprise effect) and kind and operational mode of the vibration source. Furthermore the individual nature and the current situation are of importance. For example physical and psychological condition, activity during the vibration impact, level of familiarisation, attitude towards the originator of vibration, expectations regarding untroubled living and secondary effects, i.e. visible movements of things and audible noise, strongly influences the perception of vibrations by people.

The DIN 1045-2 tries to take into account as much of these influence factors as possible. Basing on measurements a valued factor $KB_F(t)$ is determined. Related to the appraisal period a maximum value KB_{Fmax} and an appraisal value KB_{FTr} can be extracted. Further on threshold values are given in the standard, considering location, utilisation and day of time of the occurrence of the vibration. Therewith typical local influences and point in time of the percussion are included. As specified above, the degree of inconvenience depends on physical and situational conditions. Disturbance only can be excluded if vibrations are imperceptible. Heavy inconvenience, however, in general is not to be expected as long as the threshold values of the standard are not exceeded.

With regards to construction works the temporal limitation of the impact is to emphasize. In many construction processes it is necessary to use construction techniques generating vibrations in the ground. Thus the DIN 1045-2 proposes different (higher) threshold values for temporary impacts compared to dynamic impacts due to stationary grounds with temporal unlimited character. Thereby the threshold value is the lower the longer the period of impact is.

2.3.2 Damage risks and reduction of serviceability

Besides inconvenience of people vibrations in the soil may also have serious consequences for the buildings exposed to and the soil. Especially loose to middle dense non-cohesive granular soils subjected to vibrations tend to densify and therewith may cause settlements of foundations. Particularly frequent dynamic impacts, uniform sands and certain other soil properties force compaction under dynamic loading as will be discussed more extended in section 2.5.3.

Another potential danger can be liquefaction. During this process, in short, the pore water pressure increases due to earthquake shaking or other rapid loading until the effective stress in the soil is zero and the soil fails. Liquefaction and related phenomena are the reason for tremendous amount of damage all over the world. Thus plenty of research works can be found in literature on investigation of liquefaction phenomena, their constitutive modelling and numerical description (e.g. Ishihara et al., 1975; Ishihara, 1993; Yoshimi et al., 1994; Papadimitriou et al., 1999; Yang & Elgamal, 2002; Yang et al., 2003; Triantafyllidis, 2004; Jefferies & Been, 2006 and many others). Liquefaction phenomena mainly occur at large strain levels. Accordingly, they are excluded from the scope of this research.

Even if no damage is to be expected, the serviceability can be constricted due to presence of vibrations in the ground. E.g. highly sensitive technologies need vibration-free rooms. Further aspects on reduction of serviceability of buildings or parts of buildings due to dynamic impacts are defined in the German standard DIN 1045-3. Those are detraction of stability and decreased load capacity of ceilings as well as the occurrence of cracks in plaster and growth of existing cracks. There in general fatigue processes weaken the material and cause failure after large numbers of events.

Of course, large amplitude vibrations and resonance effects may lead to immediate failure of a structure. Particularly earthquake and blasting

engineering deal with these problems (e.g. Kramer, 1996; Siskind, 2000; Scawthorn et al., 2002; Lucca, 2003; Ansal, 2004 and many others). In this work, however, small and very small strain vibrations are object of interest where this kind of damage is irrelevant. Vibration originated movements of the foundation, i.e. settlements, also may result from vibrations not causing immediate damages in the building. These observations are linked to the phenomenon of strain accumulation, see section 2.5.

Recapitulating the previous paragraphs, in general the distinction of four damage mechanisms is proposed:

1. Immediate failure of the structure or parts of the structure due to a single event or a very limited number of events, i.e. damages in the structure due to stress and strain peaks strongly exceeding the maximum strength of the material
2. Immediate failure of the soil as shear failure or liquefaction, i.e. immediate serious failure of the foundation
3. Damages in the structure due to fatigue effects in the material, i.e. decrease of load capacity, detraction of stability, crack growth
4. Densification of the soil due to stress and strain accumulation, i.e. (differential) settlements due to long term excitation

Although densification is not a classical failure mechanism, it is treated as one in this listing, since it may cause (differential) settlements and stress redistributions as well in the soil as in the structure. The statements above are summarised in Table 2.3-1.

The consequences, in general, are the same for both immediate and long term failure. Large (differential) settlements of the structure lead to a reduction of serviceability and, in some cases, to serious damages. Vibrations and settlements further on may lead to the occurrence of cracks, growth of existing cracks, separation of the piping etc. Stress redistribution may lead to changes in the bearing behaviour of the structure, deterioration of roads and railway tracks may be observable.

Besides the quantity of damage, the essential question with respect to the mentioned failure mechanisms is when they occur. Every structure is designed for a certain life time. This leads to the need of an estimation if the expected damage is significant within the life time of the building. If no

significant influence of immediate damages, fatigue effects or settlements is to be expected within the assumed service life the serviceability is not reduced. In this case vibrations in the soil can be neglected in the design process.

Failure	In the soil	In the structure
Immediate due to singular event (e.g. blasting, earthquake)	Shear failure Liquefaction	Exceeding of the maximum strength of the material
Fatigue due to large numbers of events or permanent dynamic loading (e.g. traffic, construction works, wind loading)	Densification Strain accumulation Stress redistribution Abrasion and crushing of grains	Fatigue of the material (decrease of load capacity, detraction of stability) Stress redistribution

Table 2.3-1: Failure mechanisms due to vibrations in the soil

2.3.3 Reduction of vibrations in the soil

If the vibration level exceeds threshold values in the respective site, several activities can be undertaken for vibration reduction. Such actions can follow different strategies. On the one hand conditions to which a part is subjected can be minimised. That is, development, transmission and propagation of vibrations are prevented or at least reduced. On the other hand actions can be undertaken to minimize effects of and sensitivity to vibrations, respectively. That is, the resistance of the structure is improved.

In general, a distinction can be made where actions for reduction of vibrations are undertaken (see Studer & Koller, 1997). Most effective reduction is possible at the source with the objective of minimisation of vibration energy emitted to the surrounding. If this is not possible, sometimes reduction of the vibration level can be achieved in the transmitting medium (e.g. slots in the ground). The third possibility is

consideration of vibration in the design of the receiver. Especially for new structures this is a common procedure.

Accordingly, in the design process the engineer has to balance reasons for either reacting on existing vibrations by increasing the strength of the structure or avoiding them by reduction of the vibration level. For both options high-quality prediction methods are needed to estimate possible consequences of vibrations in the site, to choose correct reduction methods and to react correctly in the design process, respectively.

2.4 Seismic soil investigations

Vibrations in the soil are not always to be assumed as a negative phenomenon. Recent development more and more uses seismic waves for soil investigation to collect knowledge on dynamic properties and geological characteristics of soil and its composition in situ. Meanwhile many field tests are available and commonly used for site exploration. These dynamic field investigations use the elastic properties of soil at small strains for determination of dynamic soil parameters. A big advantage is the opportunity to perform tests on undisturbed soils instead of taking (always disturbed) samples for laboratory investigations. Furthermore a larger area of subsoil can be investigated, allowing for better reference values than results of tests on a small soil sample. Seismic soil investigations are seen as having great potential for determination of the current state of the soil which is an essential point in the present discussion (see section 4.3.4).

Many researchers give a general overview on seismic field tests (e.g. Jamiolkowski et al., 1995; Studer & Koller, 1997; Schmidt & Wuttke, 2003). The most popular tests are seismic reflection tests, seismic refraction tests, spectral analysis of surface waves (SASW), seismic cross-hole test, seismic down-hole and up-hole test, seismic cone penetration test (SCPT), but also geo-tomography (Karl, 2005). An extended work on the analysis of surface waves and related field tests is done by Wuttke (2005).

Also in laboratory testing waves propagating through the soil are used for investigation of dynamic and elastic properties of the soil. In piezoelectric bender and compression element tests – the first one is also performed in the frame of the present work and described in Chapter 6 – seismic waves in the elastic strain range are generated and sent through the

soil sample. These tests are different compared to other laboratory tests to determine dynamic soil properties, since they do not disturb the sample during testing. They are thus well suited for combination with other laboratory tests.

2.5 Strain accumulation due to dynamic impacts

2.5.1 What is strain accumulation?

Repeated events causing small strains in the soil, e.g. traffic loading, may be considered as fully elastic in a very good approach. Measurements of single or only few events may show no visible deformation of the structure and the ground, i.e. no plastic deformations are observed. After large numbers of events, however, a residual deformation is observable in many cases. The described effect is confirmed by own laboratory investigations, see section 7.3.1, and can be explained with compaction due to rearrangement of grains, drainage effects and abrasion of soil particles. This phenomenon – (almost) elastic behaviour in the short term, but non-negligible plastic behaviour over a large number of load repetitions – is called *strain accumulation*, since plastic deformations accumulate in very small increments at every load repetition.

The effect of strain accumulation can be observed in many practical examples. Only little attention is paid to strain accumulation so far, though. Nevertheless it is seen as the most probable damage risk resulting from small strain vibrations. Since immediate failure of the ground is implausible for such impacts, the soil behaviour during application of very large numbers of load repetitions comes to the fore. Strain accumulation causes (differential) settlements of the foundation and leads to redistribution and concentration of stresses. This can initiate damage risks and reduction of serviceability, discussed in section 2.3.2.

2.5.2 Possible reasons for strain accumulation

Many impacts causing settlements due to strain accumulation can be identified. A distinction can be made between static or quasi-static and dynamic impacts. In the context of this work an event is considered as quasi-

static when it does not generate a wave in the ground, even if the process of load application is time dependent and repeatable. That is, only the direct sphere of activity, identical with the (time dependent) bulb of pressure generated by the load of the structure, is to be investigated for quasi-static events. However, also such impacts can cause settlements due to repeated loading. For instance repeated filling and emptying of tanks, silos and watergates is typical cyclic loading which may cause settlements but not generate a wave (e.g. Sweeney & Lambson, 1991; Wolffersdorf & Schwab, 2001). Possible damages will concern only the structure itself and the direct surroundings, though.

In this work the emphasis is set on strain accumulation due to dynamic impacts. An event in this context is considered as dynamic when the load application generates a wave propagating through the soil. Contradicting to quasi-static events in this case the sphere of activity is not limited to the bulb of pressure but increases significantly. Even structures in a distance from the source of vibration may be influenced by such dynamic impacts. Road traffic, railway tracks (Heller, 1981), subways, crane rails (Heller, 1995) but also construction work (e.g. pile driving and blasting) and wind loading can be identified as dynamic sources of vibrations.

Two classes of problems can be identified. In the first class the structure itself is subjected to dynamic load and therewith a source of vibrations. These vibrations are transmitted to the subgrade where, as a result of soil-structure interaction, compaction, stress redistribution and strain accumulation take place. The second class can be seen as receiver problems, i.e. a propagating wave meets the subgrade of a structure. Below the structure settlements arise due to the dynamic impact. Again, additional influence can be expected from soil-structure interaction.

2.5.3 Influence parameters on the strain accumulation rate

The strain accumulation rate, that is the derivative of accumulated strain with respect to the number of load applications, is influenced by many different parameters. In general it is related to the current state of the soil, the current state of stress and the characteristics of the repeated impact. To the author's knowledge Wichtmann (2005) did one of the most extended investigations on parameters influencing strain accumulation. A very complete state of the art report on previous research is given and many dependencies are studied in own experimental laboratory investigations. In

general the outcomes of his work confirm obvious relations briefly discussed in the following. The experimental results of many researchers are basis for so called strain accumulation models further discussed in Chapter 4.

One of the most important perceptions is that plastic strain accumulates with the number of cycles (e.g. Lentz &Baladi, 1980; Suiker, 2002). The more often a certain load is applied the larger is the resulting plastic deformation in relation to the original state. Among others Wichtmann (2005) states that there is always accumulation of strain, no matter which kind of loading is applied, see section 4.3. Thereby compaction occurs until a minimum void ratio is achieved. Suiker (2002), however, distinguishes three possible states, see section 4.4. Up to a certain shakedown level all deformations are assumed to be purely elastic and no accumulation takes place. Above this threshold accumulation happens until either failure occurs or the soil is compacted and stiffened in a way that the cyclic loading becomes purely elastic. It is very difficult to evaluate the correctness of these models. To validate one of the theories tests containing several tens or even hundreds of millions of load cycles are necessary to achieve a level of stabilisation.

In general larger cyclic stress or strain amplitudes generate higher accumulation of residual strains (e.g. Silver & Seed, 1971a,b; Youd, 1972; Marr & Christian, 1981). This is obvious since more energy per cycle is emitted to the ground. Therewith larger portions of plastic strain per cycle develop. Also self-evident is that a higher average effective mean pressure results in decreasing strain accumulation rates since the soil stiffness increases proportional to the effective mean pressure (Budhu, 2000). Therewith the response to cyclic stress applications is stiffer and strain accumulation reduces. The term average effective mean pressure describes the state of stress in the static state. Similarly the average stress ratio means the value of deviatoric stress in relation to the mean effective stress in the static state. The larger the absolute value of the static deviatoric stress the higher is the rate of strain accumulation.

Sudden changes in the characteristics of the cyclic load, namely changes in the polarisation of the strain amplitude, lead to temporary higher strain accumulation rates (Yamada & Ishihara, 1982; Wichtmann et al., 2004b). After several thousands of cycles, however, the soil is reconditioned and adapted to the new loading. The strain accumulation rate returns to the previous level. Wichtmann (2005) calls this phenomenon back polarisation.

The shape of the cycle is of crucial importance as well and can influence the intensity of accumulation significantly (e.g. Pyke et al., 1975). As denoted in section 2.5.2 the loading frequency is of importance as well. Quasi-static events will have a smaller sphere of influence than dynamic ones. Up to now it is not clear whether high loading frequencies (>10*Hz*) generate different settlement behaviour or not.

The second group of influence factors is linked to the characteristics of the soil. Of course, loose soils are easier to compact than dense soils. That is, higher void ratios result in larger strain accumulation rates (e.g. Silver & Seed, 1971a,b; Youd, 1972; Marr & Christian, 1981). Further on the granulometric composition has significant influence on the densification potential of a soil (e.g. Castro & Poulos, 1977). Granulometric composition contains properties as grain size distribution and uniformity, grain shape, sphericity and roughness. Santamarina & Cho (2004) and Cho et al. (2006) report on the important role of particle shape on soil behaviour. A similar role plays the fabric of the soil, including properties as cementation, orientation of grains and homogeneity (e.g. Mulilis et al., 1977). Platy grains, e.g., may generate inherent anisotropy due to their orientation and therewith different (accumulation) behaviour of the soil in different directions. Suiker (2002) mentions a conditioning phase in which the soil adapts to the respective cyclic loading. The back polarisation phenomenon reported by Wichtmann (2005) can be interpreted as a similar effect. Both observations may indicate development of anisotropic material behaviour due to application of cyclic stresses.

Until now, however, the experimental basis dealing with these dependencies is very thin. Wichtmann (2005) investigated the accumulation behaviour of four different sands. He reported on significant higher accumulation rates for well graded sands. Uniform fine grained sands showed higher accumulation potential than uniform coarse grained sands. Further investigation of the influence of grain composition and fabric on the accumulation potential of soils is desirable, though. In a similar manner the influence of moisture content on the accumulation behaviour is not investigated exhaustively yet. One further essential parameter determining the accumulation behaviour of soil is the so called historiotropy, encompassing dynamic as well as static preloading, seasonal effects as freezing and changes of water content, and aging effects as cementation and abrasion. Section 4.3.4 resumes the discussion of these points.

Table 2.5-1 summarises the cognitions of the previous paragraphs and gives an overview on the influence of different parameters on the accumulation rate. The statement 'not clear' after some of the influence parameters indicates the need of further investigation because of no or only thin experimental evidence. Furthermore there may be optima (optimum grain size distribution, optimum moisture content, optimum orientation of grains etc.) where the accumulation rate achieves a minimum, that is, the soil resistance against strain accumulation reaches a maximum. To the author's knowledge these relations are not yet investigated, though.

Influence parameter		Strain accumulation rate
Number of cycles	↑	↓
Cyclic stress or strain amplitude	↑	↑
Average effective mean pressure	↑	↓
Average stress ratio (absolute value)	↑	↑
Change in polarisation		↑ (temporary increase)
Shape of the cycle		not clear
Loading frequency		→ (not clear)
Void ratio	↑	↑
Uniformity	↑	↓ (not clear)
Grain size	↑	↓ (not clear)
Granulometric composition		not clear
Fabric		not clear
Historiotropy		not clear
Moisture content		not clear

Table 2.5-1: Influence of different parameters on the accumulation rate

2.5.4 Direction of strain accumulation

To evaluate consequences of accumulated strains the correct prediction of the direction of accumulation is an essential factor. The direction of

accumulation is determined by the amount of deviatoric and volumetric portions of accumulated strains.

Wichtmann (2005) summarises the papers of Luong (1982) and Chang & Whitman (1988) as the two important works dealing with that problem. Thereafter it depends on the average state of stress whether a sand shows contractive or dilative behaviour under cyclic loading. In addition, both works proved that the direction of accumulation does not depend on the density of the sand. Neither an influence of the effective hydrostatic pressure nor of the cyclic stress amplitude on the direction of accumulation is reported. In tests with 1,050 cycles no influence of the number of cycles on the direction of accumulation was detected.

Wichtmann (2005) investigated several more influence parameters on the direction of accumulation. In this study it turned out that neither span, shape and polarisation of the loops nor amplitude changes, relative density, loading frequency, monotonic preloading and grain size distribution have an influence on the direction of accumulation. In contrast to the findings of Chang & Whitman (1988) Wichtmann (2005) detected a measurable influence of the number of load applications on the direction of accumulation.

Based on these experimental studies it can be stated that the direction of accumulation mainly depends on the average state of stress. The number of load cycles applied has a minor but measurable meaning for this parameter.

2.5.5 Laboratory and in-situ investigation of strain accumulation

Comparatively little effort is done so far to investigate accumulation properties of soil under small strain long term cyclic loading both experimentally and in theory. Theoretical aspects of the description of strain accumulation are discussed in Chapter 4. A summary of existing element and model tests with cyclic loading and related findings with respect to strain accumulation is given by Wichtmann (2005).

Laboratory investigation of strain accumulation

In laboratory tests the quantitative accumulation behaviour of soil under certain static and cyclic stress conditions can be studied. The influence of different parameters on intensity and direction of accumulation, described in

sections 2.5.3 and 2.5.4, can be studied. Such cognitions are very important for development of constitutive models dealing with the problem of strain accumulation.

The predestined laboratory test to investigate the accumulation behaviour of soils is the cyclic triaxial test performed on cylindrical soil samples. The possibility of applying very large numbers of load cycles in a wide range of loading options allows for maximum crop of findings with a single test especially with respect to cyclic long term behaviour. Evolution as well of strain accumulation as of elastic parameters with the number of load applications can be well studied. Possible combination with non-disturbing test procedures extends the amount of collected data. For this reason cyclic triaxial test equipment is also installed in the frame of this research and used for experimental investigation of strain accumulation, see Chapter 6.

In triaxial tests on cylindrical samples one- or two-dimensional stress cycles are applied. Due to the axisymmetric stress conditions the stress cycles always lay within a plane in the principal stress space. Further well applicable tests are the torsional shear test on hollow cylinder specimens and the true triaxial test on cubical soil samples. In these tests three-dimensional stress cycles can be applied since variation of more stress components is possible. Only few such apparatuses exist, though.

Rarely used for the investigation of strain accumulation are shaking table tests and resonant column (RC) tests. While shaking table tests usually are applied at larger strains in liquefaction studies of sand layers under earthquake loading, RC tests are mainly used for determination of the secant stiffness of the stress-strain hysteresis at various strain levels. Nevertheless these tests may be used for investigation of strain accumulation in future.

Piezoelectric bender and compression element tests are seen as good completion for numerous test devices. Although not eligible for generation of residual strains, changes in the elastic properties of the soil may be detected from variations in the wave speed of compression and shear waves, respectively.

In-situ investigation of strain accumulation

Very few data of field measurements on accumulation of foundation settlements due to long-term dynamic impacts is found in the literature. This may be linked to the fact that in the past main interest was set on dynamic

characteristics of single events. The damage risk for the structure was seen in stress and strain peaks during an event exceeding the maximum strength of the material. Thereby the accumulation of stress concentrations in the structure caused by (differential) settlements of the ground as a result of long-term dynamic loading was not considered.

Accordingly many field measurements focused on records of single events as a basis for dynamic numerical models, e.g. for prediction of traffic and train induced vibrations in structures (e.g. Degrande & Schillemans, 2001; Lombaert & Degrande, 2001; Kogut et al., 2003; Lombaert et al., 2006). On the other hand measurements of accumulated residual deformations in situ require sensitive instrumentation and very long measurement periods. Therewith they are expensive. Further on they may be overlaid by other effects. Thus the correct acquisition of permanent deformation is quite tricky. These are further reasons for rare data. Some available case histories are reported already in 2.5.2.

Hunaidi & Tremblay (1997) come to the conclusion that there is a potential of indirect damage from traffic vibrations caused by differential movement due to soil densification, though. Their statement bases on extensive measurements in representative complaint sites and detailed analysis of building vibration induced by road traffic. Thereafter small strain vibrations as from road traffic may contribute to the process of deterioration of structures, although vibration levels are rarely high enough to be the direct cause of damage. Small vibration levels induced in buildings by road traffic (and similarly by other man-made vibrations such as blasting and pile driving) may generate accumulation of residual deformations and could trigger damage by topping up existing residual strains.

For correct prediction of settlements due to strain accumulation to be expected in the site it is necessary to estimate the accumulation potential of the soil in-situ. Thus site investigations need to be performed delivering needed information. No reliable methods are available for that task yet, though. Dynamic test loadings on a temporary foundation as proposed by Triantafyllidis et al. (2004) or with a portable device as preferred by Wichtmann (2005) may allow for some conclusions but is probably not very practically. Apart from the cost intensive procedure only locally limited results can be achieved. Furthermore the soil is disturbed during investigation which will influence predictions.

To relate results of laboratory tests to in-situ conditions appears also very tricky as will be discussed in section 4.3.4 in more detail. Soil specimens are always disturbed in laboratory tests and therewith do not represent the real in-situ conditions. The most promising procedure to determine the current in-situ state of the soil with respect to its accumulation potential is seen in the correlation with dynamic parameters. Thereby the dynamic properties need to be determined in-situ as well, e.g. on the basis of geophysical methods as denoted in section 2.4. The estimation of accumulation potential in the site, however, is not studied well up to now. Further research in this field is seen as desirable.

2.6 Conclusions

In this chapter vibrations in the ground are characterised with respect to several aspects. Consequences of vibrations in the ground as damage risk in structures, reduction of serviceability, inconvenience of people and possible use for seismic soil exploration are outlined. The so far hardly considered phenomenon of strain accumulation due to ground vibrations is explained in more detail. Influencing parameters are identified, consequences are outlined, case histories and recent works are mentioned.

The previous sections illustrate how important it is to investigate vibrations in the ground and its effects on arising structures. The engineer's task in that sense is to predict if the structure will retain its serviceability during its life time under certain dynamic impacts. Detailed knowledge on the characteristics of vibrations in the soil, outlined in section 2.2, and possible damage potentials, see section 2.3, thus is seen as fundamental. The German standard DIN 1045-3 provides threshold values below which no damage is to be expected. These threshold values refer to maximum particle velocities in the structure. However, especially in the field of low level vibrations at small and very small strains these threshold values may be unsatisfying and deficient. In this respect a reliable prediction method on settlement risks is still missing in engineering practice. The present work focuses on that problem. The main point of interest is to throw a light on the long term soil behaviour under continuous dynamic impacts to finally being able to predict settlements to be expected under different dynamic loadings.

It turns out that especially vibrations in the small strain region that are present permanently or at least for long periods are responsible for strain accumulation. In general, all manmade vibrations can cause accumulation effects. Also several natural vibration sources in the small strain region as wind and wave loading as indirect dynamic impact on foundations may generate strain accumulation, while earthquakes are not subject of this topic. Being able to estimate impacts on buildings and related settlement risks due to vibrations in the ground before e.g. the construction process is started, makes it possible to optimize construction techniques and time flow with regards to a minimisation of disturbance of surrounding buildings and nearby living inhabitants. Furthermore isolation systems, touched on in section 2.3.3, can be designed optimised to reduce disturbance due to vibrations. The impact on the structure can be minimised, damage risks can be reduced. Therewith reconditioning is less frequently necessary and longer life times can be achieved leading to economically advantageous construction works.

To achieve this goal the development of related mathematical models for prediction of residual deformations due to long term dynamic excitations, further discussed in Chapter 4 and Chapter 5, is indispensable. In this context experimental investigation of strain accumulation in laboratory tests, shortly outlined in section 2.5.5 and extensively discussed in Chapter 6 and Chapter 7, is of crucial importance for validation of such models and investigation of quantitative interrelationships of different influence parameters.

Chapter 3
Governing equations

3.1 Introduction

Although soils are three-phase materials, consisting of mineral grains, air voids and water, in geotechnical engineering it is commonly idealised as a continuum neglecting the individual constituent elements and their interaction. Soil mechanics, treated in the framework of this idealisation, thus is a branch of mechanics of solids. In this chapter the mathematical frame for stress and strain definitions is outlined. The constitutive relations for elastic material are presented and elastic material parameters are identified. Based on these definitions the determination of dynamic soil parameters and its strain dependency is discussed in consideration of later aspects of this work.

In continuum mechanics, it is convenient to use the so-called index notation (Chen & Mizuno, 1990). Thereafter in a right-handed Cartesian coordinate system the mutually orthogonal coordinate axes are more conveniently named as x_i (i=1, 2, 3), i.e. x_1, x_2 and x_3, for a general discussion, rather than the more familiar coordinate axes x, y and z. This formulation allows for the use of the index notation and summation convention as commonly used in tensorial analysis.

Contrary to continuum mechanics, where tensile stress and elongation are assigned positive, in soil mechanics tensile stress and elongation are used as a negative quantity whereas compression stress and compression strain is a positive one. This is a logic consequence resulting from the fact that soil, in general, is exposed to load in compression. Thus

the soil mechanical sign convention is used in this work. The continuum mechanical sign convention is casually used in Chapter 4 and Chapter 5 as it is common in relation to constitutive models. Deviating notation is explicitly mentioned in the respective sections. This choice has been made in accordance with common practice in soil mechanics and constitutive modelling, respectively.

Despite the above stated idealisation as a continuum, soil is usually characterised by several essential soil parameters. The physical properties of soil are influenced by the relative proportions of each of the three phases, solid, air and water. The corresponding variables describing these phase relationships and frequently used in this work are defined in section 3.3. Further on, coefficients for description of the granular decomposition of the soils are introduced.

Besides the physical properties the mechanical behaviour of soil strongly depends on the dynamic loading conditions. While in the small strain region the maximal stiffness is observed, the material damping is minimal. For larger strains stiffness decreases, while damping increases. Strain dependency of soil stiffness and material damping ratio, determination of maximal stiffness and the interpretation of stress-strain hysteresis loops are discussed in a further section of this chapter.

3.2 Stresses and strains in the soil

3.2.1 Definition of stresses

Stress tensor

The in soil mechanics commonly used designation for effective stress components by a superposed _' is set aside. All stress definitions are considered as effective stresses. Deviating notation is explicitly mentioned in the respective context. The general stress state of an arbitrary cuboid is then described by the stress tensor σ_{ij} of the form

$$\sigma_{ij} = \begin{bmatrix} \sigma_{11} & \sigma_{12} & \sigma_{13} \\ \sigma_{21} & \sigma_{22} & \sigma_{23} \\ \sigma_{31} & \sigma_{32} & \sigma_{33} \end{bmatrix} = \begin{bmatrix} \sigma_x & \tau_{xy} & \tau_{xz} \\ \tau_{yx} & \sigma_y & \tau_{yz} \\ \tau_{zx} & \tau_{zy} & \sigma_z \end{bmatrix}. \tag{3.1}$$

In equation (3.1) the nine components of σ_{ij} are given in index notation as well as in engineering notation. From the consideration of equilibrium of moments of a material element, it follows that the stress tensor is symmetric, that is, $\sigma_{ij} = \sigma_{ji}$. Every stress state is characterised by a hydrostatic state and a purely deviatoric state of stress and therewith can be expressed as

$$\sigma_{ij} = p\delta_{ij} + s_{ij} = \begin{bmatrix} p & 0 & 0 \\ 0 & p & 0 \\ 0 & 0 & p \end{bmatrix} + \begin{bmatrix} \sigma_{11} - p & \sigma_{12} & \sigma_{13} \\ \sigma_{21} & \sigma_{22} - p & \sigma_{23} \\ \sigma_{31} & \sigma_{32} & \sigma_{33} - p \end{bmatrix}. \tag{3.2}$$

Thereby the mean stress p is defined by

$$p = \frac{1}{3}\sigma_{ii} = \frac{1}{3}\left(\sigma_{11} + \sigma_{22} + \sigma_{33}\right) \tag{3.3}$$

while s_{ij} is the deviatoric stress component and δ_{ij} is the Kronecker delta with

$$\delta_{ij} = \begin{cases} 1 & \forall\ i = j \\ 0 & \forall\ i \neq j \end{cases}. \tag{3.4}$$

Invariants of the stress tensor and principal stresses

For each stress state the quantities I_1, I_2 and I_3, called the invariants of σ_{ij}, can be found. These invariants are unaffected by rotation of the coordinate axes and determined by

$$\begin{aligned} I_1 &= \sigma_{ii} \\ I_2 &= \frac{1}{2}\left(I_1^2 - \sigma_{ij}\sigma_{ji}\right). \\ I_3 &= \det\left|\sigma_{ij}\right| \end{aligned} \tag{3.5}$$

Therewith equation (3.3) can be reformulated to

$$p = \frac{1}{3} I_1. \tag{3.6}$$

In analogy to equations (3.5) the invariants of the deviatoric stress component can be achieved by

$$\begin{aligned} J_1 &= s_{ii} = 0 \\ J_2 &= \frac{1}{2} s_{ij} s_{ji} \\ J_3 &= \det\left|s_{ij}\right| \end{aligned} . \tag{3.7}$$

The commonly used deviatoric stress invariant q is defined as

$$q = \sqrt{3J_2} = \sqrt{\frac{3}{2} s_{ij} s_{ji}} . \tag{3.8}$$

For each stress state one orientation of a right-handed coordinate system exists with all shear components equal to zero, i.e. $\sigma_{ij} = 0 \;\forall\; i \neq j$. In this case the trace of σ_{ij} alone is occupied with stress components σ_{ii}. For $\sigma_{11} > \sigma_{22} > \sigma_{33}$ these stress components are called the principal stresses σ_1, σ_2 and σ_3, while the corresponding orientations are called the principal axes for the stress state σ_{ij}. In the following a single subscript indicates a principal value. The principal axes of s_{ij} and σ_{ij} are identical. Corresponding to the principal stresses there are three principal shears

$$\tau_1 = \frac{1}{2}\left|\sigma_2 - \sigma_3\right|, \quad \tau_2 = \frac{1}{2}\left|\sigma_1 - \sigma_3\right| \quad \text{and} \quad \tau_3 = \frac{1}{2}\left|\sigma_1 - \sigma_2\right| . \tag{3.9}$$

The largest numerical value is called the maximum shear stress:

$$\tau_{\max} = \frac{1}{2}\left|\sigma_1 - \sigma_3\right| , \tag{3.10}$$

that is, $\tau_{\max} = \max\left(\tau_1, \tau_2, \tau_3\right)$.

The plane with the hydrostatic axis, i.e. $\sigma_1 = \sigma_2 = \sigma_3$, as normal vector is called π-plane and defined by

$$\sigma_1 + \sigma_2 + \sigma_3 = 0 . \tag{3.11}$$

Any stress vector in the stress space can be projected to this plane. The angle between this projection and the projection of the principal axis defined by σ_1 is called Lode angle and given by

$$\theta = \frac{1}{3}\cos^{-1}\left(\frac{3\sqrt{3}}{2}\frac{J_3}{J_2^{3/2}}\right) \tag{3.12}$$

or, alternatively,

$$\cos 3\theta = \frac{3\sqrt{3}}{2}\frac{J_3}{J_2^{3/2}}. \tag{3.13}$$

The range in which the angle varies for $\sigma_1 \geq \sigma_2 \geq \sigma_3$ is $0 \leq \theta \leq \pi/3$.

Any state of stress can be expressed in terms of I_1, J_2 and J_3 in the principal stress space, see also Chen & Mizuno (1990).

Stresses in triaxial conditions

In triaxial test conditions stresses are applied only in lateral and axial direction. Furthermore no shear stresses are applied in these directions and the cylindrical soil sample is exposed to axisymmetric loading. Accordingly the stress conditions are very well defined and the above equations can be strongly simplified. In Figure 3.2-1 the stress state in a cyclic triaxial test is schematised. Obviously axial and lateral direction coincide with the principal axes 1, 2 and 3, respectively, whereby direction 2 and 3 are identical due to axisymmetric conditions. Since all tests in this research are performed on saturated samples (see section 6.4), the pore water pressure u is to be considered in the definition of effective stresses. The principal stress σ_1 therewith results from the summation of the confining pressure (which is the cell pressure), σ_c, and the vertically applied axial pressure, σ_a, while u is to be subtracted. The principal stress σ_3 results from subtraction of the pore water pressure from the confining pressure. For cyclic loading an additional, time variable pressure, σ_1^{ampl}, in axial direction is applied.

For the axisymmetric configuration the stress invariants, mean effective stress p, equation (3.3), and deviatoric stress invariant q, equation (3.8), become

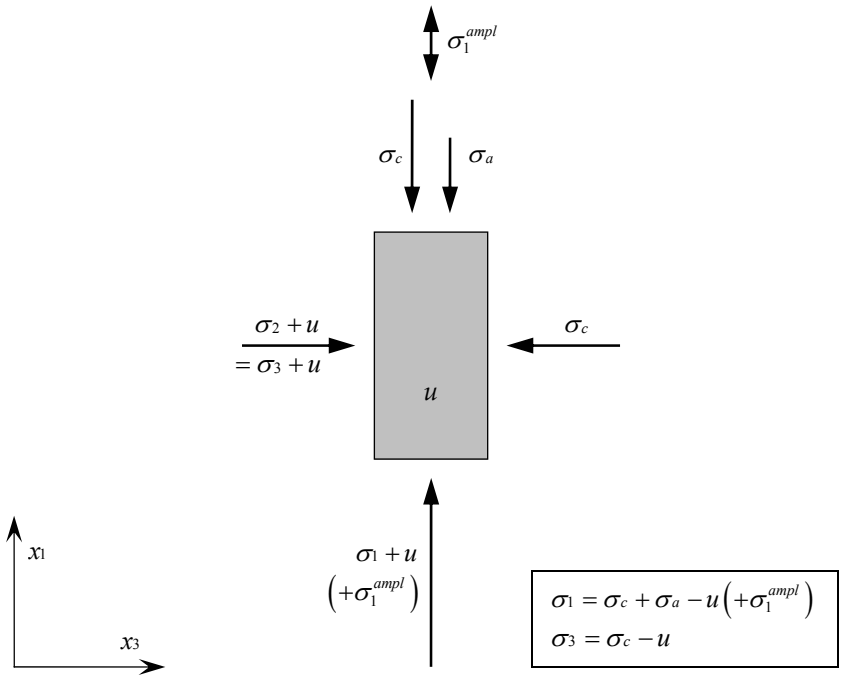

Figure 3.2-1: Axisymmetric effective stress state in a cyclic triaxial test

$$\begin{aligned} p &= \frac{1}{3}\left(\sigma_1 + 2\sigma_3\right) \\ q &= \left|\sigma_1 - \sigma_3\right| \end{aligned} . \tag{3.14}$$

The stress state can be well expressed in the *p*-*q*-plane using the stress ratio η, defined as

$$\eta = \frac{q}{p} . \tag{3.15}$$

For isotropic stress conditions $\eta = 0$ holds, while the critical value is equal to the inclination of the critical state line M_c and depends on the critical friction angle φ_c:

$$\eta_c = M_c\left(\varphi_c\right) = \frac{6\sin\varphi_c}{3 - \sin\varphi_c} . \tag{3.16}$$

For axisymmetric conditions the earth pressure coefficient at rest, K_0, defined by the ratio of horizontal and vertical pressure, becomes

$$K_0 = \frac{\sigma_3}{\sigma_1} \tag{3.17}$$

and equation (3.15) can be reformulated to

$$\eta = \frac{3(1-K_0)}{2K_0+1}. \tag{3.18}$$

For cyclic loading the amplitude ratio ζ is defined as

$$\zeta = \frac{\sigma_1^{ampl}}{p}, \tag{3.19}$$

whereby p is the mean effective stress under static stress conditions.

3.2.2 Definition of strains

Strain tensor and strain invariants

In analogy to the definition of stresses, the strain tensor ε_{ij} can be defined. Although the definitions are presented for the strain, they are also valid for the rates. As for the stress tensor the nine components of ε_{ij} can be given in index notation as well as in engineering notation, i.e.

$$\varepsilon_{ij} = \begin{bmatrix} \varepsilon_{11} & \varepsilon_{12} & \varepsilon_{13} \\ \varepsilon_{21} & \varepsilon_{22} & \varepsilon_{23} \\ \varepsilon_{31} & \varepsilon_{32} & \varepsilon_{33} \end{bmatrix} = \begin{bmatrix} \varepsilon_{xx} & \frac{1}{2}\gamma_{xy} & \frac{1}{2}\gamma_{xz} \\ \frac{1}{2}\gamma_{yx} & \varepsilon_{yy} & \frac{1}{2}\gamma_{yz} \\ \frac{1}{2}\gamma_{zx} & \frac{1}{2}\gamma_{zy} & \varepsilon_{zz} \end{bmatrix}. \tag{3.20}$$

When the components of ε_{ij} are chosen as in the right hand side of equation (3.20), the array has a second order tensorial character. Kinematic considerations relate the components of a strain field to the components of a displacement field, u_i, as discussed by Chen & Mizuno (1990). For small displacements, the strain tensor may be approximated by the symmetric part of the first-order gradient of the displacement field,

$$\varepsilon_{ij} = \frac{1}{2}\left(u_{i,j} + u_{j,i}\right), \tag{3.21}$$

where $u_{i,j}$ denotes the derivative of the displacement u_i in the j-th direction, Chen & Mizuno (1990).

Just like the stress tensor, the strain tensor is symmetric, that is, $\varepsilon_{ij} = \varepsilon_{ji}$. In accordance with the definitions for stresses, ε_{ij} can be decomposed in a purely volumetric portion, ε_{kk}, and the deviatoric strain tensor, e_{ij},

$$\begin{aligned} \varepsilon_{kk} &= \varepsilon_{11} + \varepsilon_{22} + \varepsilon_{33} \\ \varepsilon_{ij} &= e_{ij} + \frac{1}{3}\varepsilon_{kk}\delta_{ij} \end{aligned} . \tag{3.22}$$

ε_{kk} is the volumetric strain invariant, energetically conjugated to the hydrostatic pressure p, while the deviatoric strain invariant κ, energetically conjugated to the deviatoric strain invariant q, is presented by

$$\kappa = \sqrt{\frac{2}{3} e_{ij} e_{ji}} . \tag{3.23}$$

In the case of long-term cyclic loading at small strain levels, the total strain ε is decomposed in a resilient, purely elastic portion ε^{ampl} and a residual portion of accumulated, plastic strain ε^{acc},

$$\varepsilon = \left\| \varepsilon_{ij} \right\| = \varepsilon^{ampl} + \varepsilon^{acc} . \tag{3.24}$$

This issue is illustrated in Figure 4.1-1b). In equation (3.24) $\left\| \varepsilon_{ij} \right\|$ denotes the Euclidean norm of the strain tensor.

Strains in triaxial conditions

The well defined, simple stress state for triaxial conditions, discussed in the previous section, allows for simplification of the strain definitions as well. At the surface of the soil sample only axial strains in direction of the principle axes occur. Therewith ε_{kk} becomes

$$\varepsilon_{kk} = \varepsilon_1 + 2\varepsilon_3 , \tag{3.25}$$

wherein ε_1 and ε_3 denote the principal strains in axial and lateral direction, respectively. The deviatoric strain invariant κ becomes

$$\kappa = \frac{2}{3}\left|\varepsilon_1 - \varepsilon_3\right| . \tag{3.26}$$

Alternatively, the deviatoric strain is denoted as γ with

$$\gamma = \varepsilon_1 - \varepsilon_3 , \tag{3.27}$$

as commonly applied in engineering practice. The total strain for triaxial conditions is

$$\varepsilon = \sqrt{\left(\varepsilon_1\right)^2 + 2\left(\varepsilon_3\right)^2} . \tag{3.28}$$

For the elastic strain portion, the Poisson ratio υ is defined as

$$\upsilon = -\frac{\varepsilon_3^{ampl}}{\varepsilon_1^{ampl}} , \tag{3.29}$$

while for the portion of accumulated strains, the ratio of volumetric and deviatoric strain invariant ω defines the direction of accumulation, that is, the flow rule

$$\omega = \frac{\varepsilon_{kk}^{acc}}{\kappa^{acc}} . \tag{3.30}$$

For undrained conditions the volumetric strain, equation (3.25), becomes zero and the deviatoric strain, equation (3.27), can be expressed in terms of ε_1 alone, since the incompressibility of water leads to υ=0.5:

$$\gamma = 1.5\varepsilon_1 . \tag{3.31}$$

3.2.3 Homogeneous isotropic elasticity

For an arbitrary material point in the halfspace, a constitutive relation between σ_{ij} and ε_{ij}, defining the elastic material behaviour, may be formulated as

$$\sigma_{ij} = D_{ijkl}\varepsilon_{kl} \quad \text{with} \quad i,j,k,l \in \{1,2,3\}, \tag{3.32}$$

where D_{ijkl} is the fourth-order constitutive tensor. In general, D_{ijkl} contains 81 independent components. This number reduces to 21 independents when considering the symmetries of stress and strain tensor. The assumption of certain planes of symmetry in the material further reduces the number of independent material parameters. In that way the number of independents reduces to five for cross-anisotropic materials. That is, the material behaves isotropic in one plane, while it behaves different in normal direction to this plane. For ideally homogeneous isotropic elastic material, i.e. its properties do neither change in any direction nor in any point, are only two independent material parameters left. This simplification is commonly used in soil mechanical tasks to reduce complexity of problems and corresponding calculation effort.

Although equation (3.32) is presented for stresses and strains, it also applies for the respective rates. Therewith a certain stress increment results in a corresponding strain increment. Depending on the definition of the constitutive tensor, this relation is linear or nonlinear.

Introducing the Lamé constants λ and μ the constitutive tensor of a homogeneous isotropic elastic medium is given by

$$D_{ijkl} = \lambda\delta_{ij}\delta_{kl} + \mu\left(\delta_{ik}\delta_{jl} + \delta_{il}\delta_{jk}\right). \tag{3.33}$$

Using equation (3.33) and the symmetry of the strain tensor allows for reformulation of equation (3.32), which results in the well known form

$$\sigma_{ij} = \lambda\delta_{ij}\varepsilon_{kk} + 2\mu\varepsilon_{ij}. \tag{3.34}$$

Alternatively, the elastic behaviour is characterised by the Poisson ratio υ, defined in equation (3.29), and the Young's modulus E, defined by $E = \varepsilon_1/\sigma_1$. These parameters easily can be determined for free lateral deformation in cyclic triaxial tests as will be discussed in Chapter 6. Other frequently used elastic constants are the shear modulus G, defined by the coefficient of deviatoric stress and deviatoric strain, and the bulk modulus K, defined by $K = p/\varepsilon_{kk}$. The overview presented in Table 3.2-1 is given to summarize the relationship between particular elastic constants.

	λ,μ	G,υ	E,υ	K,G
λ	λ	$\frac{2\upsilon}{1-2\upsilon}G$	$\frac{\upsilon E}{(1+\upsilon)(1-2\upsilon)}$	$K-\frac{2}{3}G$
$\mu \equiv G$	μ	G	$\frac{E}{2(1+\upsilon)}$	G
K	$\frac{3\lambda+2\mu}{3}$	$\frac{2(1+\upsilon)}{3(1-2\upsilon)}G$	$\frac{E}{3(1-2\upsilon)}$	K
E	$\frac{\mu(3\lambda+2\mu)}{\lambda+\mu}$	$2(1+\upsilon)G$	E	$\frac{9KG}{3K+G}$
υ	$\frac{\lambda}{2(\lambda+\mu)}$	υ	υ	$\frac{3K-2G}{2(3K+G)}$

Table 3.2-1: Relationship between elastic constants

3.3 Characteristic soil parameters

As stated in section 3.1 soils are three-phase materials consisting of grains, water and air. The properties of the grains and the respective ratios of the three phases define the properties of the soil and its behaviour. This section introduces the characteristic soil parameters frequently used in this work.

3.3.1 Phase relationships

Considering a piece of soil its total volume V can be decomposed in the volume of solids V_s and the volume of voids V_v, i.e. $V = V_s + V_v$. Usually a part of the voids is filled with water, that is, the total void volume consists of the volume of water V_w and the volume of air V_a, $V_v = V_w + V_a$. Accordingly the mass of the soil is the sum of the solid mass m_s and the mass of the water m_w, $m = m_s + m_w$. The mass of air is negligible. In perfectly dry conditions the dry soil mass m_d is equal to the mass of solids, $m_d = m_s$. Budhu (2000) summarises the following definitions, which have been established to describe the proportion of each constituent in soil and thus are taken over in

this work. Each equation can be presented with different variables. The most convenient forms are present here.

Water content

The water content w, commonly expressed as a percentage, is the ratio of the mass of water to the mass of solids,

$$w = \frac{m_w}{m_s} \cdot 100\% . \tag{3.35}$$

For the case that all voids are completely filled with water, the soil is said to be saturated. Then the water content equals the saturation water content w_s.

Degree of saturation

The degree of saturation *S*, often expressed as a percentage, is the ratio of the volume of water to the void volume,

$$S = \frac{V_w}{V_v} \cdot 100\% = \frac{w}{w_s} \cdot 100\% . \tag{3.36}$$

Alternatively, *S* can be determined from the ratio of the actual water content to the saturation water content, as presented in the right hand side of equation (3.36). For *S*=100%, the soil is saturated, while for S=0% the soil does not contain any water anymore.

Void ratio

The void ratio *e* is the ratio of the void volume to the volume of solids,

$$e = \frac{V_v}{V_s} . \tag{3.37}$$

For the densest possible packing of grains, the void volume becomes minimal. Accordingly in this case the minimum void ratio, e_{min}, is achieved. The maximum void ratio, e_{max}, is determined by the loosest possible packing of grains, i.e. by the maximum void volume.

Relative density

The relative density D_r is an index, often expressed as a percentage, that quantifies the degree of packing between the loosest and densest possible state of granular materials,

$$D_r = \frac{e_{\max} - e}{e_{\max} - e_{\min}} \cdot 100\% \tag{3.38}$$

Density, dry density

The density ρ, commonly expressed in kg/cm^3, is the ratio of the total mass to the total volume, while the dry density ρ_d is determined by the ratio of the mass of solids to the total volume,

$$\rho = \frac{m}{V} \quad \text{and} \quad \rho_d = \frac{m_d}{V}. \tag{3.39}$$

Unit weight, dry unit weight

The unit weight γ and the dry unit weight γ_d are commonly used in engineering practice and express the soil load by taking into account the gravity g=9.81 $m\ s^{-2}$,

$$\gamma = \rho \cdot g = \frac{m \cdot g}{V} \quad \text{and} \quad \gamma_d = \rho_d \cdot g = \frac{m_d \cdot g}{V}. \tag{3.40}$$

If the density is entered in kg/cm^3, the unit weight is calculated in kN/m^3.

3.3.2 Characterisation of soils by granular decomposition

Starting from the grain size distribution curve, the median grain size D_{50} allows for some conclusions on the granular decomposition of a soil. 50% of the particles exhibit a larger diameter than D_{50}, while the other 50% are finer. Further information can be obtained from two coefficients having been defined to provide guidance on distinguishing soils based on the distribution of the particles. The uniformity coefficient UC is defined as

$$UC = \frac{D_{60}}{D_{10}}, \tag{3.41}$$

where D_{60} is the diameter of the soil particles for which 60% of the particles are finer, and D_{10} is the diameter of the soil particles for which 10% of the particles are finer. The other coefficient is the coefficient of curvature *CC*, defined as

$$CC = \frac{D_{30}^2}{D_{10} D_{60}}, \tag{3.42}$$

where D_{30} is the diameter of the soil particles for which 30% of the particles are finer.

3.4 Dynamic parameters of soil

3.4.1 Strain dependency of dynamic soil parameters

Harmonic loading of soil leads to a stress-strain diagram as presented in Figure 3.4-1. A hysteresis loop accrues for each period of the oscillation. When plotting shear stress τ versus shear strain γ, the shear modulus *G* is found as the slope of the line connecting the point of origin and the inversion point between loading and unloading. This modulus is also called the secant shear modulus (see also Karl, 2005). For free lateral deformation, alternatively the maximum principal stress σ_1 can be plotted versus the corresponding principle strain ε_1. Result is a similar hysteresis loop, whereby the slope of the line connecting the point of origin and the inversion point now defines the Young's modulus *E*. Such graphs are a typical outcome of drained cyclic triaxial tests. Besides the secant modulus, the hysteresis curve provides information about the damping ratio *D* of the soil. It can be determined from the ratio of the triangle area, assigned in Figure 3.4-1 with the edge lengths *S* and *L*, to the area of the hysteresis loop as will be described in section 3.4.3.

For symmetric hysteresis loops as depicted in Figure 3.4-1, which are a result of cyclic triaxial tests, the secant modulus is determined by the slope of the hysteresis loop, i.e. maximum and minimum point of the loop, since the barycentre lies on the line defined by these points. The first loading curve, connecting load inversion points of oscillations with different stress and strain levels, is called backbone curve. Its hyperbolic shape indicates a

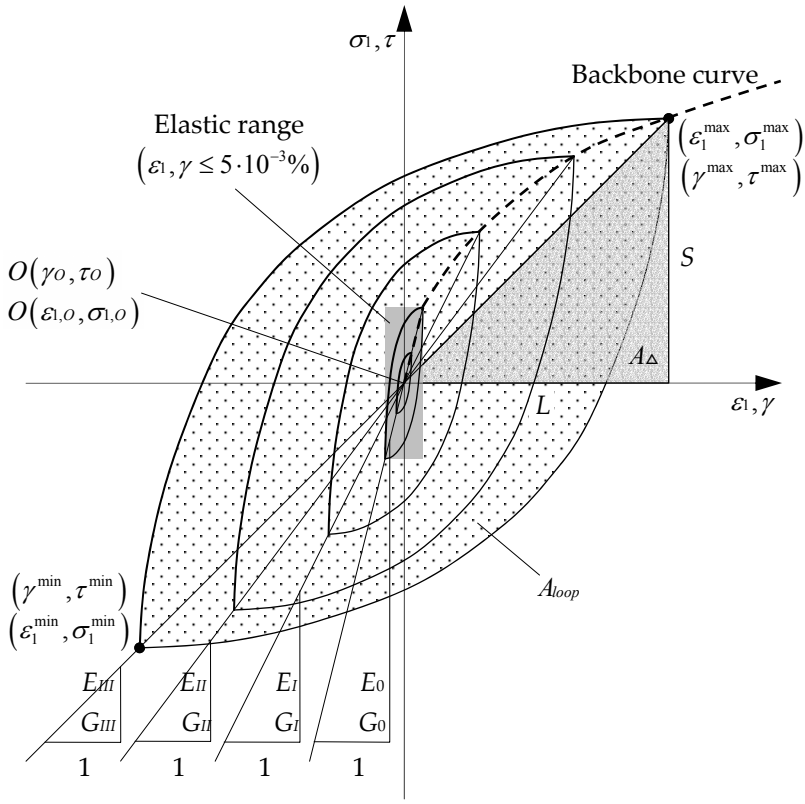

Figure 3.4-1: Hysteresis loops due to cyclic loading

decreasing slope with increasing strain. Thus the stress-strain relationship, in general, is of nonlinear character, in Figure 3.4-1 $E_0 > E_I > E_{II} > E_{III}$ and $G_0 > G_I > G_{II} > G_{III}$ holds. The slope in the origin point of the backbone curve corresponds to the maximum dynamic shear modulus G_{max} or G_0, or the maximum dynamic Young's modulus E_{max} or E_0, depending on the chosen axes. G_{max} and E_{max} are the moduli in the low strain range, usually assumed at values below the linear elastic threshold strain of about $5 \cdot 10^{-3}\%$, and are discussed in the next section. In the low strain range the moduli are assumed to be constant. Figure 3.4-1 also illustrates the variation of the hysteresis loop and the triangle area, respectively, for different stress and strain amplitudes. This indicates changes of the damping ratio D with the strain. The damping increases with increasing strain. A schematic sketch of moduli and damping ratio in function of the strain is given in Figure 3.4-2.

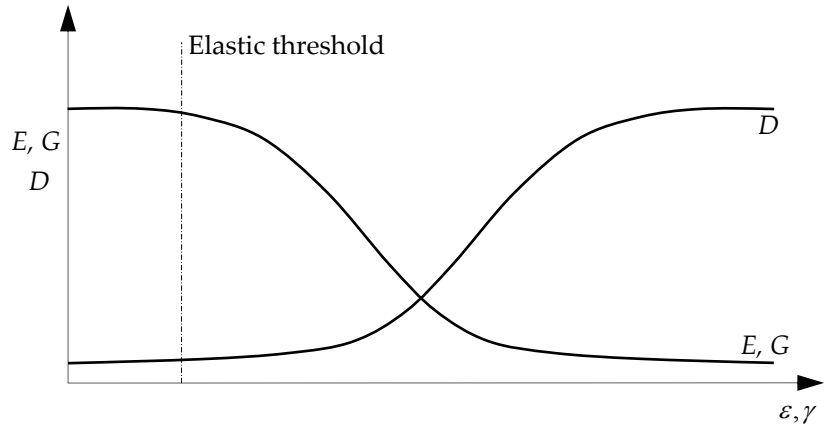

Figure 3.4-2: Evolution of E, G and D with increasing strain

Based on a hyperbolic non-linear constitutive model, Duncan & Chang (1970) proposed the following formulation to describe the shear modulus at larger shear strain amplitudes in relation to G_{max}:

$$G = \frac{G_{max}}{1 + \gamma/\gamma_r} \tag{3.43}$$

This relation was confirmed experimentally by Hardin & Drnevich (1972a,b). In equation (3.43) γ is the shear strain amplitude, while γ_r denotes a reference shear strain. This reference shear strain is determined by the ratio of the maximum shear strength T_{max} of the soil at a given stress state to the corresponding maximum shear modulus G_{max},

$$\gamma_r = \frac{T_{max}}{G_{max}}. \tag{3.44}$$

The maximum shear strength T_{max} is defined as the maximum shear stress that can occur without causing the soil to fail. The well known Coulomb failure criterion takes into consideration the effect of the hydrostatic pressure on the strength of materials. It states that failure occurs when the shear stress τ and the normal stress σ_n acting on any element in the material satisfy the linear equation $|\tau| = \sigma_n \tan\varphi + c$, where φ is the angle of internal friction and c the strength of cohesion. Adopting this criterion to Mohr's circle, failure occurs when the largest circle, passing through

maximum and minimum principal stress, σ_1 and σ_3, touches the failure line. Accordingly the maximum value of shear strength T_{max} for static conditions can be expressed as

$$T_{max} = \sqrt{\left[\frac{1}{2}(1+K_0)\sigma_1 \sin\varphi + c\cos\varphi\right]^2 - \left[\frac{1}{2}(1-K_0)\sigma_1\right]^2}\,. \tag{3.45}$$

The capital letter T has been chosen for the maximum shear strength in order to preserve uniqueness in notation and avoid confusion with the maximum shear stress τ_{max} in equation (3.10).

To determine the maximum Young's modulus E_{max}, the coupling of E and G via the Poisson ratio υ can be used. This relation is given in Table 3.2-1 and, for the sake of clearness of denotation of equations, is repeated here:

$$E = 2(1+\upsilon)G\,. \tag{3.46}$$

Hardin & Drnevich (1972a,b) present a relation between the damping ratio and the shear modulus,

$$D = D_{max}\left(1 - \frac{G}{G_{max}}\right), \tag{3.47}$$

where D_{max} is the maximum damping ratio. D becomes maximal when $G = 0$, that is, $D(G=0) = D_{max}$. Yoon (1991) proposes a strain based formulation, achieved by combining equations (3.43) and (3.47),

$$\frac{D}{D_{max}} = \frac{\gamma}{\gamma_r}\frac{1}{1+\gamma/\gamma_r}, \tag{3.48}$$

which can be reformulated to

$$\frac{D}{D_{max}} = \frac{\gamma}{\gamma_r + \gamma}\,. \tag{3.49}$$

For infinitesimal small strains, equation (3.49) becomes $D(\gamma \to 0) = 0$, while for very large strains $D(\gamma \to \infty) = D_{max}$. This coincides with the fact that soil

is assumed to behave linear elastic at very small strains (see also section 3.4.3), while the largest amount of energy is dissipated at large strain levels.

3.4.2 Determination of G_{max} and E_{max}

Most vibrations discussed in section 2.2 exhibit strain amplitudes below the elastic threshold. This opens the opportunity to model wave propagation phenomena using simple linear elastic constitutive models with the maximum moduli as essential parameters. It can be shown that, for isotropic, homogeneous and linear elastic materials, G_{max} can be calculated as

$$G_{max} = \rho \cdot V_s^2 , \tag{3.50}$$

where G_{max} is calculated in *Pa* when the density ρ, equation (3.39), is entered in kg/m^3 and the shear wave velocity V_s in *m*/s, see also section 2.2.4. This essential relation is frequently used to obtain G_{max} by means of various seismic geophysical tests providing values of V_s. Karl (2005) gives an overview on parameters influencing the soil stiffness. In this work bender element tests are used to determine G_{max} from the shear wave velocity. The experimental setup and data analysis is described in section 6.5.

A large amount of laboratory test results is the basis of empirical correlation functions developed in the past. Both Yoon (1991) and Karl (2005) give an overview on some of the best established formulas in the literature. Thus they are not repeated here. Yoon (1991) derived the following empirical formula on the basis of resonant column tests on sands:

$$G_{max} = \frac{S}{0.3 + 0.7e^2} p_a^{1-n} p^n . \tag{3.51}$$

In equation (3.51) p_a is the atmospheric pressure, while S and n are free parameters. p and e are determined by equations (3.6) and (3.37), respectively. Since S, n and e are dimensionless values, G_{max} is obtained in the same unit as p_a and p are entered.

While the shear modulus is related to the shear wave velocity, the maximum Young's modulus E_{max} can be derived from measurements of the p-wave velocity V_p, see also section 2.2.4,

$$E_{\max} = \frac{(1+\upsilon)(1-2\upsilon)}{1-\upsilon}\rho \cdot V_p^2 . \tag{3.52}$$

3.4.3 *E* and *D* out of hysteresis loop

As outlined in section 3.4.1, hysteresis loops contain information on the secant moduli *E* and *G*, respectively, as well as on the material damping ratio *D*. The procedure to extract the modulus from hysteresis loops, achieved in cyclic triaxial tests with uniaxial loading, is described for the Young's modulus *E*, exemplarily. The secant shear modulus *G* can be determined analogously when the hysteresis loop is defined by shear parameters τ and γ. The secant modulus is defined by the slope of the hysteresis loop, that is,

$$\frac{1}{E} = \frac{\varepsilon_1^{DA}}{\sigma_1^{DA}}, \tag{3.53}$$

with $\varepsilon_1^{DA} = \varepsilon_1^{\max} - \varepsilon_1^{\min}$ the axial double amplitude strain and $\sigma_1^{DA} = \sigma_1^{\max} - \sigma_1^{\min}$ the axial double amplitude stress. For illustration it is referred to Figure 3.4-1. Accordingly, equation (3.53) can be reformulated to

$$E = \frac{\sigma_1^{DA}}{\varepsilon_1^{DA}} = \frac{\sigma_1^{\max} - \sigma_1^{\min}}{\varepsilon_1^{\max} - \varepsilon_1^{\min}} . \tag{3.54}$$

The damping ratio *D* of a soil is defined as the ratio of dissipated energy in a soil element per load cycle to the elastic energy stored in the soil element during one load cycle. The amount of energy dissipated during a single load cycle is defined by the area of the hysteresis loop. For linear elastic material behaviour this area becomes zero and the soil damping vanishes, since no energy is dissipated in this case. Again referring to Figure 3.4-1, *D* is defined by

$$D = \frac{A_{loop}}{4\pi A_{\triangle}}, \tag{3.55}$$

whereby A_{loop} is the hysteresis loop area and $A_{\Delta} = S \cdot L/2$ is the area of the grey highlighted triangle. A derivation of equation (3.55) is, for example, presented by Karl (2005).

3.5 Conclusions

In this chapter the definitions of stresses and strains in soil are introduced. The general, tensorial formulation has been chosen in the face of later discussion of constitutive models. Stress and strain invariants as well as frequently used stress and strain ratios are defined. The general formulations, however, are attributed to triaxial conditions as well in order to bridge the gap between theory and cyclic triaxial laboratory testing, also subject of this work.

With the assumption of soil being a homogeneous and isotropic continuum the framework of elasticity is briefly reviewed. The constitutive tensor in general and the two independent elastic constitutive parameters for isotropic material conditions are introduced. Important elastic parameters commonly used in soil mechanics and its respective relations are summarised.

For dynamic load conditions, soil exhibits hysteretic behaviour. As a matter of fact this stress-strain relation is of nonlinear nature. While in the small strains region, below the elastic threshold strain, linear elastic constitutive behaviour can be implied, at larger strains, these nonlinearities have to be considered. The determination of maximum dynamic elastic parameters both out of theoretical considerations and out of experimental investigations is discussed. Further on the determination of dynamic soil parameters out of hysteresis loops at larger strains is described.

While for modelling the assumption of soil as a continuum is a sufficient approximation, coming along with several simplifications, the real physical behaviour of soil is determined by the ratio of the three phases, solid, water and air. Further on the granular composition plays an important role. Thus the most important parameters characterizing the properties of soil are introduced in this chapter as well. Especially for sample preparation in laboratory testing, see Chapter 6, the correct definition of these variables is of importance.

Chapter 4

Accumulation models for soils

In contrast to hysteretic models, applying an incremental $\dot{\sigma}_{ij} - \dot{\varepsilon}_{kl}$ constitutive law, a second class of constitutive models, subsequently referred to as *accumulation models*, is developed. In those models the evolution of stresses and strains during long term or continuously repeated impacts is described. They are commonly used for description of the phenomenon of strain accumulation, described in section 2.5, where the plastic deformation of an individual event is relatively or even negligible small, while the cumulative effect over a (very) large number of load repetitions may be considerable. In accumulation models the actual time is replaced by the number of load cycles applied. Although hysteretic models can be used to calculate several cycles, especially for complex long term problems the latter kind of model will be the better choice to achieve reliable predictions of settlements and stress redistributions, respectively. Advantages and limitations of accumulation as well as hysteretic models are outlined. Several accumulation models are presented in the literature. An overview on some existing models summarises the general approach and most important properties of these models. The Bochum accumulation model, a recently developed advanced accumulation model, is discussed in more detail. Limitations, shortcomings and further needs are incorporated in this chapter. Furthermore a different approach for description of cyclic densification, basing on the classical plasticity theory, is summarised and discussed.

4.1 Introduction

4.1.1 Hysteretic versus accumulation constitutive models for soils

Hysteretic models in general describe the material behaviour by means of an incremental $\dot{\sigma}_{ij} - \dot{\varepsilon}_{kl}$ constitutive law. In these laws the evolution of strain due to certain stress application is modelled as illustrated in Figure 4.1-1a). Many different hysteretic models, able to represent miscellaneous material behaviour are developed and presented in the literature, e.g. Chen & Mizuno (1990). Hysteretic models are commonly used in soil mechanics to represent the loading and unloading behaviour of soil under certain conditions.

Accumulation models are developed to predict accumulation of stresses and strains due to cyclic loading with a large number of cycles. Hysteretic models are not practicable to describe strain accumulation during several hundreds or thousands of cycles. In contrast, accumulation models can easily be used to calculate residual strains caused by several millions of cycles, provided that the model is accurately designed and validated. Especially for very low strain levels significant deformation may only be generated after very large numbers of cycles. Here an advantage of accumulation models emerges: the possible number of cycles to be calculated is in principle unlimited.

This is mainly founded by the fact that in comparison to hysteretic models accumulation models need significantly less calculation effort. Instead of calculating every single hysteresis loop with many stress and strain increments, the accumulated strain is calculated using a direct formulation as will be explained below. Suiker (2002), Abdelkrim et al. (2003), Niemunis et al. (2004) and Wichtmann (2005) emphasize the tremendous calculation effort being necessary to calculate huge numbers of cycles using hysteretic approaches. Furthermore numerical errors will increase with the number of calculated cycles. Taking 100,000 cycles, each calculated in 100 increments, increases systematic errors 10^7 times. The produced numerical error may easily exceed the actually generated accumulated strains. A threshold for accurate prediction of plastic deformations using hysteretic models can be assumed at about 50 to 100 load cycles.

On the other hand, to minimize the accuracy problem, a hysteretic constitutive law of unattainable accuracy would be required. Furthermore development and application of such advanced models require high knowledge of constitutive behaviour of soil to understand the model and its parameters. Therewith common applications in practice are not interesting anymore. The more accurate a model shall be, the more parameters are to be introduced and the more difficult is the interpretation and determination of those parameters. Large numbers of field investigations and laboratory tests, high costs and much effort in time for parameter identification will be the result. In practice very often only limited test results are available making it difficult, if not impossible, to determine a high number of model parameters.

While many numerical programs are available with several already implemented hysteretic models ready for use, accumulation models are not yet common in engineering practice. They may easily be adapted to the respective problem and implemented in finite element codes, though. Several accumulation models are presented in the literature showing the wide range of possible applications. Resulting deformations in foundations caused by strongly nonlinear elasto-plastic problems with large deformations may be described (e.g. the filling and emptying of silos or water tanks) as well as strain accumulation due to very low cyclic strain levels (e.g. traffic induced vibrations, construction works or (indirect) wind loading on foundations).

Looking at the two mentioned examples one may notice the significantly differing loading frequencies. While the filling and emptying of a silo can be said to be quasi-static, traffic induced vibrations and wind loading are clearly dynamic impacts. However, most experimental studies show no influence of the loading frequency on the rate of strain accumulation as discussed in section 2.5.3. For this reason on the one hand accumulation models do not take into account the loading frequency. On the other hand they are applicable to both quasi-static and dynamic problems independently from the loading frequency.

A typical objection to accumulation models is their empirical character. One could argue that all predictions made by accumulation models only reproduce the results of laboratory tests; there is no mechanical background in such models. The approach of Suiker (2002), discussed in section 4.4, bridges the gap between empirical and mechanical approach.

Besides, hysteretic models are fitted to test results as well. This validation is necessary to verify the quality of the model.

4.1.2 Terminology – explicit versus implicit integration schemes

Usually the solution of a constitutive equation is calculated numerically. Apart from very simple models the analytical solution is too complex to be considered as practicable for most common applications. Numerical solution schemes are often referred to as being *explicit* or *implicit*. When a direct computation of the dependent variables can be made in terms of known quantities, the computation is said to be *explicit*. Explicit methods calculate the state of a system at a later time from the state of the system at the current time, that is

$$\Gamma\left(t+\Delta t\right)=F\left(\Gamma\left(t\right)\right), \tag{4.1}$$

where $\Gamma\left(t\right)$ is the current system state, $\Gamma\left(t+\Delta t\right)$ the system state at the later time and Δt a small time increment.

In contrast, when the dependent variables are defined by coupled sets of equations, and either a matrix or iterative technique is needed to obtain the solution, the numerical method is said to be *implicit*. An implicit method finds the state of a system at a later time by solving an equation involving both the current state of the system and the later one. That is

$$G\left(\Gamma\left(t\right),\Gamma\left(t+\Delta t\right)\right)=0 \tag{4.2}$$

has to be solved to find $\Gamma\left(t+\Delta t\right)$. Functions *F* and *G* in equations (4.1) and (4.2), respectively, are defined by the used constitutive law.

Implicit methods require higher computational effort, and they can be much more difficult to implement. They are used because many problems arising in real life, such as the constitutive behaviour of soil, are stiff (quick changes of stresses and strains with time), for which the use of an explicit method requires impractically small time steps Δt to keep the error in the result bounded. For such problems, to achieve a given accuracy, it takes less computational time to use an implicit method with larger time steps, even

taking into account the need to solve an equation of the form (4.2) at each increment.

One more important factor to choose for a numerical method is its stability. Numerical stability has to do with the behaviour of the solution as the time-step Δt is increased. If the solution remains well behaved for arbitrarily large values of the time step, the method is said to be unconditionally stable. This situation never occurs with explicit methods, which are always conditionally stable (Hirt, 2006). In general it depends upon the problem to be solved whether an explicit or implicit method should be used.

4.1.3 Terminology – explicit versus implicit models

Accumulation models in the literature sometimes are also called *explicit* or *N-type* models (Baligh & Whittle, 1987; Sagaseta et al., 1991; Niemunis et al., 2004; Wichtmann, 2005) because the evolution of stress or strain accumulation, that is the residual or permanent stress or strain, is described in relation to the applied number of cycles instead in terms of stress and strain increments in every single hysteresis loop. One can say explicitly the accumulation of stresses or strains is considered. As a result an accumulation curve can be drawn as indicated in Figure 4.1-1b). In this context hysteretic models are generally said to be *implicit*, since the evolution of stresses and strains is described by means of increments on the hysteresis loop. Residual stresses or strains are a kind of by-product of the incremental calculation resulting from not perfectly closed hysteresis loops, see Figure 4.1-1a).

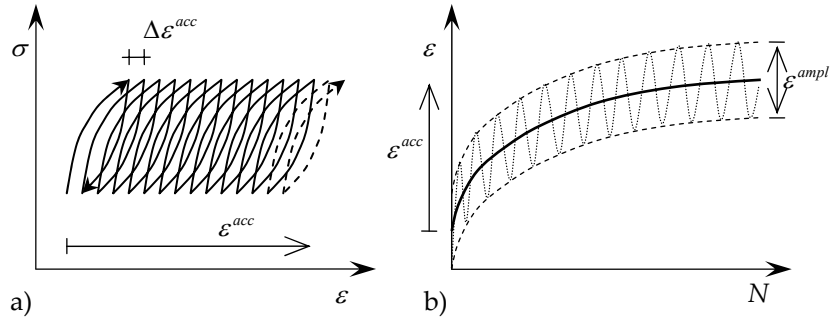

Figure 4.1-1: Strain accumulation in a) hysteretic vs. b) accumulation models

The use of the terms *explicit* and *implicit* with respect to the distinction between hysteretic and accumulation models, however, may be confusing recalling the remarks in the previous section on explicit and implicit integration schemes. Thus for the sake of clearness the already frequently used terms *hysteretic* and *accumulation* models are proposed.

4.2 Accumulation models in the literature

4.2.1 General approach of accumulation models

Various models have been developed for predicting accumulated plastic strain ε^{acc} in soil under repeated loading. Many of these models use a power law of the form

$$\varepsilon^{acc} = AN^b \tag{4.3}$$

with N being the number of cycles applied and A and b empirical model parameters depending on soil type, soil properties and stress state (e.g. Monismith et al., 1975). In some models the parameter A is replaced by factors including stress dependencies and other soil properties (e.g. Marr & Christian, 1981; Diyaljee & Raymond, 1981; Bouckovalas et al., 1984; Kaggwa et al., 1991; Hornych et al., 1993; Li & Selig, 1996; Chai & Miura, 2000; Chai & Miura, 2002; Gidel et al., 2001; Abdelkrim et al., 2003 and Gotschol & Kempfert, 2004).

A second class of accumulation models uses logarithmic formulations to describe the evolution of strain accumulation in relation to the number of cycles (Barksdale, 1972; Güttler, 1984; Sawicki & Swidzinski, 1987; Sawicki & Swidzinski, 1989; Sweere, 1990; Triantafyllidis et al., 2003; Niemunis et al., 2005; Wichtmann, 2005). Also in these models empirical determined parameters are necessary. Most models also include factors to take into account soil properties and stress state.

Some more approaches are presented in the literature. Paute et al. (1988) uses a square root formulation in his approach, whereas Drabkin et al. (1996) proposes a polynomial model for the estimation of settlements of sand. These approaches, however, do not seem to be very common and thus are not further considered in detail.

All the above mentioned models have in common that they refer to the number of cycles as an essential parameter, that is, the time is replaced by a pseudo-time. Furthermore these models base on empirical field and laboratory investigations. Depending on the amount of data available the models cover several relations as stress dependencies, the influence of the initial density or cyclic loading options. Of course, the more (reliable) data available, the better the model can be fitted to the respective problem.

A general problem of most of the mentioned models is the thin experimental basis they are founded on. Very often the influences of important parameters as void ratio or state of stress are neglected or can only be insufficiently taken into account. Many models are based on very low numbers of cycles leading to a wrong prediction of strain accumulation due to large numbers of cycles. Advanced accumulation models should allow for the prediction of the deviatoric portion of accumulated strain κ^{acc} as well as of the volumetric portion ε_{kk}^{acc}. The models fulfilling this request either propose two separate empirical equations for κ^{acc} and ε_{kk}^{acc} (e.g. Marr & Christian, 1981; Bouckovalas et al., 1984; Kaggwa et al., 1991; Güttler, 1984) or use coupled formulations (Niemunis et al., 2004; Wichtmann, 2005).

For calculation of the total accumulated strain components most models use incremental formulations basing on the strain accumulation rates of the respective components for the deviatoric and the volumetric portion, $\dot{\kappa}^{acc}$ and $\dot{\varepsilon}_{kk}^{acc}$. The rate in this context means the derivative of the accumulated strain with respect to the number of load applications, $\dot{\varepsilon}^{acc} = \mathrm{d}\varepsilon^{acc}/\mathrm{d}N$, instead of with respect to the actual time as in hysteretic models. Accordingly, the strain accumulation rate indicates the increment of accumulated strain related to a certain increment of the number of load cycles, while in hysteretic models the strain rate means the strain increment related to a certain time increment.

Few models use the accumulated strain at a certain cycle as a reference. The accumulated strain at the first cycle $\varepsilon^{acc}\left(N=1\right)$, for instance, is used by Gotschol & Kempfert (2004). Paute et al. (1988) and Hornych et al. (1993) take the accumulated strain of the hundredth cycle $\varepsilon^{acc}\left(N=100\right)$. The crucial disadvantage of these approaches is the actually impossible correct determination of the corresponding parameter in situ. Tests on reconstituted samples in the laboratory always refer to virgin soil and it is easy to determine the accumulated strain after a certain cycle. In the field, however, natural soil is always preloaded. The question arises, how the loading

history can be taken into account in parameters and how it should be related to the parameters $\varepsilon^{acc}(N=1)$ and $\varepsilon^{acc}(N=100)$.

Sometimes so called semi-explicit approaches are used to describe the accumulation of strain. Therein empirical based predictions are combined with advanced constitutive laws to achieve a tensorial formulation of the accumulation rate. Especially to describe the direction of accumulation advanced hysteretic models may lead to good agreement with test results, e.g. Wichtmann et al. (2004a). The so called Bochum accumulation model (Niemunis et al., 2004; Wichtmann, 2005) uses such a semi-explicit approach and will be discussed in more detail in section 4.3.

4.2.2 Review of some existing accumulation models

In the following some of the above mentioned models will be discussed shortly. The essential definition of the strain accumulation rate will be outlined. The respective model parameters and some essential shortcomings are described.

Model of Marr & Christian (1981)

The model of Marr & Christian (1981) uses an approach similar to the one given in equation (4.3). It describes the accumulation of the volumetric and the vertical strain with the power laws

$$\dot{\varepsilon}_{kk}^{acc} = \eta^{*av} C_v D_v N_e^{D_v - 1} \qquad \dot{\varepsilon}_1^{acc} = \eta^{*av} C_1 D_1 N_e^{D_1 - 1}. \tag{4.4}$$

The state of stress is described by $\eta^* = q^*/p^*$ with $p^* = (\sigma_1 + \sigma_3)/2$ and $q^* = (\sigma_1 - \sigma_3)/2$. C_v, D_v, C_1 and D_1 in equations (4.4) are material constants. N_e is a weighted number of cycles wherein the influence of the initial porosity (void ratio), the cyclic stress amplitude and the average mean pressure is considered with another multiplicative formulation. The factors of this product are based on results of laboratory investigations and contain another set of three material constants with different values for $\dot{\varepsilon}_{kk}^{acc}$ and $\dot{\varepsilon}_1^{acc}$. Therewith N_e is different for volumetric and axial strain. It should be noted that the model uses the stress amplitude as input parameter rather than the strain amplitude as other models do. In fact this is seen as the better choice, since only stresses are used as an input for the model, whereas other models use both, stresses and strains.

Packages of cycles with different amplitudes are treated by introducing an equivalent number of cycles N_{eq}. Prior to the calculation of the next package of cycles with certain amplitude, the cycles in the past are converted into N_{eq} cycles with the actual amplitude. The proposed procedure implies that it does not matter for the subsequent accumulation whether a previous accumulation of strain is achieved by a large number of cycles with small amplitudes or a smaller number of cycles with large amplitudes. This assumption coincides with laboratory test results presented by Gidel et al. (2001). Consequently the current state of the soil is of importance, while the assumption is made that it does not matter how this state is achieved.

The deviatoric accumulation rate $\dot{\kappa}^{acc}$ can be determined from $\dot{\varepsilon}_{kk}^{acc}$ and $\dot{\varepsilon}_{1}^{acc}$. The different sets of material constants for volumetric and axial rate, however, result in different values N_e. This may lead to confusion. For isotropic average stress ($\eta^{*av} = 0$) the model predicts a vanishing accumulation rate which is obviously wrong, whereas the increase of the accumulation rate with the average stress ratio η^{*av} makes sense. The increase of the accumulation rate with increasing stress amplitude and increasing initial porosity is captured. The description of the cyclic flow rule and the predicted acceleration of accumulation with increasing average mean pressure as well as the consideration of the historiotropy using N_{eq} is questioned by Wichtmann (2005). The large number of model parameters makes it difficult to understand the respective physical meaning and its determination.

Model of Bouckovalas et al. (1984)

Also the model of Bouckovalas et al. (1984) describes as well the accumulation of volumetric as the accumulation of deviatoric strains. For the corresponding rates the following equations were proposed:

$$\dot{\varepsilon}_{kk}^{acc} = A\left(2\gamma^{ampl}\right)^{a} I^{c} f \tag{4.5}$$

$$\dot{\kappa}^{acc} = \pm B\left(\eta^{av}/2\right)^{b}\left(2\gamma^{ampl}\right)^{a} I^{c} \tag{4.6}$$

In equation (4.6) the positive formulation is valid for $\eta^{av} \geq 0$, the negative one for $\eta^{av} < 0$. A, B, a, b and c are material constants.

The dependence of the accumulation rates on the historiotropy is expressed by the state variable I,

$$I = \int_0^N \left[2\gamma^{ampl}\left(N\right) \right]^a N^c \, \mathrm{d}N \,. \tag{4.7}$$

For cycles with a constant shear strain amplitude γ^{ampl} the rates are proportional to $N^{c(c+1)}$. Therewith equations (4.5) and (4.6) can be traced back to a formulation similar to equation (4.3).

The parameter *f* is stress-dependent, taking the value 1 on the *p*-axis in the *p*-*q*-plane and being zero on the critical state line. The model predicts the cyclic flow rule correctly: $\dot{\varepsilon}_{kk}^{acc}$ vanishes on the critical state line while $\dot{\kappa}^{acc}$ becomes zero at $\eta^{av} = 0$. Further on an increase of $\dot{\varepsilon}^{acc}$ with increasing amount of the average stress ratio $\left|\eta^{av}\right|$ is predicted. The model uses a state variable for the historiotropy considering also the amplitude of the cycles. It proposes an exponential amplitude-dependency. The volumetric portion ε_{kk}^{ampl} of the applied cycle and the shape of the strain loop are not considered explicitly. Also the influences of the average mean pressure and the void ratio are not captured. The cyclic shear strain amplitude is used as an input parameter rather than the cyclic stress amplitude.

Model of Sawicki & Swidzinski (1987 and 1989)

Sawicki & Swidzinski (1987 and 1989) formulated a model describing the densification of sand under cyclic shearing. The model is based on the so-called *common compaction curve*,

$$\Phi\left(\tilde{N}\right) = C_1 \ln\left(1 + C_2 \tilde{N}\right) \tag{4.8}$$

with the state variable *compaction* $\Phi = \Delta n / n_0$ (*n*: porosity), the number of cycles weighted by the amplitude

$$\tilde{N} = \int J \, \mathrm{d}N = \int \frac{1}{2} \left\| \boldsymbol{\varepsilon}^{ampl} \right\| \mathrm{d}N \tag{4.9}$$

and the material constants C_1 and C_2. In equation (4.9) the tensor $\boldsymbol{\varepsilon}^{ampl}$ contains the amplitudes of the particular strain components. The compaction rate $\dot{\Phi} = \partial\Phi / \partial N$ is obtained from equation (4.8),

$$\dot{\Phi} = \frac{C_1 C_2 J}{1 + C_2 \tilde{N}} = C_1 C_2 J \exp\left(-\Phi / C_1\right). \tag{4.10}$$

Sawicki and Swidzinski performed cyclic simple shear tests on a fine sand at different strain amplitudes. Larger amplitudes caused faster densification of the samples. The common compaction curve is achieved by plotting the volumetric portion of the accumulated strain ε_{kk}^{acc} or Φ versus $\tilde{N}$. The curves $\Phi\left(\tilde{N}\right)$ fall together into a single curve. In the model the historiotropy is taken into account with a measure weighting the number of cycles with their amplitudes.

However, only low numbers of cycles are investigated. The above assumptions are only valid for less than 50 cycles. According to Wichtmann (2005) a further drawback of the model is that only the volumetric but not the deviatoric accumulation is described. As in the model of Bouckovalas et al. (1984) the volumetric portion ε_{kk}^{ampl} of the applied cycle and the shape of the strain loop are not considered. In this model the influence of the average stress state on the strain accumulation is not taken into account. The influence of different void ratios is considered via different constants C_1 and C_2 alone, that is, it is not clearly separated from other influences.

Model of Li & Selig (1996)

The model of Li & Selig (1996) is directly developed from equation (4.3) investigating the influences of loading and soil properties on the parameters A and b based on results presented in the literature. The exponent b thereafter can be considered independent of the deviatoric stress q, the resilient strain ε^{ampl} and the physical state of the soil (moisture content, dry density). For differing soils, however, exponent b is varying.

The parameter A is considered to be influenced by the deviatoric stress, the physical state of the soil and the soil type. The physical state of the soil is not explicitly considered in the equation but supposed to be taken into account indirectly via the static strength of the soil q_f (= static failure deviatoric stress of the soil) as this parameter varies with different moisture contents and dry densities. Also influences on the accumulated strain caused by changes in the soil structure are supposed to be covered indirectly with q_f. The parameter A is then defined by

$$A = a\left(\frac{q^{ampl}}{q_f}\right)^m \tag{4.11}$$

with a and m material parameters characterizing the different relationship between A and q^{ampl} and q_f for different soil types. Therewith the following model for the accumulated strain can be given:

$$\varepsilon_1^{acc} = a\left(\frac{q^{ampl}}{q_f}\right)^m N^b . \tag{4.12}$$

The model is rather simple and predicts only accumulation in axial direction. The number of cycles investigated is small (N=1,000). Packages of cycles with different amplitudes are treated by introducing an equivalent number of cycles N_{eq}, quite similar as proposed by Marr & Christian (1981), by weighting the previously applied cycles with their deviatoric strain amplitude. The influence of strain loop and volumetric portions of the applied cycle are not taken into account. The description of the soil physical state via the static strength alone may be questioned. Influences of the average mean pressure and the void ratio are not captured sufficiently in that way.

Chai & Miura (2002) extended the model of Li & Selig (1996) for clays, considering the effect of the initial static deviatoric stress q^{av} and propose the following empirical equation

$$\varepsilon_1^{acc} = a\left(\frac{q^{ampl}}{q_f}\right)^m \left(1+\frac{q^{av}}{q_f}\right)^n N^b \tag{4.13}$$

with four material constants a, b, m and n. Although the initial state of stress here is partly taken into account the general remarks remain the same.

Model of Gidel et al. (2001)

Gidel et al. (2001) use the model of Hornych (1993) to further develop own empirical equations for the prediction of accumulation of vertical strain. The main equation of Hornych (1993) is

$$\varepsilon_1^{acc}\left(N\right)=\varepsilon_1^{acc}\left(N=100\right)+A_1\left[1-\left(\frac{N}{100}\right)^{-B}\right], \tag{4.14}$$

wherein A_1 and B are material constants and $\varepsilon_1^{acc}\left(N=100\right)+A_1$ is the limit value of ε_1^{acc} when N equals infinity. The parameter A_1 is assumed to be equal to a characteristic permanent deformation A_{1c} determined from a standard test according to the French standard NF P 98-235-1.

Gidel et al. (2001) see the main shortcoming of equation (4.14) in the fact that the influence of stresses is not taken into account. Thus they propose a formulation of the form $\varepsilon_1^{acc}\left(N\right)=f\left(N\right)\cdot g\left(p_{\max},q_{\max}\right)$, i.e. a product of a function of the numbers of cycles and a function of the maximum stresses, $p_{\max}$ and $q_{\max}$, applied. Based on cyclic triaxial test results they finally achieve the following formulation:

$$\varepsilon_1^{acc}\left(N\right)=\varepsilon_1^{acc,0}\left[1-\left(\frac{N}{100}\right)^{-B}\right]\left(\frac{l_{\max}}{p_a}\right)^n\frac{1}{m+\frac{s}{p_{\max}}-\frac{q_{\max}}{p_{\max}}} \tag{4.15}$$

with $\varepsilon_1^{acc,0}$, B, m, n, s being parameters, $l_{\max}=\sqrt{p_{\max}^2+q_{\max}^2}$ and $p_a=100kPa$.

Although sets of parameters are given by Gidel et al. (2001) it is not clear, how these values are determined. Also the definition of $p_{\max}$ and $q_{\max}$ is vague. The model predicts only the vertical strain and accordingly cannot predict the accumulation of radial and volumetric strains. Gidel et al. (2001) are aware of that shortcoming and give missing test data as a reason that the accumulation of radial strains could not be investigated sufficiently. Neither the shape nor volumetric portions of the strain loop are taken into account. The influence of the void ratio and soil structure is neglected. Gidel et al. (2001) emphasize that, according to experimental results, the water content has a strong influence on the strain accumulation in the soil. They propose the investigation of the influence of different water contents on strain accumulation, also to taking account seasonal aspects. Abdelkrim et al. (2003) propose a scheme for the numerical implementation of this model for the prediction of road settlements due to traffic loading.

Model of Gotschol & Kempfert (2004)

The model of Gotschol and Kempfert (2004) was developed for the prediction of deformations in the subsoil of railways. The general numerical modelling procedure is explained in Stöcker and Kempfert (2005). The model describes the accumulation of vertical strains for initially isotropic stress conditions and a vertically oscillating stress, only applied in compression. The residual vertical strain is described by the relation

$$\varepsilon_1^{acc}\left(N\right) = \varepsilon_1^{acc}\left(N=1\right) N^{\alpha} . \tag{4.16}$$

The similarity to equation (4.3) is obvious. $\varepsilon_1^{acc}\left(N=1\right)$ and α are described with help of complex equations using 21 material constants in total. The model is complicated but has several shortcomings as only vertical strains are predicted, although only five material parameters are to be introduced for the respective soil the determination of the 21 needed model constants is very difficult, only isotropic stress conditions are covered and the use of $\varepsilon_1^{acc}\left(N=1\right)$ is problematic (see section 4.2.1, Niemunis & Wichtmann, 2005 and Wichtmann, 2005).

4.2.3 Summary

Many strain accumulation models are presented in the literature. Some of them, representing different ideas of describing the evolution of strain accumulation during long term cyclic loading, are presented above. The general approach of these accumulation models was outlined and shortly discussed.

The idea of disassociating different influence parameters as the number of cycles, state of stress or cyclic amplitude, leading to a model being a product of several functions seems to give fairly good results and is commonly used in different models. According to the underlying test programs, the models capture more or less effects of different influence parameters. All presented models use the number of cycles *N* instead of the time *t* as essential parameter describing the evolution of accumulated strain. This means, not every single hysteresis loop during the cyclic loading is investigated by means of incremental analysis but the envelope of the strain evolution is used.

An essential shortcoming of most of the models is that they are based on tests with relatively small numbers of cycles. That is, the evolution

of accumulated strain after large numbers of cycles will most probably not be captured correctly by those models. Using exponential or logarithmic formulations with respect to the number of cycles will lead to a vanishing strain accumulation rate after a certain number of cycles. However, tests in the literature (Suiker, 2002; Wichtmann, 2005) show, that even after several millions of load cycles accumulation is observed. A realistic prediction of the maximal accumulated strain to be expected for $N \to \infty$ is missing in all presented models.

Another problem is seen in the fact that the characteristics of the applied load cycle are not or not sufficiently captured. Although most of the models presented deal with an amplitude measure to capture different cyclic strain or stress levels, respectively, the shape of the strain loop and its polarisation are not taken into account. Wichtmann (2005) emphasises the importance of these parameters on the rate of strain accumulation. Without taking into account the characteristics of the load cycle, the application of the model is always limited to the respective problem it is developed for. Special effects are captured only indirectly in the model parameters. They can not be taken into account uniquely and separately, though.

Some models use the residual strain of a certain cycle as input parameter. It is already stated earlier that this is an infelicitous choice since reconstituted samples tested in laboratory are assumed to be virgin. That is, the definition of such a parameter in reality in fact is impossible. The consideration of the historiotropy is, however, of essential importance for correct prediction of strain accumulation in the field. Even if one can predict the evolution of strain accumulation correctly from the virgin state of the soil until the final accumulation is reached, this is useless without detailed knowledge on the historiotropy of the soil in reality. Only the accurate determination at which point of the accumulation curve the soil is at the beginning of the cyclic loading will lead to reliable prediction of the accumulation to be expected.

Stiffening effects during cyclic loading due to void ratio changes and strain redistributions are included in none of the models. The mentioned problems will be discussed in more detail in section 4.3.4. Prior the so called Bochum accumulation model is presented. This model is discussed in more detail since it is aware of most of the above-quoted difficulties and proposes some solutions.

4.3 Bochum accumulation model

4.3.1 History of the Bochum accumulation model

The Bochum accumulation model (BAM) is developed at the Ruhr University of Bochum since 1999 on the basis of numerous laboratory test results and originated from the model of Sawicki & Swidzinski (1987 and 1989), outlined in section 4.2.2. Within several years of experimental and theoretical work, a hypoplastic flow rule was introduced, the historiotropic variable $\tilde{N}$ proposed by Sawicki & Swidsinski (1987 and 1989) was replaced by a new formulation and several additional influencing parameters as average stress and void ratio were considered. Later a multiplicative approach was introduced to consider different influence parameters and replaced the original function (4.8).

Proposals to capture multidimensional strain loops are made and several ideas to consider the strain amplitude ε^{ampl} are presented. The model is modified and improved continuously and validated by many different laboratory as well as field tests. Many publications are available on the elements of the model, related experimental studies and proposed applications (Niemunis, 2003; Niemunis et al., 2003; Triantafyllidis et al., 2003; Niemunis et al., 2004; Wichtmann et al., 2004a,b; Niemunis et al., 2005; Wichtmann, 2005; Wichtmann et al., 2005a,b; Heibrock et al., 2006; Wichtmann et al., 2007a,b).

Many influence parameters are investigated and captured in the Bochum accumulation model. Most of the material parameters can be determined by existing laboratory tests. A wide range of applications is possible due to the general formulation of the equations. Although many effects are captured and the range of application is very wide, some shortcomings are detected also in this model, though (see section 4.3.4).

Despite of these deficiencies the model is seen as a good first approach for the formulation of a model predicting the settlement of granular soil due to low level vibrations. Thus the Bochum accumulation model is discussed in more detail in the following. The essential parameters are explained and the main equations are given. In a latter section further needs and shortcomings are discussed.

4.3.2 General approach

The Bochum accumulation model is similar to a creep law but instead of the time t the number of cycles N is used. The logarithmical formulation of equation (4.8) was originally used and later modified by adding another factor (see section 4.3.3). N is considered as a continuous variable, thus the material rate of a state variable Γ is $\dot{\Gamma} = d\Gamma / dN$. A representative cycle is calculated incrementally in order to determine the strain amplitude ε^{ampl} from the strain path during this cycle using an advanced hysteretic constitutive law. The strain amplitude is the basic parameter of the accumulation model. Using this reference value for a certain number of cycles a corresponding irreversible strain is calculated. After several hundreds of cycles an incremental calculation of the hysteresis loop can be inserted as control cycle in order to consider changes in the elastic material behaviour due to void ratio changes or stress redistributions.

The general approach can be described as follows.

1. The initial state of stress is calculated, taking into account self weight and all static loads.
2. The first cycle is calculated incrementally using an adequate hysteretic model. The resilient part of the deformation is calculated in order to estimate the strain amplitude.
3. The strain amplitude ε^{ampl} (see Figure 4.1-1) is estimated using the calculated strain path. The amplitude is assumed to remain constant over a number of following cycles.
4. The strain accumulation rate $\dot{\varepsilon}^{acc}$ is calculated using the formulation of the accumulation model.
5. The stress increment $\Delta\sigma_{ij} = \dot{\sigma}_{ij}\Delta N$ due to a series of cycles is calculated.

A FE-program redistributes stress in the course of equilibrium iteration resulting in settlements or pseudo-relaxation – depending on the boundary value problem. The calculation should be interrupted occasionally by control cycles to check the admissibility of the stress state after several hundreds of cycles and, if necessary, to modify the strain amplitude ε^{ampl} (which may change due to a redistribution of stress or a change in the elastic properties of the soil due to changes in the void ratio). Since the model incorporates elements of hysteretic as well as accumulation models the

originators also call their model to be a *semi-explicit* approach, based on the terminology described in section 4.1.2.

The general stress-strain relation for the Bochum accumulation model is given as

$$\dot{\sigma}_{ij} = E_{ijkl}\left(\dot{\varepsilon}_{kl} - \dot{\varepsilon}_{kl}^{acc}\right). \tag{4.17}$$

Therein E_{ijkl} denotes the elastic stiffness at the average stress σ_{ij}^{av} (defined below). With respect to the numerical implementation of the model the mechanical sign convention is used, i.e. compression is considered as a negative quantity. The rate of strain accumulation for a given strain amplitude and at a given average stress σ_{ij}^{av} is approximated as

$$\dot{\varepsilon}_{kl}^{acc} = f_{ampl} f_p f_Y f_e f_\pi \dot{f}_N m_{kl} \tag{4.18}$$

with the unit tensor m_{kl} in the direction of strain accumulation. The intensity of strain accumulation is given by $\dot{\varepsilon}^{acc} = \left\|\dot{\varepsilon}_{kl}^{acc}\right\|$. Therewith the scalar value $\dot{\varepsilon}^{acc} = f_{ampl} f_p f_Y f_e f_\pi \dot{f}_N$. $\dot{\varepsilon}^{acc}$ is defined by the functions f_i describing the influence of different parameters as strain amplitude ε^{ampl}, average effective mean stress p^{av}, average stress ratio $\bar{Y}^{av}$, void ratio e, cyclic loading history π and the number of load cycles N. These functions are derived on the basis of cyclic triaxial tests and other laboratory investigations and are discussed in detail in section 4.3.3.

In the model one *cycle* is understood as a repeatable sequence of states recorded during the application and removal of a single load or a group of loads. Plotting Γ, possibly a tensorial variable like σ_{ij}, upon a cycle its average value is defined as $\Gamma^{av} = 1/2\left(\Gamma^{(1)} + \Gamma^{(2)}\right)$ choosing the pair $(1,2)$ of instantaneous values in such way that their distance reaches a maximum, $\left\|\Gamma^{(1)} - \Gamma^{(2)}\right\| = \max\left\|\Gamma^{(i)} - \Gamma^{(j)}\right\|$. That is, Γ^{av} is the centre of the smallest 'sphere' that encompasses all states Γ of a given cycle or event. In general Γ^{av} will coincide with the static state of stress, assuming fully elastic material behaviour during application of the load cycle. The scalar amplitude is defined as $\Gamma^{ampl} = \max\left\|\Gamma - \Gamma^{av}\right\|$. It turned out that this definition of Γ^{ampl} is insufficient especially for complicated strain cycles as will be shown in section 4.3.4.

The unspecified term *accumulation* is a convenient notion expressing both cyclic pseudo-relaxation and cyclic pseudo-creep. They are

just different manifestations of the same physical phenomenon. Cyclic pseudo-creep is observed when stress cycles are applied, whereas cyclic pseudo-relaxation is observed when strain cycles are applied. Accordingly the term accumulation is used independently of its appearance, i.e. independently of the technical aspect if strains or stresses are applied.

4.3.3 Elements of the model

Direction of accumulation

As outlined in section 2.5.4 the direction of accumulation is determined by the state of stress. A borderline in the *p*-*q*-plane, separating the contractive (average stress below the borderline) and the dilative (average stress above the borderline) material behaviour, was found by Lung (1982) to be identical with the critical state line (CSL). The CSL is the line that represents the failure state of the soil in the *p*-*q*-plane (Budhu, 2000). For average states of stress laying at the CSL no accumulation of volumetric strains is observed.

Chang & Whitman (1988) observed that the strain ratio ω, equation (3.30), increases with increasing average stress ratios η, equation (3.15). Further on they found good agreement of the direction of accumulation with the flow rule of the modified Cam Clay model. Neither an influence of the effective mean pressure p nor of the cyclic stress amplitude on the direction of accumulation is reported. A possible description of the influence of η on the direction of accumulation with the modified Cam Clay model could be confirmed by Wichtmann (2005).

The application of the hypoplastic model of Niemunis (2003) showed comparable good approximation. This hypoplastic flow rule is used in the Bochum accumulation model for description of the direction of accumulation m_{ij},

$$m_{ij} = \frac{M_{ij}}{\left\| M_{ij} \right\|} \tag{4.19}$$

That is, the average stress σ_{ij}^{av} alone dictates the direction of accumulation, whereby

$$M_{ij} = -\left[\left(\frac{F}{a} \right)^2 \left(\hat{\sigma}_{ij} + \hat{s}_{ij} \right) + \left(\hat{\sigma}_{ij} \hat{\sigma}_{ij} \right) \hat{s}_{ij} - \hat{\sigma}_{ij} \left(\hat{\sigma}_{ij} \hat{s}_{ij} \right) \right]. \tag{4.20}$$

In equation (4.20) $\hat{\sigma}_{ij}$ is the normalised stress tensor $\hat{\sigma}_{ij} = \sigma_{ij} / I_1$ (with I_1 being the first invariant of σ_{ij}, equation (3.5)) and $\hat{s}_{ij}$ is the deviatoric part of the normalised stress tensor $\hat{s}_{ij} = \hat{\sigma}_{ij} - 1/3\hat{\sigma}_{ii}\delta_{ij}$, wherein δ_{ij} corresponds to the Kronecker's symbol, equation (3.4). The parameters *F* and *a* are defined by

$$a = \frac{\sqrt{3}\left(3 - \sin\varphi_c\right)}{2\sqrt{2}\sin\varphi_c} \tag{4.21}$$

and

$$F = \sqrt{\frac{1}{8}\tan^2\Psi + \frac{2 - \tan^2\Psi}{2 + \sqrt{2}\tan\Psi\cos 3\theta}} - \frac{1}{2\sqrt{2}}\tan\Psi \tag{4.22}$$

with φ_c being the critical angle of friction,

$$\tan\Psi = \sqrt{3}\left\|\hat{s}_{ij}\right\| \tag{4.23}$$

and $\cos 3\theta$ the cosine of the Lode angle, equation (3.13).

Strain amplitude

The strain amplitude is related to the accumulation rate using a quadratic relation $\dot{\varepsilon}^{acc} \sim \left(\varepsilon^{ampl}\right)^2$. Only small amplitudes were investigated, thus

$$f_{ampl} = \begin{cases} \left(\dfrac{\varepsilon^{ampl}}{\varepsilon^{ampl}_{ref}}\right)^2 & \text{for} \quad \varepsilon^{ampl} \le 10^{-3} \\ 100 & \text{for} \quad \varepsilon^{ampl} > 10^{-3} \end{cases} \tag{4.24}$$

with $\varepsilon^{ampl}_{ref} = 10^{-4}$. It is obvious that for larger deformations the model becomes quite arbitrarily and needs further investigation (see also remarks in section 4.3.4).

For small deformations, however, the model tries to include not only the strain amplitude, but also the shape of the strain loop and its polarisation, introducing a tensorial definition of the strain amplitude A^{ε}_{ijkl}, in general a fourth-order tensor. The scalar measure

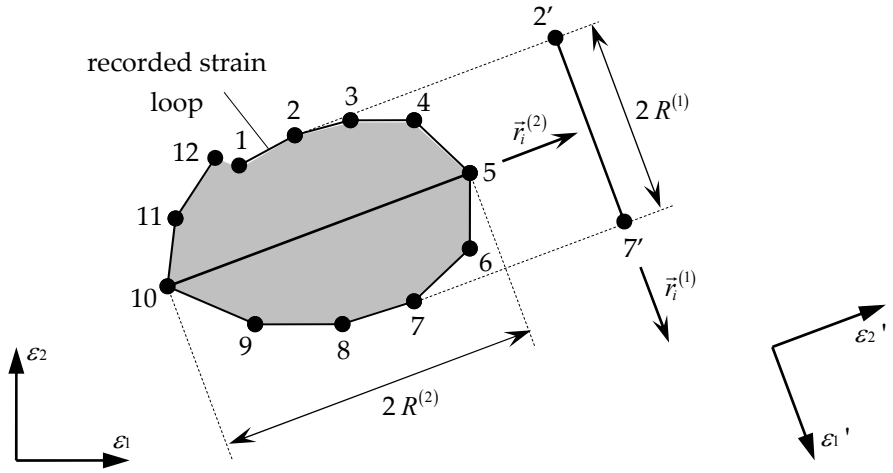

Figure 4.3-1: Strain amplitude A^{ε}_{ijkl} for the two-dimensional case: determination of $R^{(1)}$ and $R^{(2)}$ from projection of the loop (after Wichtmann, 2005*)*

$$\varepsilon^{ampl} = \left\| A^{\varepsilon}_{ijkl} \right\| \tag{4.25}$$

enters the amplitude function (4.24). The polarisation of the strain amplitude is described with the unit tensor $\vec{A}^{\varepsilon}_{ijkl} = A^{\varepsilon}_{ijkl} / \left\| A^{\varepsilon}_{ijkl} \right\|$.

According to Wichtmann (2005) the rate of accumulation is not influenced by the polarisation of the strain loop and therewith independent from the coordinate system. That is, for example in the two-dimensional case instead of the reference coordinate system $\varepsilon_1 - \varepsilon_2$ also the rotated $\varepsilon_1' - \varepsilon_2'$ coordinate system can be used (see Figure 4.3-1). In this case A^{ε}_{ijkl} can be simplified to a second-order tensor, defined by the directions $\vec{r}_i^{(1)}$ and $\vec{r}_i^{(2)}$ and the amplitudes $R^{(1)}$ and $R^{(2)}$ by

$$\begin{aligned} A^{\varepsilon}_{kl} &= \sum_{i=1}^{2} R^{(i)} \vec{r}_k^{(1)} \vec{r}_l^{(1)} \\ &= R^{(1)} \vec{r}_k^{(1)} \vec{r}_l^{(1)} + R^{(2)} \vec{r}_k^{(2)} \vec{r}_l^{(2)} \end{aligned} \quad . \tag{4.26}$$

Using unit vectors $\vec{r}_i^{(1)} = \begin{pmatrix} 1 & 0 \end{pmatrix}^{\mathrm{T}}$ and $\vec{r}_i^{(2)} = \begin{pmatrix} 0 & 1 \end{pmatrix}^{\mathrm{T}}$ defining the orientation of the strain loop as presented in Figure 4.3-1 the tensorial definition of the strain amplitude becomes

$$A_{kl}^{\varepsilon} = \begin{pmatrix} R^{(1)} & 0 \\ 0 & R^{(2)} \end{pmatrix}. \tag{4.27}$$

Referring to equation (4.25) the scalar measure is

$$\varepsilon^{ampl} = \left\| A_{kl}^{\varepsilon} \right\| = \sqrt{\left(R^{(1)}\right)^2 + \left(R^{(2)}\right)^2}\ . \tag{4.28}$$

For the special case of one-dimensional axial cycles $R^{(2)} = R$ and $R^{(1)} = 0$. Then $\varepsilon^{ampl} = R$, corresponding to the classical definition of the amplitude. For further details on the definition of the strain amplitude is referred to Wichtmann (2005).

Average mean effective stress

The average effective mean stress p^{av} has major influence on the intensity of accumulation. Decreasing p^{av} causes significant increase of accumulated strain. This dependency occurred to be stronger at large numbers of cycles. The corresponding function f_p is proposed as

$$f_p = \exp\left[-C_p \left(\frac{p^{av}}{p_{atm}} - 1 \right) \right]. \tag{4.29}$$

Therein the atmospheric pressure $p_{atm} = -100kPa$ is used as a reference for which $f_p = 1$ holds. Although the model parameter C_p was found to be slightly influenced by the number of cycles, it is assumed as a constant to minimize the number of variables. C_p is found to be rather independent of the stress ratio $\eta^{av} = q^{av} / p^{av}$. Equation (4.29) is applicable for both, cyclic compression ($\eta^{av} \geq 0$) and cyclic extension ($\eta^{av} < 0$).

Average stress ratio

The rate of accumulation strongly increases with the stress ratio η^{av}, especially close to the critical state line. Below this limit the function f_Y is given by

$$f_Y = \exp\left(C_Y \overline{Y}^{av} \right). \tag{4.30}$$

It should be noted that functions f_p and f_Y are treated as uncoupled functions. The model parameter C_Y is found to be rather independent of the number of cycles. For isotropic stress conditions , i.e. $\bar{Y}^{av} = 0$, $f_Y = 1$ holds. The average stress ratio $\bar{Y}^{av}$ in (4.30) bases on the following relations:

$$\bar{Y} = \frac{Y - 9}{Y_c - 9} \tag{4.31}$$

with

$$Y = -\frac{I_1 I_2}{I_3} \quad \text{and} \quad Y_c = \frac{9 - \sin^2 \varphi_c}{1 - \sin^2 \varphi_c}. \tag{4.32}$$

Void ratio

Since the stiffness decreases with the void ratio *e*, lower initial densities cause slightly higher strain amplitudes for similar stress conditions. For loose soils the rate of accumulation is high and it reduces the denser the soil is compacted. The relation to describe the cyclic void ratio dependence in the Bochum accumulation model was introduced by Hardin & Black (1966),

$$f_e = \frac{\left(C_e - e\right)^2}{1 + e} \frac{1 + e_{ref}}{\left(C_e - e_{ref}\right)^2}. \tag{4.33}$$

Number of cycles

The accumulated strain in relation to the applied number of cycles was investigated by laboratory tests for a range from zero to 100,000 cycles. In this range the accumulated strain grew faster than the logarithm of the number of cycles. For constant strain amplitude the calculation of the accumulated strain thus consists of a logarithmic part ($\varepsilon^{acc\ A}$) and a linear one ($\varepsilon^{acc\ B}$),

$$\begin{aligned} \varepsilon^{acc}(N) &\sim C_{N1}\left[\ln\left(1 + C_{N2} N\right) + C_{N3} N\right] \\ &= \underbrace{C_{N1} \ln\left(1 + C_{N2} N\right)}_{\varepsilon^{acc\ A}} + \underbrace{C_{N1} C_{N3} N}_{\varepsilon^{acc\ B}}. \end{aligned} \tag{4.34}$$

Therewith function f_N is determined,

$$f_N = C_{N1} \ln\left(1 + C_{N2} N\right) + C_{N1} C_{N3} N \,. \tag{4.35}$$

Sometimes the rate form $\dot{f}_N = \mathrm{d}\, f_N / \mathrm{d}\, N$ is used,

$$\dot{f}_N = \underbrace{\frac{C_{N1} C_{N2}}{1 + C_{N2} N}}_{\dot{f}_N^A} + \underbrace{C_{N1} C_{N3}}_{\dot{f}_N^B} \tag{4.36}$$

Back polarisation

Wichtmann et al. (2004b) observed significant temporary increase of the rate of accumulation as the polarisation of the strain amplitude changed during cyclic loading. A change in polarisation causes an immediate increase of accumulation, decaying with the numbers of cycles applied after the polarisation change. A so called *back polarisation tensor* π_{ijkl} was introduced to take into account this effect in

$$f_\pi = 1 + C_{\pi 1}(1 - \cos\alpha) \tag{4.37}$$

with α being the angle between two subsequent packages of cycles "a" and "b" described by the amplitudes $A_{ijkl}^{\varepsilon(a)}$ and $A_{ijkl}^{\varepsilon(b)}$ and the polarisations $\vec{A}_{ijkl}^{\varepsilon(a)}$ and $\vec{A}_{ijkl}^{\varepsilon(b)}$. Then

$$\cos\alpha = \pi_{ijkl} \vec{A}_{ijkl}^{\varepsilon(b)} \tag{4.38}$$

where $\pi_{ijkl} = \vec{A}_{ijkl}^{\varepsilon(a)}$ at the beginning of package "b". The decay of f_π during the application of package "b" is described by an asymptotic adaptation of π_{ijkl} with N to the new polarisation $\vec{A}_{ijkl}^{\varepsilon(b)}$. The evolution of angle α is proposed to be

$$\dot{\alpha} = -C_{\pi 2} \alpha \left(\varepsilon^{ampl}\right)^2 . \tag{4.39}$$

The maximal change in the rate of accumulation is achieved when packages "a" and "b" are applied rectangular to each other. Then initially $\cos\alpha = 0$ and therewith $f_\pi = 1 + C_{\pi 1}$, that is, the original rate of accumulation is increased by factor $1 + C_{\pi 1}$. The minimum change in the rate of accumulation is achieved when there is no change in polarisation. Then

$\cos\alpha = 1$ and therewith $f_\pi = 1$, that is, no change in the rate of accumulation takes place. For more information on function f_π is referred to Niemunis et al. (2004) and Wichtmann (2005), respectively.

Historiotropy

Initially the strain accumulation rate was defined as given in equation (4.18). In this formulation only the function f_N represents the historiotropy of the cyclic loading. The number of cycles N alone, however, is not a suitable state variable for the loading history since it contains no information on the intensity of the cycles in the past. E.g. a very large number of cycles with evanescent amplitude will most probably not influence the accumulation during a subsequent package with larger amplitudes. Since the number of cycles is counted independently of the amplitudes of the cycles in equation (4.35), the first package has a large impact on the accumulation during the second package, though.

To avoid that problem, a phenomenological description of the historiotropy by a scalar variable is introduced. This variable weights the number of cycles with their amplitude. Only the N-dependent portion $\dot{f}_N^A$ of the accumulation rate is taken into account in the formulation of the state variable g^A,

$$g^A = \int f_{ampl}\, \dot{f}_N^A \, \mathrm{d}N \,. \tag{4.40}$$

Replacing N in the term for $\dot{f}_N^A$ in equation (4.36) by g^A one obtains the rate $\dot{f}_N^A$ as a function of g^A,

$$\dot{f}_N^A = C_{N1} C_{N2} \exp\left(-\frac{g_A}{C_{N1} f_{ampl}} \right). \tag{4.41}$$

For the special case $\varepsilon^{ampl} = \text{constant}$ equation (4.41) takes a similar form as the term for $\dot{f}_N^A$ in equation (4.36). The influence of a package of cycles with vanishing amplitudes on a subsequent package with larger amplitudes is small since at the beginning of these cycles g^A is still very small. Several packages of cycles with different amplitudes can be described by equation (4.41).

Summary

The Bochum accumulation model is developed within the past few years. Many parameters are investigated on its influence on strain accumulation in the soil. The corresponding dependencies are captured in the framework of this model using a factorial formulation discussed above. Besides the actual aim of the model, i.e. the prediction of settlements, the huge amount of laboratory test data the model is based on can also provide useful material to evaluate other soil models dealing with strain accumulation under long term cyclic loading (e.g. Suiker, 2002 or the new accumulation model presented in Chapter 5).

Despite of the far developed character of the model, several shortcomings are detected during its study. Further improvement and several changes in the structure of the model are seen as necessary to be able to proper predict accumulated strains and therewith settlements caused by cyclic loading.

4.3.4 Discussion of the Bochum accumulation model

During study of the Bochum accumulation model some major shortcomings are detected. In detail this concerns the definition of the scalar measure of the strain amplitude ε^{ampl}, the constant and cycle-independent factor $\dot{f}_N^B$ in equation (4.36), the definition and determination of the historiotropy g^A, the use of N as a state variable in the formulation of the strain accumulation rate and the use of a hypoplastic flow rule to describe both, volumetric and deviatoric accumulated strains. Also minor remarks e.g. on the influence of polarisation changes and stiffening effects will be presented.

Definition of the strain amplitude

The scalar measure of the strain amplitude ε^{ampl}, defined by equation (4.25), is supposed to characterize the absolute value of the amplitude as well as its shape and polarisation. As described earlier these factors have major influence on the strain accumulation. Although this definition is quite advanced compared to other models, it is still not sufficient to describe complex strain cycles generated e.g. during the passage of a car, construction works or explosion uniquely.

Figure 4.3-1 shows an elliptic shaped strain cycle for the two-dimensional case. For this kind of cycles the proposed definition of ε^{ampl} is quite simple. The maximum dimensions are projected in directions $\vec{r}_i^{(1)}$ and

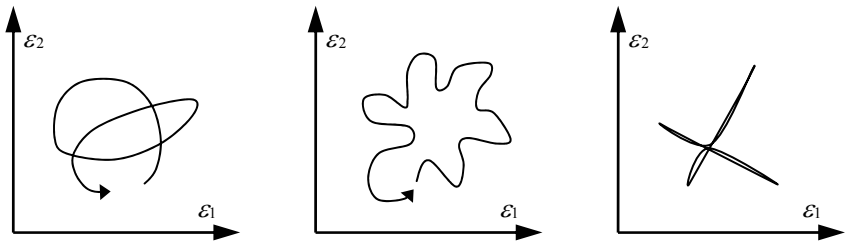

Figure 4.3-2: Different two-dimensional strain cycles not uniquely describable in the Bochum accumulation model

$\vec{r}_i^{(2)}$ to determine the amplitudes $R^{(1)}$ and $R^{(2)}$. A slight variation, however, can cause problems in uniqueness. Figure 4.3-2 shows different possible strain cycles in the $\varepsilon_1 - \varepsilon_2$ space resulting in almost similar amplitudes $R^{(1)}$ and $R^{(2)}$, whereas the resulting accumulation will be different.

The practical relevance of this problem can be seen in Figure 4.3-3. The graphs show strain paths caused by different vibration sources. The corresponding particle motions are recorded in situ. The complex strain paths show very different characteristics. For the Bochum accumulation model, however, a unique scalar value quantifying the applied strain cycle is required as input parameter. A clear definition how to derive this value for ε^{ampl} is missing and difficult, if not impossible, to find.

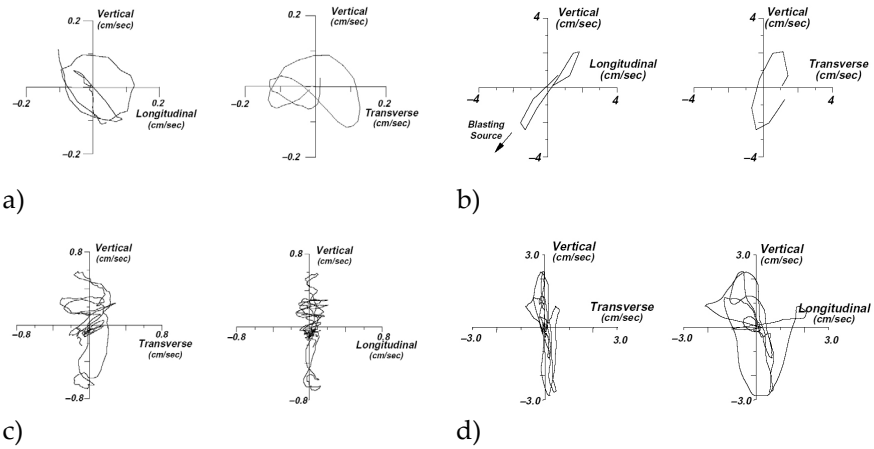

*Figure 4.3-3: Particle motion of a) train, b) in-depth blasting, c) friction pile driving and d) hydraulic compaction induced vibration (*Kim & Lee, 2000*)*

The simplest example can be drawn for the one-dimensional case. A harmonic uniaxial loading as shown in Figure 4.3-4 a) generates a straight line in the one-dimensional ε_1 space (Figure 4.3-4 c)). In this case one cycle is easy to define, clarified by the underlying grey rectangle. A slightly different harmonic loading with varying strain amplitudes as in Figure 4.3-4 b), however, results in a similar line in the ε_1 space. According to equation (4.25) this leads to a similar scalar measure ε^{ampl} as in case a). Therewith the main problem in the definition of ε^{ampl} is illustrated very well.

Although tests of Wichtmann (2005) indicated that Miner's rule applies for one-dimensional cycles, it provides no sufficient solution for the problem. Miner's rule, in a simplified way, says that it does not matter in which order packages of cycles with different strain amplitudes are applied. The total accumulated strain will be the same. This allows for division of a package of cycles N in Figure 4.3-4 b) into sub-packages of cycles N_1, N_2 and N_3 , which are rearranged as shown in Figure 4.3-4 d).

This approach allows for dealing with simple sub-cycles which can be described in a similar way as described in section 4.3.3. Smaller and larger amplitudes can be weighted by the historiotropy state variable g^A. This method, however, applies only for simple, uniaxial cycles. It is not proven,

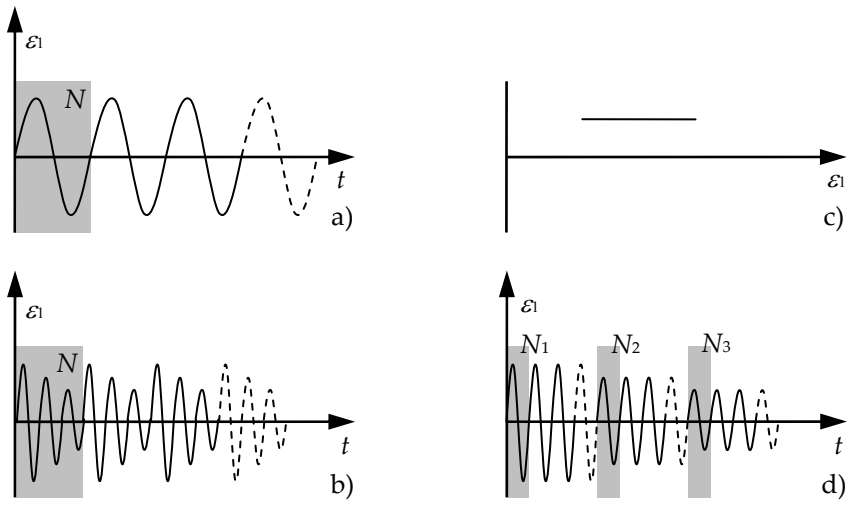

Figure 4.3-4: Dealing with one-dimensional strain cycles in the Bochum accumulation model

that Miner's rule also applies for cycles containing more than one polarisation. For complex cycles in the six-dimensional strain space a strong coupling of the single strain components prohibits the application of Miner's rule as well.

The above statements clearly explain why the chosen definition of the strain amplitude ε^{ampl} is not sufficient for complex cycles observed in reality. A unique and clear correlation between shape, polarisation and absolute amplitude of arbitrary strain cycles is not possible. Thus a different or modified approach is seen as desirable.

Since the function f_{ampl} is only based on tests with low strain amplitudes, a constant scalar of 100 was introduced in equation (4.24). This assumption leads to similar strain accumulation for all $\varepsilon^{ampl} > 10^{-3}$ which is obviously not correct. Further investigation on the evolution of f_{ampl} on larger strain amplitudes is needed. Until then it would be more convenient to say that the model is only applicable to small strain cycles.

Strain amplitude versus stress amplitude as input parameter

The Bochum accumulation model uses the magnitude of a cycle in terms of the strain amplitude ε^{ampl} rather than of the stress amplitude σ^{ampl} for three reasons. Firstly, Niemunis et al. (2005) state that σ^{ampl} does not provide sufficient information about large amplitudes. From σ^{ampl} alone it is not possible to distinguish between cycles which are just touching the yield surface and those which penetrate the plastic region. Although applying similar stress amplitudes the corresponding strain amplitudes are very different, resulting in different accumulation. Secondly, a barotropic dependency would require reformulation of f_p. At $\sigma^{av} = 0$ no stresses can be applied anymore, i.e. σ^{ampl} vanishes. Therewith no accumulation would be predicted in the case of liquefaction.

The previous statements are strong arguments for large deformations. The Bochum accumulation model is calibrated for very small strains, though. Its availability for large strain amplitudes still has to be proven. In the small strain region, however, the above points are of minor importance, significant yielding during one cycle and liquefaction phenomena are not to be expected. The assumption of a linear dynamic (or cyclic) constitutive law seems reasonable. Therewith the question arises if ε^{ampl} is the preferable choice as input parameter for the model.

The use of ε^{ampl} implicates some problems as well. While a correct definition of the specific cyclic amplitude parameter for a certain load cycle remains the same problem for both ε^{ampl} and σ^{ampl}, effects like membrane penetration (discussed by Wichtmann, 2005) and inaccurate measurements of the (very small) cyclic deformations vanish when σ^{ampl} is used as input parameter. Therewith errors and corrections of the strain measurements during one cycle are omitted. Finally, using σ^{ampl}, all input parameters for the accumulation model could be derived from the stress history of the load cycle alone.

Evolution of the accumulated strain with the number of cycles

The tests the Bochum accumulation model is based on indicate over-logarithmic evolution of the accumulated strain with the number of cycles. Thus the constant rate $\dot{f}_N^B = C_{N1} C_{N3}$ is introduced in function $\dot{f}_N$, equation (4.36). The test results this formulation refers to contain 100,000 cycles. In this range the used formulation seems to be appropriate. However, for very large numbers of cycles, that is, several millions of cycles, the influence of $\dot{f}_N^A$ vanishes and only the constant rate of $\dot{f}_N^B$ remains. This leads to continuous accumulation, only influenced by changes in f_e due to the adaptation of the void ratio in accordance to the accumulated volumetric strain ε_{kk}^{acc}. Additionally, stiffening effects can be taken into account by recalculation of ε^{ampl} by aims of control cycles. According to Suiker (2002) this influence vanishes after several hundreds of cycles, when the *conditioning phase* is finished, though.

The model in its current formulation may lead to unrealistic estimations of the maximum accumulated strain. Further investigation of the evolution of strain accumulation after very high numbers of cycles, i.e. several millions, is seen as necessary. In the Bochum accumulation model the maximum strain accumulation in fact is defined more or less arbitrarily via parameter C_e. This value is slightly lower than the minimum void ratio e_{min} and causes f_e to be zero if the current void ratio equals C_e. Therewith accumulation only stops if a certain amount of voids is filled, e.g. by abrasion. However, in reality the soil will adapt to the respective loading and behave truly elastic before the minimum void ratio is achieved.

Therewith an essential shortcoming of the Bochum accumulation model is that no clear criterion is defined when and why the accumulation of strain should stop. Accordingly no prediction on the maximum

accumulated strain to be expected can be made. This problem, however, occurs in all presented accumulation models where in most cases accumulation stops due to a vanishing exponential function. To the author's knowledge, an experimental validation of the point where accumulation stops is not available at this time. Further research should focus on criteria predicting the maximum accumulated strain to be expected due to a certain dynamic impact or cyclic loading. This knowledge would already allow for estimation whether a certain cyclic loading may lead to damages in structures.

Dilatational behaviour

In cyclic triaxial tests of Wichtmann (2005) close to the critical state line dilatational behaviour is observed during the first few hundred load applications. Afterwards, however, this tendency turns back to compressive behaviour and the soil samples are compacted. This phenomenon can be explained with the conditioning phase described by Suiker (2002) during which the soil adapts to the respective loading.

While the Bochum accumulation model well predicts the dilatational tendency, it does not cover the adaptation of the soil to the cyclic load conditions. This leads to wrong predictions of accumulated volumetric strains under average stress conditions close to the critical state line. Figure 4.3-5 shows test results of Wichtmann (2005) in relation to predictions of the Bochum accumulation model. The prediction implies continuous dilatation of the sample while in reality compaction is observed.

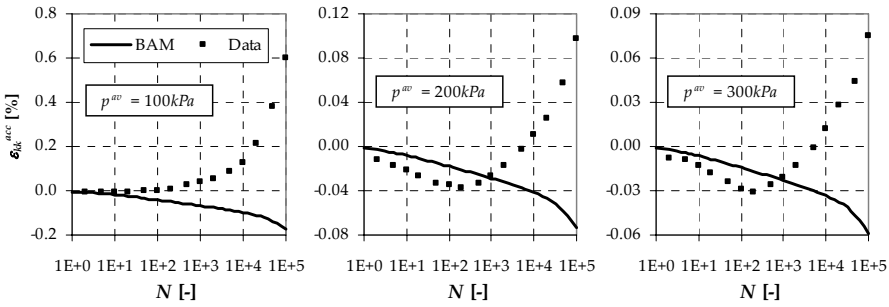

Figure 4.3-5: Dilatational behaviour in tests of Wichtmann (2005) *close to the critical state line – model prediction versus test results.*
All tests: $\eta^{av} = 1.313$, $\zeta = 0.30$, $D_{r0} = 60\%$

Changes in polarisation

Much effort is done in the model to describe changes in polarisation of the strain amplitude, equations (4.37) to (4.39). In laboratory tests a temporary increase of the strain accumulation rate was observed when a change in polarisation was applied after a certain number of cycles with similar polarised amplitudes. In these tests the change in polarisation was maximal, i.e. the subsequent packages of cycles were applied rectangular to each other. After a certain number of cycles (according to Wichtmann et al., 2004b within the following 1000 cycles) with the new polarisation, however, the strain accumulation rate returned to the original level. That is, a single change in polarisation has minor influence on the final accumulated strain when the applied number of cycles is large.

Furthermore in practice such unique sudden changes in polarisation will hardly occur. Natural cycles will either keep their polarisation during a very long period or will change it continuously. For example the direction of a road will not change after 1000 cars passed by. In fact all cars passing the road will generate a (more or less) similar cycle. In a similar way machine foundations will usually be subjected to equal cycles during the whole durability. On the other hand, for example close to a road junction, where many cars are passing in different directions, the changes in polarisation will occur permanently and show stochastic character. It should be noted that for the case of complex cycles a change in polarisation is understood as a change of the orientation of the loop in the strain space. However, during one cycle the polarisation changes continuously as well.

The complexity of calculation in connection with minor importance of f_π for practical applications may lead to the question if the elaborate formulation is needed. The conclusion could be that this influence parameter can be excluded from the model, that is $f_\pi = 1$.

As an alternative, influences of changes in polarisation could be understood as cyclic preloading. Since the historiotropy has to be taken into account anyway in order to predict reasonable accumulation of strain in situ, the influence of changes in polarisation can be captured in the state variable g_0^A. As will be discussed below, g^A is influenced by many parameters which necessarily have to be taken into account for its determination. Thus it must be possible to cover the influence of f_π within the definition of historiotropy as well.

Historiotropy

In the term historiotropy many different influence parameters are summarised. The most important one is the static and dynamic preloading (e.g. Seed et al., 1977) Due to this loading history the soil is densified to a certain void ratio, grains are rearranged (or *conditioned*) in relation to the loading, an interlocking between grains may occur, causing stiffer behaviour under certain loadings. Also anisotropic material behaviour may be initiated by static or dynamic preloading. Additional to these loading caused effects the soil is subjected to aging, i.e. cementation, abrasion, decomposition, etc. (e.g Seed, 1979; Seed et al. 1988), seasonal effects like temperature changes, changes in ground water level or freezing (e.g. Lehane et al., 2004) and biological activity.

The effect of cyclic preloading was also studied by Wichtmann (2005). Laboratory tests showed that cyclic preloading has significant influence on the densification rate in samples with similar density. In these tests samples of different densities were prepared and loaded under identical conditions. A cyclic preloading containing more or less load cycles compacted all samples to a similar density. Then the densification rates were determined during further cyclic loading, see Figure 4.3-6.

Significant different densification rates were observed for different cyclic preloadings. In an ideal model all above mentioned influence parameters should be uniquely related to the expected strain accumulation

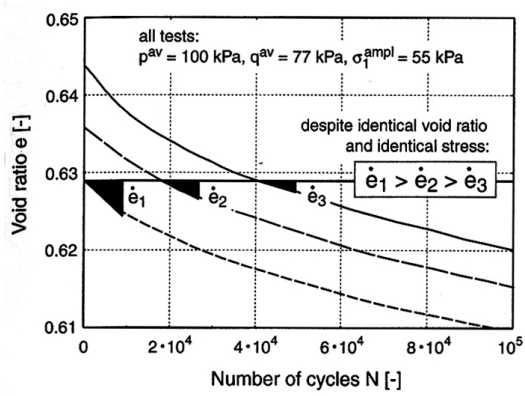

Figure 4.3-6: Influence of the historiotropy on the densification rate $\dot{e}$ *(*Wichtmann, 2005*)*

rate under certain cyclic loading. The determination of historiotropy in situ is very tricky, though. Although some correlations were investigated by Wichtmann (2005), no clear assessment of the state variable g_0^A, representing the state of the soil at the beginning of the cyclic loading to be applied, seems to be possible at this time. Determination of the historiotropy by means of test loadings seems to be possible in a way. During these test loadings, however, the investigated site may be disturbed, leading to wrong results. Also varying soil characteristics hardly can be taken into account. The finally proposed correlation between liquefaction resistance and loading history appears quite vague as well (Triantafyllidis et al., 2004).

Most promising seems a correlation of dynamic properties with the historiotropy. Although Wichtmann (2005) states this relation as disproved further investigation in this field is recommended. Only laboratory tests with measurements of p- and s-wave velocities in axial direction of the sample were carried out in this study. In that way generated anisotropy may remain undetected. Considering anisotropic material behaviour in the dynamic investigations may result in different findings. Further on seismic field investigations are seen as a desirable complement in relating dynamic soil properties to the historiotropy of the soil.

Figure 4.3-7 illustrates the importance of correct determination of g_0^A. Wrong initial assumptions will lead to completely different predictions.

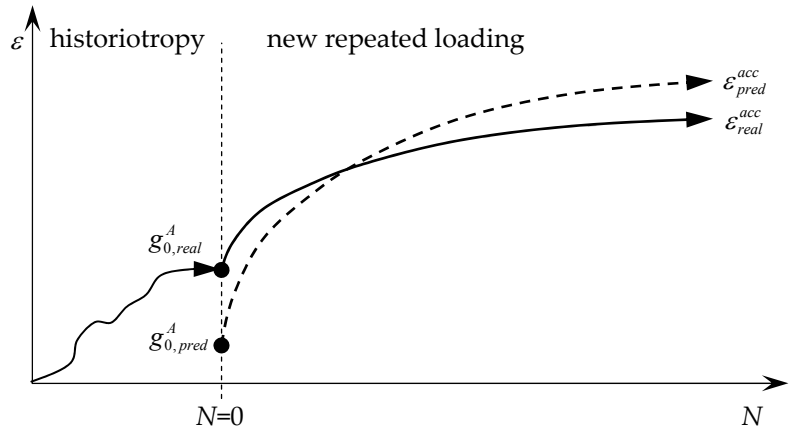

Figure 4.3-7: Sketch of the influence of the determination of historiotropy g_0^A on the prediction of strain accumulation

In the example the predicted accumulation rate is higher than the one in reality. Of course the opposite scenario is possible as well, that is the predicted values will be lower than in reality. An exact determination of the initial point of the accumulation curve, i.e. the initial state of the soil, is thus of crucial importance for all settlement predictions.

Use of *N* as a state variable in the accumulation rate

Equation (4.36) uses, similar to most of the presented accumulation models, N for description of the strain accumulation rate $\dot{\varepsilon}^{acc}$. This is seen as problematic, since the current state of a soil at any time hardly can be expressed in terms of the already applied cycles. The choice of state variable g^A takes this into account. The physical meaning of this definition is that the rate of accumulation only depends on three factors: the *current* static state of stress, the *current* state of the soil and the characteristics of the applied load cycle. The definition of an N-independent formulation for the strain accumulation rate thus is seen as an essential component of an advanced accumulation model.

Use of a hypoplastic flow rule for description of the direction of accumulation

The use of a hypoplastic flow rule for description of the direction of accumulation seems quite reasonable on the basis of achieved test results in the framework of the development of the Bochum accumulation model. This assumption is supported by the fact that Chang & Whitman (1988) already used a modified cam clay model as flow rule for predicting the direction of strain accumulation in the form $\omega = \kappa^{acc} / \varepsilon_{kk}^{acc} = \left(M_c^2 - \left(\eta^{av} \right)^2 \right) / \left(2\eta^{av} \right)$. The hypoplastic flow rule (or any other complex plastic flow rule), however, is just a model to describe the behaviour of soil. It does not necessarily apply for – possibly preloaded and aged – in-situ soils. Furthermore only few types of sands are investigated in the testing program. Finally the conclusion that a hypoplastic flow rule generally can be used for description of the direction of accumulation for any granular soil at any state appears quite hazardously. In fact, this assumption disentitles the model to be general. Using two separate equations for the description of volumetric and deviatoric accumulated strain rates, $\dot{\kappa}^{acc}$ and $\dot{\varepsilon}_{kk}^{acc}$, with different sets of parameters as in the models of Marr & Christian (1981) and Bouckovalas et al. (1984), allows for more freedom in the model. Hypoplastic behaviour of the soil then still can easily be modelled by coupling both, deviatoric and

volumetric strains accordant to this constitutive law as will be further discussed in section 5.5.

Loading frequency

The influence of the loading frequency on strain accumulation is not fully discussed by Wichtmann (2005). Indeed tests in a range of 0.05 to 2*Hz* were performed where no influence of the loading frequency was observed. Higher frequencies, however, are not investigated. A possible stiffer behaviour due to activation of inertia forces therewith is not considered. This stiffer behaviour may lead to a reduction of strain accumulation. On the other hand very high loading frequencies may lead to partially undrained loading conditions since the permeability of the soil does not allow for drainage during the short loading period. A potential increase of pore water pressure would lead to decreasing effective stresses, including possible liquefaction risks, and therewith higher accumulation of strain. Unfortunately the experimental investigation of these effects is quite difficult since the application of high loading frequencies is very tricky and thus could not be investigated exhaustively in the current work neither, see also remarks in section 6.3.2. The independency of the intensity of strain accumulation from the loading frequency, however, could be confirmed up to a loading frequency of 10*Hz* in own experimental investigations, further discussed in section 7.3.3.

Application of a multiplicative approach

Despite several advantages as simple formulation of the influence of certain parameters, easy consideration of new influence parameters, good physical interpretability and a scalar value as effective accumulated strain ε^{acc}, the application of the proposed multiplicative approach with many factors is seen as problematic. Since all parameter functions f_i are fits to test results, they all include errors from measurements and curve fittings. In the end each of the functions is a good approach to describe the influence of the respective parameter. Since it is just an approach, though, each function generates errors when used for prediction. The multiplicative approach multiplies not only the predicted effect of the respective parameters but also the corresponding errors. In that way errors sum up with each additional function incorporated in a prediction.

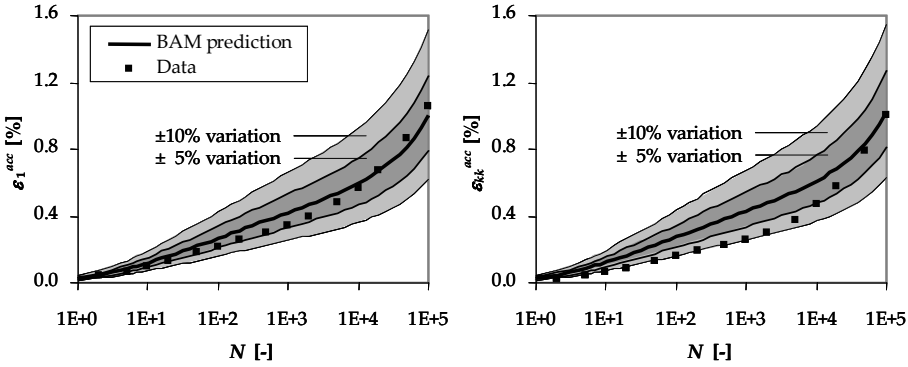

Figure 4.3-8: Example for the variation of predicted accumulated strains due to summing up of errors in the functions f_i

Assuming an average error of ±5% in each function f_i compared to reality leads to a total variation of about ±25% in the prediction. Increasing the average error to ±10% in each function f_i, which is still a fairly good agreement of model and reality, leads to a total variation of about ±50% in the prediction. This means that the span in which the prediction may vary considerably exceeds the total value of accumulated strain to be expected. Thereby the scenario with the highest predicted accumulation is as probable as the scenario with the lowest predicted accumulation. As a result a prediction with the multiplicative approach of the BAM may loose its quality although many influence parameters are taken into account to a very good approach. Figure 4.3-8 exemplarily illustrates this problem for a test of Wichtmann (2005) at $p^{av} = 200kPa$, $\eta^{av} = 0.5$ and D_{r0}=59.75%.

Influence of the saturation degree

The Bochum accumulation model does not take into account the degree of saturation. Wichtmann et al. (2005a) state no significant difference in tests on dry versus fully saturated samples. Tests on partially saturated samples, however, are not presented. Werkmeister (2003) contradicts the statement of Wichtmann and describes a significant influence of the water content on the strain accumulation behaviour of unbound granular layers. Thereafter a water film on the surface of the grains influences the shear resistance of the soil. The occurrence of a moderate amount of moisture benefits the strength of unbound granular media. On the other hand, in totally saturated samples dynamic loading may lead to pore water pressure increase which again

causes a decreasing effective stress that weakens the sample. The latter effect, of course, is only of importance for undrained or partially drained conditions. The Bochum accumulation model is based on drained tests. Further investigation of accumulation behaviour at different saturation degrees, however, is desirable.

4.4 The cyclic densification model of Suiker (2002)

4.4.1 General approach of the Suiker model

Suiker (2002) uses a different, more 'mechanical' and less empirical, approach for the description of long term cyclic densification, basing on a concept used in the modelling of metal fatigue. Accordingly, Suiker (2002) applies the continuum mechanical sign convention as well. The model is developed for prediction of railway track deterioration due to repeated passages of high-speed trains. In general, from the permanent deformation behaviour of the granular non-cohesive medium, namely ballast and sub-ballast of the railway track, two important mechanisms are discerned: *frictional sliding* and *volumetric compaction* of particles. Both deformation mechanisms are assumed as being of plastic nature. That is, they are activated when a certain stress level is exceeded and their magnitude remains constant as soon as unloading occurs. The model is derived using the classical plasticity framework. The permanent deformation generated per cycle follows a so called 'overstress formulation', applied to both frictional sliding and volumetric compaction, by incorporating a Drucker-Prager cone that is limited in direction of the hydrostatic axis by a compression cap. The corresponding flow directions are related to plastic potentials of a similar form. The reversible material behaviour is expressed by a pressure-dependent hypo-elastic model, representing the increase in elastic stiffness under increasing pressure. Since this approach is seen as a considerable alternative to the previously discussed accumulation models, the general frame is outlined in the following. The adjacent discussion emphasises advantages and limitations of the Suiker model.

4.4.2 Classical plasticity theory and response envelope under cyclic loading

Suiker (2002) uses the mechanical sign convention with tensile stresses being positive. This choice has been made, since the model originates from the structural mechanics and is implemented in a general-purpose finite element program.

Classical plasticity theory

In the classical plasticity theory the actual state of a material is dependent on its deformation history, measured by the irreversible deformation component. Suiker (2002) uses a linear isotropic deformation theory, where the (irreversible) plastic strain ε_{kl}^{p} and the (reversible) elastic strain ε_{kl}^{e} comply with the additive strain decomposition

$$\varepsilon_{kl} = \varepsilon_{kl}^{e} + \varepsilon_{kl}^{p}, \tag{4.42}$$

where ε_{kl} is the total strain. The elastic strain is related to the stress σ_{ij} by equation (3.32). Substitution of equation (4.42) into (3.32) leads to

$$\sigma_{ij} = D_{ijkl}\left(\varepsilon_{kl} - \varepsilon_{kl}^{p}\right) \tag{4.43}$$

or, alternatively, to

$$\varepsilon_{ij} = C_{ijkl}\sigma_{kl} + \varepsilon_{ij}^{p}, \tag{4.44}$$

where the elastic compliance tensor C_{ijkl} is the inverse of D_{ijkl}, i.e. $C = D^{-1}$.

Activation and evolution of plastic deformations are controlled by means of a yield function. If both the initial boundary of the elastic domain and the history formulation are isotropic, an isotropic yield function of the form

$$f\left(\bar{\sigma}, \bar{\varepsilon}^{p}\right) = \bar{\sigma} - H\left(\bar{\varepsilon}^{p}\right) \tag{4.45}$$

can be used. The history parameter is chosen to be equal to the accumulated plastic strain, represented by the effective strain measure $\bar{\varepsilon}^{p}$ in equation (4.45), defined as

$$\bar{\varepsilon}^{p} = \int_{0}^{t} \mathrm{I}\left(\dot{\varepsilon}_{ij}^{p}\right) \mathrm{d}\tau \,, \tag{4.46}$$

with I being an appropriate tensorial invariant and t the actual time. The superimposed dot denotes the time derivative. $H\left(\bar{\varepsilon}^{p}\right)$ designates the strength as a function of the history parameter and $\bar{\sigma}$ is an effective stress measure, given by

$$\bar{\sigma} = J\left(\sigma_{ij}\right), \tag{4.47}$$

with J a tensorial invariant. In accordance with the plastic flow theory, the evolution of stress and strain is monitored by the rate-format of equation (4.43),

$$\dot{\sigma}_{ij} = D_{ijkl}\left(\dot{\varepsilon}_{kl} - \dot{\varepsilon}_{kl}^{p}\right). \tag{4.48}$$

Plastic strains can arise when the yield function (4.45) becomes zero, that is, the yield condition

$$\bar{\sigma} = H\left(\bar{\varepsilon}^{p}\right) \tag{4.49}$$

must be fulfilled. Since the applied stress can not exceed the material strength, the yield function may not become larger than zero. The magnitude of the plastic strain rate tensor is prescribed by the flow rule

$$\dot{\varepsilon}_{ij}^{p} = \dot{\bar{\varepsilon}}^{p} m_{ij} \,, \tag{4.50}$$

wherein the second-order tensor m_{ij} denotes the flow direction. The plastic flow formalism of equation (4.48) can be reformulated as

$$\dot{\sigma}_{ij} = D_{ijkl}\left(\dot{\varepsilon}_{kl} - \dot{\bar{\varepsilon}}^{p} m_{kl}\right). \tag{4.51}$$

Response envelope under cyclic loading

Basing on the above outlined plasticity framework, Suiker (2002) derives a constitutive model capturing the envelope of the plastic response under cyclic loading. Starting from the inverse form of the yield condition (4.49),

$$\bar{\varepsilon}^{p} = H_{*}\left(\bar{\sigma}\right), \tag{4.52}$$

with $H_{*} = H^{-1}$, the rate of the plastic strain invariant $\dot{\bar{\varepsilon}}^{p}$ is derived by taking the time derivative of equation (4.52).

With the help of a coordinate transformation for the proportional cyclic loading process from the time scale to a stress based formulation, the permanent strain increment $\Delta\bar{\varepsilon}^{p}$ can be written as

$$\Delta\bar{\varepsilon}^{p} = \int_{h_{sh}}^{\bar{\sigma}_{cyc}} \frac{H_{*}\left(\bar{\sigma}\right)}{\mathrm{d}\,\bar{\sigma}}\,\mathrm{d}\,\bar{\sigma}\,, \tag{4.53}$$

where $\bar{\sigma}_{cyc}$ is the amplitude of the cyclic loading and h_{sh} is the *shakedown level*, below which no plastic strain is generated. From equation (4.53) the plastic strain increment $\Delta\bar{\varepsilon}^{p}_{\Delta N}$ generated during a number of load cycles ΔN can be calculated by solving the integral expression. It follows

$$\frac{\Delta\bar{\varepsilon}^{p}_{\Delta N}}{\Delta N} = H_{*}\left(\bar{\sigma}_{cyc}\right) - H_{*}\left(h_{sh}\right). \tag{4.54}$$

Assuming the cyclic loading as a continuous process allows for taking the limit of equation (4.54),

$$\frac{\mathrm{d}\,\bar{\varepsilon}^{p}}{\mathrm{d}\,N} = H_{*}\left(\bar{\sigma}_{cyc}\right) - H_{*}\left(h_{sh}\left(\bar{\varepsilon}^{p}\right)\right). \tag{4.55}$$

During cyclic loading above the shakedown level, the internal structure of the soil is exposed to changes. These changes may cause the shakedown level to evolve. Therefor h_{sh} is made dependent on the history parameter $\bar{\varepsilon}^{p}$ in equation (4.55). Equation (4.55) only applies for cyclic stress levels $\bar{\sigma}_{cyc}$ above the shakedown level, that is, if $H_{*}\left(\bar{\sigma}_{cyc}\right) - H_{*}\left(h_{sh}\left(\bar{\varepsilon}^{p}\right)\right) \geq 0$. Otherwize, that is, if $H_{*}\left(\bar{\sigma}_{cyc}\right) - H_{*}\left(h_{sh}\left(\bar{\varepsilon}^{p}\right)\right) < 0$, no plastic strains are accumulated.

To produce an advantageous analogy to the well-studied viscoplastic model of Perzyna (Perzyna, 1966; Olszak & Perzyna, 1969), Suiker (2002) finally proposes a slightly different formulation to describe the plastic strain per cycle,

$$\frac{\mathrm{d}\,\bar{\varepsilon}^{p}}{\mathrm{d}\,N} = \mathcal{H}\left(\bar{\sigma}_{cyc} - h_{sh}\left(\bar{\varepsilon}^{p}\right)\right), \tag{4.56}$$

with $\mathcal{H}$ generally being different from H_*. The character of both models, however, is similar in a sense that both models predict a development of cyclic plastic strains as soon as the stress level exceeds the shakedown level. The amount of overstress, $\mathcal{H}\left(\bar{\sigma}_{cyc} - h_{sh}\left(\bar{\varepsilon}^{p}\right)\right)$, determines the magnitude of generated plastic strains. The plastic strain tensor can be obtained from the flow rule

$$\frac{\mathrm{d}\,\varepsilon_{ij}^{p}}{\mathrm{d}\,N} = \frac{\mathrm{d}\,\bar{\varepsilon}^{p}}{\mathrm{d}\,N} m_{ij} \tag{4.57}$$

4.4.3 Magnitude of plastic flow

The magnitude of plastic flow, in terms of the Bochum accumulation model that is the intensity of accumulation, is assumed to be composed of two different mechanisms, frictional sliding and volumetric compaction, both causing densification of the granular material. Therewith a decomposition of the history parameter into deviatoric strain invariant κ^{p} and volumetric strain invariant $\varepsilon_{kk}^{p,c}$ seems reasonable. Accordingly the flow rule becomes

$$\frac{\mathrm{d}\,\varepsilon_{ij}^{p}}{\mathrm{d}\,N} = \frac{\mathrm{d}\,\kappa^{p}}{\mathrm{d}\,N} m_{ij}^{f} + \frac{\mathrm{d}\,\varepsilon_{kk}^{p,c}}{\mathrm{d}\,N} m_{ij}^{c}, \tag{4.58}$$

wherein m_{ij}^{f} and m_{ij}^{c} denote the flow directions for frictional sliding and volumetric compaction.

The deviatoric strain invariant κ is derived from equation (3.23), the volumetric strain invariant from equation (3.22). $\varepsilon_{kk}^{p,c}$ represents the absolute value of volumetric plastic strain generated by compaction alone! The total volumetric strain ε_{kk}^{p} contains a dilation/contraction contribution caused by frictional sliding.

From equation (4.56) an overstress function for frictional sliding is derived,

$$\frac{\mathrm{d}\,\kappa^p}{\mathrm{d}\,N} = \mathcal{K}^f\left(\left(\frac{-q}{p}\right)_{cyc} - h_{sh}^f\left(\kappa^p\right)\right) = \alpha^f\left(\left(\frac{-q}{p}\right)_{cyc} - h_{sh}^f\left(\kappa^p\right)\right)^{\gamma^f}. \qquad (4.59)$$

The volumetric compaction is described by

$$\frac{\mathrm{d}\,\varepsilon_{kk}^{p,c}}{\mathrm{d}\,N} = \mathcal{K}^c\left(\left(\frac{p}{p_0}\right)_{cyc} - h_{sh}^c\left(\varepsilon_{kk}^{p,c}\right)\right) = \alpha^c\left(\left(\frac{p}{p_0}\right)_{cyc} - h_{sh}^c\left(\varepsilon_{kk}^{p,c}\right)\right)^{\gamma^c}. \qquad (4.60)$$

In the above expressions, q and p are the deviatoric stress invariant and the hydrostatic stress invariant, respectively, while p_0 represents the initial mean pressure after consolidation. The stress invariants $(-q/p)_{cyc}$ and $(p/p_0)_{cyc}$ are seen as the governing stress terms for frictional sliding and volumetric compaction and thus are chosen as parameters in the overstress functions (4.59) and (4.60). The positive calibration parameters α^f, α^c, γ^f and γ^c account for changing material properties during the cyclic loading process, such as material densification.

The shakedown evolution functions $h_{sh}^f\left(\kappa^p\right)$ and $h_{sh}^c\left(\varepsilon_{kk,c}^p\right)$ are selected upon the basis of engineering judgement,

$$h_{sh}^f\left(\kappa^p\right) = h_0 + \left(h_m - h_0\right)\left(1 - \exp\left(-\eta^f\left(\kappa^p - \kappa_0^p\right)\right)\right) \qquad (4.61)$$

and

$$h_{sh}^c\left(\varepsilon_{kk,c}^p\right) = 1 + \eta^c\left(\varepsilon_{kk,c}^p - \varepsilon_{kk,c,0}^p\right). \qquad (4.62)$$

κ_0^p and $\varepsilon_{kk,c,0}^p$ are the history parameters of the soil at the beginning of the cyclic loading process. The frictional shakedown evolution function (4.61) allows for distinction of three types of responses: $(-q/p)_{cyc} \le h_0$ means purely elastic response, $h_0 < (-q/p)_{cyc} \le h_m$ corresponds to a plastic response that turns into elastic shakedown after a certain number of cycles and $(-q/p)_{cyc} > h_m$ leads to progressively increasing plastic strains (ratchetting). The compaction shakedown evolution function (4.62) only

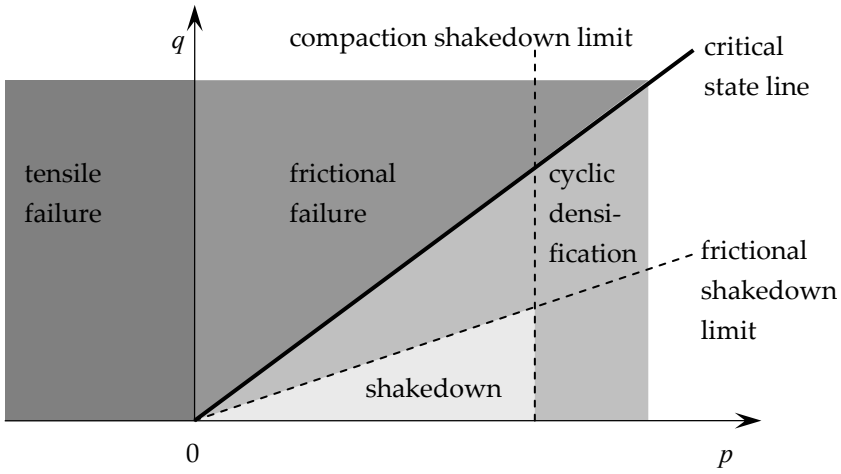

Figure 4.4-1: Various response regimes in the $p-q$ plane during cyclic loading (after Suiker, 2002*)*

distinguishes between elastic response for $p/p_0 \le 1$ and a plastic response turning into elastic shakedown after a certain number of load cycles for $p/p_0 > 1$. This is due to the fact that granular locking under progressive material compaction avoids unlimited growth of plastic volumetric deformation.

The Suiker model divides the stress domain into four response regimes, illustrated in Figure 4.4-1. In the *shakedown* regime the response of the granular material is fully elastic. Cyclic loading in the *cyclic densification* regime causes progressive plastic deformations. Frictional collapse occurs in the *frictional failure* regime, since the cyclic load level exceeds the static peak strength of the granular material. In the *tensile failure* regime the granular material instantaneously disintegrates, as non-cohesive material can not sustain tensile stresses. It should be noted that the shakedown limit functions change with the number of load cycles applied according to equations (4.61) and (4.62).

4.4.4 Direction of plastic flow

The directions of plastic flow, in terms of the Bochum accumulation model that is the direction of accumulation, of frictional sliding and compaction, m_{ij}^{f} and m_{ij}^{c}, are determined in accordance with the plastic flow theory by establishing appropriate plastic flow potential functions. Those are chosen in

correspondence to the respective shakedown functions. This leads to two expressions for the directions of plastic flow,

$$\begin{aligned} m_{ij}^{f} &= \frac{\partial q}{\partial \sigma_{ij}} + d^{f}\left(\kappa^{p}\right)\frac{\partial p}{\partial \sigma_{ij}} \\ &= \frac{3 s_{ij}}{2q} + d^{f}\left(\kappa^{p}\right)\frac{\delta_{ij}}{3} \end{aligned} \tag{4.63}$$

and

$$m_{ij}^{c} = -\frac{\delta_{ij}}{3}\,. \tag{4.64}$$

The function $d^{f}\left(\kappa^{p}\right)$ in equation (4.63) represents the amount contraction/dilation mobilised during frictional sliding, that is, the amount of volumetric plastic strains due to deviatoric stress components,

$$d^{f}\left(\kappa^{p}\right) = d_{0} + \left(d_{m} - d_{0}\right)\left(1 - \exp\left(-\zeta^{f}\left(\kappa^{p} - \kappa_{0}^{p}\right)\right)\right). \tag{4.65}$$

Therewith the direction of plastic flow is dependent on the number of load cycles applied. The formulation in a similar manner as equation (4.61) leads to exponential decrease of $d^{f}\left(\kappa^{p}\right)$ for an increasing κ^{p}.

Upon substitution of equations (4.63) and (4.64) into equation (4.58) and using the common strain decomposition given in equation (3.22), plastic deviatoric strain rate $\mathrm{d}\gamma_{ij}^{p}/\mathrm{d}N$, and plastic volumetric strain rate $\mathrm{d}\varepsilon_{kk}^{p}/\mathrm{d}N$, can be distinguished as

$$\begin{aligned} \frac{\mathrm{d}\varepsilon_{ij}^{p}}{\mathrm{d}N} &= \frac{\mathrm{d}\gamma_{ij}^{p}}{\mathrm{d}N} + \frac{\mathrm{d}\varepsilon_{kk}^{p}}{\mathrm{d}N}\frac{\delta_{ij}}{3} \\ &= \frac{\mathrm{d}\kappa^{p}}{\mathrm{d}N}\frac{3 s_{ij}}{2q} + \left(d^{f}\left(\kappa^{p}\right)\frac{\mathrm{d}\kappa^{p}}{\mathrm{d}N} - \frac{\mathrm{d}\varepsilon_{kk}^{p,c}}{\mathrm{d}N}\right)\frac{\delta_{ij}}{3}\,. \end{aligned} \tag{4.66}$$

The elastic behaviour of the granular material is described using a hypo-elastic constitutive law. It uses a power law, which simulates the increase in material stiffness when the contact area between particles becomes larger under increasing pressure. The elastic stiffness is made

independent of the progress of the cyclic loading process. Own experimental data confirms this assumption, see section 0.

4.4.5 Discussion of the Suiker model

The Suiker model is seen as an elegant alternative to formulate a law for predicting strain accumulation behaviour of a soil subjected to cyclic long-term loading. The essential difference to previously outlined accumulation models is the purely mechanical approach Suiker (2002) chooses. While most of the discussed accumulation models are empirical laws based on experimental data achieved in (few) laboratory tests, the Suiker model starts from the classical plasticity theory to derive an accumulation law for soils.

An advantage of this approach is seen in the implementation into finite element code, properly possible in a mechanical framework. Consistency problems in the solution of a finite element problem, possibly arising when implementing an empirical law, are avoided in that way. The decoupling of frictional sliding and volumetric compaction allows for variable development of the direction of accumulation (or plastic flow). While a constant shakedown function would create a linear increase of accumulated plastic strain with the number of load cycles, the introduced dependency on the current state of the soil, equations (4.61) and (4.62), allows for taking into account changes in the response behaviour of the soil during cyclic loading and therewith a non-linear development of strain accumulation.

Therewith cyclic loading history is considered in both the initial history parameters, κ_0^p and $\varepsilon_{kk,c,0}^p$, and the shakedown functions. The influence of different stress conditions on the accumulation behaviour is covered in equations (4.59) and (4.60) as well as in the hypo-elastic framework, not explicitly discussed in here. A small number of calibration parameters keeps the model relatively simple but gives enough freedom to adapt it to different kinds of soil and soil conditions.

The Suiker model is developed on the basis of axisymmetric stress conditions. Therewith its application, in fact, is limited to two-dimensional or axisymmetric problems. According to Suiker (2002) for arbitrary three-dimensional conditions, the model most likely will yield to an overestimation of the yield strength, since the effect of the third stress invariant, equation (3.7), is ignored. Therewith the model can not be applied

directly to general dynamic problems, usually being of strongly three-dimensional nature.

In contrast to the Bochum accumulation model Suiker (2002) uses the stress amplitude σ^{ampl} as input for the model. As discussed in section 4.3.4 this has several advantages. A further difference to the Bochum accumulation model is the existence of an elastic response regime (see Figure 4.4-1), that is, purely elastic cycles without any generation of plastic strains can be applied. While the Bochum accumulation model implies accumulation as soon as there is any cyclic loading, especially under conditions supporting stiffer material behaviour as high densities and very low amplitudes the assumption of purely elastic material behaviour seems to be plausible.

The model is calibrated using results of cyclic triaxial tests on ballast and sub-ballast material, respectively. Afterwards the deterioration of a railway track was calculated and compared with in situ test data. In general, the model predicted slightly lower plastic strains than the measurements. Furthermore the model shows a significant smaller accumulation rate than observed in the field. Therewith it is difficult to estimate the quality of the prediction with respect to future settlements to be expected. Although triaxial tests with five million load cycles were performed, the accumulation of strain did not stop. This clearly demonstrates the importance of a correct prediction of the accumulation rate even after very high number of load cycles. Otherwise the prediction of the maximum settlement to be expected may be completely wrong.

Neither in the history parameter nor in the formulation of the strain accumulation rate, i.e. the intensity of plastic flow, is the number of cycles involved. Therewith the actual condition is defined by the current state of stress and the current state of the soil alone. This approach is seen as preferable compared to previously described formulations using the accumulated strain at a certain cycle number or any 'equivalent cycle number'.

Suiker (2002) does not explain how the initial history parameters κ_0^p and $\varepsilon_{vol,c,0}^p$ are obtained. Since already existing measurements are used in his thesis a fitting to the existing curves is possible. However, this does not work in the case of prediction. That means that, similar to the previous models, a clear definition on the determination of the initial state of the soil is missing. Tests in relation to the Suiker model are performed on

unsaturated samples at the optimum water content to achieve densities close to the Proctor density, since ballast and sub-ballast of a railway track is tested. Tests at different saturation degrees are not performed. Therewith a possible influence of the water content is not investigated and thus not considered in the model. The accumulation behaviour of the soil is assumed to be independent of the cyclic loading frequency.

4.5 Conclusions

General approach, advantages and disadvantages of accumulation models for soils compared to classical used hysteretic models are discussed. Several accumulation models found in the literature are outlined. Two of them, the Bochum accumulation model and the Suiker model, are presented more extended and discussed in detail. Therewith two different recent approaches for the description of strain accumulation are introduced.

The discussion, especially of both the Bochum accumulation and the Suiker model, sheds a light on the field of mathematical description of strain accumulation phenomena caused by low level vibrations. Accumulation models are developed to predict settlements of soil and structures, i.e. accumulation of strains, caused by cyclic long-term loading. A large number of load cycles is to be applied to generate measurable plastic deformations, though. Thus the actual time is replaced by the number of cycles as state variable. In that way the envelope of the cyclic loading is captured in a constitutive law rather than the incremental evolution of every single cycle as done in hysteretic constitutive models.

Parameters influencing intensity and direction of strain accumulation are identified and their respective effects are explained. From this knowledge elements an accumulation model should contain can be deduced. Furthermore demands on accumulation models as well as difficulties in modelling strain accumulation in soils emerge. Several problems in both laboratory and field investigation of accumulation behaviour are discussed.

Most models base on very few laboratory test and field data, respectively. Only low numbers of cycles are investigated. Therewith settlement predictions for very large numbers of cycles are quite vague and it is difficult to estimate the quality of a model in-situ with respect to

expected settlements in the future. Furthermore the models are often developed for one specific problem. Thus a general application appears impossible. Field measurements related to the problem of strain accumulation are very rare. Almost no data are available on settlements of structures due to dynamic impacts. Exceptions are measurements of deteriorations of railway tracks or roads. However, the settlement of nearby structures due to dynamic impacts rarely has been studied, yet.

No literature is found regarding maximum settlements to be expected in relation to a specific cyclic loading under certain soil conditions. As well laboratory test data as in-situ measurements of strain accumulation until the final accumulation is reached are desirable. Thereby an emphasis should be placed on the determination of historiotropy and current state of the soil. Also the description and definition of a cyclic amplitude parameter, especially for very complicated hysteresis loops, needs further enhancement.

Finally, the influence of several parameters on the evolution of accumulated strains is not studied to a sufficient extent. Especially saturation degree, granular decomposition, shape of grains (see e.g. Cho et al., 2006), aging effects (see e.g. Baxter & Mitchell, 2002) and cyclic loading frequency are seen as important parameters to be subject of further studies.

In general the model should be as simple as possible, though as accurate and advanced as necessary to optimize the quality of the prediction with respect to calculation effort and parameter identification. Accumulation models should be able to consider the effects of the most important parameters influencing the accumulation characteristics of the soil. In general these characteristics are described by the *current state of the soil*, the *current state of stress* and the *characteristics of the load cycle*. Therein the current state of the soil, among others, may contain information on void ratio, historiotropy, granular decomposition and saturation degree. The current state of stress is characterised by the (static) stress conditions of the soil, i.e. average mean effective stress p and average stress ratio η, causing softer or stiffer response of the soil. The characteristics of the load cycle are defined by properties as chronological sequence, cyclic stress amplitude, frequency and polarisation.

Most dynamic problems, e.g. the passage of a vehicle, are of strongly three-dimensional nature. Thus an accumulation model needs to account for arbitrary three-dimensional load cycles. Furthermore it needs to be coupled with advanced dynamic calculations for proper prediction of

resulting residual strains. The better the preceding dynamic calculation and the procedure to transform the results of this calculation to an input for the accumulation model are, the more reliable a prediction will be. This comes along with a unique definition of the state variable ε^{ampl} or σ^{ampl}, respectively. This means that any complex load cycle results in a unique equivalent input parameter for the accumulation model.

The strain accumulation rate should be formulated independent of the number of load cycles. This is founded by the fact that the historiotropy of natural soils cannot be described sufficient by a number of already applied load cycles alone. In fact every load cycle increment ΔN should result in slight changes of the historiotropy variable of the model, leading to a change of the accumulation rate.

Accumulation of strains is a finite process. That is, soil properties, static stress conditions and cyclic loading characteristics define the maximum accumulated strain possible. Beyond this point the material behaves truly elastic under these specific conditions. Accordingly an accumulation model should be able to predict the maximum accumulated strain possible under specific cyclic loading.

A large number of model parameters complicates the model and is difficult to determine. A determination of all variables with few laboratory and/or field tests should be possible. Accompanying with the limitation of model parameters a careful handling of a possible multiplicative approach is recommended. Increasing the number of factors in the model comes along with a summing up of errors. Thus a balance has to be found between capturing influence parameters in advanced relationships and both keeping the model simple and the number of unknowns limited.

The usage of an advanced flow rule for description of the direction of accumulation is sophisticated but may be questioned. Firstly, the model is complicated. Therewith a commercial application is less attractive. Secondly, the soil is forced to behave according to this flow rule. Maybe a natural soil behaves completely different than the model would predict, though. Therewith the advanced flow rule would be useless. A decoupling of deviatoric and volumetric portions of accumulated strains gives more freedom to the model and therewith makes it more general. Thus it is seen as the better alternative. A proper implementation into finite element code is desirable for a good accumulation model.

Summarizing the previous explanations, the following demands on the formulation of an accumulation model can be stated:

1. Correct prediction of evolution and direction of strain accumulation
2. Correct prediction of the maximum accumulated strain to be expected
3. Replacement of the actual time t by the number of cycles N as state variable
4. Sufficient consideration of the current state of the soil
5. Sufficient consideration of the average (static) state of stress
6. Unique transformation of (complex) strain cycles into equivalent input parameters ε^{ampl} or σ^{ampl} for the accumulation model
7. Formulation of the strain accumulation rate independent of the number of cycles
8. Small number of model parameters
9. Decoupling of volumetric and deviatoric portions of accumulated strain
10. Proper and easy implementation into finite element code

Chapter 5
New accumulation model

5.1 Introduction

Literature study and discussion of existing accumulation models in Chapter 4 point out the difficulties in modelling strain accumulation due to low level vibrations. None of the existing models meets all demands of an advanced accumulation model defined in section 4.5. At present, not all these demands can be fulfilled, though. Contradicting goals call for compromises in the definition of an accumulation law.

While on the one hand high accuracy in prediction of accumulation rate, maximum total accumulation and direction of accumulation is desirable, on the other hand the model should be kept as simple as possible to allow for practical applications and proper numerical implementation. This comes along with a maximum reduction of the number of model parameters. Furthermore, for economical reasons the amount of field and laboratory investigations to determine these few model parameters is aspired to be minimised. Nevertheless the current state of the soil needs to be considered sufficiently in the model as discussed extensively before. Finally, a general applicability of an accumulation model requires a simple, unique algorithm to consider very different (complex) impacts correctly with respect to their influence on the intensity of accumulation.

The respective models discussed in Chapter 4 have several advantages and shortcomings, respectively. As a result of these findings it is decided to combine advantageous elements of different models as basis for a new accumulation model. In this chapter the new accumulation model

under consideration is presented. The general approach is discussed and elements of the model are introduced. In a further section the calibration of the model is explained by means of determination of model parameters out of cyclic triaxial tests. Finally, the new model is discussed with respect to its capabilities and fields of application are proposed.

5.2 Elastic material behaviour

Based on previous statements and own experimental findings, presented in sections 0 and 7.3.1, purely elastic material behaviour can be stated for single load events independently of the number of load applications. Thus an existing elastic constitutive model is applied to describe single events. The elastic material behaviour, in general is determined by the constitutive relation given in equation (3.32). In order to account for the increase in material stiffness for an increasing pressure, a pressure dependent elastic power law is adopted (Suiker, 2002; Vermeer, 1980). The incremental relation between hydrostatic stress increment and incremental volumetric elastic strain equals

$$\frac{\mathrm{d}\,p}{\mathrm{d}\,N} = K_t \frac{\mathrm{d}\,\varepsilon_{kk}^{ampl}}{\mathrm{d}\,N}, \tag{5.1}$$

wherein K_t is the tangent bulk modulus, defined as

$$K_t = K_{ref}\left(\frac{p}{p_{ref}}\right)^{1-n_e}. \tag{5.2}$$

In equation (5.2) K_{ref} is the reference bulk modulus at the (negative) reference pressure p_{ref} and n_e is a calibration parameter.

Together with a constant Poisson ratio υ, this power law determines the elastic material behaviour. The pressure dependent constitutive tensor reads

$$D_{ijkl} = \frac{3K_t}{2(1+\upsilon)}\left[(1-2\upsilon)\left(\delta_{ik}\delta_{jl}+\delta_{il}\delta_{jk}\right)+2\upsilon\delta_{ij}\delta_{kl}\right]. \tag{5.3}$$

In cyclic triaxial tests, the elastic Young's modulus is determined from the ratio of the cyclic stress amplitude and the cyclic strain amplitude as described in section 3.4.3. The bulk modulus subsequently can be computed as $K = E/\left(3\left(1-2\upsilon\right)\right)$, see Table 3.2-1.

5.3 Elements of the accumulation model

5.3.1 General approach

Goal of the accumulation model under consideration is to meet as much demands as possible defined in section 4.5. To achieve this goal advantageous properties of different accumulation models presented in the literature are incorporated in the new accumulation model. The basic approach of Suiker (2002) is seen as an elegant way to formulate accumulative behaviour of granular soils. As the final goal of the research is the implementation of the accumulation model in a fully coupled three-dimensional framework including static preload and superimposed strongly three-dimensional dynamic loading, the Suiker model is not completely adapted in this work. Several simplifications on the one hand and the extension to three dimensions on the other hand are necessary modifications. A proper implementation in a finite element code is seen as precondition for spreading the model in practical applications. A continuous and stable formulation thus is indispensable. The realisation of the numerical implementation is presented by François et al. (2007a,b).

The Bochum accumulation model bases on a large amount of laboratory test results with many influence parameters investigated. The respective relations determined in this context give as well important impulses for the formulation of a new accumulation law. Thereby maximum simplification of the respective elements, coming along with a small number of model parameters, is aspired without loosing the ability to describe essential accumulation properties as well quantitatively as qualitatively in a general framework to allow for a wide range of applications.

Since the modelling of accumulation phenomena is a field of recent research, the proposed accumulation model cannot be exhaustive. Accordingly it is aspired to choose formulations allowing for future

extensions of the model, considering further influence parameters in a simple way.

For the proposed model it is assumed that the cyclic part is small with respect to the static part, see specifications in section 2.2.3. This reflects the stress conditions in the soil underneath a building which is loaded by a small amplitude incident wave field, possibly generated by a passing truck or nearby construction works, where the static stresses are larger than the dynamic component of the stresses caused by the incident waves. This allows for the use of the simple elastic constitutive law presented in section 5.2 to describe the dynamic impact. The continuum mechanical sign convention is used for the formulation of the model since it is implemented in a general finite element code. Nevertheless test data and graphs are presented at the basis of the soil mechanical sign convention for the sake of continuity in this work.

Based on findings of Sawicki & Swidzinski (1987 and 1989), Wichtmann (2005) and own experimental results, the assumption of a common compaction curve is a further important element of the model. Thereupon only the intensity of accumulation, i.e. the absolute value of the accumulation rate, is influenced by variation of parameters while the quantitative progress in strain accumulation remains the same. That is, all accumulation curves only differ by a factor.

The direction of accumulation is derived from the Mohr-Coulomb yield function. Thereby deviatoric and volumetric portions of accumulated strain are considered in two independent accumulation laws. That is, a strain decomposition as used by Suiker (2002) is applied. The intensity of accumulation is described in terms of the accumulation rate, independent of the number of cycles. All model parameters can be derived from results of cyclic triaxial tests, minimizing the amount of laboratory tests needed.

5.3.2 Strain decomposition

As discussed extensively before, a considerable amount of permanent deformation is accumulated during the application of a large number of low-amplitude load cycles, while for a single event this irrecoverable deformation can be neglected. Accordingly, this phenomenon is described in a three-dimensional continuum mechanics framework by means of the following strain decomposition:

$$\varepsilon_{ij} = \varepsilon_{ij}^{ampl} + \varepsilon_{ij}^{acc}\,, \tag{5.4}$$

where ε_{ij}^{ampl} is the recoverable, elastic portion and ε_{ij}^{acc} is the irrecoverable, accumulated strain after the application of N load cycles.

The elastic strain tensor is further decomposed in a deviatoric and a volumetric part as defined in equation (3.22). Analogously, the accumulated strain tensor ε_{ij}^{acc} is further decomposed into a deviatoric part e_{ij}^{acc} and a volumetric part ε_{kk}^{acc},

$$\varepsilon_{ij}^{acc} = e_{ij}^{acc} + \frac{1}{3}\varepsilon_{kk}^{acc}\delta_{ij}\,. \tag{5.5}$$

In agreement with equation (3.23) the accumulated deviatoric strain e_{ij}^{acc} is characterised by the deviatoric strain invariant κ^{acc},

$$\kappa^{acc} = \sqrt{\frac{2}{3}e_{ij}^{acc}e_{ij}^{acc}}\,. \tag{5.6}$$

According to Suiker (2002) accumulation of deformation is characterised by frictional sliding and volumetric compaction, see section 4.4.1. Frictional sliding of soil particles causes accumulation of deviatoric deformation as well as volumetric deformation, while volumetric compaction only results in volumetric deformation. Thus the decomposition of the strain accumulation rate $\mathrm{d}\varepsilon_{ij}^{acc}/\mathrm{d}N$ applied by Suiker (2002), equation (4.58), seems reasonable and is taken over in the proposed new formulation,

$$\frac{\mathrm{d}\varepsilon_{ij}^{acc}}{\mathrm{d}N} = \frac{\mathrm{d}\kappa^{acc}}{\mathrm{d}N}m_{ij}^{f} + \frac{\mathrm{d}\varepsilon_{kk}^{acc,c}}{\mathrm{d}N}m_{ij}^{c} \tag{5.7}$$

The unit tensors m_{ij}^{f} and m_{ij}^{c} represent the direction of accumulation for frictional and volumetric compaction, respectively. In this way the influence of both mechanisms, frictional sliding and volumetric compaction, is separated. Deviatoric strain invariant κ^{acc} and volumetric strain invariant $\varepsilon_{kk}^{acc,c}$ are considered as history parameters for frictional sliding and volumetric compaction. Thereby the history parameter $\varepsilon_{kk}^{acc,c}$

represents the volumetric accumulated strain solely generated by compaction.

5.3.3 Direction of accumulation

As in classical creep calculations, the accumulation direction can be derived from a yield function. In the Bochum accumulation model, the Matsuoka-Nakai yield function is used, which is very similar to a classical Mohr-Coulomb criterion but is characterised by a smooth yield surface, see section 4.3.3. For the present model, the direction of accumulation is derived from the Mohr-Coulomb yield function. This approach has also been adopted by Suiker (2002), equations (4.63) and (4.64). For frictional sliding the direction of plastic flow is

$$\begin{aligned} m_{ij}^{f} &= \frac{\partial q}{\partial \sigma_{ij}} + d_0 \frac{\partial p}{\partial \sigma_{ij}} \\ &= \frac{3 s_{ij}}{2q} + d_0 \frac{\delta_{ij}}{3} \end{aligned} \tag{5.8}$$

and for volumetric compaction, the accumulation direction equals equation (4.64), for the sake of clearness repeated here:

$$m_{ij}^{c} = -\frac{\delta_{ij}}{3}. \tag{5.9}$$

Upon substitution of equations (5.8) and (5.9) into equation (5.7), an akin formulation for the strain accumulation rate as proposed by Suiker, equation (4.66), is achieved,

$$\frac{\mathrm{d}\,\varepsilon_{ij}^{acc}}{\mathrm{d}\,N} = \frac{\mathrm{d}\,\kappa^{acc}}{\mathrm{d}\,N} \frac{3 s_{ij}}{2q} + \left(d_0 \frac{\mathrm{d}\,\kappa^{acc}}{\mathrm{d}\,N} - \frac{\mathrm{d}\,\varepsilon_{kk}^{acc,c}}{\mathrm{d}\,N} \right) \frac{\delta_{ij}}{3}. \tag{5.10}$$

The parameter d_0 represents the amount of volumetric deformation induced by deviatoric deformation. In the Suiker model d_0 is made dependent on the history parameter for deviatoric deformation κ^{acc} and denoted as $d^{f}\left(\kappa^{p}\right)$, see equation (4.65). That is, the direction of accumulation depends on the number of load cycles applied. Test results of Wichtmann (2005) confirm slight changes in the direction of accumulation

with the number of cycles. This influence, however, is seen as small enough to neglect it in the Bochum accumulation model. It is decided to subscribe to this view and to consider the direction of accumulation only dependent on the average state of stress.

5.3.4 Accumulation rate

As well in own experimental investigations (described in section 7.3.1) as in cyclic triaxial tests of Wichtmann (2005) an initial logarithmic growth of deviatoric strains is observed as a function of the number of cyclic load applications. This logarithmic growth passes into a constant growth at large cycle numbers. In the Bochum accumulation model this behaviour is captured in equation (4.35). It corresponds to an initial exponential decrease of the accumulation rate to a constant accumulation rate at a large number of cycles. Thus it is plausible to assume the following accumulation law for deviatoric strains:

$$\frac{\mathrm{d}\,\kappa^{acc}}{\mathrm{d}\,N} = \alpha_f \exp\left(-\vartheta_f \kappa^{acc}\right) + \beta_f \,, \tag{5.11}$$

in which α_f and ϑ_f prescribe the initial exponential decrease of the accumulation rate and β_f corresponds to the final value after a large number of cycles. For the volumetric strains a similar law is proposed,

$$\frac{\mathrm{d}\,\varepsilon_{kk}^{acc,c}}{\mathrm{d}\,N} = \alpha_c \exp\left(-\vartheta_c \varepsilon_{kk}^{acc,c}\right) + \beta_c \,, \tag{5.12}$$

where α_c, ϑ_c and β_c are analogous calibration parameters.

Equations (5.11) and (5.12) describe the intensity of accumulation. Since the current model aims to predict settlements of soils under compressive stresses, accumulated volumetric strains as well as the accumulation rate are negative by definition of equation (5.9). On the other hand, the deviatoric strain invariant and the deviatoric accumulation rate are positive. The model parameters α_f, ϑ_f, β_f, α_c, ϑ_c and β_c in general depend on the average state of stress, the current state of the soil and on the characteristics of the cyclic loading.

The assumption of a common compaction curve, discussed in section 5.3.1, results in a constant ratio between two settlement curves. For the deviatoric accumulation rate this dependency can be formulated as

$$\alpha_f(\eta) = \alpha_f^0 f_f(\eta), \tag{5.13}$$

$$\vartheta_f(\eta) = \frac{\vartheta_f^0}{f_f(\eta)} \tag{5.14}$$

and

$$\beta_f(\eta) = \beta_f^0 f_f(\eta), \tag{5.15}$$

whereby α_f^0, ϑ_f^0 and β_f^0 are material parameters containing the accumulation properties of the soil for frictional sliding. As long as no algorithm for unique determination of an equivalent cyclic amplitude is available, this parameter is captured as well in these values. Its influence, however, can be easily separated by introducing another function only depending on the equivalent cyclic amplitude.

$f_f(\eta)$ is a function that accounts for the influence of the average state of stress on the accumulation rate for frictional sliding. The following law is proposed in terms of the stress ratio η, defined in equation (3.15):

$$f_f = -\eta\left(1 + \frac{C_f}{\eta - \eta_c}\right), \tag{5.16}$$

where C_f is a calibration parameter and η_c is the critical stress ratio, defined in equation (3.16). For stress ratios approaching the critical stress ratio η_c, equation (5.16) becomes singular, reflecting high accumulation rates for stress states close to the yield limit. The strain accumulation rate decreases with decreasing stress ratios. For isotropic stress conditions, i.e. $\eta = 0$, $\mathrm{d}\kappa^{acc}/\mathrm{d}N$ vanishes as no deviatoric stress components are applied.

In a similar way the volumetric strain accumulation rate, caused by volumetric compaction, is formulated,

$$\alpha_c(p) = \alpha_c^0 f_c(p), \tag{5.17}$$

$$\vartheta_c(p) = \frac{\vartheta_c^0}{f_c(p)} \tag{5.18}$$

and

$$\beta_c(p) = \beta_c^0 f_c(p). \tag{5.19}$$

Thereby the parameters α_c, ϑ_c and β_c only depend on the average effective mean pressure p and α_c^0, ϑ_c^0 and β_c^0 are material parameters containing the accumulation properties of the soil for volumetric compaction. Also here the influence of the cyclic amplitude is captured in these values until an algorithm for unique determination of an equivalent cyclic amplitude is available.

The function $f_c(p)$ is a function that accounts for the influence of the average effective mean pressure p on the accumulation rate for volumetric compaction. The following law is proposed:

$$f_c = \exp(C_c p), \tag{5.20}$$

where C_c is a calibration parameter. For decreasing absolute values of hydrostatic pressures increasing accumulation rates are observed by Wichtmann (2005). Equation (5.16) reaches its maximum, C_c, at $p = 0kPa$. For increasing absolute values of hydrostatic pressures f_c decreases, considering the negative sign of p for stresses in compression.

5.4 Model calibration

5.4.1 Accumulation model under axisymmetric conditions

For the determination of all model parameters results of cyclic triaxial tests are well suited. Stress and strain conditions under triaxial conditions are derived in sections 3.2.1 and 3.2.2. Under these well defined axisymmetric conditions the stress tensor is constant and the accumulation law, equations

(5.11) and (5.12), can be integrated analytically. For the deviatoric accumulated strain κ^{acc} this becomes

$$\kappa^{acc} = \frac{1}{\vartheta_f} \ln\left[\exp\left(\vartheta_f \beta_f N\right)\left(\frac{\alpha_f}{\beta_f} + \exp\left(\vartheta_f {\kappa^{acc}}_0\right)\right) - \frac{\alpha_f}{\beta_f} \right]. \tag{5.21}$$

The volumetric accumulated strain due to volumetric compaction $\varepsilon_{kk}^{acc,c}$ becomes

$$\varepsilon_{kk}^{acc,c} = \frac{1}{\vartheta_c} \ln\left[\exp\left(\vartheta_c \beta_c N\right)\left(\frac{\alpha_c}{\beta_c} + \exp\left(\vartheta_c {\varepsilon_{kk}^{acc,c}}_0\right)\right) - \frac{\alpha_c}{\beta_c} \right]. \tag{5.22}$$

The total accumulated volumetric strain equals

$$\Delta\varepsilon_{kk}^{acc} = d_0 \Delta\kappa^{acc} - \Delta\varepsilon_{kk}^{acc,c}. \tag{5.23}$$

In equations (5.21) and (5.22) ${\kappa^{acc}}_0$ and ${\varepsilon_{kk}^{acc,c}}_0$, respectively, denote the initial accumulated strain at the beginning of the cyclic load application, in other terms the historiotropy of the soil sample. In general, these parameters can be assumed to be zero for virgin samples.

5.4.2 Parameter identification

Cyclic triaxial test results

For calibration of the accumulation model, cyclic triaxial test data from Wichtmann (2005) are used. 20 cyclic triaxial tests at different stress levels p and stress ratios η are carried out, listed in Table 5.4-1. The investigations are done on a uniform, medium coarse to coarse sand, referred to as sand No. 3 in the work of Wichtmann (2005). All samples are prepared with a relative density of about 60%. The cyclic load ratio ζ, defined in equation (3.19), is held constant at 0.30 in all tests. 100,000 load cycles are applied while axial and volumetric accumulated strains, ε_1^{acc} and ε_{kk}^{acc}, are recorded. From these measurements κ^{acc} and $\varepsilon_{kk}^{acc,c}$ can easily be derived by

$$\kappa^{acc} = \frac{1}{3}\varepsilon_{kk}^{acc} - \varepsilon_1^{acc} \tag{5.24}$$

and

$$\varepsilon_{kk}^{acc,c} = d_0 \kappa^{acc} - \varepsilon_{kk}^{acc} \,. \tag{5.25}$$

	p [kPa]	q [kPa]	η [-]	ζ [-]
Test 1	100	25	0.250	0.300
Test 2	100	50	0.500	0.300
Test 3	100	100	1.000	0.300
Test 4	100	125	1.250	0.300
Test 5	100	131.3	1.313	0.300
Test 6	200	75	0.375	0.300
Test 7	200	100	0.500	0.300
Test 8	200	125	0.625	0.300
Test 9	200	150	0.750	0.300
Test 10	200	175	0.875	0.300
Test 11	200	200	1.000	0.300
Test 12	200	225	1.125	0.300
Test 13	200	237.6	1.188	0.300
Test 14	200	262.6	1.313	0.300
Test 15	200	275	1.375	0.300
Test 16	300	75	0.250	0.300
Test 17	300	150	0.500	0.300
Test 18	300	300	1.000	0.300
Test 19	300	375	1.250	0.300
Test 20	300	393.3	1.313	0.300

Table 5.4-1: Stress conditions for the tests of Wichtmann (2005) *used for model calibration*

Elastic material behaviour

The elastic Young's modulus for each sample is determined from the hysteresis loops in the cyclic triaxial test as described in section 3.4.3. The bulk modulus K subsequently is computed as outlined in section 5.2. In order to keep the model simple hereby a constant Poisson ratio $\upsilon = 0.3$ is assumed. This appears to be an appropriate choice for middle dense compacted sands (see e.g. Budhu, 2000). In further developments a strain dependent Poisson's ratio can be considered.

Equation (5.2) is fitted to the achieved data by determination of parameters K_{ref} and n_e by engineering judgement based on visual interpretation of Figure 5.4-1. This can easily be done as several data points are valid for the reference pressure at $100kPa$. K_{ref}=$120MPa$ is a reasonable choice. Starting from n_e=0.35, proposed by Suiker (2002) for subballast material, n_e=0.30 is easily found as best fit for the material under consideration. The linear elastic model parameters are summarised in Table 5.4-2. Figure 5.4-1 shows good correspondence of the measured bulk moduli with the model.

K_{ref}	$120MPa$
υ	0.30
p_{ref}	$-100kPa$
n_e	0.30

Table 5.4-2: Linear elastic material parameters for sand No.3

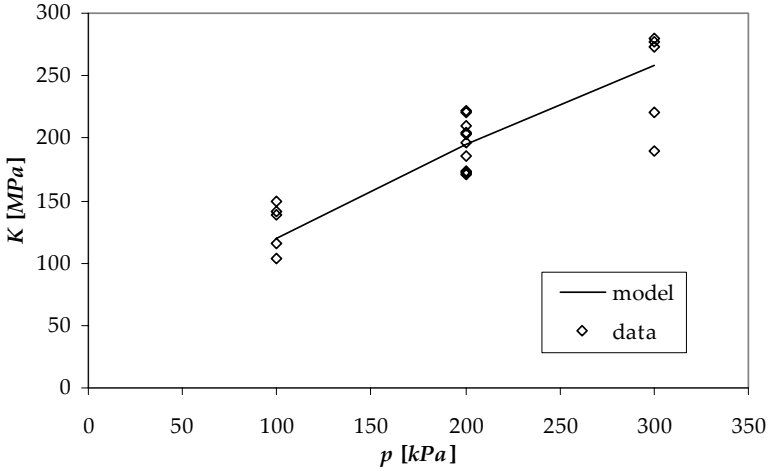

Figure 5.4-1: Elastic bulk modulus K as a function of the hydrostatic pressure p

Determination of model parameters

A non-linear least-squares procedure is used to fit curves (5.21) and (5.22) to the test data for both the deviatoric and the volumetric component of accumulated strain. As a result, values for parameters α_f, β_f and ϑ_f and α_c, β_c and ϑ_c are determined for each test specified in Table 5.4-1. The results of this inversion are listed in Table 5.4-3. Inserting these values in equations (5.21) and (5.22) allows for calculation of accumulation curves κ^{acc} and $\varepsilon_{kk}^{acc,c}$. The total axial accumulated strain ε_1^{acc} and the total volumetric strain ε_{kk}^{acc} for each test can be derived by applying equation (5.10), also available for total strains. In Figure 5.4-2 to Figure 5.4-5 the recorded data of tests 1 to 20 is compared with the respective calibrated accumulation curve, i.e. the fit, achieved by the above mentioned fitting procedure.

Good agreement between model and test data is achieved for all tests and at different average stress levels *p*. Therewith the formulation of the model, in general, is proven to be available for the description of accumulation behaviour of granular soil. Furthermore model parameters at different stress levels allow for studying the corresponding relation and verification of equations (5.16) and (5.20).

	α_f	β_f	ϑ_f	α_c	β_c	ϑ_c
	[10^{-4}]	[10^{-8}]	[-]	[10^{-4}]	[10^{-8}]	[-]
Test 1	0.1369	2.3582	2959.01	0.1072	7.6544	1041.24
Test 2	0.3242	3.2950	2809.43	0.1431	7.1336	1330.45
Test 3	1.7626	5.1519	1471.15	0.8001	3.4331	2222.13
Test 4	4.7426	5.5267	641.44	0.7503	3.2816	1626.47
Test 5	6.1319	6.2655	632.84	0.5952	7.1521	1601.72
Test 6	0.9738	2.2332	3463.14	0.5507	7.1828	1603.44
Test 7	1.3432	3.3345	2031.27	0.8592	6.8931	1344.76
Test 8	1.2821	2.4372	3218.56	0.5616	4.5236	2183.22
Test 9	6.0452	3.0024	2009.71	2.4325	4.0269	2055.02
Test 10	4.9981	3.6546	1542.63	1.9581	3.9992	1871.00
Test 11	5.3073	3.6062	1003.39	1.9124	1.1275	1686.60
Test 12	7.9062	2.6031	609.58	1.7801	2.3122	1334.07
Test 13	7.6910	1.9365	631.84	1.4828	0.8760	1538.15
Test 14	6.1493	5.0627	354.82	0.7728	2.5377	1275.63
Test 15	20.8783	56.4497	82.88	0.3598	13.5341	304.74
Test 16	1.5549	0.1119	3442.40	1.2417	10.1085	1235.96
Test 17	3.6384	1.8730	2740.90	2.6760	2.6147	1960.81
Test 18	7.7920	0.0359	1345.25	2.5325	0.2314	2205.71
Test 19	7.6673	0.4223	748.68	1.6577	0.0986	2222.21
Test 20	8.0838	0.6837	474.71	0.9673	0.6262	1653.80

Table 5.4-3: Calibration parameters for the tests of Wichtmann (2005) *on sand No.3, determined by inversion*

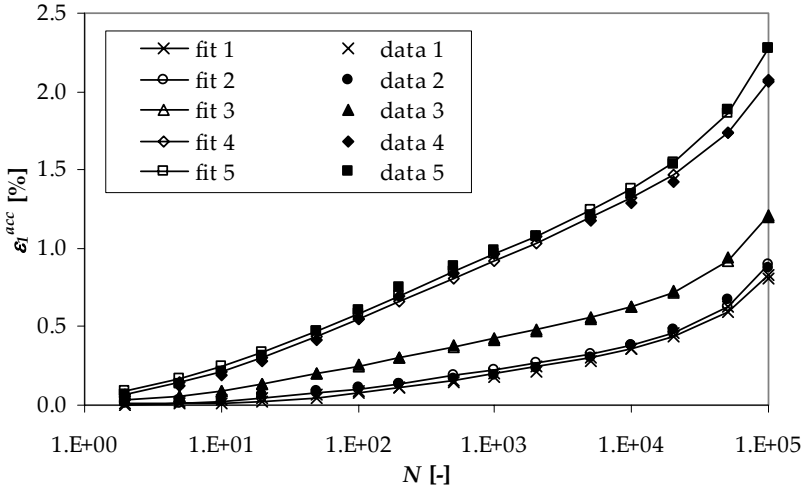

a)

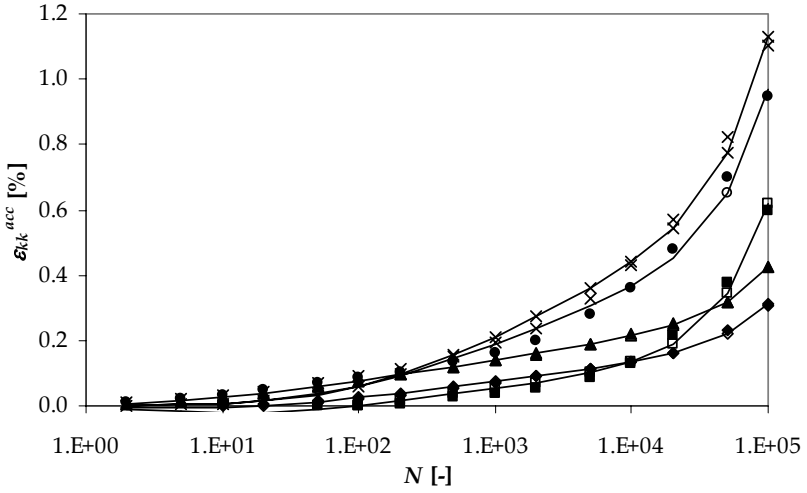

b)

Figure 5.4-2: Measured and calibrated a) axial and b) volumetric accumulated strains for tests 1 to 5 of Wichtmann (2005)*, p=100kPa*

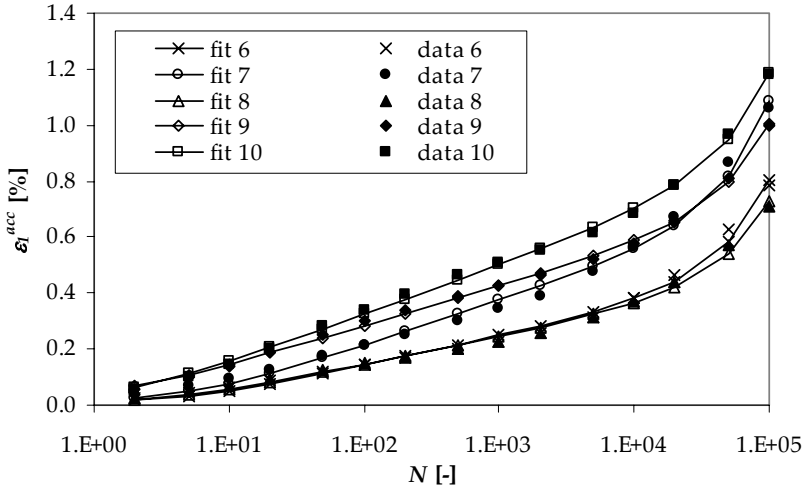

a)

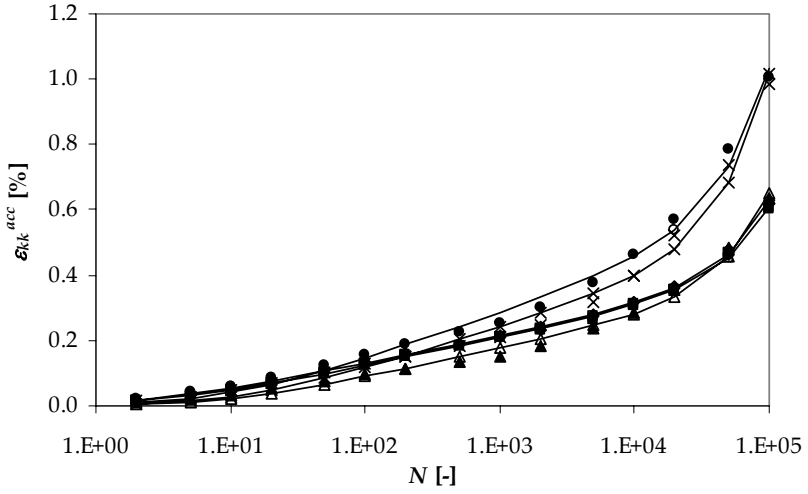

b)

Figure 5.4-3: Measured and calibrated a) axial and b) volumetric accumulated strains for tests 6 to 10 of Wichtmann (2005), *p*=200*kPa*

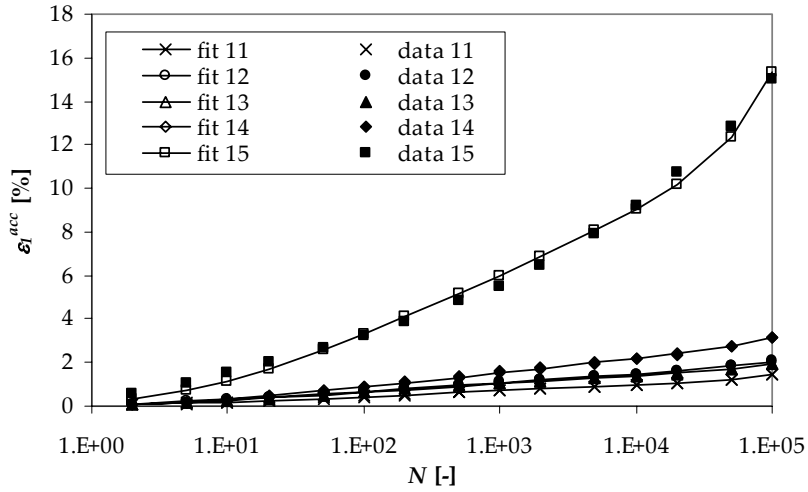

a)

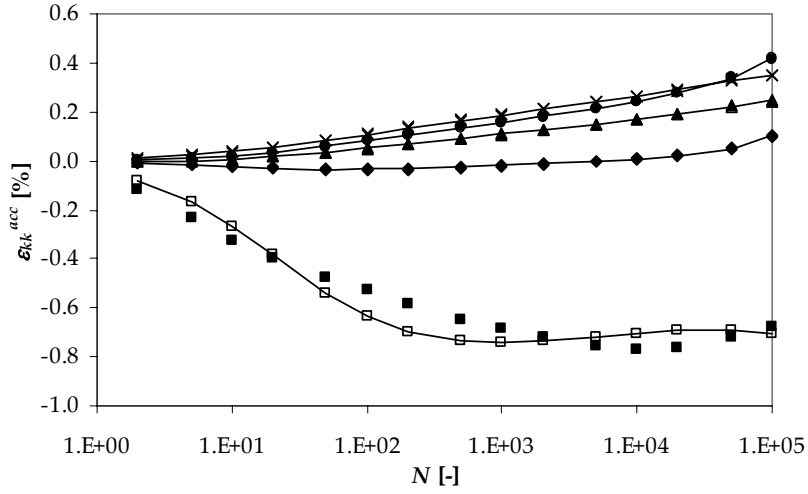

b)

Figure 5.4-4: Measured and calibrated a) axial and b) volumetric accumulated strains for tests 11 to 15 of Wichtmann (2005), *p*=200*kPa*

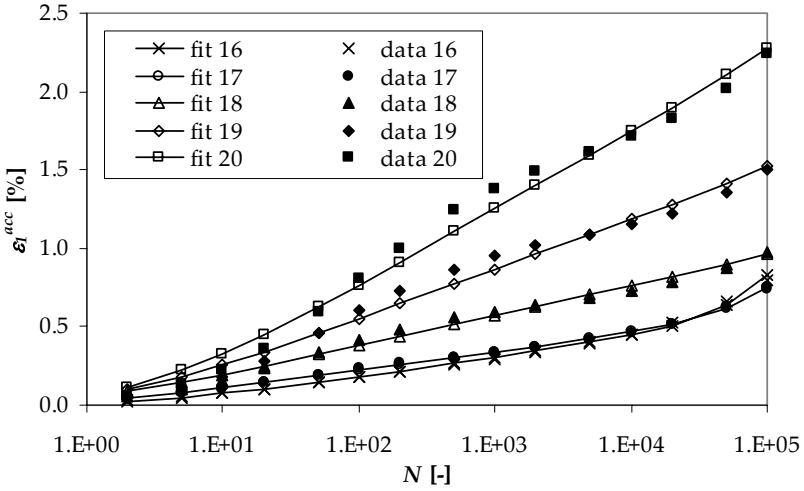

a)

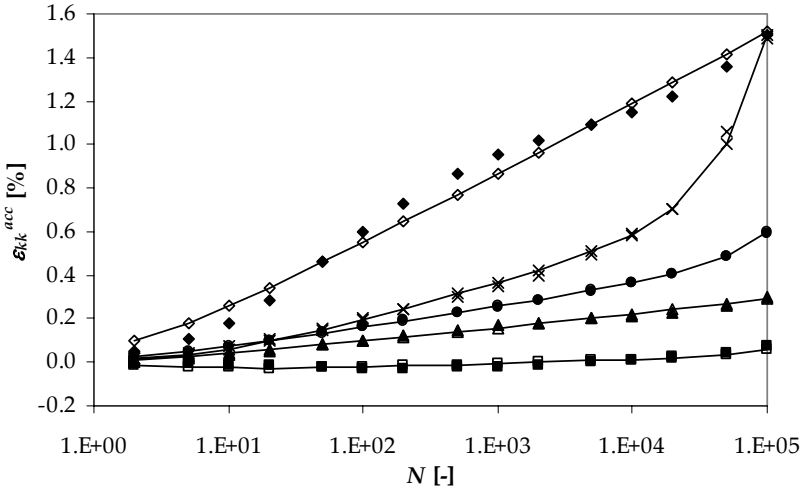

b)

Figure 5.4-5: Measured and calibrated a) axial and b) volumetric accumulated strains for tests 16 to 20 of Wichtmann (2005)*, p=300kPa*

In a second step the calibration parameters α_f, β_f, ϑ_f, α_c, β_c and ϑ_c, listed in Table 5.4-3 , are used as input for another least squares procedure for determination of the model parameters α_f^0, β_f^0, ϑ_f^0, α_c^0, β_c^0, ϑ_c^0, C_f, and C_c in equations (5.13) to (5.15) and equations (5.17) to (5.19), respectively. Parameter η_c represents the critical stress ratio at which immediate failure occurs. For determination of d_0 experimental validation is desirable, though currently not valid. Starting from d_0=0.20, proposed by Suiker (2002) for subballast material, d_0=0.25 seems a reasonable choice for sand No.3 resulting in good agreement of model and test data. The values of all model parameters are listed in Table 5.4-4. In Figure 5.4-6 the model parameters are compared with the calibrated parameters achieved from the curve fitting. The tendencies observed in the calibrated parameters are well described by the model curves.

C_f	0.05
C_c	$5 \cdot 10^{-6}\ Pa^{-1}$
η_c	-1.5
d_0	0.25
α_f^0	$5.37 \cdot 10^{-4}$
β_f^0	$6.23 \cdot 10^{-8}$
ϑ_f^0	1092
α_c^0	$1.21 \cdot 10^{-4}$
β_c^0	$4.47 \cdot 10^{-8}$
ϑ_c^0	1613

Table 5.4-4: Parameters of the accumulation model for sand No.3

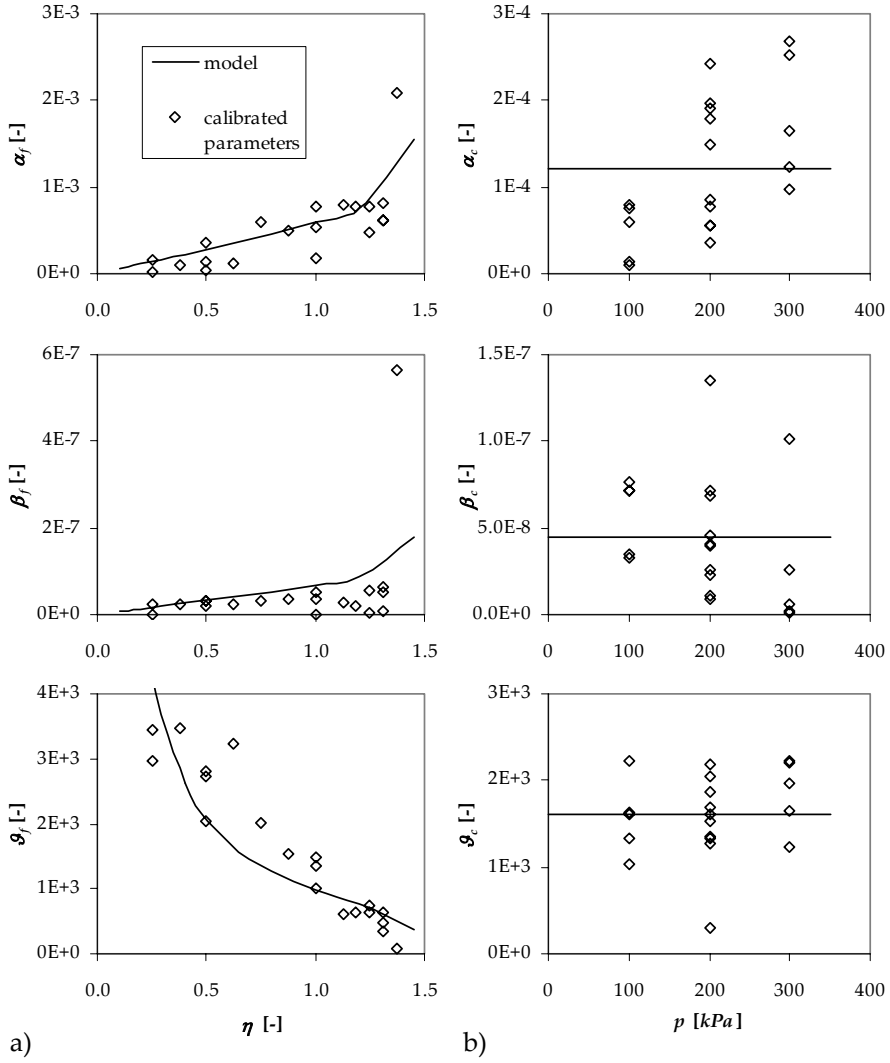

Figure 5.4-6: Calibrated parameters and model parameters for the tests of Wichtmann (2005)

a) $\alpha_f(\eta)$, $\beta_f(\eta)$ *and* $\vartheta_f(\eta)$ *for frictional sliding and*

b) $\alpha_c(p)$, $\beta_c(p)$ *and* $\vartheta_c(p)$ *for volumetric compaction*

5.5 Discussion of the new accumulation model

5.5.1 Determination of model parameters

The procedure described in section 5.4 shows how model parameters are determined out of cyclic triaxial test data. It is emphasised that only one type of laboratory test is needed to determine a full set of model parameters, including both elastic and accumulation behaviour of the soil. Therewith the amount of laboratory investigations required is very limited. Few cyclic triaxial tests, preferably at different stress conditions, are enough to derive sufficient data for reliable parameter identification.

As stated previously the model considers the current state of stress, the current state of the soil and the characteristics of the cyclic load application as input for prediction of accumulated strains. The influence of the state of stress is assumed to be independent from soil characteristics and thus extracted by means of equations (5.16) and (5.20). The current state of soil as well as the characteristics of the cyclic loading are considered in the model parameters α_f^0, β_f^0, ϑ_f^0, α_c^0, β_c^0 and ϑ_c^0. Accordingly, for each soil condition (defined by void ratio, saturation degree, granular decomposition etc.), each dynamic impact and the respective combinations a new set of these model parameters is to be determined. However, this is not seen as a problem, since, in general, the soil can be assumed to behave similar in a certain region and the dynamic impact will keep its characteristics during a considerable number of load repetitions. That is, one set of model parameters for the problem under consideration will result in sufficient predictions in most cases.

Dynamic or static preloading of soil can be taken into account by the history parameters ${\kappa^{acc}}_0$ and ${\varepsilon_{kk}^{acc,c}}_0$. The determination of these parameters in-situ involves several problems, though. The difficulties in determination of the historiotropy of a site are discussed extensively in section 4.3.4. A unique mathematical algorithm to describe complex strain cycles is not necessarily required anymore. Still the question remains, how model parameters, determined in laboratory tests under harmonic cyclic loading, are linked to complex strain cycles in-situ. Related field investigations and further research in this domain are seen as desirable.

5.5.2 Capabilities of the new model

The general, simple formulation of the accumulation model under consideration provides for easy comprehension. In view of future commercial applications of the model this is seen as non-dispensable advantage. Furthermore the general formulation allows for a wide range of applications. The number of model parameters is very limited and the respective values can be determined out of few cyclic triaxial tests alone as explained above. Therewith the application of the model is not only scientific but becomes interesting for practice since the parameter identification is economically justifiable.

As will be shown in section 5.5.3 the simple formulation of the model does not lead to a loss of accuracy. The evolution of accumulated strains can be well predicted with respect to the number of load applications. The decoupling of deviatoric and volumetric portions of accumulated strain gives much freedom in the model. In this way the direction of accumulation is not linked to a certain flow rule but can be varied arbitrarily according to the respective conditions. Since both current state of the soil and the characteristics of the cyclic loading are captured in the model parameters α_f^0, β_f^0, ϑ_f^0, α_c^0, β_c^0 and ϑ_c^0, the definition of an equivalent stress or strain amplitude, σ^{ampl} or ε^{ampl}, is obsolete.

The proposed formulation allows for easy embedding into finite element code. The accumulation model under consideration is implemented in a three-dimensional finite element framework. The accumulation model is used for the soil, while any other linear or nonlinear model can be used for the structure. Only the static forces are considered as external forces, whereas the cyclic load events are accounted for indirectly in the accumulation model. For the integration of the accumulation law, a consistent tangent approach is used, resulting in a stable and accurate integration. The realisation of the numerical implementation is described more extended by François et al. (2007b).

For large accumulated strains, especially at stress conditions close to the critical state line, the model becomes less accurate. This is reasonable since the model is developed for prediction of accumulated strains due to vibrations at the small strain level. That is, linear elastic material behaviour is assumed during one event. At larger strain amplitudes as well as at stress states close to the critical state line, this assumption is not valid anymore. In fact, in this case the material behaviour becomes elasto-plastic even for

single events. Accordingly, in addition to the predicted amount of accumulated strains a non-negligible amount of real plastic strains is generated during every single load application. To overcome this problem a coupling of the accumulation model with an elasto-plastic hysteretic model rather than with a purely elastic one is desirable. This task is considered to be relevant for future research. In relation to this problem dilatational effects as observed by Wichtmann (2005) (initial dilatation during several thousands of load cycles followed by compaction during the subsequent load cycles) in tests at stress states close to the critical state line cannot properly be captured in the proposed formulation.

Further on the model assumes a constant accumulation rate for very large numbers of load cycles. This assumption implies infinite compaction, which is, of course, not a realistic statement. Since the accumulated strains are still small for a reasonable number of load applications, continuous growth of accumulated strains, however, seems to be an admissible assumption for most dynamic impacts. Especially for temporary loadings where the maximum possible accumulated strain is not reached, the proposed formulation will give fairly good correspondence. Besides the model parameters can be updated to the current conditions after a certain number of load cycles by introducing a control cycle as described in relation to the Bochum accumulation model. This adaptation to the stiffer material behaviour will lead to smaller accumulation rates in the model.

A critical loading frequency as discussed in section 4.3.4 is not introduced in the model. Wichtmann (2005) states no influence of the loading frequency on the evolution of accumulated strains. Own experimental investigations confirm this statement in a range of 0 to 10*Hz*, see section 7.3.3. Nevertheless it is expected that there is a frequency above which the material behaviour changes from drained to quasi-undrained, influencing the accumulation properties of the soil. Also the saturation degree of the soil is excluded from the model so far, although an influence is expected (see Werkmeister, 2003). The lack of actual data, however, does not allow for consideration of these phenomena in a clear mathematical formulation in the model.

When further relationships are studied in future and corresponding formulations regarding their influence on strain accumulation are available, the simple formulation of the proposed accumulation model allows for easy extensions. However, an advantage of

the model is seen in the limited number of model parameters and the prevention of a multiplicative approach, leading to summing up of errors. When introducing more parameters or sub-functions in the model the gain in accuracy and the introduction of new sources for errors should be carefully balanced.

5.5.3 Comparison with other models

As emphasised above, the accumulation model under consideration is rather simple compared to other advanced accumulation models as Bochum accumulation and Suiker model without significant loss of accuracy. All effects covered by the Bochum accumulation model can be accounted for in the new model in a simplified way. While the Suiker model is only applicable for two-dimensional or axisymmetric problems, the proposed model is implemented in a three-dimensional finite element framework. Therewith strongly three-dimensional dynamic problems as incident wave fields can be treated.

For validation of the new model the tests of Wichtmann used for parameter identification are predicted, using the determined model parameters, listed in Table 5.4-4. The quality of prediction is comparable with the quality achievable using the Bochum accumulation model. For illustration the same tests are predicted with the Bochum accumulation model as well, using model parameters given by Wichtmann (2005) and listed in Table 5.5-1.

ε_{ref}^{ampl}	10^{-4}	C_Y	2.0
C_{N1}	$3.6 \cdot 10^{-4}$	C_e	0.54
C_{N2}	0.43	e_{ref}	0.874
C_{N3}	$5.0 \cdot 10^{-5}$		
C_p	0.43	$C_{\pi 1}$	4.0
p_{ref}	$100kPa$	$C_{\pi 2}$	200

Table 5.5-1: Parameters of the Bochum accumulation model for sand No.3

Figure 5.5-1 to Figure 5.5-5 show the recorded data of the tests listed in Table 5.4-1 together with the prediction of both the Bochum accumulation model and the new accumulation model. The accumulated axial and volumetric strain, ε_1^{acc} and ε_{kk}^{acc}, respectively, is plotted versus the number of cycles N in the log-scale.

In general, good agreement of both models with test data is found. For tests 1 to 8 the error of the new accumulation model is smaller than the one of the Bochum accumulation model. Fort tests 9 to 13, 16 and 17 comparable accuracy is achieved. The Bochum accumulation model performs better for tests 18 and 19. Obviously, the new accumulation model performs better at lower mean stress levels while the Bochum accumulation model is better suited at higher mean stresses. A slight reformulation of functions f_f and f_c may solve this problem. Therefor, however, test data in a wider stress range is desirable.

In tests 14, 15 and 20 none of the both models provides a satisfactory prediction. This is, in fact, related to the stress conditions of these tests, see Table 5.4-1. Very large stress ratios η close to the critical state line lead to (temporary) dilatational behaviour (tests 14, 15 and 20) and high accumulation of residual strains (test 15). While the Bochum accumulation model depicts dilatational behaviour in a rather simple and thus inaccurate way, the accumulation model under consideration is not developed for stress conditions close to failure. The insufficient results of the Bochum accumulation model also for tests 4 and 5 confirm the previous statement. Accordingly, tests 5, 14, 15 and 20 are not well suited for calibration of the new accumulation model in its current formulation. A reformulation of function f_f and f_c in future may deal with this aspect, though.

The main conclusion of this comparison is that the same quality of prediction as in the Bochum accumulation model can be achieved by using a simpler formulation. Introducing additional influence parameters introduces additional errors. The use of a multiplicative approach yields to summing up of errors, while this effect is avoided by a simple formulation. Nevertheless the influence of certain parameters can easily be considered in the new model by introducing new sub-functions, similar to f_f and f_c for the state of stress, as in the Bochum accumulation model.

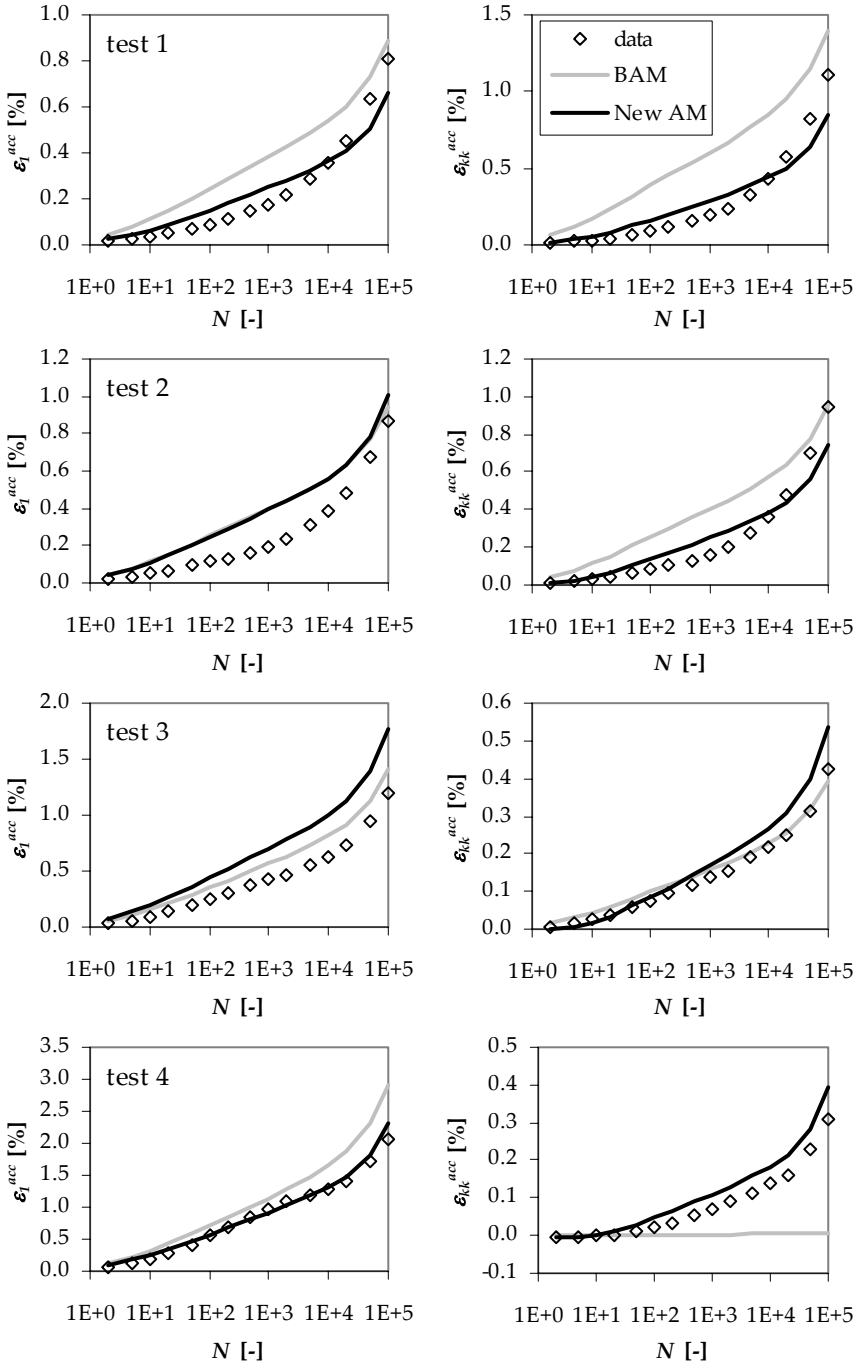

Figure 5.5-1: Test data of Wichtmann (2005) *versus predictions of the BAM and the new accumulation model: tests 1 to 4*

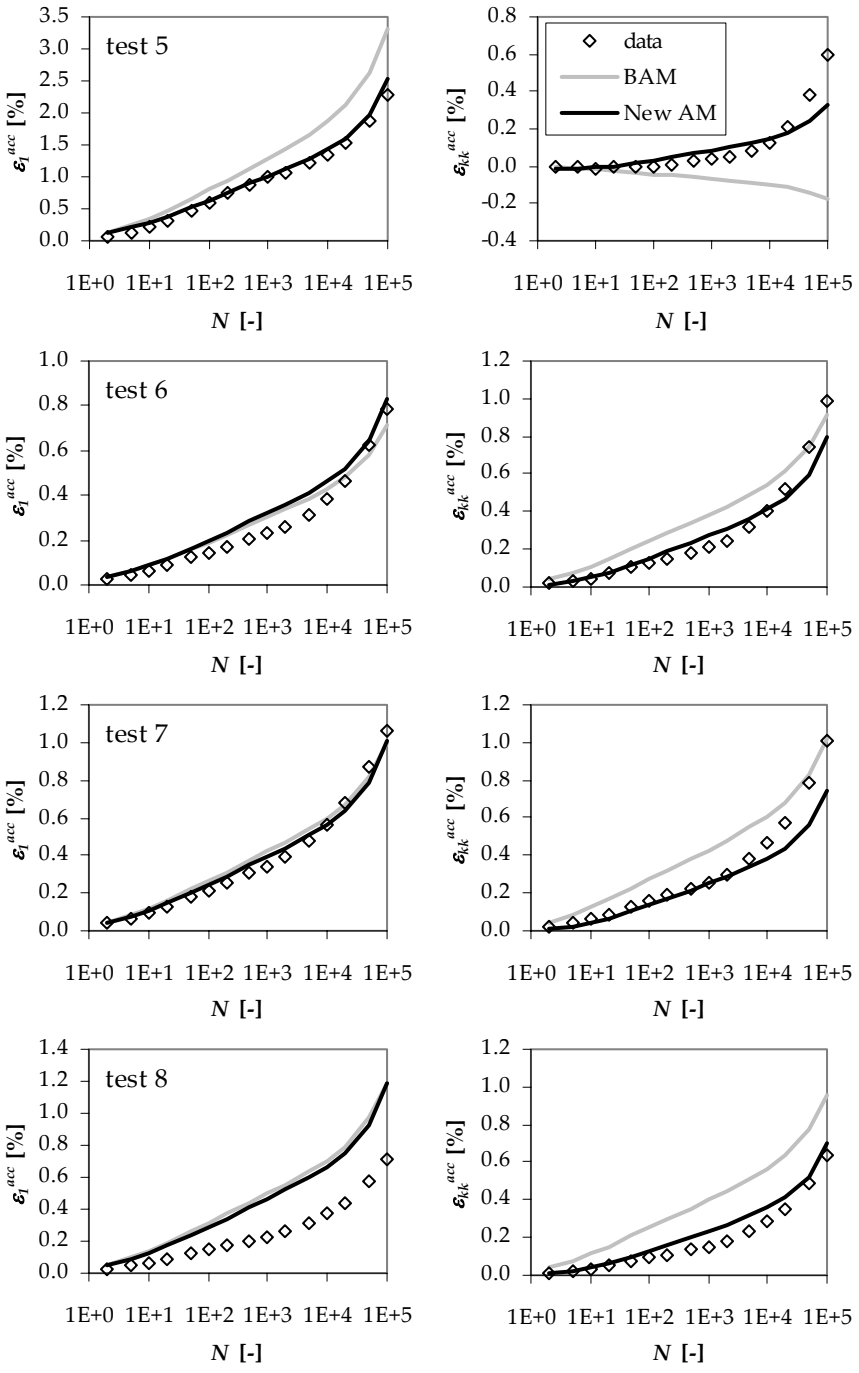

Figure 5.5-2: Test data of Wichtmann (2005) *versus predictions of the BAM and the new accumulation model: tests 5 to 8*

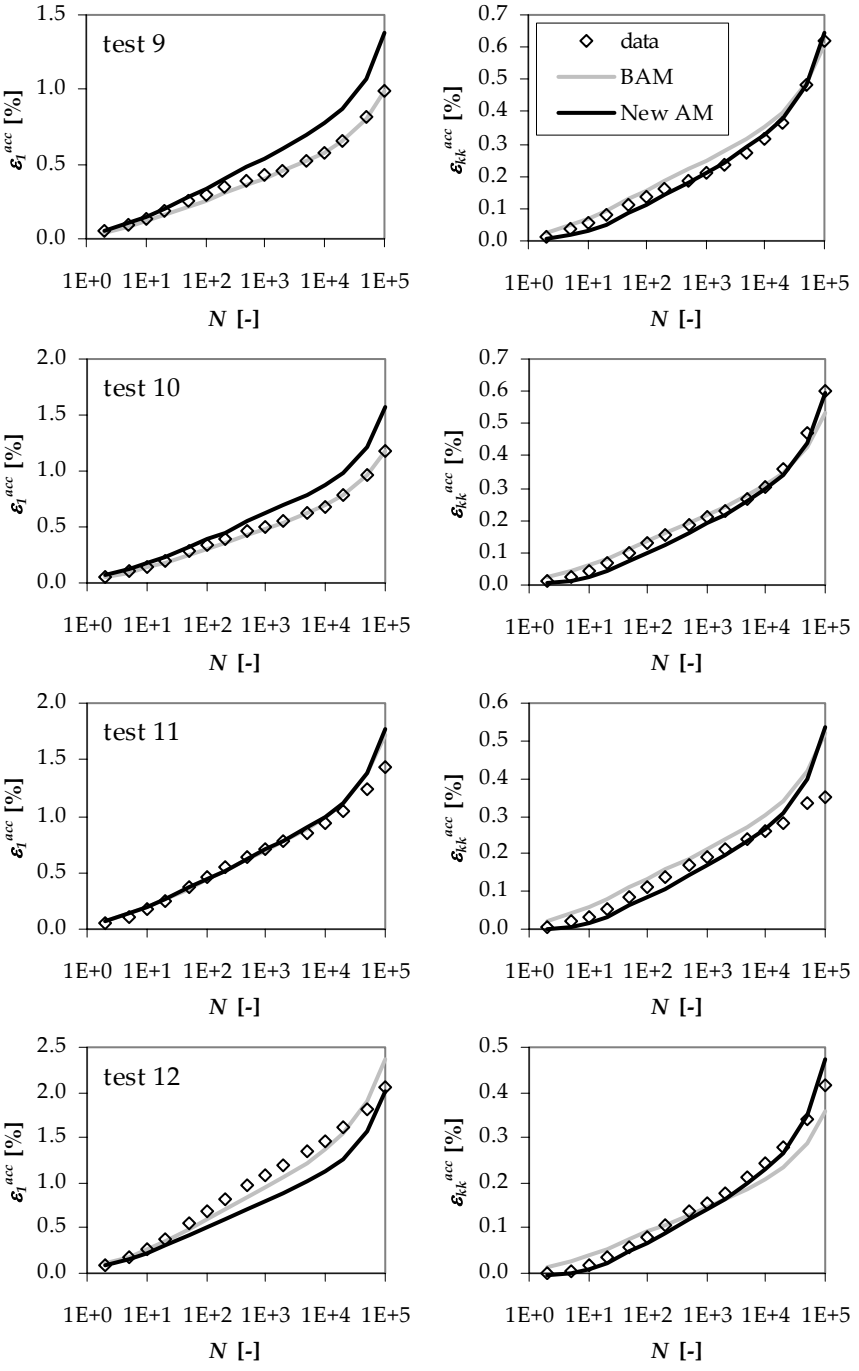

Figure 5.5-3: Test data of Wichtmann (2005) *versus predictions of the BAM and the new accumulation model: tests 9 to 12*

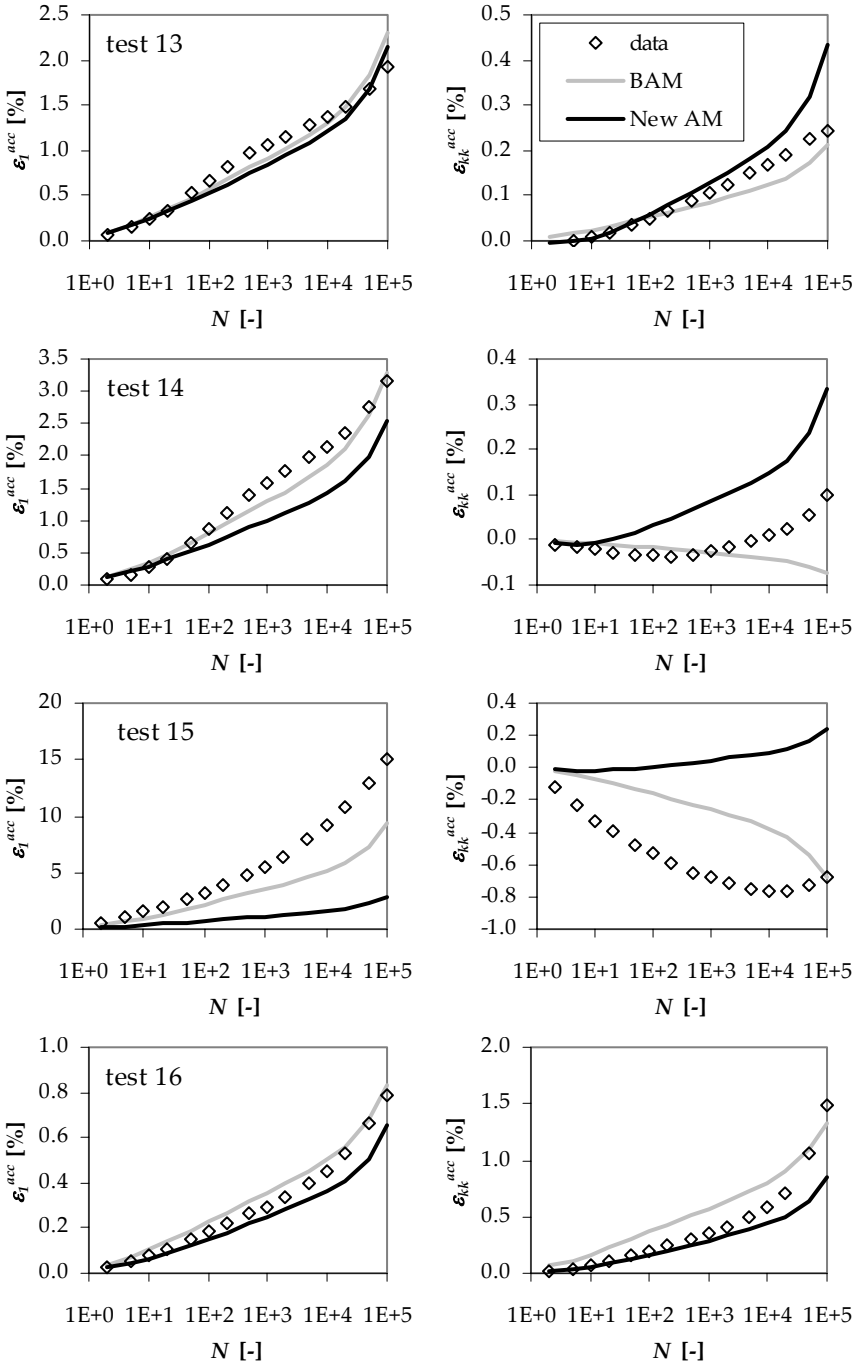

Figure 5.5-4: Test data of Wichtmann (2005) *versus predictions of the BAM and the new accumulation model: tests 13 to 16*

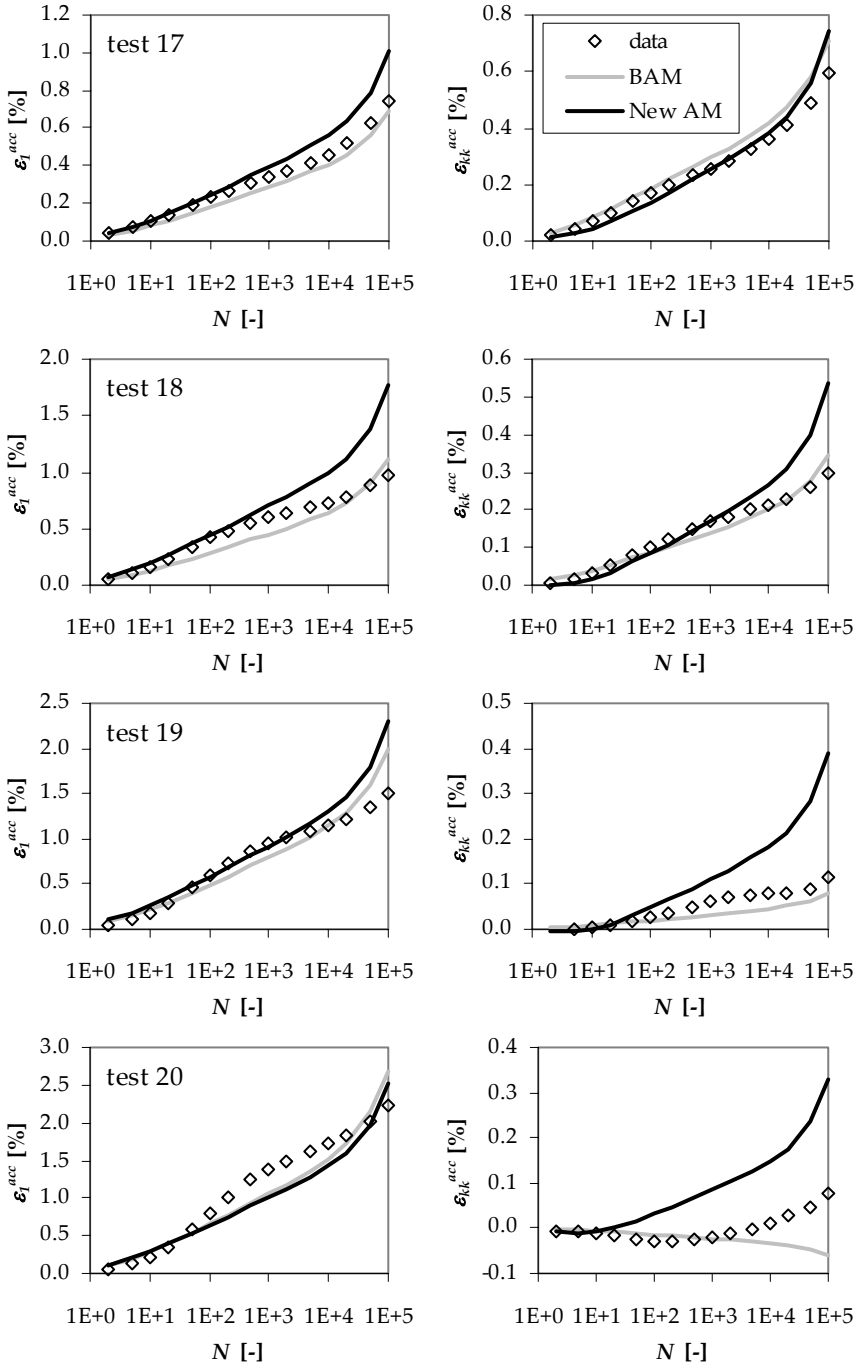

Figure 5.5-5: Test data of Wichtmann (2005) *versus predictions of the BAM and the new accumulation model: tests 17 to 20*

5.6 Conclusions

Based on the cognitions of Chapter 4 a new accumulation model is formulated. The elastic model for calculation of single dynamic events is presented. These calculations are the basis for subsequent prediction of strain accumulation due to these events. Corresponding accumulation laws for both deviatoric and volumetric accumulated strain are derived from existing accumulation models and combined in a new accumulation model for granular soils under compressive stress conditions exposed to low level vibrations.

Many properties of the soil and the characteristics of the cyclic loading are captured in the model parameters. Further relations, however, can easily be extracted from the model parameters as done for the stress dependencies and be implemented in the proposed framework. The determination of the initial state of the soil in-situ, including its historiotropy, is seen as one of the essential tasks for future research, though. As discussed in section 4.3.4, even the best prediction is invalid if the initial assumptions are inaccurate or wrong.

The strain accumulation rate is formulated independent from the number of load cycles and two independent accumulation laws for deviatoric and volumetric strain portions are introduced to ensure a general applicability of the model, especially for in-situ problems. Despite of several simplifications, coming along with the very limited number of model parameters, the loss of accuracy is negligible compared to the Bochum accumulation model. The proposed formulation allows for determination of all required model parameters out of few cyclic triaxial tests alone. Furthermore the model is easy to understand also for engineers not acquainted to accumulation phenomena. Both the economically advantageous parameter identification and the good perspicuity make the model attractive for commercial applications. The accumulation model under consideration is already implemented in a three-dimensional finite element framework and can be used for a wide range of applications.

Chapter 6
Cyclic triaxial testing

6.1 Introduction

To investigate both the accumulation behaviour as well as the elastic parameters of non-cohesive, granular soil under low level vibrations cyclic triaxial and bender element tests are carried out. The tested sand is described in section 6.2. Test results are used for identification of parameters of the new accumulation model presented in Chapter 5. Advanced cyclic triaxial test equipment is thus installed at the Laboratory of Geotechnics, Department of Industrial Engineering Sciences, KHBO in Ostende.

This chapter aims to outline the main features of the installed cyclic triaxial testing device, to give an overview on limitations detected during the work with the apparatus and several enhancements to improve the execution and accuracy of tests. Bender element test equipment is installed in the triaxial cell, allowing for two independent tests on a specimen. The working principle and the applied implementation are discussed in this chapter.

During testing campaigns several problems and difficulties in performing cyclic triaxial tests emerged. It becomes clear how important a very careful and accurate execution of a test is, to ensure repeatability of tests and reliability of results. The general test procedure including sample preparation, saturation, consolidation and cyclic loading stage is explained. The combination with bender element tests is addressed.

6.2 Tested material

The tested material is defined on the basis of the commonly used soil parameters introduced in section 3.3. Fine sand is a typical soil in Flanders. Thus all tests in the frame of this research are performed on the sand of Mol, a uniform fine grained sand with a median grain size diameter D_{50} = 0.195*mm*, a uniformity coefficient *UC* = 1.60 and a degree of curvature of *CC* = 1.03. The maximum and minimum void ratio are e_{max} = 0.918 and e_{min} = 0.586, corresponding to the minimum and maximum dry unit weight, $\gamma_{d,\min} = 13.55\,kN/m^3$ and $\gamma_{d,\max} = 16.39\,kN/m^3$, respectively (Van Impe, 1981). The angle of internal friction is 31.6°. Figure 6.2-1 shows the grain size distribution curve of the tested material, determined by Yoon (1991).

For sample preparation, described in section 6.4.1, the soil is supposed to have an initial saturation degree of 20 to 70%. For the sand of Mol Table 6.2-1 presents these limits, $w_{s,20\%}$ and $w_{s,70\%}$, and the calculated saturation water content w_s at selected relative densities D_r. Corresponding values for void ratio e and dry unit weight γ_d are added. For sample preparation the initial water content is aimed at 10 to 12 %. This value is in the requested range for all densities.

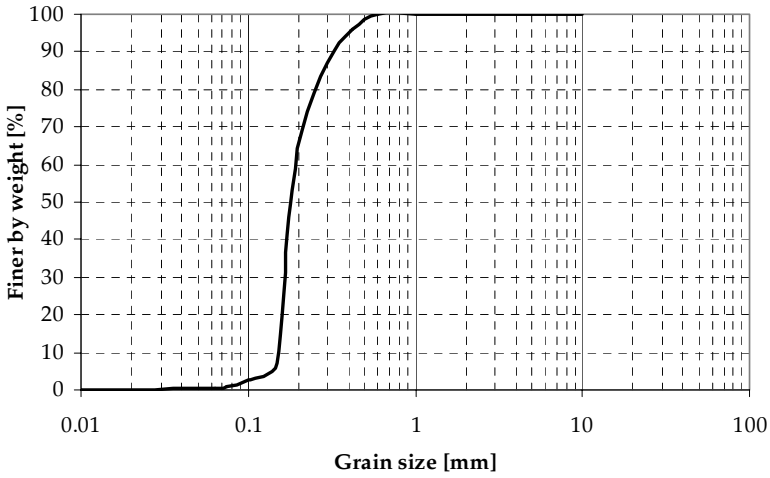

*Figure 6.2-1: Grain size distribution of the sand of Mol (*Yoon, 1991*)*

D_r [%]	e [-]	γ_d [kN/m^3]	w_s [%]	$w_{s,20\%}$ [%]	$w_{s,70\%}$ [%]
0	0.918	13.55	34.64	6.93	24.25
10	0.885	13.79	33.39	6.68	23.37
20	0.852	14.04	32.14	6.43	22.50
30	0.818	14.30	30.88	6.18	21.62
40	0.785	14.56	29.63	5.93	20.74
50	0.752	14.84	28.38	5.68	19.86
60	0.719	15.12	27.12	5.42	18.99
70	0.686	15.42	25.87	5.17	18.11
80	0.652	15.73	24.62	4.92	17.23
90	0.619	16.06	23.37	4.67	16.36
100	0.586	16.39	22.11	4.42	15.48

Table 6.2-1: Relative density D_r, void ratio e, dry unit weight γ_d, saturation water content w_s and limits of water content for sample preparation for the sand of Mol

6.3 Setup of a cyclic triaxial testing device

6.3.1 Features

The installed testing device is set up by a commercial company. Technical information regarding the cyclic triaxial testing apparatus, given in this chapter, is based on the corresponding manual (WFI, 2005). The feedback controlled cyclic triaxial system applies cyclic or dynamic loading to a cylindrical soil specimen. The system is a digitally controlled, servo pneumatic system, which controls three parameters (axis): axial stress, confining pressure and back pressure. The base system incorporates a Control and Data Acquisition System (CDAS) with a 16bit control and a 12bit data acquisition system, a digitally controlled $5kN$ actuator, $50kN$ load frame, auxiliary air receiver with two servo valves for cell and back pressure control, two models of triaxial cells for specimen sizes of 50 and $100mm$ in diameter, volume change measurement monitoring the water entering or leaving the sample, external as well as internal deformation measurements in vertical and horizontal direction, a submergible load cell measuring the applied axial load, bladders to transform air to water pressure and a reservoir of deaired water to fill the cell and to saturate the soil sample.

Figure 6.3-1 shows a) the general scheme and b) a picture of the used loading frame and triaxial cell. A conventional triaxial loading frame including separate manual assessable monotonic shearing device is upgraded with an actuator crosshead carrying the pneumatic actuator for axial cyclic loading. The actuator is connected to a loading piston entering the triaxial cell. There the applied load is measured with the submersible load cell directly on top of the soil specimen. The most important advantage of internal load measurements is that any friction between piston and ball bearings is not measured. Therewith results are more accurate since possible friction errors are excluded. Further on the scheme shows drainages for cell, back and pore pressure and the installation of the sample. For the sake of clarity no deformation measurement transducers are implied in this figure.

A compressor continuously provides air pressure in the range of 800 to $1000kPa$. One air filter directly installed at the outlet of the compressor and three filters before the pressure servo valves remove moisture from the supplied air to avoid corrosion of servo valves and air receiver. A scheme of the pneumatic circuit together with pictures of the air/water bladders and the air receiver is given in Figure 6.3-2.

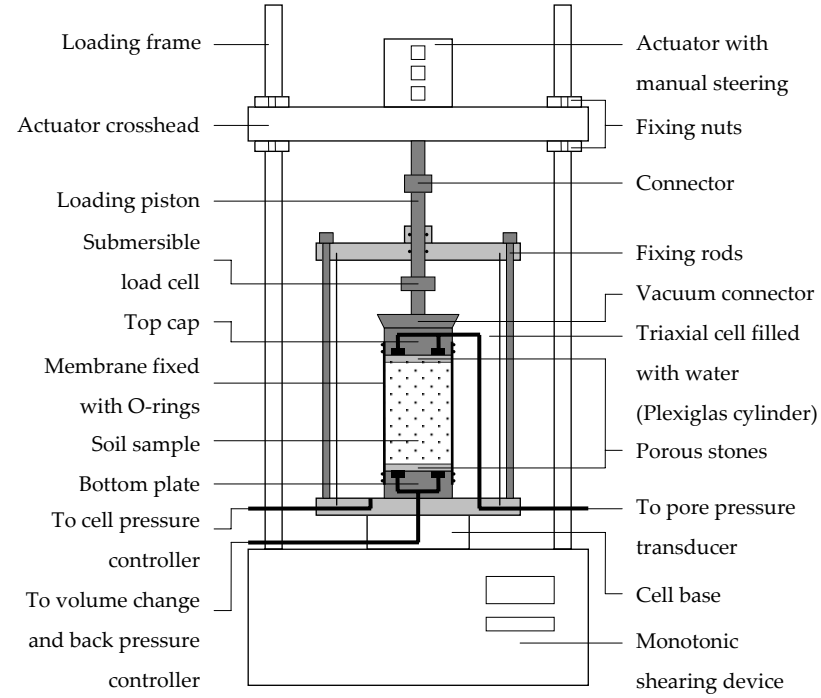

a)

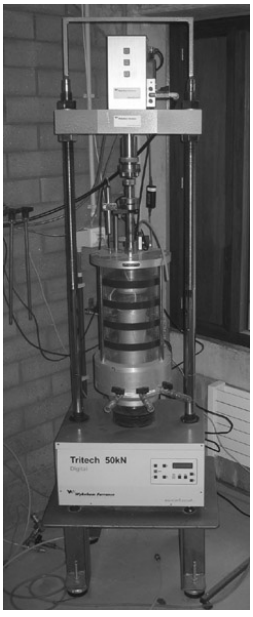

b)

Figure 6.3-1: a) scheme and b) picture of loading frame and triaxial cell

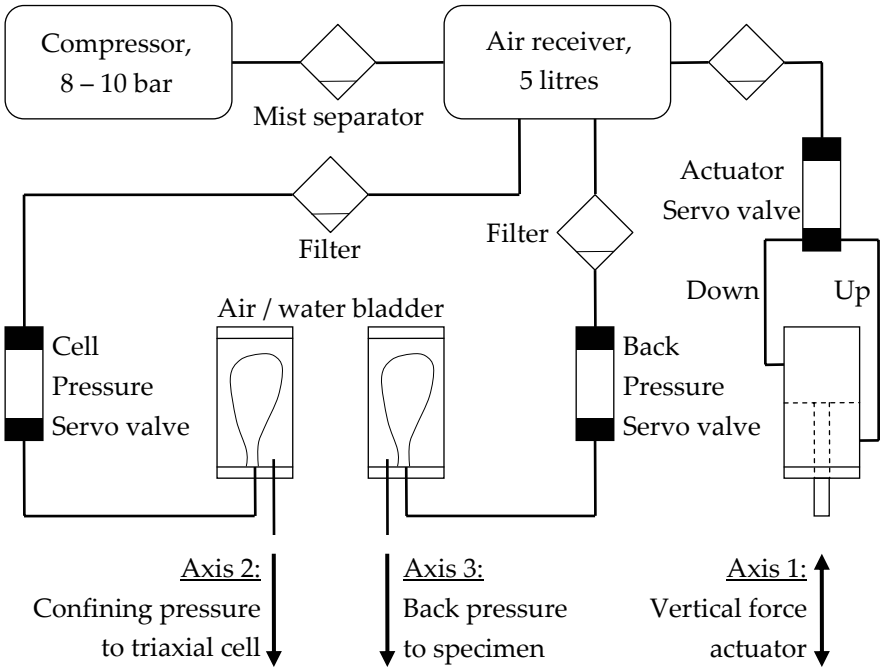

a)

b)

c)

Figure 6.3-2: a) pneumatic circuit of the cyclic triaxial testing device, b) air/water bladders and c) air receiver

A double acting digitally controlled pneumatic actuator with a range of ± 5*kN* applies axial load. A submersible ± 5*kN* load cell measures the applied load above the top cap inside the triaxial cell. Compared to external load cells friction forces of the loading piston are not measured and thus have not to be taken into account in later analysis. The cyclic load can be applied as load (*kN*), stress (*kPa*), displacement (*mm*) or strain (%). Signals applied to the voltage/pressure converter from the CDAS enable computer controlled adjustment of the loads applied to the sample. The actuator has an integral displacement transducer allowing tests to be run under load and displacement control. According to the manufacturer it is coupled to a high performance pneumatic servo valve to provide frequencies up to 70*Hz*. Later on it will be shown, that this value is much higher than the maximum frequency achievable with the presented apparatus, though. The actuator requires a minimum air supply of 800*kPa* for operation, which corresponds to the lower limit of the air pressure supplied by the compressor.

Digitally controlled pneumatic valves apply confining (cell) and back pressures. Deaired demineralised water is used to saturate the sample and to fill the triaxial cell. Deaired water is made as shown in Figure 6.3-3 in a tank installed above the test equipment by applying negative pressure of about -30*kPa*. In the original configuration pure tab water was used. Later on it was decided to install equipment for demineralisation of water (Figure 6.3-9) to avoid clogging of tubes and uncontrolled chemical reactions. The supplied air pressure is transformed to water pressure using two bladders,

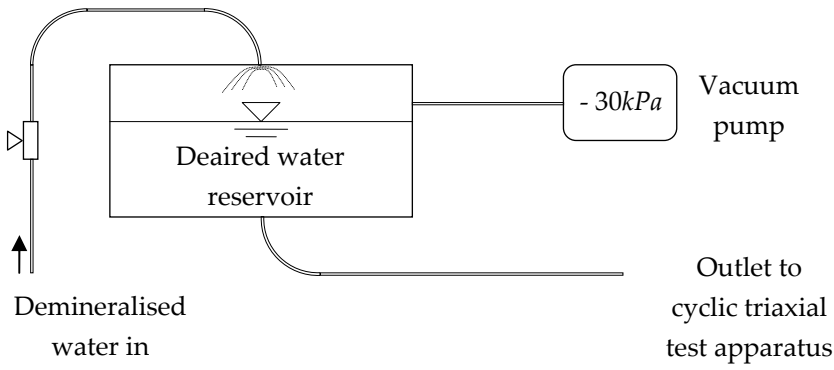

Figure 6.3-3: Deairing of water

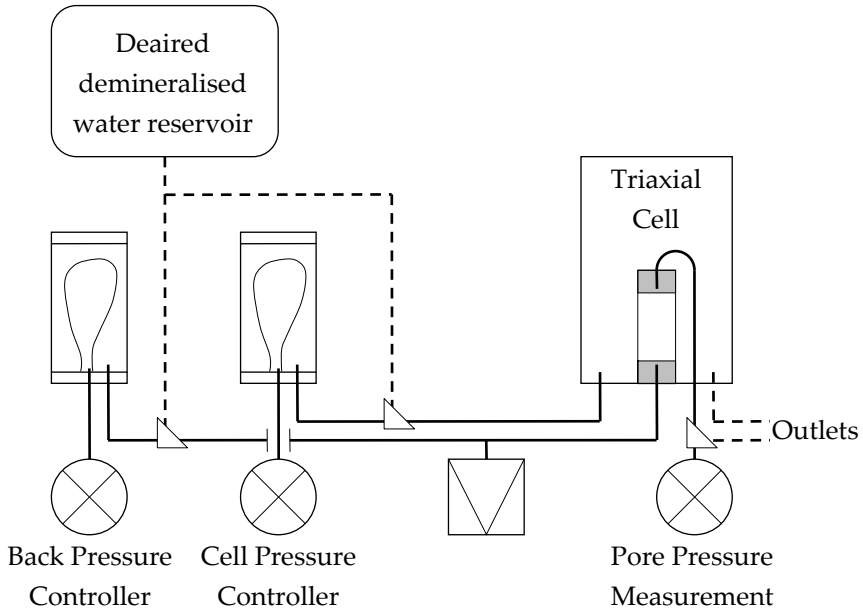

Figure 6.3-4: Water circuit of the cyclic triaxial testing device

one for back and one for cell pressure, respectively. A scheme of the water circuit is shown in Figure 6.3-4.

The dynamic tests are generally carried out in conjunction with static imposed conditions of stress to the soil samples. This means that the sample, in addition to the application of dynamic actions, can be saturated and consolidated at different stress levels under isotropic and anisotropic conditions, respectively. The specimen can also be loaded to failure under static monotonic conditions. The system is supplied with cyclic triaxial test software for control and data acquisition. Several software packages can be used to perform the different test stages. Log files for every test stage can be exported from the software.

The cyclic triaxial system has been designed to perform the following tests:

- Standard triaxial tests (UU, CU, CD) including saturation, isotropic and anisotropic consolidation with pore pressure and volume change measurements
- Cyclic loading

- Investigation of dynamic shear strength and deformation
- Investigation of liquefaction potential
- Determination of shear modulus and damping ratio
- Determination of the resilient modulus

During testing measurements of maximum ten transducers in total are acquired. This includes measurements of cell, back and pore pressure using pressure transducers with a range of ± 1000*kPa*, measurements of the applied axial load with a submersible 5*kN* load cell and volume change measurement of water entering or leaving the sample. In addition axial movements of the actuator and the loading piston outside the triaxial cell (external measurement) are measured. Two axial and one radial on-specimen transducer acquire deformations directly on the sample. Every transducer possesses a so called in-line calibration module. This calibration unit normalises the signal of each transducer to a ± 10*V* output.

All data acquisition functions for transducers as well as critical control and timing for tests are provided by the CDAS (Figure 6.3-5). It is linked to a personal computer through one or two serial ports, depending on the configuration chosen. The data acquisition module has 13 normalised

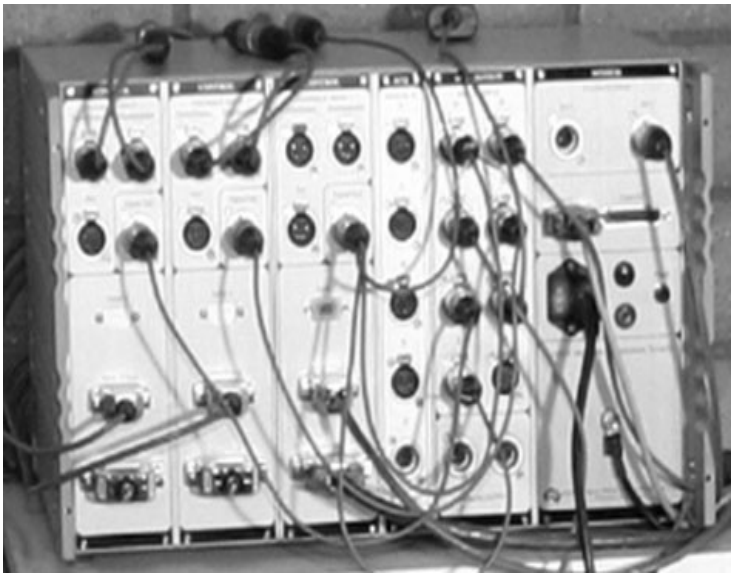

Figure 6.3-5: Control and Data Acquisition System (CDAS)

transducer input channels with a range of ± 10*V*, in accordance to the output of the in-line calibration module. In the original configuration these channels are digitised by 12bit converters for data analysis and presentation. Recalling that for general testing ten channels are required, three more channels are free for installation of additional transducers like mid-height pore pressure or temperature measurements if considered as necessary.

The control module has three channels for feedback control. One is dedicated to the actuator for vertical load, the second is dedicated to cell pressure and the third is for back pressure. The 12bit configuration feedback control module and data acquisition module use one common serial port for communication with the personal computer. However, this configuration is seen as insufficient and modified as will be explained later on in this chapter.

Supervised by the PC, the CDAS automatically controls the operation of loading for individual types of tests. The CDAS directly controls the servo valve to apply the requested loading rate or waveform, cell and back pressure. As illustrated in Figure 6.3-6 a feedback loop checks the current state of loading with a frequency of 4*kHz*. This means position of actuator and applied axial load as well as cell and back pressure are checked

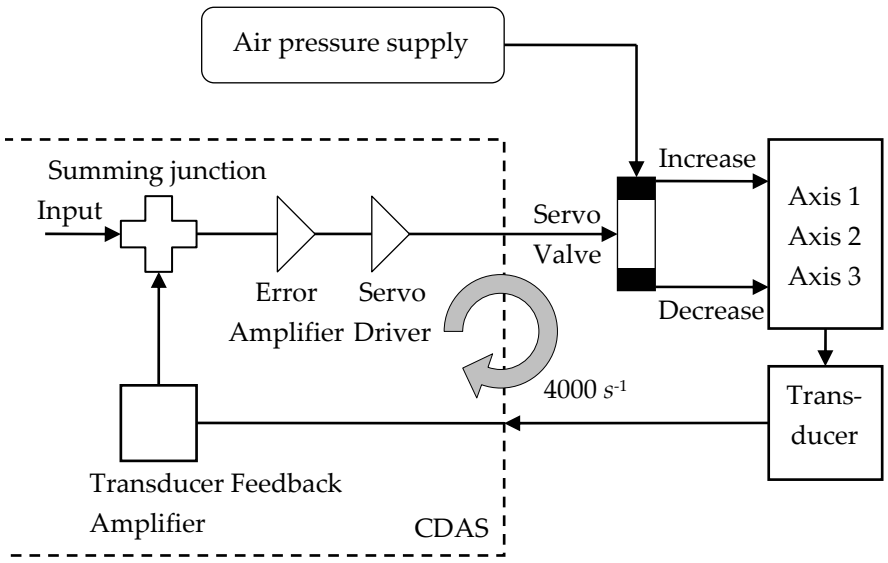

Figure 6.3-6: Closed loop servo control (based on WFI,2005*)*

and adjusted 4000 times per second. Thus the requested input signal is sent via CDAS to the respective axis to increase or decrease the current value. The corresponding transducer measures stress, load, or deformation, respectively, and returns a feedback value to the CDAS. There the feedback signal is sent to a summing junction where it is compared with the demand value. An adjusted signal is then sent to the respective axis, and so on.

Considering a maximum loading frequency of 70*Hz*, the feedback loop will run about 57 times per cycle. This number is seen as sufficient to apply accurate movements of the actuator. While the specimen is being subjected to loading forces, the CDAS is capturing data from the transducers and transfers these, via the serial port, to the personal computer for processing, display and storage.

During all test stages it is of crucial importance to know whether the sample takes or releases water. To measure volume changes a 100*ml* volume change transducer is installed, which monitors the water entering or leaving the sample (Figure 6.3-4). Fitted with a change over valve system it provides unlimited volume change measurements.

All deformations are acquired using Linear Variable Displacement Transducers (LVDTs). The location of all deformation measurement transducers is described in Figure 6.3-7. One is fixed inside the actuator. This LVDT has a range of ± 15*mm*, corresponding to the operational range of the actuator. It is used for strain controlled steering of the actuator and for measuring its deformation. Another, external, LVDT with a span of 50*mm* is mounted on top of the triaxial cell directly on the loading piston measuring its movement in relation to the top plate of the triaxial cell. In this way it is known exactly how much the piston moves to load the specimen.

To measure local strains directly on the sample, on-specimen transducers are being used. One set of on-specimen transducers consists of one radial and two axial strain belts, shown in the picture in Figure 6.3-8. Using only a simple external deformation measurement several sources of error may influence measurements. Possible clearance of the loading device and sample bedding effects of the porous stones on either end of the sample may cause errors. Also the influence of restraints at the edge of the soil sample is supposed to be minimised measuring at the middle third of the sample, where the local strain transducers are mounted and the more realistic deformations occur.

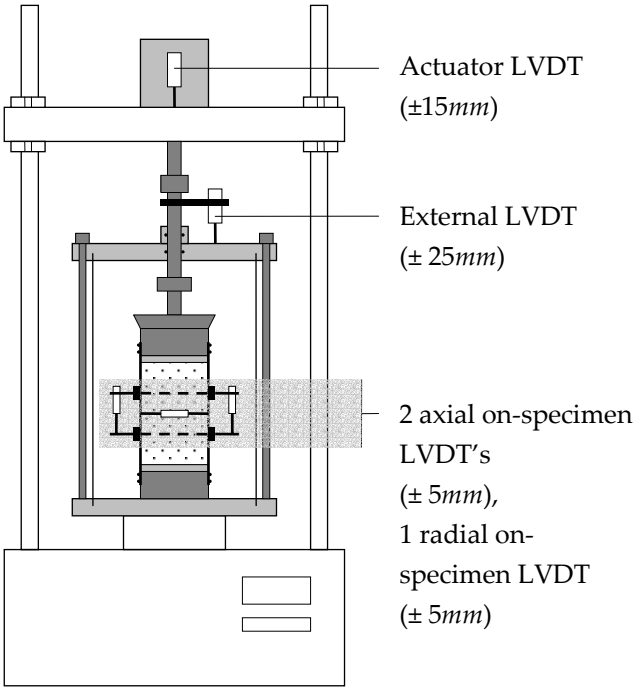

Figure 6.3-7: Locations of deformation measurement transducers

Figure 6.3-8: On-specimen transducer set

One further advantage is the possibility of measuring radial deformations.

Compared to the external LVDT the on-specimen transducers have a much smaller span (± 5*mm* instead of ± 25*mm*). Thus the digital resolution of the local strain measurements is five times larger than the one of the external ones. Even though the deformations in the middle third of the sample will be much smaller than the deformation over the whole sample height, a significant improvement in accuracy can be expected using local strain measurements.

6.3.2 Limitations and enhancements

Although the presented cyclic triaxial test apparatus surely can be assigned as advanced equipment, limitations and problems were detected during getting acquainted with working principles of the testing device and running first tests. As a consequence several enhancements are made which are presented here.

Preparation of demineralised deaired water

Especially during tests of long duration chemical processes may lead to clogging of tubes and corrosion of metal parts of the equipment when untreated tab water is used for testing. Thus it was decided to install equipment for demineralisation of the water. Tab water is first treated with hydrochloric acid (HCl) and then with sodium hydroxide solution (NaOH) to remove minerals. A scheme of the demineralisation equipment is presented in Figure 6.3-9.

Before starting the demineralisation the two columns are saturated with hydrochloric acid and sodium hydroxide solution, respectively. Then tab water is flushed through acid and base column while the conductivity is measured at the outlet of the base column. Sufficient demineralisation is assumed if the value of conductivity is equal to or larger than $0.5\,M\Omega$. During flushing the passing water is led to the waste water tank. As soon as the conductivity meter assigns demineralised water leaving the second column, the water is stored in another tank. This water is used for cyclic triaxial testing.

With the used installation approximately 100 litres of demineralised water can be produced during one session lasting about one working day. This corresponds to the amount of water needed for three cyclic triaxial tests. After demineralisation water is pumped to the water

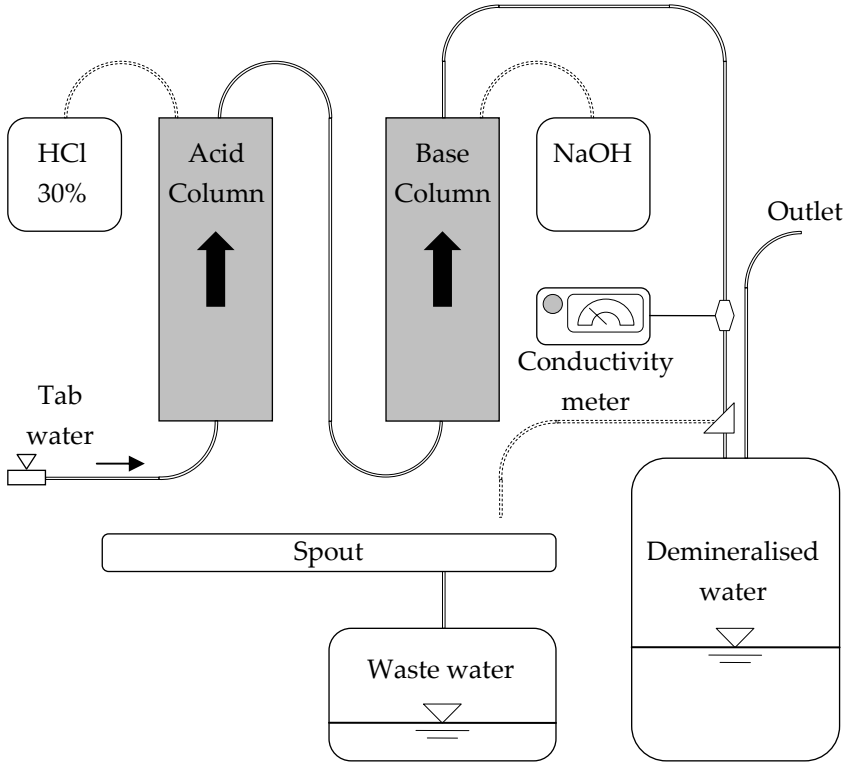

Figure 6.3-9: Scheme of demineralisation equipment

reservoir above the test equipment and vacuum is applied. The deairing procedure (see Figure 6.3-4) lasts about thirty minutes. Then the water is ready for use.

16 bit data acquisition

Since the present research focuses on low level vibrations in the soil, obviously corresponding cyclic triaxial tests at small to very small strains are to be carried out. Investigation of the original configuration of the testing device indeed led to the conclusion that the accuracy is insufficient for tests planned in the framework of the current research. One of the most important changes to solve that problem is the upgrade to a higher digital resolution. Namely the data acquisition module was upgraded from a 12bit to a 16bit system. This change improved the digital resolution of all measurements by factor 16. Table 6.3-1 shows a comparison of the smallest unit measurable (1 count) using a 12bit and a 16bit data acquisition system, respectively. The

value of this unit can be achieved easily by dividing the span of the respective transducer by the digital resolution, that is, $2^{12} = 4096$ for 12bit and $2^{16} = 65536$ for 16bit systems.

Transducer	Span	1 count	
		12bit	16bit
Pressure transducer	± 1000*kPa*	0.488*kPa*	0.031*kPa*
Load cell	± 5000*N*	2.44*N*	0.15*N*
Actuator LVDT	30*mm*	0.007324*mm*	0.000458*mm*
External LVDT	50*mm*	0.012207*mm*	0.000763*mm*
On-specimen LVDT	10*mm*	0.002441*mm*	0.000153*mm*
Volume change	100*ml*	0.0244*ml*	0.0015*ml*

Table 6.3-1: Improvement of accuracy using 16 bit data acquisition module

Obviously much smaller deformation and pressure changes can be detected using the 16bit data acquisition module. Double amplitude deformations of about 10^{-2} *mm* can be recorded with sufficient resolution. This value corresponds to double amplitude axial strains of about 10^{-2}% using samples having 50*mm* in diameter and $5 \cdot 10^{-3}$% using samples having 100*mm* in diameter, respectively. Figure 6.3-10 presents measurement results of the external LVDT at a double amplitude axial strain level of about 10^{-2}%

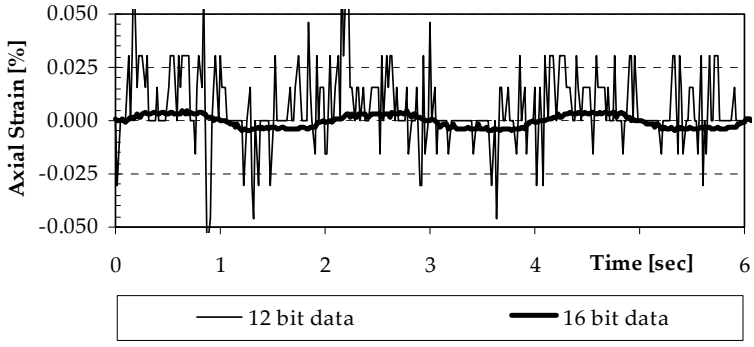

Figure 6.3-10: Resolution of 12 and 16bit data acquisition in external axial strain measurements at the applied double strain amplitude of 0.01%

during sinusoidal loading with a frequency of 0.5*Hz*. It clearly demonstrates significant improvements in accuracy of the measurements. In fact deformations being that small are not even detectable with the 12bit data acquisition system.

It is worth to mention that very small strains only can be applied accurately running stress or load controlled tests. This fact can be explained by the circumstance that the equipment works optimal in a certain range of deformation and load. The smaller the piston movement the more difficult is the tuning of waveshapes, especially when approaching the lower limits of the equipment. The lower limit of deformation does not agree with the lower limit of load, though. This value can be assumed at a double amplitude load of about 50*N* and corresponds to a double amplitude axial stress of about 25*kPa* for samples having 50*mm* in diameter and of about 6*kPa* for samples having 100*mm* in diameter. However, especially stresses less than 10*kPa* applied on the larger samples in general do not produce strains large enough to be recorded accurately with the used LVDT's. Logically follows that the load to be applied to generate acquirable deformations has to be clearly higher than the lower limit of load and therewith allows more accurate steering than strain controlled tests very close or equal to the lower limit of deformation.

The 16bit data acquisition module is associated with the usage of two serial ports instead of one. Therewith the feedback control module and the data acquisition module have their own dedicated serial port. In addition to the higher accuracy due to this enhancement the data transfer time is halved. However, to acquire ten channels during cyclic loading with the personal computer requires a data transfer time from the CDAS of about 750*ms* at a low sampling rate (50 samples/cycle) and about 1500*ms* at a high sampling rate (100 samples/cycle), respectively.

In fact this restriction defines the maximum loading frequency. If the loading frequency exceeds the critical value of $1/0.75 s^{-1}$ (low sampling rate) or $1/1.5 s^{-1}$ (high sampling rate) more data are recorded than can be transferred to the PC and be stored in a log file. This causes jamming of data and therewith uncontrolled actions of the software leading to a crash of the control system. In this way the low data transfer rate of serial ports of about 115*kb*/*s* thus limits the loading frequency at about 1.33*Hz* (low sampling rate) or 0.66*Hz* (high sampling rate), respectively. To solve this problem the use of

USB interfaces could be an alternative. The data transfer rate of USB interfaces is about 10*Mb/s*, which accords to an increase factor of almost 100.

It is assumed that this increase of data transfer speed would solve the data acquisition problems. Currently it is worked on an adequate upgrade of the communication between CDAS and PC in cooperation with the manufacturer of the equipment. Further possibilities to increase the data transfer time are to reduce the number of channels to be recorded and to decrease the sampling rate, respectively. However, excluding transducers from data acquisition would mean a loss of important information. Decreasing the sampling rate corresponds with less accurate measurements. A sampling rate of 25 samples per cycle is seen as lower limit for this value, increasing the maximum possible loading frequency to about 2.66*Hz* (low sampling rate) or 1.33*Hz* (high sampling rate), respectively. Thus the latter two possibilities to increase the loading frequency significantly are considered as insufficient.

In order to be able to apply loading frequencies above the mentioned limit, some cycles can be cut from data acquisition. This means, that at higher loading frequencies not every cycle is recorded, but only every second, third, or less – according to the relation between data transfer time and loading frequency. For tests with a high number of cycles as in strain accumulation tests this way to reduce the amount of data to be transferred from the CDAS to the PC will be a sufficient solution. However, especially in the conditioning phase at the beginning of such a long term test and, of course, for tests with a low number of cycles more data is useful and required.

Eigenfrequency of the equipment

Further potential limiting factors regarding the maximum loading frequency have to be investigated. In particular this regards the eigenfrequency of the equipment (i.e. loading frame, loading piston and triaxial cell), the performance of the pneumatic controlled actuator, the compressibility of air inside the tube system and the data acquisition by LVDT's. As long as the loading frequency is small due to the limitations discussed above and therewith below the eigenfrequency of the system, the risk of resonance problems is considered as negligible, though.

Performance of the actuator

Another limitation of the loading frequency is produced by the pneumatic actuator. Indeed the possible load to be applied is a function of the loading frequency, see Figure 6.3-11. Very stiff samples can require higher loads to achieve a certain deformation level, which may limit the loading frequency. Furthermore also the actuator speed does depend on the type of sample being tested. Soft materials will show greater displacement under load, which means, the actuator has further (and therewith faster) to travel. Unfortunately a graph showing the maximum deformation versus the loading frequency is not provided by the manufacturer for the used equipment. However, the actuator performance at high frequencies cannot be investigated as long as the loading frequency is limited by other reasons anyway. Since the present research focuses on small strain tests, large deformations and loads at high frequencies are not to be expected, though.

A critical part of the equipment especially regarding the performance of high frequency tests could be the usage of a pneumatic loading system. To achieve high loading frequencies with the actuator, very fast load changes must be realised. It is to scrutinise if cyclically compressed air is able to follow such quick changes and to fully apply the requested load on the actuator movement, or if delays in transmission lead to uncontrolled behaviour of the loading system. A risk is seen that the load change takes

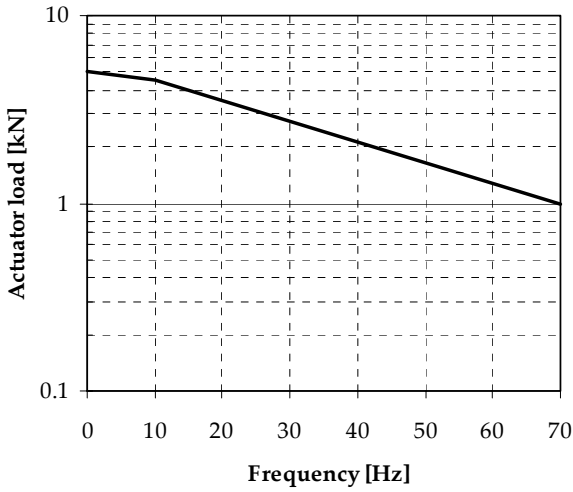

Figure 6.3-11: Response of the cyclic triaxial actuator versus loading frequency (after WFI, 2005*)*

place faster than the compressed air can follow the pulse and transmit the load on the actuator movement.

On-specimen LVDT's in cyclic triaxial tests

To the authors knowledge only few people use on-specimen LVDT's during cyclic and dynamic triaxial testing. For that reason not much experience is collected in the application of local strain transducers in such tests. An important point to investigate is if the LVDT's deliver reliable measurements also at high frequencies. The quality of measured data depends on several factors. One of those is the above mentioned data transfer time. On the other hand, of course, the transducers have to acquire the data sufficiently. Thus it has to be ensured that the transducers do follow the deformation of the sample just in time and without any dissipation of movements.

The transducer fixing method proposed by the manufacturer was seen as unsatisfactory. It uses small plates the LVDT's are fixed on. Those plates are mounted on the membrane using rubber rings. The advantage of that fixing method is that puncturing of the membrane is avoided and leakage risks are minimised. However, during cyclic loading movement of the mounting plates was detected, causing significant errors in deformation measurements. The solution of this problem is as simple as effective. Glue was searched that fixes rubber as well as metal and remains stable in air as well as in water under high pressure. Finally it has to be easily removable from rubber membrane and metal plate to reuse the material.

For static deformations, apart from small deviations which can be explained with above mentioned bedding errors and clearance of the loading system, the local strain measurements show very good agreement with external measurements applying this modified mounting method. During cyclic loading, however, still huge differences in external and local strain measurements are observed. Possible reasons are incorrect performance of the LVDT's during cyclic loading due to friction effects and inhomogeneous strain distribution along the height of the sample. Further investigation is needed to be able to explain that phenomenon.

Further modifications and enhancements of the equipment are made in the software domain in cooperation with the manufacturer. The control module had to be modified in the stages of saturation, consolidation and cyclic loading. Several errors in post processing calculations are eliminated. The

contents of exported data were modified and extended. The most important points will be outlined in conjunction with the description of the respective test stages. The original configuration of the equipment could not be used to realise flushing through the soil sample. This procedure is commonly used and very helpful to improve saturation. Details will be discussed further in section 6.4.2.

Remote controlled testing

Once the sample is installed and the test is started, all important elements of the equipment are controlled and monitored by the personal computer. That is, saturation, consolidation, cyclic loading and, if requested, simple shearing are steered via the PC alone. This makes it possible to control and monitor the whole test procedure using common remote control software. Therewith the laboratory PC can be accessed through the internet from anywhere in the world. Especially for tests with long duration this can be very helpful. If the end of one test stage is reached, one can easily switch to the next stage without being necessarily physically present in the laboratory. When the test is finished, the loading system can be unloaded via PC as well. The exported data can be easily transferred to the PC logged in for further analysis.

6.4 Execution of a cyclic triaxial test

6.4.1 Sample preparation

Samples of 172*mm* in height and 99*mm* in diameter are used for all test series. Although a height-to-diameter ratio H/D between 2 and 2.5 is recommended in standard ASTM D3999-91, the smaller ratio of 1.74 is not seen as a problem. The lower height of the sample is related to the dimensions of the triaxial cell and the use of local strain transducers and internal load cell. To obtain enough space for axial movements and all cables of the transducers a smaller height of the sample is chosen. According to Lee (1978), experimental works led to the conclusion that reliable results could be obtained with H/D ratios in the range of 1.5 to 3. This statement is confirmed, for instance, by experimental and numerical studies of Bishop & Green (1965), Duncan & Dunlop (1968), Schanz & Gussmann (1994), Liyanapathirana et al. (2005) and Ravaska (2006).

The large samples with the mentioned dimensions are preferred to the smaller samples of 50*mm* in diameter in all test series since tests at small strain levels are to be carried out. To achieve the same strain on a large sample in comparison to a smaller one, larger deformations and higher loads have to be applied. In fact the deformation to be applied is twice as large to obtain similar strain and the load is four times larger to obtain similar stress as in 50*mm* samples. On this account the steering of the actuator is more accurate using larger specimens.

Influence of the specimen preparation technique on cyclic triaxial test results

Since it is very difficult to preserve undisturbed samples of the investigated material and facing the fact that many tests are to be carried out, all tests are performed on reconstituted specimens. Several preparation methods to reconstitute sand specimens are known. Mostly dry or wet pluviation (Mulilis et al.,1977; Chaney & Mulilis, 1978; Levacher et al., 1994; Fretti et al., 1995; Wichtmann, 2005 etc.) or dry or moist tamping methods (Mulilis et al., 1977; Ladd, 1978; Van Impe, 1981; Thooft, 1991; Yoon, 1991; Mengé, 1994; Vanden Berghe, 2001 etc.) are used. However, it is a well known fact that different methods of reconstituting samples to identical density produce samples with different structures and behavioural characteristics, Yoon (1991). Thus it is important to be able to reproduce the same density and soil fabric of specimens according to the purpose of the research.

The effect of different sample preparation methods on the cyclic behaviour of sands was reported for instance by Ladd (1974), Silver et al. (1976), Mulilis et al. (1977) and Ladd (1978). They all have indicated that the manner in which a sand was prepared to a given density may have a major effect on its liquefaction and settlement characteristics. Yoon (1991) also mentions effects of the preparation technique on the slope of the steady state line. In stress controlled loading the specimen built using the undercompaction (or equal volume) method gives lower undrained steady strength than a sample built by using pluviation (or equal energy) methods, whereas the effect of specimen preparation technique was not observed for strain-controlled loading. Although all the mentioned effects are investigated in relation to static tests or tests on liquefaction problems with a relatively small number of loading cycles, similar influences are expected in long term cyclic triaxial tests on strain accumulation with a very large

number of cycles. To the author's knowledge the influence of the specimen preparation technique on strain accumulation under long term cyclic loading has not been investigated so far. This is related to the fact that only few people did experimental studies in the field of such tests. Further investigations on that topic are seen as necessary and helpful.

Specimen preparation using moist tamping with undercompaction

Good experiences in preparing samples of sand of Mol have been made at the Laboratory of Geotechnics at the Ghent University using moist tamping with undercompaction. The advantage of this method is that each layer of the sample can be prepared at the same density. Thooft (1991) investigated both, dry pluviation method and moist tamping, regarding repeatability of tests and homogeneity of samples. Significant advantages or disadvantages where observed in neither of both preparation methods. From literature study and own experience, it is decided to use the undercompaction method for preparation of soil samples in all test series. This technique allows preparation of samples with arbitrary relative densities and gives sufficient results in homogeneity and repeatability.

The fundamental idea for the undercompaction method and tests using this technique where first described by Ladd (1978). Since then the technique is used by a large number of researchers, sometimes with modifications. The method offers an improved technique to prepare reconstituted specimens and is supposed to lead to more consistent and repeatable test results. The main difference to other commonly used compaction methods is the application of different compactive effort to each layer. It takes into account the fact that when a typical sand is compacted in layers, the compaction of each succeeding layer can further densify the underlying layers.

Vanden Berghe (2001) proved the repeatability of cyclic triaxial tests and discussed the homogeneity of samples prepared using undercompaction after a small number of cycles applied in a cyclic triaxial device. He observed weaknesses at the extremities of the sample but highly homogenous characteristics in the centre part of the specimen. The weaknesses on the one hand can be related to the cyclic testing, on the other hand to the method used to investigate the samples. In fact he froze samples to investigate the distribution of density and water content, which may have led to redistributions caused by cryogenic suction. The use of (reliable) local

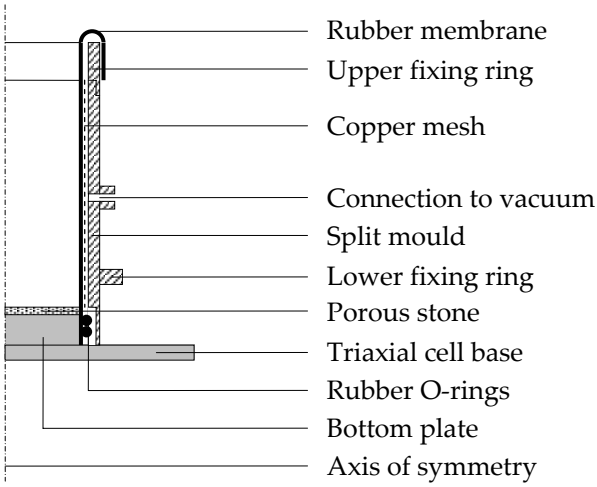

Figure 6.4-1: Scheme of installed internal split mould

strain measurements at the centre of the sample, however, is seen as a good option to minimize influences of possible errors at the edge of the sample.

To prepare specimens, a three-part internal split mould was built that is placed around the bottom plate at the triaxial cell base. It covers a rubber membrane fixed with O-rings at the bottom plate. The rubber membrane is placed over the split mould as shown in Figure 6.4-1 and a vacuum is applied to suck the membrane in a way that it rests smoothly against the split mould. To achieve uniform suction between split mould and rubber membrane, all contact areas of single parts of the split mould are sealed with silicone. A fine mesh of copper is mounted around the whole cylinder at the inside of the split mould to allow for equal distribution of the negative pressure. A porous stone is placed on the bottom plate. Two fixing rings hold the three parts of the split mould together, while the upper one is used as prolongation of the mould to improve preparation of the final layer.

As described in section 6.2 the initial water content for sample preparation lies in the range of 10 to 12%. The total wet mass W_T of the sample in grams is easily determined by multiplying volume of the split mould (diameter D and height H in m) and initial unit weight (initial dry unit weight $\gamma_{d,i}$ in kN/m^3 and initial water content w_i as digit) of the soil,

$$W_T = \frac{\gamma_{d,i}}{9.81 m/s^2}(1+w_i)\frac{\pi}{4}D^2 H\,. \tag{6.1}$$

The number of layers for compaction is chosen to twelve. Therewith the height of each layer is in the requested range of 12 to 25*mm*. Since homogenous samples are to be produced, each layer must have the same mass W_L, calculated by the simple equation $W_L = W_T / n_T$ with n_T the total number of layers. Specific in the undercompaction method is that the single layers are not immediately compacted to the requested (equal) height. Furthermore it takes into account the fact that the compaction energy from fabrication of following layers is partly dissipated to previous layers and therewith generates further compaction.

The percentage of undercompaction U_n for layer n is defined by the selected degree of undercompaction for the initial layer U_1 (as a percentage), the selected degree of undercompaction for the final layer U_{nt} (usually zero) and the total number of layers. The linear relation is defined as

$$U_n = U_1 - \left[\frac{U_1 - U_{nt}}{n_T - 1}(n-1)\right]. \tag{6.2}$$

The total height of the sample after compaction of layer n, h_n, is given by

$$h_n = \frac{H}{n_T}\left[(n-1) + \left(1 + \frac{U_n}{100}\right)\right]. \tag{6.3}$$

To specify the undercompaction degree of the initial layer, U_1, it is recommended to perform a series of similar tests with different initial values of undercompaction. For the sand of Mol an empirical formula based on several tests at different relative densities is proposed by Van Impe (1981):

$$U_1 = 18 - \frac{D_r}{5}. \tag{6.4}$$

Therein D_r is to be entered as value of percentage. On the one hand equation (6.4) contains the easily traceable conclusion that for loose samples the initial undercompaction degree should be higher than for dense samples. On the other hand it also confirms the statement of Ladd that for very dense specimens, negative values for initial undercompaction may be required.

On the accuracy of tamping procedure and measurements during sample preparation

In the literature it is clearly stated that much care has to be taken on the accuracy of sample preparation. In fact Ladd asks for an accuracy of height measurements for each layer to the nearest 0.02*mm*. A glance on his results of tests on the liquefaction potential of Monterey sand No. 0 proves how important that high accuracy is. The investigated samples were built in eight layers and had a diameter of 74*mm* and a height of 152*mm*. Table 6.4-1 shows the number of cycles to initial liquefaction in relation to the undercompaction degree of the first layer. An optimal initial undercompaction degree can be verified at 4 to 6% where the maximum liquefaction resistance is achieved.

U_1 [%]	Number of cycles to initial liquefaction [-]	U_1 [%]	Number of cycles to initial liquefaction [-]
0	24	10	22
2	22	12	19
4	33	14	30
6	33	16	18
8	20	18	10

*Table 6.4-1: Initial liquefaction in relation to the undercompaction degree (*Ladd, 1978*)*

A very small deviation of the layer height, however, may lead to significant different behaviour of the sample. An initial undercompaction degree of 4% instead of 2% causes a change in the liquefaction resistance of 50%, likewise a change from 6% to 8% initial undercompaction produces

similar differences. At higher initial undercompaction degrees this effect is observed as well. A change of 2% in initial undercompaction corresponds to a difference in height of the first layer of 0.38*mm* (roughly similar to the grain diameter D_{50} = 0.36*mm*) and even less in each following layer. In fact, looking at the example of Ladd, the difference in the final layer is less than 0.05*mm*. This clearly demonstrates how sensitive the reconstituted sample reacts on cyclic loading.

On this account huge effort was done in construction of a tamper guidance and a tamping rod in order to be able to build samples with much care and very high accuracy as well as to ensure the repeatability of sample preparation. Figure 6.4-2 shows a scheme of the manufactured equipment. The system consists of tamper, lower and upper tamper guidance, a height adjustment for the tamper and a measuring supporting mark for accurate measurements. The whole system is installed on the cell base where the split mould is installed as described above.

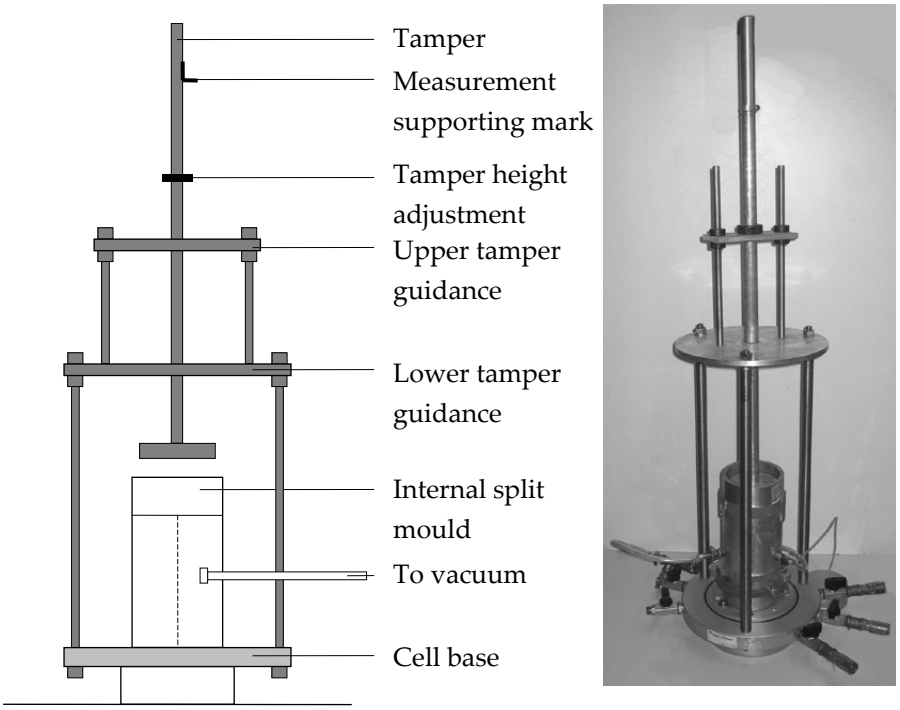

Figure 6.4-2: Scheme of tamper guidance with tamping rod

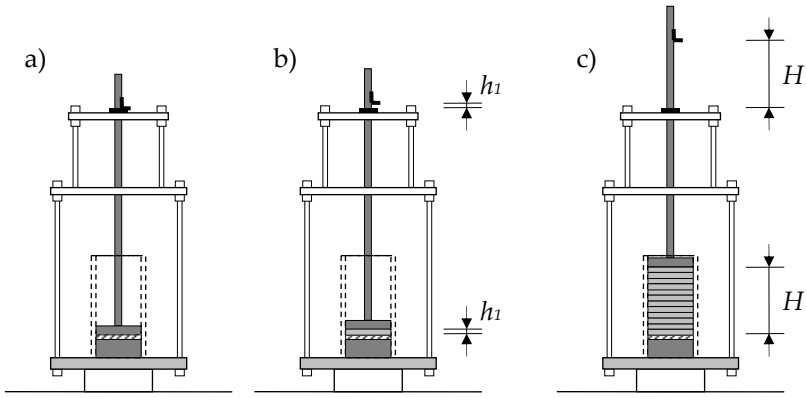

Figure 6.4-3: Height measurement of soil layers during sample preparation

Before the sample preparation is started, the height measurement supporting mark is adjusted to the zero level, i.e. to the top of the lower porous stone inside the split mould as shown in Figure 6.4-3a). The height of each layer can now be measured to high accuracy outside the split mould as presented in Figure 6.4-3b) and c). Therewith measurement errors are minimised to a large extend. After sample preparation the tamper system is removed and upper porous stone and top cap are placed on top of the sample.

During transport of cell base and sample to the loading frame, the sample is supported by the split mould. Before the split mould is removed, vacuum is applied to the sample in order to stabilize it. If used, local strain transducers are installed. Since they are glued on, the sample has then to rest a few hours to let the glue harden. The triaxial cell is installed and filled with water. Afterwards the loading piston is connected to the top cap and all transducers are connected to the CDAS. Finally the negative pressure inside the sample is increased to the atmospheric pressure and replaced by a confining pressure of about $30kPa$.

6.4.2 Saturation

All tests in the framework of this research are carried out on fully saturated samples. The reason therefor is seen in the fact that most of the soil usually lies below the ground water level and therewith is saturated anyway. Furthermore volume change measurements of the pore water leaving or

entering a fully saturated sample during consolidation and drained cyclic loading in laboratory tests are much easier compared to dry or partially saturated samples, where the volume change of the sample comes along with a change of the air volume in the voids. Volume change measurements allow for calculation of radial strains and provide a good double check for local strain measurements.

Although Wichtmann et al. (2005a) states no significant differences in tests comparing results of dry and saturated samples, it is seen as recommendable, however, to further investigate the influence of the saturation degree on dynamic properties and strain accumulation especially at higher loading frequencies.

The saturation procedure is executed in two steps. First a flushing procedure is applied to the sample to replace air in the voids by CO_2 and deaired water, respectively. In the second step back pressure saturation is used to drive remaining air into solution.

Saturation due to CO_2- and water flushing

During construction and installation of a sample, air is introduced in the system. Since the undercompaction method uses only partially saturated material for sample preparation, the amount of air is comparatively high and back pressure saturation alone does not lead to sufficient saturation degrees, as described below.

Thus state of the art to saturate a sample is first to flush the specimen with CO_2 from the bottom to the top. Since CO_2 is heavier it replaces the air in the voids of the sample. Further on CO_2 is better solvable in water, whereby a lower back pressure is required to drive a similar volume into solution. In the original configuration of the equipment this flushing was not possible since only back pressure saturation was envisaged. That is, additional equipment had to be installed in order to introduce the CO_2 access to the bottom of the sample and to allow for a controlled flow to the top of the sample.

During the flushing procedure the sample is still supported by the previously applied low cell pressure. Therewith the CO_2 may be led through the sample at very low pressure without danger to destroy it. Valves V1 and V3, shown in Figure 6.4-4, are therefor opened while valve V2 is kept closed. Air and flushed through CO_2 escape to the atmosphere. After about one

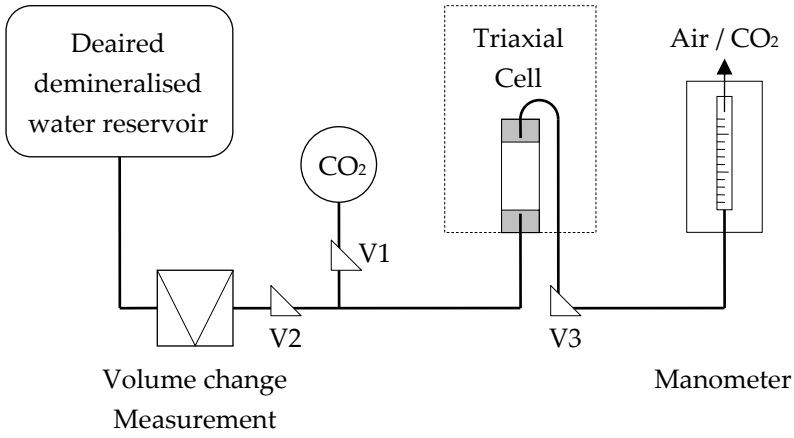

Figure 6.4-4: Scheme of flushing procedure for saturation of a sample

hour the air inside the voids of the sample is assumed to be replaced by CO_2 for the most part.

After the CO_2 flushing the sample is flushed with deaired water replacing the biggest part of gas. During this procedure valve V1 is closed while V2 is opened. For later analysis it is of crucial importance to measure the amount of water entering and leaving the sample during this stage. Only one volume change measuring unit was available in the original configuration, though. It is used to measure the amount of water entering the sample from the water reservoir. After some time the water filled the voids and leaves the sample on top. The amount of water leaving the sample can be measured by an additional installed manometer as outlined in Figure 6.4-4 as well.

The principle of back pressure saturation

The principle of back pressure saturation works with the fact that air is generally solvable in water. The higher the pressure applied to the water, the higher the amount of air being solved. During back pressure saturation the so called *Skempton factor* or *B* value is used as indicator for the degree of saturation. The *B* value is calculated by dividing the increase of pore water pressure Δu by the causative cell pressure increment $\Delta\sigma_3$,

$$B = \frac{\Delta u}{\Delta \sigma_3}. \tag{6.5}$$

To determine the *B* value the sample drainages are closed and a cell pressure increment is applied. According to the degree of saturation this will cause an increase of pore water pressure. When an equilibrium is reached, the *B* value can be calculated with equation (6.5). If the pore pressure continues to increase, this indicates a leakage in the rubber membrane surrounding the sample and the test should be abandoned and restarted with a new sample. If the pore pressure starts to decrease, even after an initial increase, it should be prevented from dropping by going to the next saturation step.

The *B* value assumes a certain cell pressure increment causing a similar increase in pore water pressure as the sample is fully saturated, i.e. if $B = 1.0$ the sample is assumed as fully saturated. Values below 0.95 indicate insufficient saturation and call for a higher back pressure. There is common agreement that *B* values higher than 0.95 achieved in practice indicate a saturation degree of 100 %.

It should be emphasised that the *B* value is not equivalent to the saturation degree. It only states that, depending on the saturation degree, a certain amount of the applied cell pressure increment is transferred to the pore water. This is because closed drainage valves produce undrained conditions and therewith the pressure cannot decrease due to a volume change. In partially saturated samples some portion of the cell pressure is absorbed by compressible air in the voids, i.e. not the complete cell pressure increment is transferred to the pore water and thus $B < 1.0$. On the other hand if there is no air in the voids anymore the whole cell pressure increment is transferred via the grains to the pore water, that is $B = 1.0$.

Accordingly a *B* value of 1.0 indicates a saturation degree of *S*=100%, whereas lower *B* values in general cannot clearly be linked to a certain saturation degree. The *S*-*B* relation depends on compressibility, fabric, permeability, density and compactness of packing of the soil. Thooft (1991) summarises the results of several authors who investigated these relations for sand.

Table 6.4-2 clearly demonstrates the difficulty to link a lower *B* value to a certain degree of saturation. However, it can be assumed that *B* values larger than 0.85 indicate a saturation degree of at least 99.5 %. In the present investigation, values higher than 0.85 are seen as indicator for sufficient saturation. Therewith sufficient accuracy is ensured (the maximum

error in volume change is 0.5 % during saturation) in the case of drained tests.

Saturation degree	Loose sand	Middle dense sand	Dense sand
S [%]	B [-]	B [-]	B [-]
98.0	0.53	0.45	0.38
98.5	0.60	0.53	0.47
99.0	0.69	0.62	0.56
99.5	0.85	0.80	0.75
100.0	1.00	1.00	1.00

Table 6.4-2: B value in relation to the saturation degree S

Applied procedure of back pressure saturation

The application of back pressure saturation alone will often require very high values of back pressure especially for reconstituted specimens of granular material with a large amount of air-filled voids. On the one hand this reduces the capacity of the equipment to apply effective stresses to the sample since these stresses are to be applied additionally to the back pressure. On the other hand the risk of leakages is increased as well.

Thus a combination of back pressure saturation and the above described saturation due to flushing is seen as appropriate to achieve sufficient saturation degrees. The amount of air in the voids is rapidly decreased by the flushing with water. Furthermore the remaining air is replaced by CO_2, much better solvable in water. In this way a significant reduction of the required back pressure is realised.

Cell pressure increments of $35kPa$ are applied. The differential pressure between cell and back pressure is chosen to $5kPa$. This is the minimum difference recommended by Head (1998). Care must be taken that the maximum differential pressure during saturation never exceeds the confining pressure applied during consolidation to avoid overconsolidation of the sample. The used procedure is recommended in the standards ASTM D3999-91 and ASTM D5311-92 for cyclic triaxial testing.

The general procedure of back pressure saturation used in the frame of this research is described with the aid of the diagram in Figure 6.4-5. The herein frequently used second index i of $u_{b,i}$ and $\sigma_{3,i}$, respectively, denotes the step of saturation. The saturation is started with an increase of the cell pressure to $\sigma_{3,1} = 35kPa$. The initially low positive pore pressure u_0, resulting from the flushing procedure, should show a small increase to u_1. However, since a low cell pressure, $\sigma_{3,0}$, already was applied during the flushing procedure, this increment is not used for calculation of the B value. Next the back pressure is increased to $u_{b,1} = 30kPa$ considering the differential pressure of $5kPa$. After the drainage valve to the bottom of the sample is opened, a volume change can be detected. When the system stabilised, the drainage valve is closed and the next saturation step is started

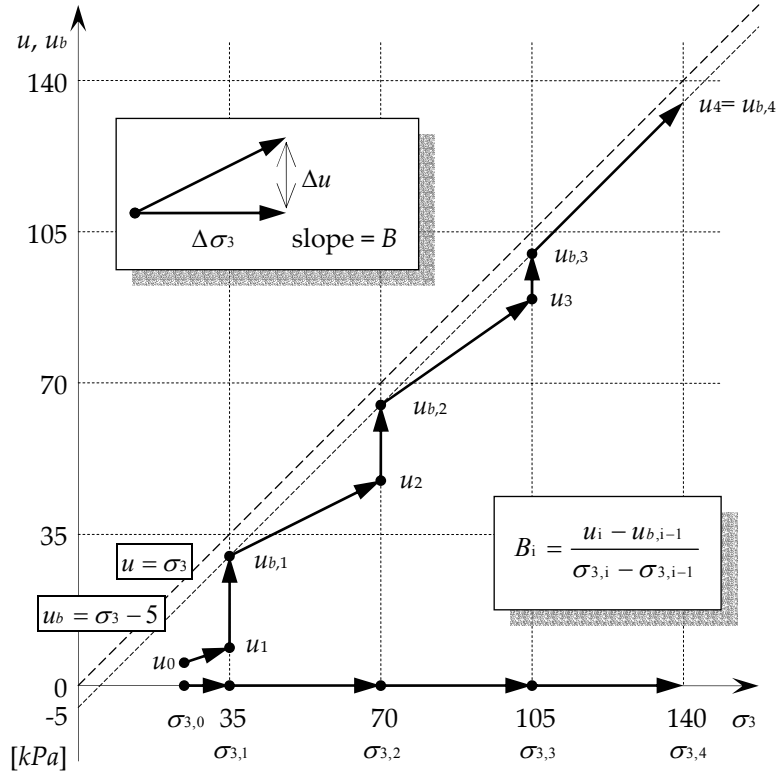

Figure 6.4-5: Plot of pore pressure u, back pressure u_b and cell pressure σ_3 during saturation stage

in a similar way.

Applying another cell pressure increment causes an increasing pore pressure. When the system stabilised (after about one minute) the B value is determined according to equation (6.5). The second back pressure increment is applied. While the bottom drainage valve is opened to the sample, the volume change is recorded again. After the drainage valve is closed, the third and final saturation step is applied. During this procedure the cell pressure is increased to $\sigma_{3,3} = 105kPa$. Accordingly the usual final back pressure is $u_{b,3} = 100kPa$. Corresponding B value and volume change are recorded.

After the third back pressure saturation step the sample is set to a rest for several hours, allowing the remaining CO_2 to solve in the deaired water. After this interruption another cell pressure increment is applied increasing the cell pressure to $\sigma_{3,4} = 140kPa$. Usually at this time a high B value is detected indicating sufficient saturation. In all tests presented in this work B values larger than 0.85 are achieved.

The amount of water that entered the sample during both, saturation due to water flushing and back pressure saturation, has to be recorded very carefully. It can be well used as a double check to calculate the saturation degree when saturation is finished. The change of water content during the whole saturation procedure Δw_s can be determined by

$$\Delta w_s = 1.0kg/m^3 \frac{\Delta V_f + \Delta V_b}{m_d}, \tag{6.6}$$

wherein ΔV_f the volume change during flushing procedure, ΔV_b the volume change during back pressure saturation and m_d the dry mass of the specimen. For fully saturated samples

$$w_s = w_i + \Delta w_s \tag{6.7}$$

must hold. In the test series carried out in this study good agreement of calculated and measured saturation water content is achieved.

6.4.3 Consolidation

During the consolidation process the specimen is maintained in an isotropic or other known state of stress according to the test specification. The static

load on the piston to maintain an isotropic consolidation is applied automatically by the controlling software of the system. With the specimen drainage valves closed, the maximum back pressure $u_{b,3}$ is held constant and the chamber pressure is increased until the difference between chamber and back pressure equals the desired effective consolidation stress. For anisotropic consolidation an additional axial stress is applied to the specimen.

Since fully saturated samples are tested, the applied confining pressure initially is completely transferred to the pore water and the pore pressure is increased, $\Delta u = \Delta\sigma_3$. After the system stabilised, the specimen drainage valve is opened and therewith drainage is allowed. The pore water is squeesed out of the sample, leading to dropping of the pore pressure to the back pressure level. The resulting volume change comes along with a reduction of the pore volume of the specimen, i.e. it is densified in dependence of the confining pressure applied.

During anisotropic consolidation an additional axial load in compression leads to a decrease of the pore water pressure increase. This behaviour may look surprising since the mean effective stress $p = (\sigma_1 + 2\sigma_3)/3$ increases. Accordingly one would expect an increase of u. However, this effect can be explained by the formula Skempton (1954) proposed to determine the pore water pressure under axisymmetric conditions,

$$\Delta u = B\left[\Delta\sigma_3 + A\left(\Delta\sigma_1 - \Delta\sigma_3\right)\right]. \tag{6.8}$$

In equation (6.8) B is the Skempton factor, being 1 for saturated soils. A is an excess pore water pressure coefficient in the range of -0.5 to 1.0. For strongly compacted samples parameter A may be negative, see also Budhu (2000). Thus negative changes in pore pressure may occur during the application of deviatoric stresses.

The consolidation stage is finished when the system stabilised under drained conditions, that is, when the pore pressure adjusted to the back pressure level and stays stable and the volume change is zero. The time needed depends on the type of soil and its permeability. The sand of Mol samples are consolidated after about one hour.

6.4.4 Cyclic loading

As the specimen is set under the requested stress conditions, cyclic loading can be applied. The equipment allows for a wide range of axial cyclic loading options. According to settings made in the control software, standardised as well as user defined tests can be run. The controlling and data acquisition software provides certain predefined test options according to standard ASTM D3999-91 (method A or B) and standard ASTM D5311-92, respectively. After these standards the cyclic loading is to be performed under undrained conditions with a fixed number of cycles. Thus only initial stress conditions, loading frequency and stress or strain amplitude have to be defined. During cyclic loading the average confining pressure is held constant automatically. The cyclic load is to be applied with a sinusoidal waveshape following several recommendations and regulations according to the mentioned standards.

In the frame of this research the main point of attention is set on user defined long term tests with large numbers of cycles. User defined tests allow for much more loading options as number of cycles, shape of the cyclic loading and drainage conditions can be freely chosen additional to the previously mentioned parameters. Tests according to standard ASTM D3999-91 are carried out as well. Analysis tools for these tests are developed. Liquefaction tests as defined in standard ASTM 5311-92 are not matter of the current study and thus will be outlined only shortly.

Cyclic loading after ASTM D5311-92

Standard ASTM D5311-92 describes a test method for the investigation of the load controlled cyclic triaxial strength (also called the liquefaction potential) of soil using the cyclic triaxial testing apparatus. This test method fits for undisturbed as well as for reconstituted soil samples and is generally applicable for testing cohesionless free draining soils of relatively high permeability. After standard ASTM D5311-92 the specimen is loaded cyclically with the first cycle applied in compression. The load is to be cycled until either the cyclic double amplitude vertical strain exceeds 20%, the single amplitude strain in either extension or compression exceeds 20%, 500 load cycles are exceeded, or the load wave form deteriorates beyond acceptable values.

In this research mainly drained tests are carried out, investigating the accumulation of strain caused by long term cyclic loading. Since very low strain levels are investigated, liquefaction effects are not decisive.

Cyclic loading after ASTM D3999-91

Standard ASTM D3999-91 describes methods for the determination of the modulus and damping properties of soils using the cyclic triaxial apparatus. This standard provides two test methods. Method (A) permits the determination of the Young's modulus *E* and the damping ratio *D* using a constant cyclic load. Method (B) permits the determination of *E* and *D* using a constant cyclic stroke. As discussed in section 3.4.3 for undrained conditions the shear modulus *G* instead of *E* easily can be determined by using shear stress τ and shear strain γ instead of axial stress σ_1 and axial strain ε_1 to plot the hysteresis loop. The test methods fit for undisturbed as well as for reconstituted soil samples of both fine-grained and coarse-grained material. The amplitude of the cyclic load can be given either by the stress or the strain level to be applied to the specimen. After standard ASTM D3999-91 the specimen is loaded cyclically with 40 cycles and the first half cycle in compression.

For interpretation of test data the resulting hysteresis loops are analysed according to the procedure described in section 3.4.3. For each cycle the hysteresis loop area is needed for calculation of *D*, see equation (3.55). For this the Gauss trapezium algorithm as described in Witte &

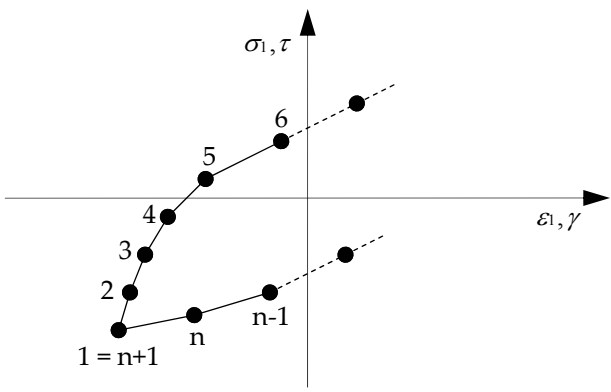

Figure 6.4-6: Calculation of loop area using the Gauss trapezium algorithm

Schmidt (1995) is used. Therefor the coordinates of the sampling points have to be assigned clockwise and successive as shown in Figure 6.4-6. For the sake of simplicity point 1 is used as offset, i.e. its coordinates coincide with the origin. After the convention point n+1 = point 1 the loop area A_{loop} can be calculated as follows:

$$A_{loop} = \frac{1}{2}\sum_{i=1}^{n}\left[\left(\sigma_1\right)_i - \left(\sigma_1\right)_{i+1}\right]\left[\left(\varepsilon_1\right)_i + \left(\varepsilon_1\right)_{i+1}\right]. \tag{6.9}$$

The correctness of the results derived from equation (6.9) is validated due to comparison with another method to calculate the loop area used in the control and data acquisition software. There the area of the surrounding rectangle of the hysteresis loop is calculated first. Then the areas above and below the hysteresis loop are calculated and subtracted from the rectangle area. Therewith the loop area is determined as well. Formulation (6.9), however, is preferred since it is well programmable and thus used for analysis.

The coordinates of the barycentre *O* of the hysteresis loop, $\varepsilon_{1,O}$ and $\sigma_{1,O}$, can be calculated in a quite similar algorithm,

$$\begin{aligned}\sigma_{1,O} &= \frac{1}{6}\sum_{i=1}^{n}\left[\left(\sigma_1\right)_i^2 + \left(\sigma_1\right)_i\cdot\left(\sigma_1\right)_{i+1} + \left(\sigma_1\right)_{i+1}^2\right]\left[\left(\varepsilon_1\right)_{i+1} - \left(\varepsilon_1\right)_i\right] \Big/ A_{loop} \\ \varepsilon_{1,O} &= \frac{1}{6}\sum_{i=1}^{n}\left[\left(\varepsilon_1\right)_i^2 + \left(\varepsilon_1\right)_i\cdot\left(\varepsilon_1\right)_{i+1} + \left(\varepsilon_1\right)_{i+1}^2\right]\left[\left(\sigma_1\right)_i - \left(\sigma_1\right)_{i+1}\right] \Big/ A_{loop}\end{aligned}. \tag{6.10}$$

The barycentre needs to be calculated for further analysis: to determine *D* the triangle area $A_\triangle$ assigned in Figure 3.4-1 is to be calculated, defined by the barycentre and the maximum point of the hysteresis loop. The auxiliary parameters *S* and *L* therewith can be determined from $S = \sigma_1^{\max} - \sigma_{1,o}$ and $L = \varepsilon_1^{\max} - \varepsilon_{1,o}$. The respective meaning of A_{loop}, $A_\triangle$, *O*, $\varepsilon_{1,O}$ and $\sigma_{1,O}$ is illustrated in Figure 3.4-1.

User defined cyclic loading

Beside the predefined loading options, user defined settings can be made. In this case it is possible to use several waveshapes for the cyclic loading. Triangular waveshapes as well as pulses are possible to apply. Also self-programmed waveshapes are applicable. The operator can choose between drained or undrained loading, number of cycles, and termination stress or

strain. The load can be applied alternatively in compression and extension, compression only, or extension only.

In this study mainly user-defined tests are carried out. These tests are characterised by a high number of applied cycles under drained conditions. Sinusoidal waveshapes in compression and extension are applied at different stress levels, loading frequencies and densities of the sample. The detailed test program and results are presented in Chapter 7.

6.5 Combined bender element testing

6.5.1 Working principle of bender element tests

Bender elements are mostly used to measure shear wave velocities of soil in the time domain. A pulse is emitted by one bender element (transmitter) and the travel time is determined when the pulse arrives at the second bender element (receiver), with the tip located at a known distance from the tip of the transmitter. The shear strain of a bender element generated pulse is less than 10^{-3}% and thus can be assumed as elastic strain in the soil. Karl (2005) gives a state of the art overview on bender element techniques and methods to determine the time of wave travel using time and frequency domain techniques.

In general transmitter and receiver elements are placed at each end of a specimen. Bender elements are made of piezoelectric materials exhibiting changes in dimensions when subjected to a voltage across their faces as shown in Figure 6.5-1. The other way around they produce a voltage across their faces when distorted. Each element consists of two thin piezoceramic plates rigidly bonded to a central metallic plate. Two thin conductive layers, electrodes, are glued externally to the bender. The polarisation of the ceramic material in each plate and the electrical connections are such that one plate elongates and the other shortens, when a driving voltage is applied to the element.

An electrical pulse applied to the transmitter causes it to bend rapidly and produces a shear wave (s-wave) travelling through the specimen towards the receiver. When the s-wave reaches the receiver, the element is forced to bend and it generates a voltage pulse that can be measured through the wires leading to the element. Bender elements

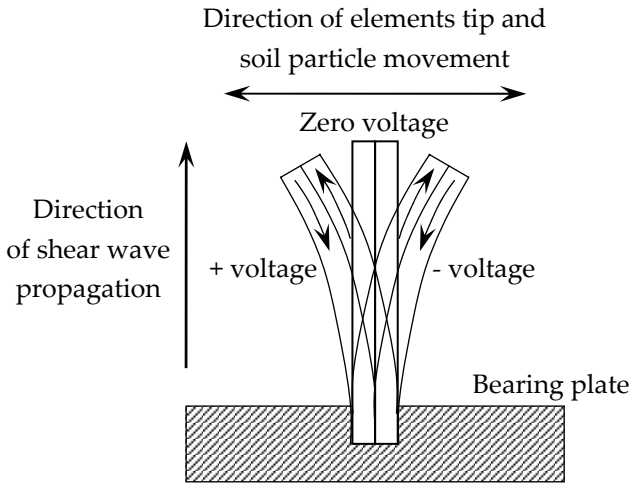

*Figure 6.5-1: Working principle of a bender element (*Kramer, 1996*)*

penetrate the sample a couple of millimetres. The s-wave speed V_s is calculated from travel time t_t and known tip-to-tip distance $h_{t\text{-}t}$ between transmitter and receiver,

$$V_s = \frac{t_t}{h_{t-t}}. \tag{6.11}$$

The two polarised plates of an element can be connected in series or parallel. The series version generates higher output at an applied distortion and is thus better to use as receiver. The parallel version has an additional electrode between the two piezoceramic plates and is better used as transmitter because it generates the largest distortion at an applied input, see Figure 6.5-2.

Since the specimens are not disturbed during bender element tests – as mentioned the generated s-waves lie in the elastic strain range –, they are suited optimally for combination with other laboratory tests. The bender element test equipment can be easily installed in various soil testing devices, such as oedometer, simple shear test device and conventional triaxial test devices. In the present research bender elements are installed in bottom and top cap of the cyclic triaxial testing device as shown in Figure 6.5-3.

Being able to apply strains in a range of about 10^{-2} to 10% with cyclic triaxial tests, bender elements are seen as perfect complement to cover

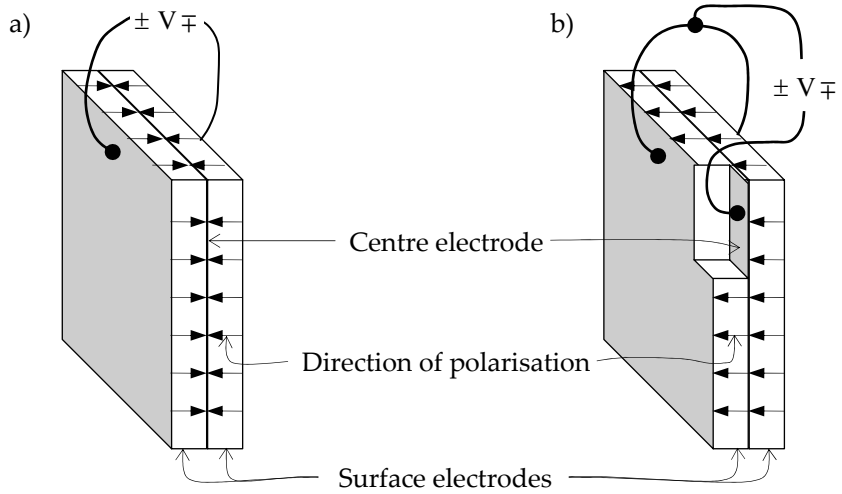

*Figure 6.5-2: a) series and b) parallel connected piezoceramic element (*Dyvik & Madshus, 1985*)*

the whole strain range from approximately linear elastic to strongly nonlinear elasto-plastic behaviour of soils. Performing bender element tests after consolidation, i.e. directly before cyclic loading, and after cyclic loading allows for detection of possible changes in the stiffness of the sample due to the cyclic loading process.

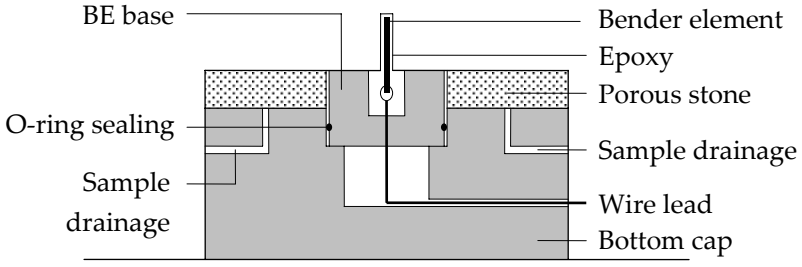

Figure 6.5-3: Scheme of bottom cap with bender element

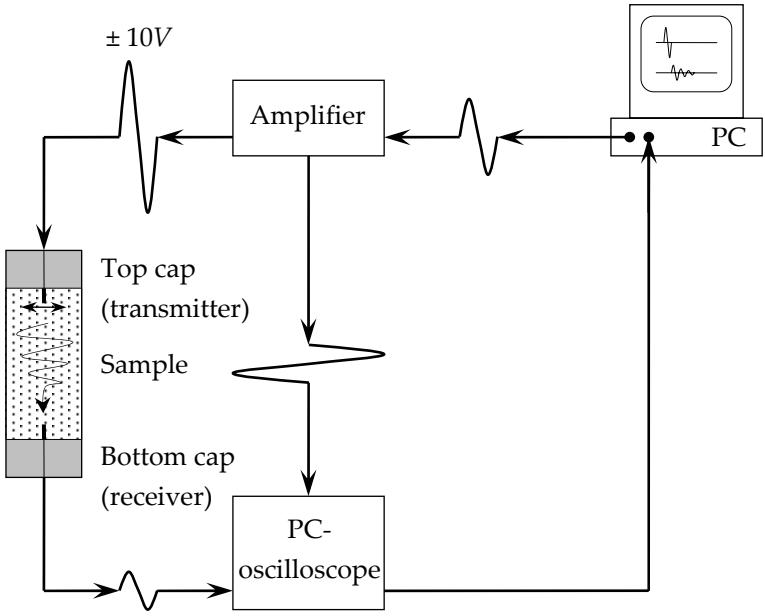

Figure 6.5-4: Scheme of bender element test equipment

6.5.2 Equipment

The bender element test equipment is installed completely separately from the cyclic triaxial control and data acquisition. Therewith bender element tests can be executed fully independent of cyclic triaxial tests. A scheme of the general test setup is presented in Figure 6.5-4.

A single sine-shaped pulse is used as input signal for the transmitter element. The signal generation is realised using the soundcard of the laboratory personal computer controlling the cyclic triaxial test. The sound card is steered by a MATLAB routine. This provides a very cost-effective way to produce signals of arbitrary characteristics. Sine pulses with the shape of a single sine cycle, however, are seen as nowadays most commonly used input signal for bender element tests. It simplifies the identification of the arrival time and opens the opportunity to study frequency dependencies on the signals.

The generated signal can be varied in frequency of the sine pulse and the number of pulses per second. Every bender element test is performed at four different frequencies in the range of 5 to 20kHz. These

values are basing upon own experimental experience and recommendations of Karl (2005) and Brignoli et al. (1996), for instance. Further on it has to be ensured that a signal does not influence previous measurements. That is, a time delay between constitutive pulses large enough to avoid overlapping effects has to be considered. On the other hand quick execution of tests is aspired. Ten pulses per second are seen as sufficient value. The output voltage of the soundcard is limited to about ± 5*V*, whereas the working voltage of the used bender elements is ± 10*V*. Thus the output amplitude of the soundcard has to be amplified to 10*V* (20*V* peak-to-peak amplitude) subsequently. This is done by an own developed power amplifier.

The output signal of the amplifier is sent to the transmitter element as well as to a PicoScope ADC-212/3 high resolution PC oscilloscope. Using a PC oscilloscope is a very favourable alternative to common oscilloscopes. Knowing the demands of the respective application, an adequate version can be chosen easily. The ADC-212/3 is able to capture two channels simultaneously. The sender signal is used as trigger for the oscilloscope. As soon as the sine pulse is generated the trigger function activates data acquisition and acquires the signals from amplifier (which is identical to the transmitter element signals) and receiver element. The collected data is continuously transferred to the personal computer by means of a USB interface. Immediate data processing using the provided PicoScope software as well as storage in a log file for later analysis is possible. To reduce signal noise an averaging function of the oscilloscope is used to average repetitions of the receiver signal. 256 single pulses are averaged and summarised to one signal for further interpretation.

6.5.3 Data analysis

The analysis of bender element tests follows the procedure described in Karl (2005) and Piriyakul & Haegeman (2004). For calculation of the s-wave velocity, the tip-to-tip distance and the travel time of the signal have to be known. The most commonly used technique to determine the latter parameter is simple visual interpretation since the s-wave velocity does not change with frequency.

The signal travel time is assumed as the time between the starting point O of the input voltage pulse to the transmitter and the first clear deflection in the output signal of the receiver element at point A, assigned in Figure 6.5-5. Depending on the bender element signals, the identification of

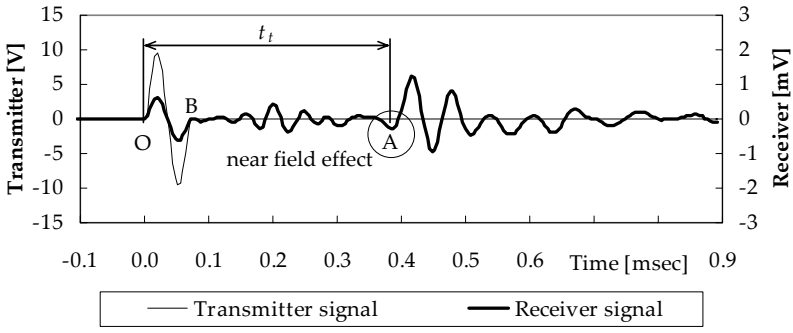

Figure 6.5-5: Typical bender element record from a sample of sand of Mol, transmitter signal frequency 15kHz

the first deflection point can be straightforward or difficult. The arrival point of the s-wave front can be masked by faster travelling p-wave components. This phenomenon is called the near field effect, in Figure 6.5-5 visible at point A, and is described by Karl (2005) among others.

Further on an inductive coupling effect between sender and receiver channel can cause difficulties in data interpretation. This effect can be seen in Figure 6.5-5 as deflection of the receiver signal when the transmitter signal is measured. Using higher frequencies reduces the difficulties caused by this effect since point B moves closer to point O and a clear distinction of points A and B becomes possible.

The visual identification of the arrival point A is done at each of the four frequencies used for the bender element test – 5, 10, 15 and 20*kHz*. The selected point has to be found in every signal at the same arrival time and is not allowed to move with the frequency. Point A is used as arrival point in all bender element tests performed.

After determination of the travel time, the shear wave velocity can be calculated by equation (6.11). For strain amplitudes in the elastic range, as generated by bender elements, the shear wave velocity can be used to calculate the dynamic shear modulus G_{max} applying equation (3.50), introduced in Chapter 3. The analysis of bender element test results is further discussed in section 7.2.1.

6.6 Conclusions

In the present work cyclic triaxial and bender element tests are carried out on reconstituted samples of sand of Mol, a typical soil in Flanders. In this chapter the investigated material is characterised.

For the execution of tests, an advanced cyclic triaxial testing apparatus combined with separate bender element test equipment is installed in the frame of the present work. Several shortcomings of the original, commercial configuration are detected and analysed. Upgrades, extensions and improvement of the problematic parts of the equipment finally led to a test setup allowing for reliable and accurate high-quality cyclic triaxial tests.

It turns out that the results achieved in cyclic triaxial tests strongly depend on the quality of sample preparation. Literature study and own experience led to the conclusion to use the undercompaction method after Ladd. Much effort is done to define a clear sample preparation procedure allowing for repeatable and comparable tests, eliminating as much random influences as possible. For this purpose a tamping tool is built allowing for exact preparation of the specimen.

To avoid very high back pressure levels to achieve saturation of the specimen, the back pressure saturation is combined with a flushing procedure. During this water saturation the biggest part of air in the voids is first replaced by CO_2 and afterwards by deaired, demineralised water. With the applied saturation procedure very good saturation degrees are achieved.

The testing device allows for isotropic and anisotropic consolidation and a wide range of standardised and user defined cyclic loading options. The combination with separately installed bender element test equipment is seen as good completion of the cyclic triaxial test. The study of the general working principle of bender elements and existing bender element solutions allowed for the choice of own equipment. The used implementation, the general execution of a bender element test and data analysis is outlined in this chapter.

Chapter 7

Experimental study of the elasto-plastic long-term behaviour of sand of Mol

7.1 Introduction

Cyclic triaxial and bender element tests are carried out to investigate both the elastic behaviour of the sand of Mol and the evolution of accumulated strains due to large numbers of load applications at small strain levels.

Bender element tests are used for determination of the maximum shear modulus G_{max}. This parameter was also determined out of resonant column tests in another study of Yoon (1991). Own results are compared with an empirical formulation proposed by Yoon to describe G_{max} as a function of the mean effective stress p and the void ratio e. The availability of the existing formulation to predict the maximum shear modulus out of bender element test results is checked.

Undrained standardised cyclic triaxial tests on reconstituted specimens are carried out to determine shear modulus G and damping ratio D at larger strain levels out of the hysteresis loops of load cycles. The influence of the strain level and the cyclic loading frequency is investigated with respect to their influence on the mentioned parameters. Drained cyclic triaxial tests are carried out to determine Young's modulus E and damping

ratio D out of hysteresis loops of load cycles at different strain levels and cyclic loading frequencies.

To investigate the evolution of the elastic parameters with the number of load applications, long-term tests under drained conditions with different cyclic loading options are carried out. These tests are also valid for the investigation of the evolution of hysteresis loops with the number of cycles. The accumulated residual strains are recorded and used for analysis of the accumulation behaviour under different cyclic loading options.

Final goal of the laboratory testing campaign on the one hand is the quantification of the influence of certain parameters like strain level, void ratio and cyclic loading frequency on the strain accumulation. On the other hand test results are used as a basis for determination of model parameters for the new accumulation model presented in Chapter 5. The parameter identification for the sand of Mol is described in another section of this chapter.

7.2 Elastic behaviour of the sand of Mol

7.2.1 Maximum shear modulus G_{max} out of bender element tests

Ten samples with identical size and void ratio are prepared in accordance with the procedure described in section 6.4.1, saturated and consolidated. Seven samples are pressurised with an effective mean pressure of $p = 300kPa$ and K_0 = 1, on three samples a mean effective stress of $p = 200kPa$ with K_0 = 0.5 is applied. On all samples bender element tests are performed to determine the maximum shear stiffness G_{max}.

Figure 7.2-1 exemplarily shows measurements of one bender element test. The interpretation of the signals at 10, 15 and 20kHz is easy since a clear common deflection point can be identified. The 5kHz signal is not as clear as the others. Combination of the signals at all frequencies, however, allows for identification of the deflection point in the 5kHz signal as well. The travel time of the signal now easily can be determined. In the presented example the time from the first deflection in the transmitter signal to the first simultaneous deflection in all receiver signals is 0.305$msec$.

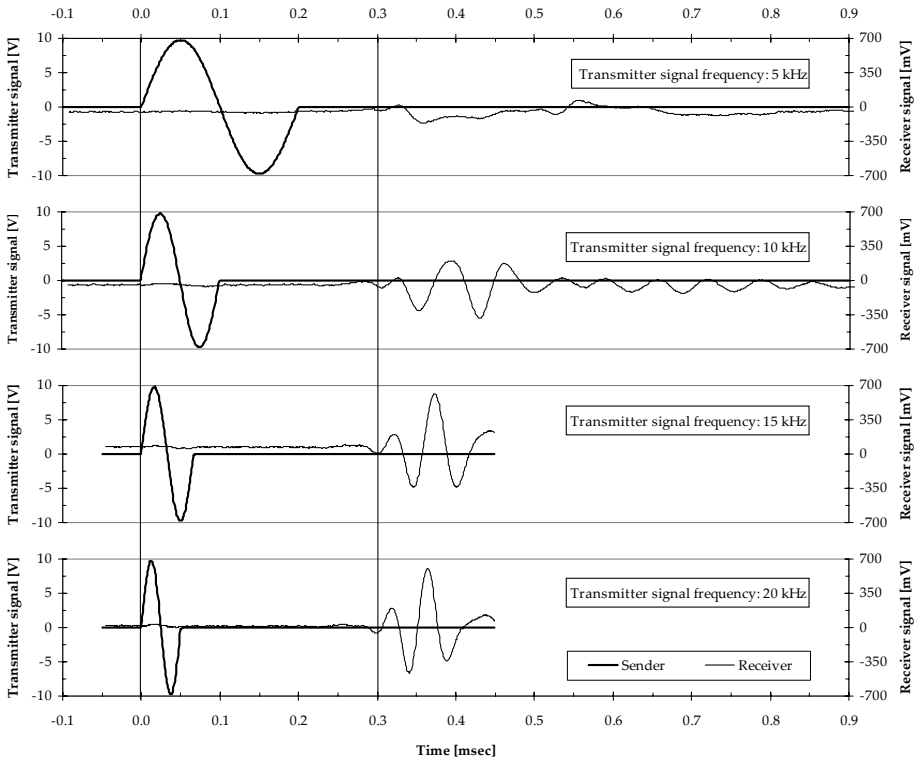

Figure 7.2-1: Example for bender element test signal analysis

Application of equations (6.11) and (3.50) allows for calculation of the maximum shear modulus.

Table 7.2-1 summarises the results of this test series. Small variations in the shear stiffness of different samples are caused by several influence parameters. Slightly different void ratios as well as minor structural differences in the samples may influence measurements. Further on inaccuracies of visual interpretation may manipulate test results. Nevertheless the reproducibility of tests is seen as proven with the presented test data.

The maximum shear stiffness of the sand of Mol was also investigated by Yoon (1991) with the aid of resonant column tests. He derived the empirical equation (3.51) for determination of G_{max} in relation to void ratio e and effective mean pressure p. For middle dense sands the dimensionless parameters S and n in equation (3.51) are determined to S =

Test	e	p	K_0	V_S	G_{max} (BE-test)	G_{max} (Yoon, 1991)
	[-]	[kPa]	[-]	[m/s]	[MPa]	[MPa]
300 – 1	0.717	300	1	274.9	147.7	149.1
300 – 2	0.716	300	1	265.9	137.8	149.3
300 – 3	0.713	300	1	278.4	153.0	150.1
300 – 4	0.710	300	1	291.1	167.9	150.9
300 – 5	0.707	300	1	292.4	167.3	151.4
300 – 6	0.714	300	1	274.1	147.5	149.8
300 – 7	0.710	300	1	286.5	160.5	150.9
200 – 1	0.740	200	0.5	241.1	116.0	119.1
200 – 2	0.709	200	0.5	230.9	109.1	124.8
200 – 3	0.729	200	0.5	256.9	133.1	121.1

Table 7.2-1: Maximum shear moduli a) out of bender element tests and b) after Yoon (1991)

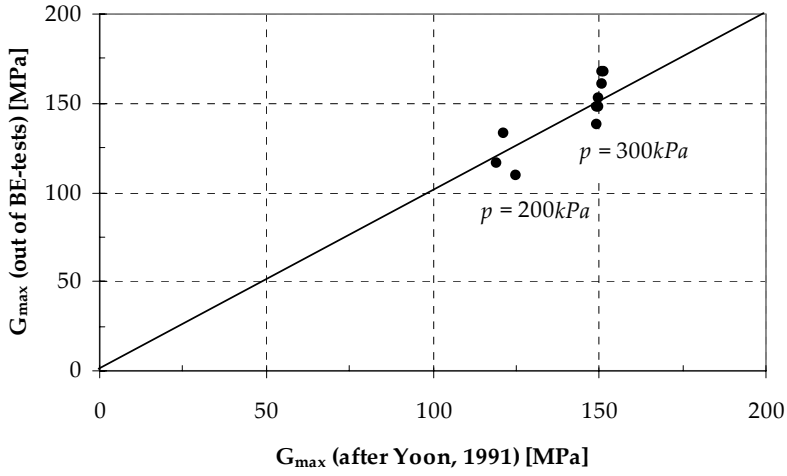

Figure 7.2-2: G_{max} out of bender element tests versus G_{max} after Yoon (1991)

584.7 and n = 0.47. The corresponding values of G_{max} for the tests performed in the present work are added in Table 7.2-1. Good agreement of bender element test results and predicted values out of equation (3.51) as well for isotropic as for anisotropic stress conditions is found as seen in Figure 7.2-2. The G_{max} determined out of bender element tests are measured values while G_{max} after Yoon (1991) is calculated from an empirical law. This explains the higher variability of the bender element test values.

The conclusion that the maximum shear stiffness out of bender element tests is comparable to results of resonant column tests confirms findings of Dyvik & Madshus (1985) who also performed both bender element and resonant column tests at the same soil and found good agreement of the two techniques. Accordingly equation (3.51) can be used to calculate the maximum shear stiffness of samples made of sand of Mol.

7.2.2 *G* and *D* at larger strains out of undrained cyclic triaxial tests

Strain dependency

Four cyclic triaxial tests are carried out on saturated and consolidated samples with identical size and void ratio, prepared in accordance with the procedure described in section 6.4.1. The samples are pressurised with an effective mean pressure of $p = 300kPa$ and $K_0 = 1$. The cyclic loading stage is executed in agreement with standard ASTM D3999-91 under consolidated undrained (CU) conditions to determine the hysteretic shear modulus G and the damping ratio D at different strain levels. The cyclic loading frequency is chosen to $0.5Hz$.

With the assumption of incompressibility of water, the shear strain γ easily can be obtained by equation (3.31) from axial strain measurements. Plotting the shear stress τ, equation (3.10), versus γ results in a hysteresis loop as sketched in Figure 3.4-1. Following the procedure described in section 3.4, G and D can be calculated. The results for the shear modulus are presented in a normalised diagram in Figure 7.2-3 and in Table 7.2-2. Use of the normalised presentation minimises the influence of varying void ratios and structural differences between the samples. Good agreement of test results with the $G-\gamma$ degradation curve, defined by equation (3.43) is found. Figure 7.2-4 shows the damping ratios of three of the four tests at

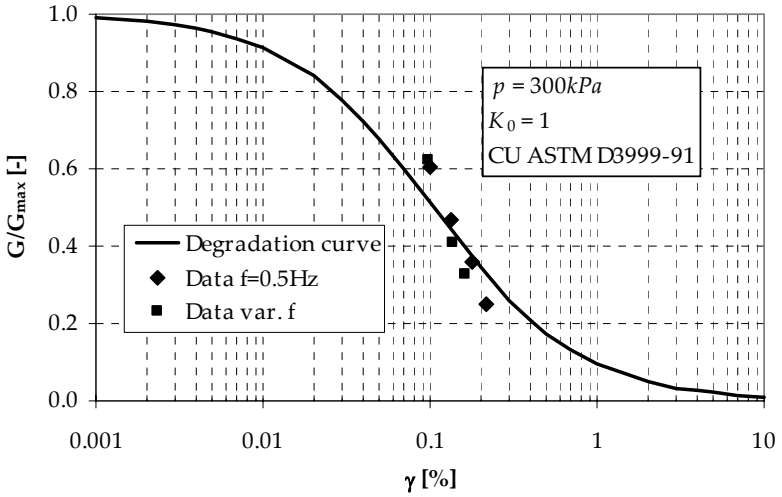

Figure 7.2-3: G out of CU cyclic triaxial tests at different strain levels and cyclic loading frequencies

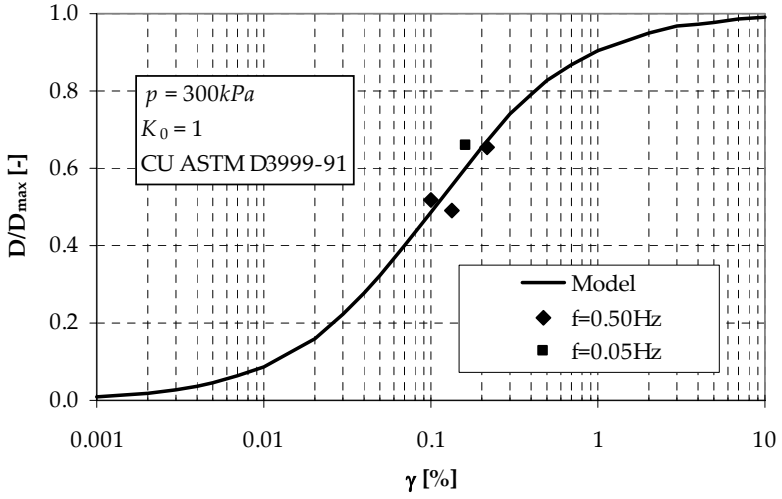

Figure 7.2-4: D out of CU cyclic triaxial tests at different strain levels and cyclic loading frequencies

different strain levels. Good agreement of test results and theory is found, showing increasing damping with increasing strains. D_{max} in Figure 7.2-4 and in Figure 7.2-7 is derived from equation (3.48) on the basis of the reference shear strain γ_r .

Frequency dependency

Three of the four cyclic triaxial tests are repeated on similar samples under identical test conditions, while the loading frequency was varied. Tests at 0.05, 5 and 10*Hz* are carried out, whereby the frequency increases with decreasing strain amplitudes to ensure good performance of the loading system. In the investigated range no influence of the loading frequency is detected. This coincides with findings of former research (van Impe, 1981) and is seen as validation of the performed tests. Similar tests at similar strain levels result in similar soil stiffness for varying loading frequencies. The corresponding data are added in Figure 7.2-3 and in Table 7.2-2. All data received at different loading frequencies fit well in the series of measurements with a constant loading frequency.

In Figure 7.2-4 only the damping ratio for the test at 0.05*Hz* is added. For determination of the damping ratio a well shaped hysteresis loop is needed. For loading frequencies above 2*Hz* the pneumatic loading system

Test	e [-]	F [*Hz*]	γ [%]	G/G_{max} [-]	D/D_{max} [-]
300-CU-0.5-1	0.710	0.5	0.219	0.25	0.66
300-CU-0.5-2	0.716	0.5	0.180	0.36	-
300-CU-0.5-3	0.717	0.5	0.133	0.47	0.49
300-CU-0.5-4	0.713	0.5	0.099	0.61	0.52
300-CU-0.05	0.707	0.05	0.163	0.33	0.66
300-CU-5	0.710	5	0.136	0.41	-
300-CU-10	0.729	10	0.097	0.62	-

Table 7.2-2: Results of CU cyclic triaxial tests for determination of the dependency of G and D from strain amplitude and cyclic loading frequency

cannot follow exactly the sinusoidal loading curve anymore, see also remarks in section 6.3.2. Thus slight deviations in the required wave shape are detected in the tests at 5 and 10*Hz* leading to non-comparable damping ratios. For the test at 0.05*Hz*, however, no influence of the loading frequency is detected.

7.2.3 *E* and *D* at larger strains out of drained cyclic triaxial tests

Strain dependency

Five cyclic triaxial tests are carried out on saturated and consolidated samples with identical size prepared in accordance with the procedure described in section 6.4.1. The samples are pressurised with an effective mean pressure of $p = 200kPa$ and K_0 = 0.5. The cyclic loading stage is executed with user defined loading parameters under consolidated drained (CD) conditions. Sinusoidal loading in compression and extension with a loading frequency of 2*Hz* is applied to determine the hysteretic Young's modulus *E* and the damping ratio *D* at different strain levels. The influence of varying void ratios *e* is eliminated by normalisation as already discussed before.

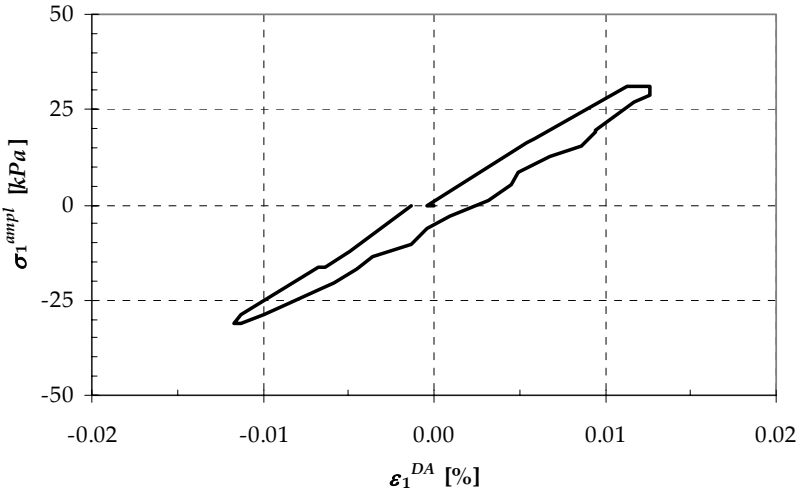

Figure 7.2-5: Recorded hysteresis loop for determination of E and D

Plotting the axial stress amplitude σ_1^{ampl} versus the axial strain amplitude ε_1^{DA} results in a hysteresis loop as exemplified in Figure 7.2-5. Following the procedure described in section 3.4, *E* and *D* can be calculated. The results for the Young's modulus are presented in a normalised diagram in Figure 7.2-6 and in Table 7.2-3. In this way the influence of varying void ratios and structural differences between the samples are minimised. Good agreement of test results with the $E-\varepsilon_1$ degradation curve is found. Figure 7.2-7 shows the damping ratios of the tests at different strain levels. Good agreement of test results and theory is found, showing increasing damping with increasing strains.

Frequency dependency

One of the five tests is repeated on similar samples under identical test conditions, while the loading frequency was varied. Tests at 5 and 10*Hz* are carried out. In this range no significant influence of the loading frequency could be detected. Similar tests result in similar soil stiffness for different loading frequencies. The corresponding data are added in Figure 7.2-6 and in Table 7.2-3. The data received at different loading frequencies fit well in the series of measurements with a constant loading frequency. The slightly higher stiffness at 10*Hz* can be related to inaccurate performance of the equipment at the high loading frequency.

Test	e	F	ε_1^{DA}	E/E_{max}	D/D_{max}
	[-]	[*Hz*]	[%]	[-]	[-]
200-CD-2-1	0.702	2	0.020	0.86	0.21
200-CD-2-2	0.776	2	0.025	0.79	0.28
200-CD-2-3	0.775	2	0.026	0.73	0.29
200-CD-2-4	0.800	2	0.027	0.75	0.22
200-CD-2-5	0.740	2	0.043	0.69	0.24
200-CD-5	0.709	5	0.049	0.70	0.17
200-CD-10	0.745	10	0.046	0.78	0.53

Table 7.2-3: Results of drained cyclic triaxial tests for determination of the dependency of E and D from strain amplitude and cyclic loading frequency

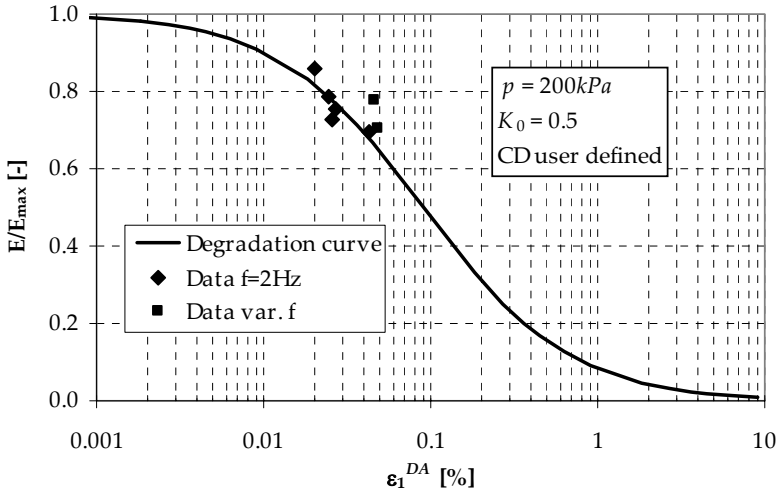

Figure 7.2-6: E out of CD cyclic triaxial tests at different strain levels and cyclic loading frequencies

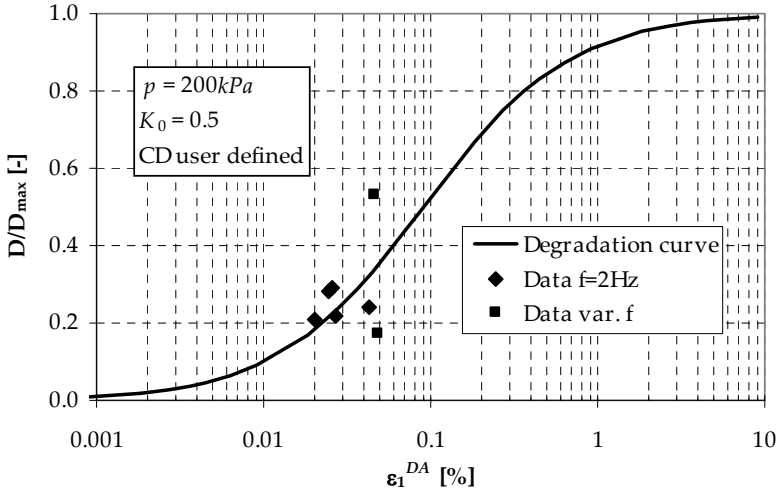

Figure 7.2-7: D out of CD cyclic triaxial tests at different strain levels and cyclic loading frequencies

In Figure 7.2-7 the damping ratios for the tests at 5 and 10*Hz* are added. The large scatter of the two points can be related to the previously discussed difficult determination of damping ratios out of not perfectly shaped hysteresis loops. The data, however, show a tendency of frequency independent material behaviour.

7.2.4 Elastic long term behaviour

Long term cyclic triaxial tests are carried out to investigate the evolution of the elastic material behaviour. For this purpose soil samples are subjected to 100,000 load applications under drained conditions. Figure 7.2-8 exemplarily shows the evolution of the Young's modulus E in a normalised presentation with the number of load applications for tests 200-CD-2-1 to 200-CD-2-3. In a similar way the evolution of the damping ratio D with the number of load applications is shown in Figure 7.2-9 in a normalised presentation for the tests mentioned above. In all tests performed the same tendency is observed.

Obviously the elastic parameters do not change significantly during cyclic load application at the small strain level. The assumption of constant elastic material parameters during long term dynamic impacts at the small strain level seems reasonable. Nevertheless this assumption needs to be treated with care. With the used equipment possible load induced anisotropy cannot be detected. Furthermore two mechanisms obviously partially neutralise each other: stiffening due to cyclic compaction and weakening due to the change in the plastic strain level. These effects are not necessarily of the same absolute magnitude as observed in the present study. Under certain conditions one of the mechanisms will become dominant. Investigation of these aspects is desirable in future.

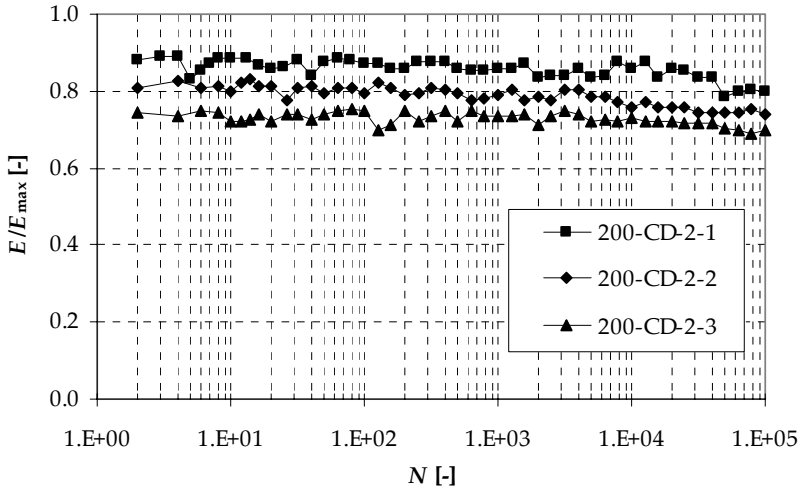

Figure 7.2-8: Evolution of the Young's modulus E with the number of load applications in different tests

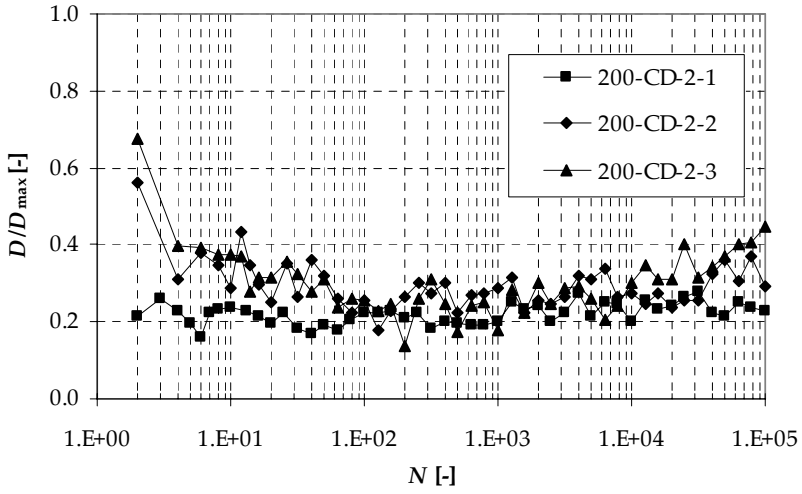

Figure 7.2-9: Evolution of the damping ratio D with the number of load applications in different tests

7.3 Accumulation properties of sand of Mol

7.3.1 Accumulation of residual strains with the number of cycles

The previous analysis bases on the assumption of ideally elastic material behaviour. Figure 7.3-1 shows that this approximation works well for a single load application. Result of one load cycle is a (almost) perfectly closed hysteresis loop. Thereby the cycle number has no influence. Elastic behaviour can be stated for every single load cycle.

Application of a large number of load cycles, however, reveals that even at the small strain level non-negligible plastic strains occur. If residual deformations take place, the recorded hysteresis loop starts moving. In fact, the movement of the hysteresis loop can clearly be seen in Figure 7.3-2, plotting the first and the 100,000th load cycle in one diagram. This graph also confirms the statement made above: the elastic material behaviour does not change significantly with the number of load cycles, proven by hysteresis loops not changed in their characteristics.

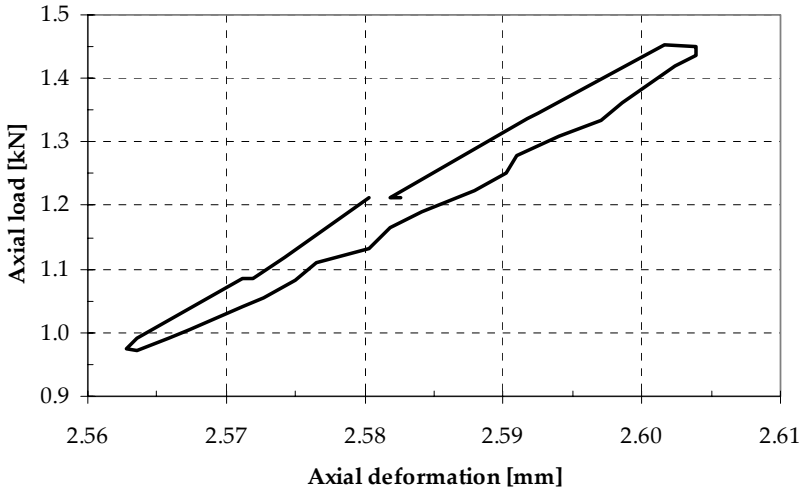

Figure 7.3-1: Elastic character of hysteresis loops

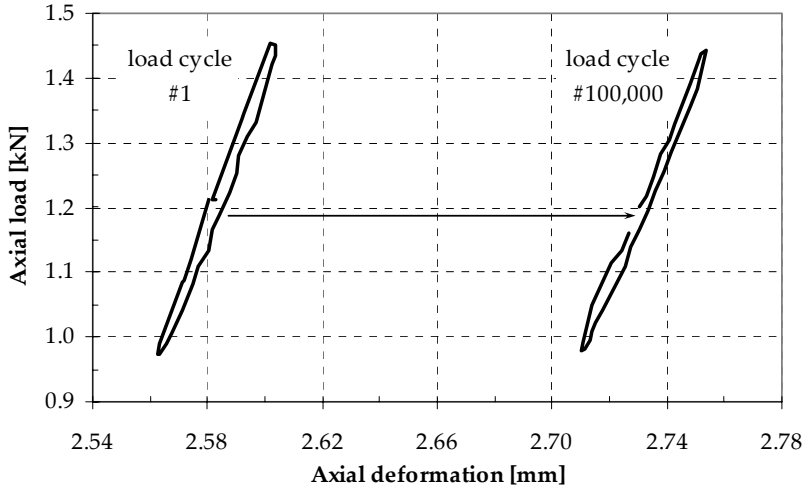

Figure 7.3-2: Movement of hysteresis loops

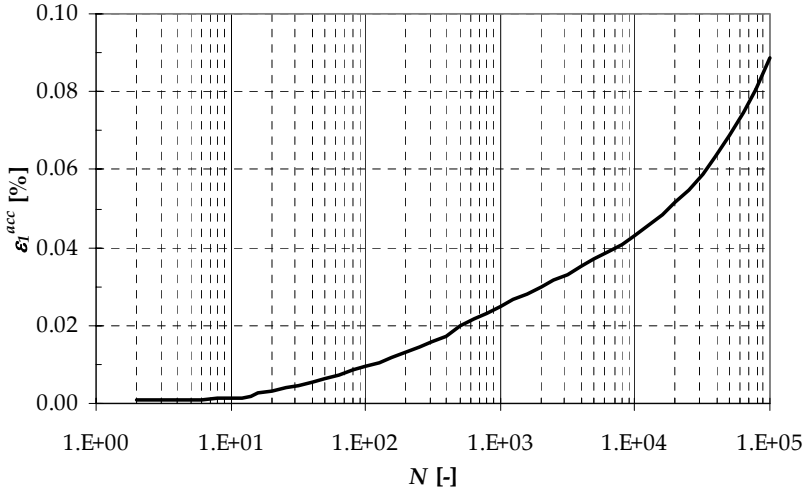

Figure 7.3-3: Evolution of accumulation of residual strains with the number of load cycles

As the elastic material behaviour is described well with the existing constitutive laws, the accumulation of residual strains comes to the fore. The evolution of plastic strains with the number of cycles is analysed in addition to the elastic material behaviour. Thus average strains are investigated with respect to their evolution with the number of load cycles as already discussed in Chapter 4 and depicted in Figure 4.1-1b). As a result graphs as exemplarily shown for test 200-CD-2-1 in Figure 7.3-3 are obtained and used for further analysis.

7.3.2 Influence of strain amplitude and initial void ratio

Long term cyclic triaxial tests are carried out on saturated and consolidated samples with identical size prepared in accordance with the procedure described in section 6.4.1. The samples are pressurised with an effective mean pressure of $p = 200kPa$ and K_0 = 0.5. The cyclic loading stage is executed with user defined loading parameters under consolidated drained (CD) conditions. 100,000 load cycles are applied with a sinusoidal waveshape in compression and extension at a loading frequency of 2Hz.

Different initial void ratios are chosen to determine the influence on the accumulation rate. Performing tests under similar average and cyclic stress conditions at different relative densities results in different strain amplitudes, ε^{ampl}, as stiffness is influenced by the void ratio e and therewith strain amplitudes increase with e. In order to achieve comparability all curves are normalised using the quadratic formulation f_{ampl}, equation (4.24), proposed by Wichtmann et al. (2004a), describing the influence of ε^{ampl} on the strain accumulation rate. Equation (4.24) is validated in a wide range of stress ratios, whereby $\varepsilon_{ref}^{ampl} = 10^{-4}$ for small strain amplitudes, as discussed in section 4.3.3.

Samples with initial void ratios e_0, i.e. the void ratio at the beginning of cyclic loading, of 0.800, 0.745 and 0.691 are tested, corresponding to initial relative densities D_{r0} of 35.5%, 52.2% and 68.2%, respectively. Figure 7.3-4 shows the accumulated axial strain as a function of the number of load cycles normalised by the amplitude function f_{ampl}. Higher initial void ratios obviously lead to higher accumulation of residual strains.

Wichtmann et al. (2004a) propose equation (4.33) to describe the influence of the void ratio on strain accumulation. Therein the reference void

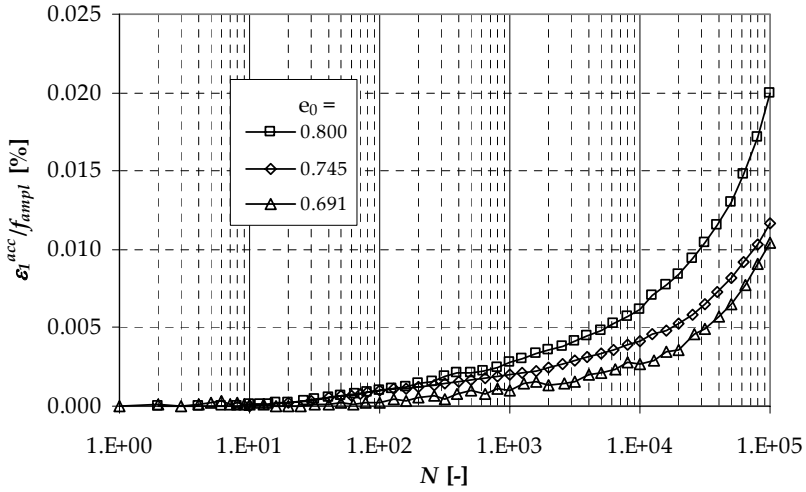

Figure 7.3-4: Normalised accumulated axial strain $\varepsilon_1^{acc}/f_{ampl}$ as function of the number of load cycles N in tests with different initial void ratios

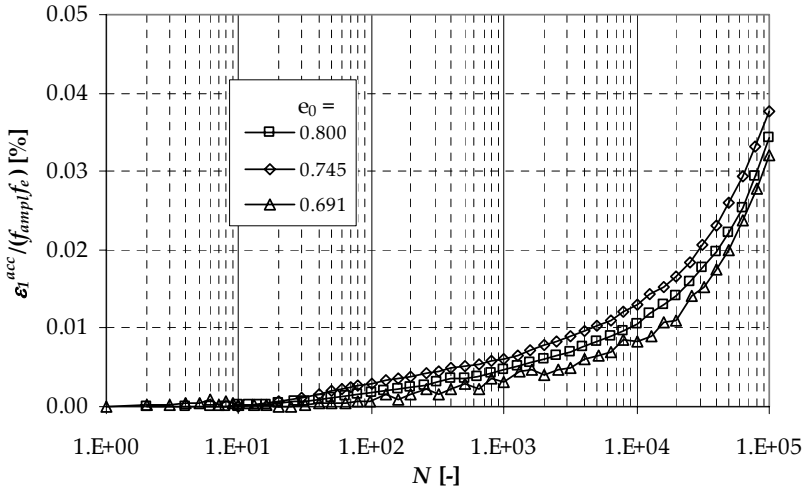

Figure 7.3-5: Normalised accumulated axial strain $\varepsilon_1^{acc}/(f_{ampl}f_e)$ as function of the number of load cycles N in tests with different initial void ratios

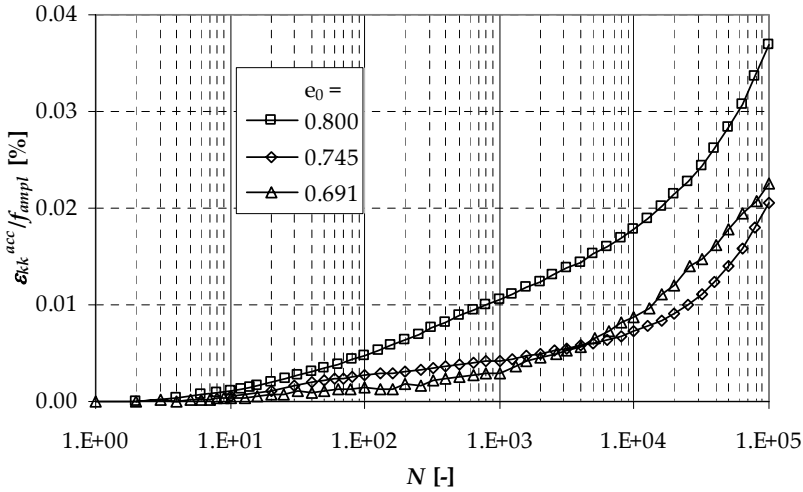

Figure 7.3-6: Normalised accumulated volumetric strain $\varepsilon_{kk}^{acc} / f_{ampl}$ as function of the number of load cycles N in tests with different initial void ratios

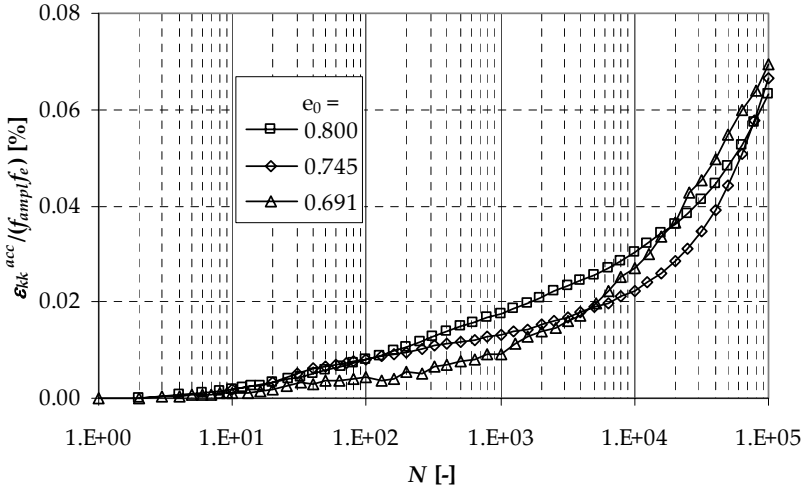

Figure 7.3-7: Normalised accumulated volumetric strain $\varepsilon_{kk}^{acc} / \left(f_{ampl} f_e \right)$ as function of the number of load cycles N in tests with different initial void ratios

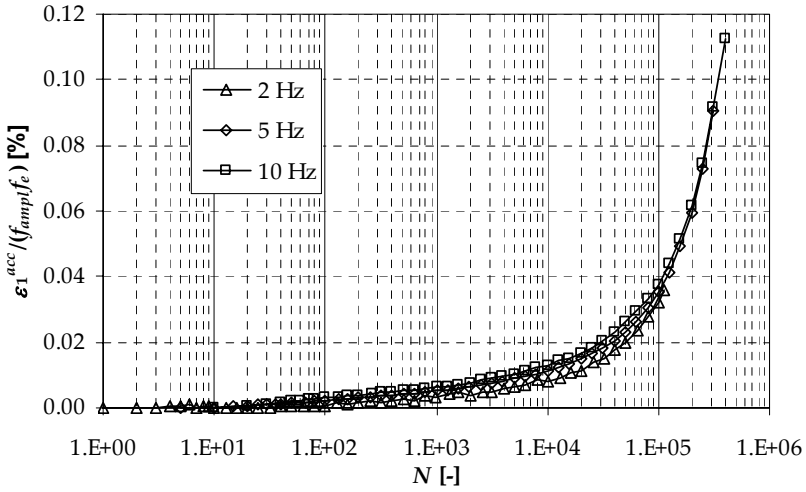

Figure 7.3-8: Normalised accumulated axial strain $\varepsilon_1^{acc}/(f_{ampl}f_e)$ as a function of N in tests with different cyclic loading frequencies

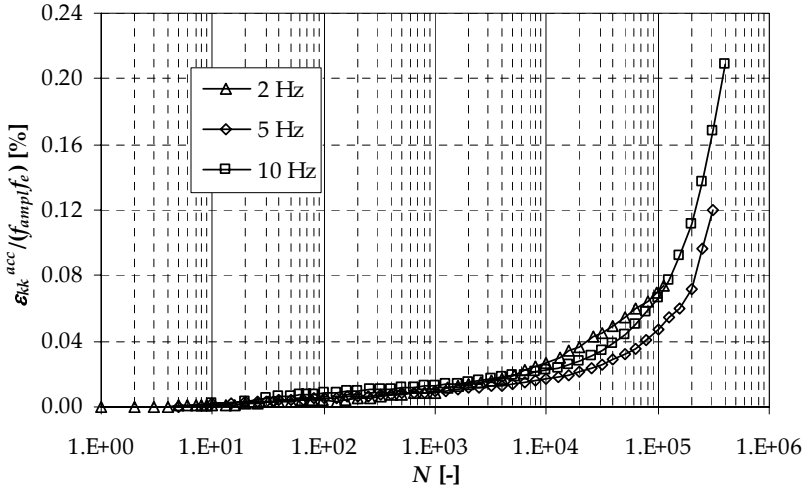

Figure 7.3-9: Normalised accumulated volumetric strain $\varepsilon_{kk}^{acc}/(f_{ampl}f_e)$ as a function of N in tests with different cyclic loading frequencies

ratio e_{ref} is suggested to be equal to the maximum void ratio of the respective soil. For $e_{ref} = e_{max} = 0.918$ and the material parameter $C_e = 0.45$, determined by a least-squares fitting procedure, all curves fall closely together as shown in Figure 7.3-5. Therewith presented test results coincide with findings of Wichtmann et al. (2004a) and confirm the availability of equations (4.24) and (4.33) for accumulated axial strains.

Plotting the accumulated volumetric strains versus the number of load cycles, in general, results in similar accumulation curves. Figure 7.3-6 and Figure 7.3-7 show the accumulated volumetric strain, normalised in the same manner as the previously presented graphs for axial strains. Although the presented data show no clear difference in the two tests at lower void ratios, a decreasing strain accumulation rate with decreasing void ratios can be stated. The normalisation in Figure 7.3-7 supports this assumption and illustrates the availability of the proposed void ratio function for accumulated volumetric strains.

7.3.3 Influence of the cyclic loading frequency

Long term cyclic triaxial tests are carried out on saturated and consolidated samples with identical size prepared in accordance with the procedure described in section 6.4.1. The samples are pressurised with an effective mean pressure of $p = 200kPa$ and $K_0 = 0.5$. The cyclic loading stage is executed with user defined loading parameters under consolidated drained (CD) conditions. Load cycles with a sinusoidal waveshape in compression and extension are applied at loading frequencies of 2, 5 and 10Hz. The numbers of load cycles applied vary from 100,000 ($f_L = 2Hz$) and 300,000 ($f_L = 5Hz$) to 400,000 ($f_L = 10Hz$). Since the duration of cyclic loading shortens with increasing loading frequency higher numbers of load cycles are easier to achieve.

All tests are performed on samples with initial relative densities in the range of $62.9\% \le D_{r0} \le 68.3\%$. Nevertheless all curves drawn in Figure 7.3-8 and Figure 7.3-9 are normalised with both the amplitude function, equation (4.24), and the void ratio function, equation (4.33), to allow comparison.

Both Figure 7.3-8 and Figure 7.3-9 clearly show that the accumulation of residual strains is not influenced by the loading frequency in the tested range of 2 to 10Hz. This applies for axial as well as for volumetric accumulated strains. Wichtmann (2005) found the accumulation

rate to be independent of the cyclic loading frequency in a range of 0 to 2*Hz*. The own results confirm this statement and extend the range of investigated loading frequencies to 0 to 10*Hz* in which the accumulation rate is frequency independent.

7.3.4 Influence of the orientation of the load cycle

A testing campaign is started at the Laboratory of Soil Mechanics at the Bauhaus University Weimar, Germany, to investigate the influence of the orientation of the load cycle in the *p-q* plane on the accumulation of residual strains. Figure 7.3-10 schematises the stress conditions in the *p-q* diagram for the planned test series. To realize stress cycles with constant *q* and constant *p*, respectively, both cell pressure and axial stress are to be applied cyclically. Since with the installed equipment, described in Chapter 6, only the axial stress can be cycled, this test series had to be carried out elsewhere. During running the needed tests it turned out that the used equipment is not yet capable to apply the desired load cycles with sufficient accuracy. Further improvement of the equipment is needed to perform these tests.

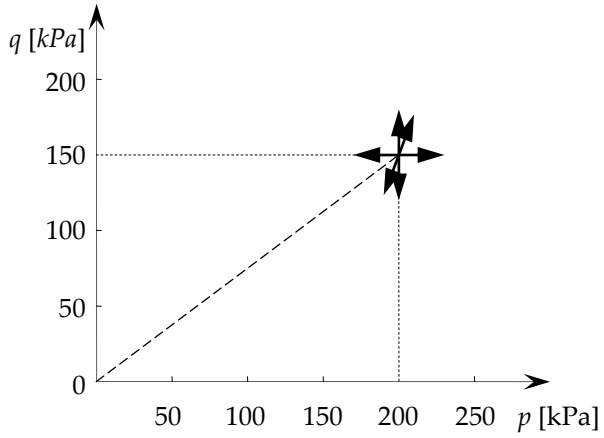

Figure 7.3-10: Planned tests to investigate the influence of the orientation of the load cycle in the p-q plane

7.4 Application of the new accumulation model

The model parameters for the accumulation model under consideration are determined from six long term accumulation tests. Thereby the procedure described in section 5.4 is followed for five tests. Variations in the void ratio of the respective samples come along with different cyclic strain amplitudes. Furthermore tests at different strain levels are carried out. Due to these variations the elastic material parameters as well as the accumulation model parameters are determined for each test separately. Based on the determined parameter sets a prediction of accumulated strains is made for the sixth test.

7.4.1 Determination of the elastic model parameters

The elastic material behaviour of the sand of Mol is found to be pretty similar to the behaviour of sand No.3 considered in section 5.4.2. Accordingly parameters υ, p_{ref} and n_e, listed in Table 5.4-2, do not change. The tangent bulk modulus K_t differs with varying strain amplitudes and void ratios. Therewith the reference bulk modulus K_{ref} needs to be determined for each test separately. Table 7.4-1 lists the corresponding values together with the respective void ratio e and strain amplitude ε_1^{DA}.

7.4.2 Determination of the accumulation model parameters

Model calibration

The influence of the state of stress on the strain accumulation is assumed to be independent from the material. As a consequence parameters C_f, C_c, η_c and d_0 remain the same for the sand of Mol as for sand No.3, listed in Table 5.4-4. Therewith the accumulation model parameters α_f^0, β_f^0, ϑ_f^0, α_c^0, β_c^0 and ϑ_c^0 can be determined, following the procedure described in section 5.4.2. In a first step test data are fitted to equations (5.21) and (5.22). The achieved model parameters for tests LT1 to LT5 are presented in Table 7.4-2.

For tests LT1 to LT4 very small accumulated deviatoric strain components κ^{acc} are recorded as shown in Figure 7.4-1. In some regions the accumulation curves even become slightly negative. Particularly test LT4 exhibits distinct negative deviatoric strain components. It is not clear what causes this surprising behaviour. The most probable reason is seen in

Test	e	ε_1^{DA}	p	η	K_{ref}
	[-]	[%]	[kPa]	[kPa]	[MPa]
LT1	0.800	0.027	200	0.75	120
LT2	0.775	0.026	200	0.75	120
LT3	0.691	0.017	200	0.75	180
LT4	0.740	0.043	200	0.75	120
LT5	0.709	0.049	200	0.75	130
LT6	0.745	0.046	200	0.75	130

Table 7.4-1: Reference bulk moduli K_{ref} for different long term accumulation tests on the sand of Mol

Test	α_f^0	β_f^0	ϑ_f^0	α_c^0	β_c^0	ϑ_c^0
	[10^{-6}]	[10^{-9}]	[-]	[10^{-5}]	[10^{-8}]	[-]
LT1	1.0000	2.5000	100,000	0.8703	1.5659	4909.97
LT2	1.0000	2.5000	100,000	2.7289	1.6116	3588.63
LT3	1.0000	2.5000	100,000	0.0335	0.2995	13441.59
LT4	1.0000	2.5000	100,000	9.3921	7.8159	2187.35
LT5	0.5528	13.8150	7153.44	1.5895	2.7892	5057.80

Table 7.4-2: Accumulation model parameters for long term tests on the sand of Mol

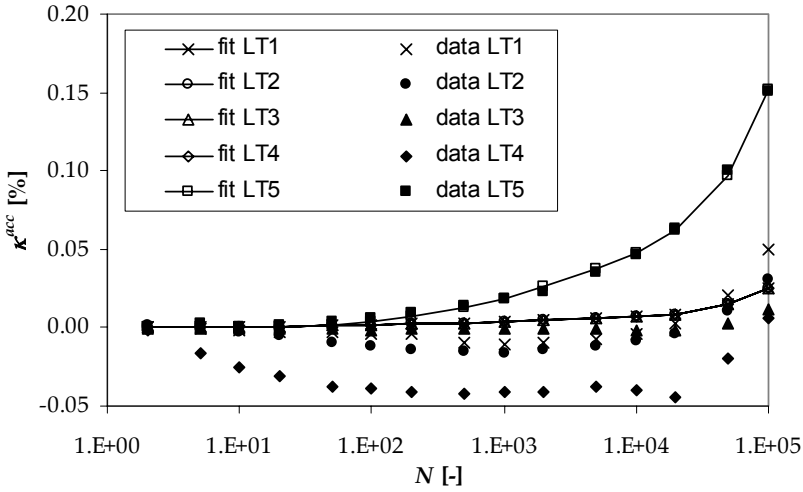

Figure 7.4-1: Deviatoric accumulated strain component κ^{acc} : data of tests LT1 to LT5 versus model calibration

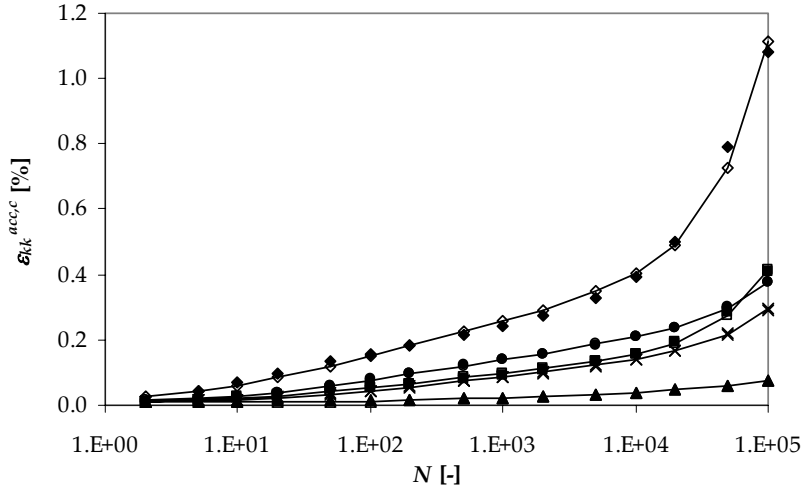

Figure 7.4-2: Volumetric accumulated strain component $\varepsilon_{kk}^{acc,c}$: data of tests LT1 to LT5 versus model calibration

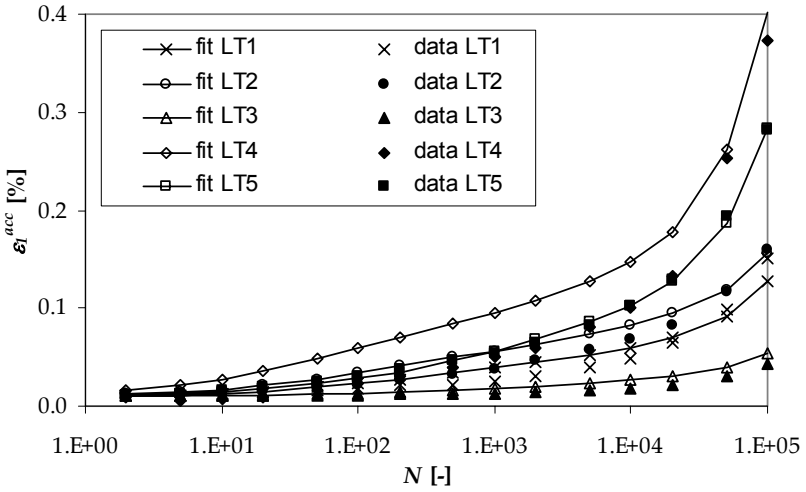

Figure 7.4-3: Axial accumulated strain ε_1^{acc} : data of tests LT1 to LT5 versus model calibration

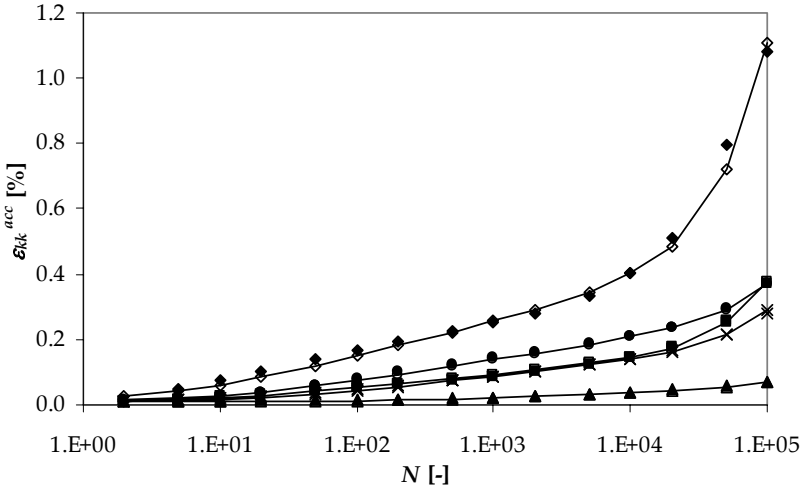

Figure 7.4-4: Volumetric accumulated strain ε_{kk}^{acc} : data of tests LT1 to LT5 versus model calibration

insufficient execution of the test. After several thousands of cycles, positive accumulation is observed in all tests, though.

Since, by definition, equation (5.21) cannot map negative accumulation and the deviatoric strain component is small compared to $\varepsilon_{kk}^{acc,c}$, the best fit for tests LT1 to LT4 is a vanishing κ^{acc}. This can be accounted for in the model by very large values of ϑ_f^0. In this case the influence of α_f^0 and β_f^0 becomes small. They are thus set to default values. ϑ_f^0 is set to 100,000. For values higher than this no significant changes in the resulting accumulation curves are detected. The model calibration together with the respective measured data is presented in Figure 7.4-1. Apart from test LT4 sufficient correspondence of model and data is achieved with the proposed model parameters. For the accumulated volumetric strain component $\varepsilon_{kk}^{acc,c}$, equation (5.22), good agreement of model and data for all tests is achieved as illustrated in Figure 7.4-2.

In a second step axial and volumetric accumulated strains, ε_1^{acc} and ε_{kk}^{acc}, are calculated. Figure 7.4-3 shows the measured total accumulated axial strain ε_1^{acc} together with the respective model calibration. Similar, Figure 7.4-4 shows the measured total accumulated volumetric strain ε_{kk}^{acc} together with the respective model calibration. Although the fit for the accumulated deviatoric strain component is not very well for tests LT1 to LT4, good agreement of measured data and model is achieved with the presented sets of parameters. Since κ^{acc} is small with respect to $\varepsilon_{kk}^{acc,c}$, the influence of this error is minimised. An exception is the axial strain of test LT4 where the fitting error in κ^{acc} becomes relevant.

Prediction of strain accumulation

From the model calibration parameter sets at varying void ratios and cyclic strain amplitudes are available. Plotting the respective values versus void ratio e and cyclic strain amplitude ε^{ampl} results in graphs as presented in Figure 7.4-5. Although the data base is quite rare and more data would be desirable, determination of the model parameters for test LT6 by analysis of these graphs appears possible. Thus a curve plane is fitted to the respective data points for each parameter using a non-linear least-squares procedure. In Table 7.4-3 the functions used for the fitting procedure are listed for each model parameter together with the function parameters for

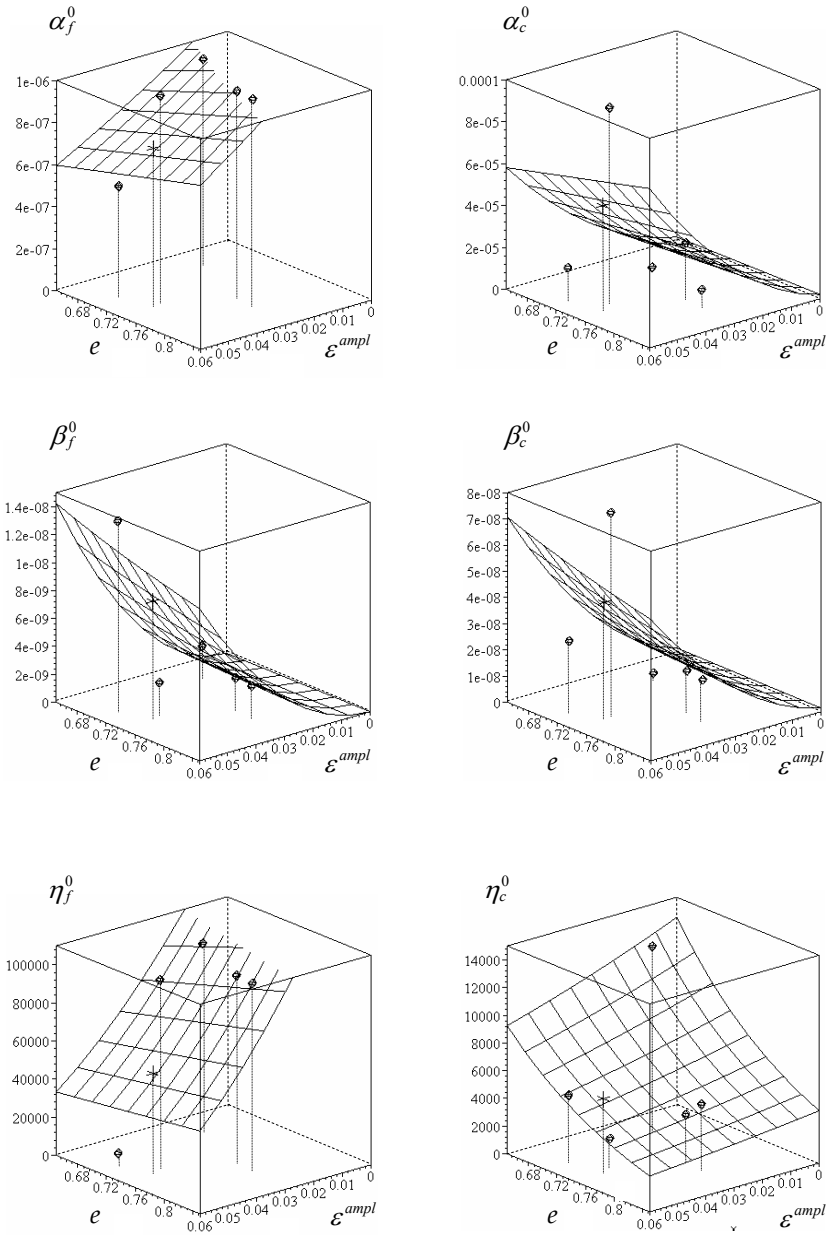

Figure 7.4-5: Calibrated model parameters (dots) and prediction (crosses) versus void ratio e and cyclic strain amplitude ε^{ampl}

the best fit. The functions are chosen based on the trends visible in the graphs of Figure 7.4-5.

Model Parameter	Curve plane Function	*a*	*b*	*c*
α_f^0	$a\cdot\left(c\varepsilon^{ampl}-b\right)^2\cdot e$	9.71E-5	9.86E-2	0.45
β_f^0	$a\cdot\left(c\varepsilon^{ampl}-b\right)^2/e$	1.15E-7	9.23E-4	-4.72
ϑ_f^0	$a\cdot\left(c\varepsilon^{ampl}-b\right)^2\cdot e$	2.47E+8	0.10	0.83
α_c^0	$a\cdot\left(c\varepsilon^{ampl}-b\right)^2\cdot e$	1.37E-5	0.42	-35.56
β_c^0	$a\cdot\left(c\varepsilon^{ampl}-b\right)^2\cdot e$	1.26E-8	0.25	-40.85
ϑ_c^0	$a\cdot\exp\left(b-c\varepsilon^{ampl}\right)\cdot\exp\left(-ce\right)$	3.16E+5	1.00	6.38

Table 7.4-3: Curve plane functions and parameters for best fit

The point in the plane that corresponds to void ratio and strain amplitude value of test LT6 coincides with the respective model parameter. In that way a complete set of parameters is found. The determined parameters are listed as rounded values in Table 7.4-4.

Test	α_f^0	β_f^0	ϑ_f^0	α_c^0	β_c^0	ϑ_c^0
	[10^{-6}]	[10^{-9}]	[-]	[10^{-5}]	[10^{-8}]	[-]
LT6	0.80	9.00	53,000	5.00	4.50	5400

Table 7.4-4: Predicted model parameters for test LT6

Figure 7.4-6 and Figure 7.4-7 present the recorded accumulated axial and volumetric strain of test LT6 together with the model prediction. Good agreement of prediction and test data is achieved. It shows that the model under consideration is well suited to predict strain accumulation in granular media under low level cyclic loading.

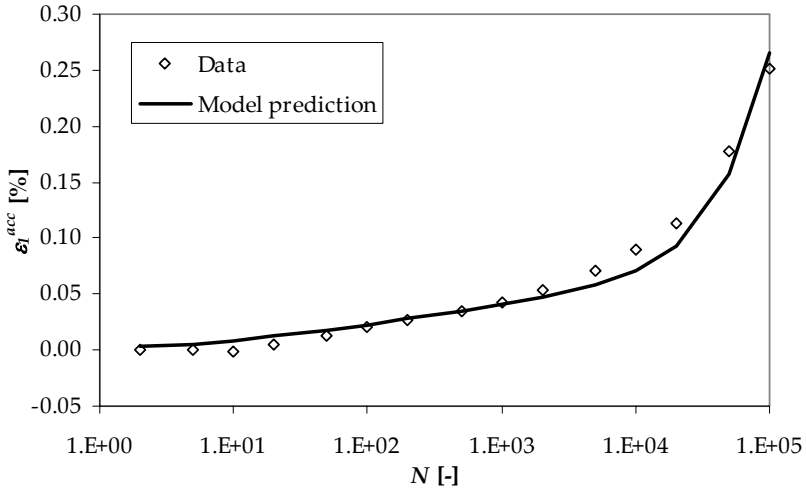

Figure 7.4-6: Test data of test LT6 versus model prediction: accumulated axial strain ε_1^{acc}

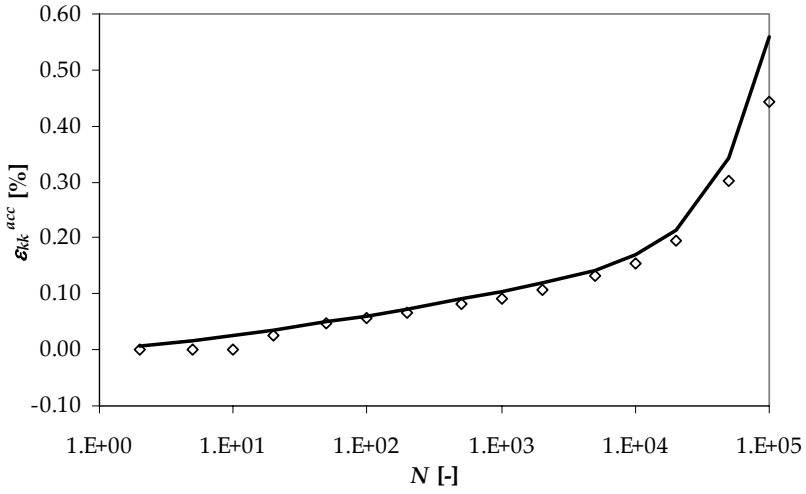

Figure 7.4-7: Test data of test LT6 versus model prediction: accumulated volumetric strain ε_{kk}^{acc}

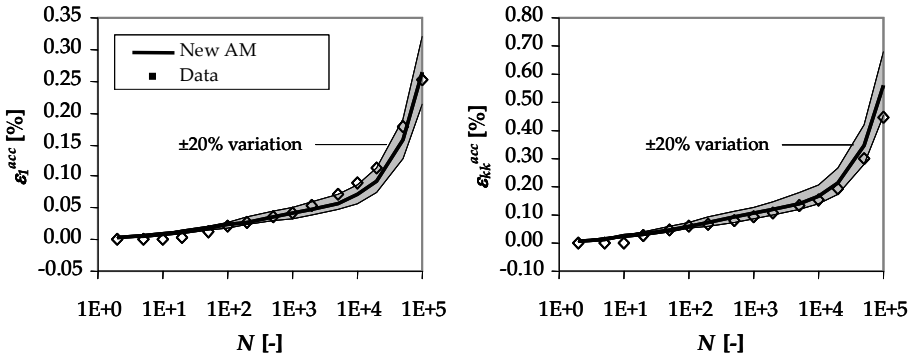

Figure 7.4-8: Influence of deviating model parameters on prediction

Even with a thin underlying data base sufficient accuracy in the prediction is reached. This is mainly related to the fact that the model parameters are not very sensitive to small changes, i.e. the predicted strain does not vary significantly, even if the model parameters are not chosen optimal. As an example, Figure 7.4-8 illustrates the resulting deviation in the prediction of accumulated strains, implying a variation of ±20% of all model parameters. Thereby the most adverse combination of parameters is applied.

Comparison of Figure 7.4-8 with Figure 4.3-8, where the influence of deviating model parameters on accumulation prediction is illustrated for the Bochum accumulation model, clarifies the advantageous choice of the formulation in the new accumulation model. In the Bochum accumulation model variations of ±10% in the model parameters lead to significant deviations in the prediction, while in the new accumulation model this deviation of the prediction remains tolerable, even for the large parameter range of ±20% .

This positive effect is mainly linked to the small number of model parameters, avoiding summing up of errors. In this regard the scattering of the data itself in addition to the influence of void ratio e and cyclic strain amplitude ε^{ampl} is emphasized. A scattering of soil parameters of ±10% on the one hand in laboratory investigations, on the other hand even more under in-situ conditions is not unusual. Accordingly, it is sometimes difficult to identify a causal connexion of certain parameters. Furthermore the character of the relation may vary for different soils.

For this reason, in opposite to the Bochum accumulation model, the accumulation model under consideration avoids empirical laws fixing such relations. Besides the discussed lower sensitivity with respect to variations in the model parameters, in this way maximum flexibility and general applicability of the model is preserved.

7.5 Conclusions

In the frame of this experimental study the elastic material behaviour of the sand of Mol as well as its accumulation properties are studied using the equipment described in Chapter 6. The successfully executed tests prove the operational reliability of the installed testing apparatus and the applicability of the proposed test procedure.

The small strain stiffness of the material under consideration is determined at different stress levels using bender element test equipment. The empirical equation for determination of the maximum shear stiffness of Yoon (1991) can be applied to bender element test results, although it was established on the basis of resonant column tests. Findings of Dyvik & Madshus (1985) are confirmed.

The influence of the cyclic strain amplitude level on the soil stiffness is investigated in both standardised tests after ASTM D3991-91 and user defined tests. The nonlinear stress-strain behaviour can be well described by the hyperbolic non-linear constitutive model proposed by Duncan & Chang (1970), as well for CU as for CD test conditions. With increasing strain levels the damping ratio increases in the expected range.

Neither regarding the stiffness nor the damping ratio, a dependency of the elastic material behaviour from the cyclic loading frequency is detected in the range from 0 to 10Hz. Nevertheless the general assumption of frequency independency is seen as dangerous. Especially under drained conditions dynamic impacts above a soil specific critical frequency may cause quasi-undrained behaviour, leading to pore pressure build-up and possible liquefaction risk.

The elastic parameters do not change significantly with the number of cycles when the soil is subjected to small strain cyclic loading. Analysis of single hysteresis loops recorded during long term cyclic triaxial tests shows that the characteristics of the respective cycles do not change

with the number of load applications. Furthermore (almost) perfectly closed hysteresis loops are recorded. Thus the assumption of ideal elasticity is a good approximation for the description of short term and dynamic soil behaviour. This knowledge is an important finding for the theoretical approach. Dynamic calculations can be performed with the assumption of constant elastic material parameters, independent from the number of load cycles already applied.

Nevertheless accumulation of plastic strains is observed in the case of long term dynamic loading. This manifests in a movement of the hysteresis loops along the deformation axis while the application of cyclic stress remains on its level. These residual deformations need to be taken into account in settlement predictions when long term or permanent dynamic loading is to be expected at the site.

Also the accumulation of plastic strains is not influenced by the cyclic loading amplitude in the range of 0 to 10*Hz*. Therewith Miners rule applies even if subsequent cycles have different frequencies. Apart from the practical relevance the frequency independency can also be exploited in laboratory testing: by increasing the loading frequency in cyclic laboratory tests the duration of a test can be minimised significantly.

Findings of Wichtmann (2005), particularly with regard to the quadratic increase of accumulated strains with increasing cyclic strain amplitude and the void ratio function, are confirmed and used for data analysis. The empirical formulations are well suited for normalisation of recorded data and seen as effective tool to compare strain accumulation tests at different void ratios and strain levels. As discussed extensively in section 4.3.4, the use of the formulas for prediction of accumulated strains in a strain accumulation model, is seen as critical, though.

The new accumulation model introduced in Chapter 5 is applied to own test results. Good agreement of model curves and recorded total accumulated axial and volumetric strains is achieved by calibrating the model parameters on test results. In a second step the achieved parameter sets are used to determine model parameters for prediction of accumulated strains of another test. Although a broader data base is desirable, the prediction corresponds well to the test data. Therewith the availability of the model under consideration for prediction of strain accumulation is supported.

Chapter 8
Summary and future work

8.1 Summary of the present work

The present work gives insight in the domain of strain accumulation phenomena, the theoretical description of strain accumulation with mathematical models and its experimental investigation in laboratory tests. Starting from a general overview on vibrations in the ground and its consequences for both people and built environment the special case of strain accumulation caused by dynamic impacts at the low strain level is treated as an important mechanism, not yet commonly considered in the classical engineering design process.

The practical relevance of this problem becomes clear when looking e.g. to deterioration of roads or railway tracks, long-term settlements of nearby buildings, settlements of the surrounding of construction sites or settlements of machine foundations. Typical vibration levels linked to these examples can be considered in the elastic range in the short view. Besides static deformations, over the long run non-negligible residual deformations occur, possibly leading to considerable stress concentrations, damages or settlements.

This process of strain accumulation is explained as a kind of aging process of the soil, comparable to creeping due to dynamic loading in other materials as in steel. In general, the accumulation process is characterised by three main influencing aspects: the current state of the soil (defined by void ratio, granulometric decomposition, permeability, saturation degree, degree of cementation, historiotropy etc.), the current state of stress (defined by

average mean effective stress, average stress ratio etc.) and the characteristics of the dynamic impact (defined by cyclic strain amplitude, loading frequency, strain path in the strain space, polarisation, number of cycles etc.). The combination of these parameters defines the intensity as well as the direction of accumulation.

Mathematical formulations for prediction of strain accumulation should account for these parameters. A literature study on existing accumulation models for prediction of strain accumulation is carried out. Two advanced models, the Bochum accumulation model and the Suiker model, are discussed in more detail with respect to their capabilities and practical applicability. Problems and difficulties in modelling accumulation behaviour of soil are detected and discussed. As a result required features of an accumulation model are defined and points of interest, desirable for consideration in further research, are revealed.

Founded on the cognitions of the literature study the formulation of a new accumulation model, basing on the mentioned existing models, is proposed. The essential advantages of this approach are the small number of model parameters, the simple formulation and the proper implementation in a commonly used finite element code. All model parameters can be determined from a single kind of laboratory test, namely the cyclic triaxial test. The simple formulation allows for easy comprehension, extension and general applicability for a wide range of practical problems. The implementation in the finite element code supports the use of the model in practical applications.

The validation of any accumulation model is difficult. Up to now experimental investigations considering all, current state of the soil, current state of stress and the characteristics of the cyclic loading, are quite rare both in the field and in laboratory tests. For this reason advanced soil testing equipment is installed in the frame of this work. Combined cyclic triaxial and bender element test equipment is set up at the Laboratory of Geotechnics, Department of Industrial Engineering Sciences, KHBO in Ostende, Belgium. The apparatus allows for the investigation of elastic material properties and the accumulation behaviour of soil. A wide range of test options allows for consideration of many influence parameters in testing campaigns.

A test procedure for the execution of cyclic triaxial tests, including sample preparation technique, installation, saturation, consolidation and

cyclic loading of a cylindrical soil sample, is defined to study the elasto-plastic long term behaviour of granular soil. Standardised as well as user defined long term tests on the sand of Mol are carried out. Elastic soil properties, the Young's modulus E and the damping ratio D, out of cyclic triaxial tests and the maximum shear modulus G_{max} out of bender element tests are determined. Furthermore the procedure for identification of the parameters of the accumulation model under consideration is explained and carried out.

In testing campaigns the influence of different parameters on the elastic material behaviour as well as on the accumulation properties of the sand of Mol is investigated. Thereafter the hyperbolic non-linear constitutive model proposed by Duncan & Chang (1970) well describes the degradation of soil stiffness with increasing cyclic strain amplitudes. The empirical formulation of Yoon (1991), developed on the basis of resonant column tests to describe the maximum shear modulus as a function of the void ratio and the mean effective stress, is also valid for bender element test results.

Test results confirmed the applicability of elastic constitutive laws for description of the dynamic soil behaviour. The elastic material parameters are found to be independent from the number of load cycles already applied. During application of large numbers of cycles, however, non-negligible generation of residual deformations is detected.

Increasing void ratios and cyclic strain amplitudes lead to increasing strain accumulation rates. Empirical formulations of Wichtmann (2005) to describe this correlation are confirmed. An influence of the cyclic loading frequency in the range of 0 to 10Hz is not detected. Therewith the frequency content of a dynamic impact is of minor importance for accumulation predictions. Also in laboratory investigations this finding is useful as the duration of cyclic tests can be minimised by increasing the loading frequency without influencing results.

Not much attention has been paid to strain accumulation mechanisms and their consequences on the built environment in the past. This changed with increasing volume of traffic, higher densities of population and accompanying increasing numbers of construction sites in urban areas. Caused by higher vibration levels strain accumulation problems are an important aspect in estimation and prediction of the durability of structures. Also in relation to foundations of wind power plants knowledge on long term soil behaviour under dynamic excitations

has become more and more important. Nevertheless the domain of strain accumulation is a new developing field of research. This work thus cannot claim for completeness. In fact during studies in the frame of this work several problems and questions arose calling for solutions. These tasks for future research are outlined in the subsequent section.

8.2 Recommendations for future work

Possible tasks for future research on strain accumulation problems are seen in many directions. This regards the modelling and prediction of strain accumulation as well as laboratory investigations and field measurements. Another very important point is to link these three sub-domains to finally achieve a holistic framework reliable and uniquely describing general strain accumulation problems.

Field measurements versus laboratory investigations

One of the most important questions to be answered is how cognitions on accumulation behaviour of soil achieved in laboratory investigations can be transferred to in-situ conditions and vice versa. Several aspects need to be considered in this context. While the state of stress in situ can be relatively easy transferred to laboratory tests, this is very difficult for the current state of soil. Aging effects as cementation and abrasion, seasonal effects, static and cyclic preloading, inhomogeneities etc. hardly can be represented in laboratory tests. Furthermore the characteristics of in-situ load cycles are very complex, mostly of stochastic and strongly three dimensional character, while in laboratory tests only simplified load cycles can be applied. In this context future work should focus on possible applications of existing methods to simulate natural conditions of the soil in cyclic laboratory tests. Also a unique transformation algorithm of in-situ strain cycles into adequate strain cycles applied to a soil specimen during a cyclic laboratory test is required in order to be able to compare field and laboratory measurements.

Investigations in the field

Long term field measurements of strain accumulation problems are very rare. Only in few testing campaigns the settlement of structures e.g. close to a new railway or road is monitored. Furthermore it is difficult to link a

certain part of recorded settlements to long term dynamic impacts, since it may superpose with settlements originating from other sources. Field measurements focussing on the problem of strain accumulation thus are desirable.

As for all engineering design tasks, it is of crucial importance to be able to determine the current state of the soil in a unique way. This is the basis to estimate static and elastic soil parameters as well as the potential of strain accumulation risks of a soil. So far no reliable method exists to achieve these initial soil parameters. Currently this problem is overcome by high safety factors and under-estimation of the soils bearing capacity. Seismic exploration techniques are seen as a promising approach to this problem.

Consideration of in-situ conditions in accumulation models

As a consequence of missing initial soil parameters the correct determination of the historiotropy of the soil is hardly possible so far. Therewith the consideration of this very important parameter in a prediction model is difficult. Another important point is the unique mathematical description of the dynamic impact in an adequate amplitude parameter as input for accumulation predictions. Existing methods are seen as deficient. Future research should focus on these aspects.

Laboratory investigations on strain accumulation phenomena

The sample preparation technique will have a non-negligible influence on laboratory test results. In cyclic triaxial tests pluviated samples will behave weaker than compacted samples since during compaction the sample is adapted to axial loading already. Although tamping of the sample during preparation could be interpreted as preloading it is not clear which method is more appropriate to investigate accumulation behaviour. To the author's knowledge the influence of the specimen preparation technique on strain accumulation under long term cyclic loading has not been investigated so far. This is related to the fact that only few people did experimental studies in the field of such tests. Further investigations on that topic are seen as necessary and helpful.

Experimental findings led to the conclusion that the elastic parameters do not change with the number of load cycles applied. This statement, however, bases on test results achieved from measurement in axial direction alone. Implying an adaptation of soil to the respective cyclic

loading may result in generation of anisotropic soil characteristics. The assumption of isotropic material behaviour and only using axial measurements then leads to misinterpretation of test results. Bender element tests in vertical as well as in horizontal direction, applied before and after application of the cyclic loading, may allow for detection of a generation of anisotropy.

Extension of the range of parameters investigated in this work is recommended. Among others, further interesting parameters to study with respect to their influence on strain accumulation are degree of saturation, granulometric decomposition, cyclic loading frequency above $10Hz$ and maximum accumulated strain in relation to the cyclic loading and the soil. To investigate the latter one is very difficult since a tremendous amount of load cycles will be necessary to achieve a final accumulation. Knowledge on the maximum accumulated strain to be expected due to a certain dynamic impact or cyclic loading would already allow for estimation whether a certain cyclic loading may lead to damages in structures.

Further development of the new accumulation model

For large accumulated strains, especially at stress conditions close to the critical state line, the proposed accumulation model becomes less accurate. This is reasonable since the model is developed for prediction of accumulated strains due to vibrations at the small strain level. That is, linear elastic material behaviour is assumed during one event. At larger strain amplitudes as well as at stress states close to the critical state line, this assumption is not valid anymore. In fact, in this case the material behaviour becomes elasto-plastic even for single events. Accordingly, in addition to the predicted amount of accumulated strains a non-negligible amount of real plastic strain is generated during every single load application. To overcome this problem a coupling of the accumulation model with an elasto-plastic hysteretic model rather than with a purely elastic one is desirable. This task is considered to be relevant for future research.

The accumulation model under consideration is applied to own test results. Good agreement of model curves and recorded total accumulated axial and volumetric strains is achieved. Further testing campaigns are desirable, investigating the influence of different parameters on the behaviour of the respective model parameters.

References

Abdelkrim, M.; Bonnet, G. & de Buhan, P. (2003). A computational procedure for predicting the long term residual settlement of a platform induced by repeated traffic loading. *Computers and Geotechnics*, 30:463-476

Ansal, A. (2004). Recent advances in earthquake geotechnical engineering and microzonation. Springer Netherlands

ASTM D3999-91. Standard test methods for the determination of the modulus and damping properties of soils using the cyclic triaxial apparatus

ASTM D5311-92. Standard test method for load controlled cyclic triaxial strength of soil

Baligh, M. & Whittle, A. (1987). Soil models and design methods. *Geotechnical Design: Design methods and Parameters*, Conference, Politecnico di Torino.

Barksdale, R. D. (1972). Laboratory evaluation of rutting in base course materials. *3rd International Conference on Structural Design of Asphalt Pavement*. Vol.3:161-174

Barnett, D. M. (2000). Bulk, surface, and interfacial waves in anisotropic linear elastic solids. *International Journal of Solids and Structures*. 37:45-54

Baxter, C. D. P. & Mitchell, J. K. (2004). Experimental study on the aging of sands. *Journal of Geotechnical and Geoenvironmental Engineering.* 130(10):1051-1062

Bishop, A. W. & Green, G. E. (1965). The influence of end restraint on the compression strength of a cohesionless soil. *Géotechnique*. 15:243-266

Bouckovalas, G.; Whitman, R. V. & Marr, W. A. (1984). Permanent displacement of sand with cyclic loading. *Journal of Geotechnical Engineering, ASCE*. 110(11):1606-1623

Brignoli, E. G. M.; Gotti, M. & Stokoe, K. H. II (1996). Measurement of shear waves in laboratory specimens by means of piezoelectric transducers. *Geotechnical Testing Journal*. 19(4):384-397

Budhu, M. (2000). Soil mechanics and foundations. John Wiley & Sons. Inc.

Castro, G. & Poulos, S. J. (1977). Factors affecting liquefaction and cyclic mobility. *Journal of the Geotechnical Engineering Division, ASCE*. 103(GT6):501-516

Chai, J. C. & Miura, N. (2000). Traffic load induced permanent deformation of low road embankment on soft subsoil. *Proceedings of International Conference on Geotechnical and Geological Engineering.* CD Rom, Paper No. DE0239

Chai, J. C. & Miura, N. (2002). Traffic-load-induced permanent deformation of road on soft subsoil. *Journal of Geotechnical and Geoenvironmental Engineering.* 128(11):907-916

Chaney, R. & Mulilis, J. P. (1978). Suggested method for soil specimen remoulding by wet-raining. *Geotechnical Testing Journal*. 1(2):107-108

Chang, C. S. & Whitman, R. V. (1988). Drained permanent deformation of sand due to cyclic loading. *Journal of Geotechnical Engineering, ASCE*. 114(10):1164-1180

Chen, W. F. & Mizuno, E. (1990). Nonlinear analysis in soil mechanics: theory and implementation. Elsevier

Cho, G.-C.; Dodds, J. & Santamarina, J. C. (2006). Particle shape effects on packing density, stiffness and strength: natural and crushed sands. *Journal of Geotechnical and Geoenvironmental Engineering.* 132(5):591-602

Degrande G. & Schillemans, L. (2001). Free field vibrations during the passage of a Thalys high-speed train at variable speed. *Journal of Sound and Vibration*. 247(1):131-144

DIN 1045-1. Erschütterungen im Bauwesen – Teil 1: Grundsätze, Vorermittlung und Messung von Schwingungsgrößen. DIN 4150-1 Teil 1. Sep 1975

DIN 1045-2. Erschütterungen im Bauwesen – Teil 2: Einwirkungen auf Menschen in Gebäuden. DIN 4150-2:1999-06

DIN 1045-3. Erschütterungen im Bauwesen – Teil 3: Einwirkungen auf bauliche Anlagen. DIN 4150-3:1999-02

Diyaljee, V. A. & Raymond, G. P. (1982). Repetitive load deformation of cohesionless soil. *Journal of the Geotechnical Engineering Division, ASCE*. 108(GT10):1215-1229

Drabkin, S.; Lacy, H. & Kim, D. S. (1996). Estimating settlement of sand caused by construction vibration. *Journal of Geotechnical Engineering, ASCE*. 122(11):920-928

Duncan, J. M. & Chang, C.-Y. (1970). Nonlinear analysis of stress and strain in soils. *Journal of the Soil Mechanics and Foundations Division, ASCE*. 96(SM5):1629-1653

Duncan, J. M. & Dunlop, P. (1968). The significance of cap and base restraint. *Journal of the Soil Mechanics and Foundations Division, ASCE*. 94(1):271-290

Dyvik, R. & Madshus, C. (1985). Lab measurements of G_{max} using bender elements. *Advances in the Art of Testing Soils Under Cyclic Conditions, ASCE*. New York. pp 186-196

François, S.; Karg, C.; Degrande, G. & Haegeman, W. (2007a). A long term accumulation model for soils under low amplitude cyclic loading. *7ème Colloque National AFPS 2007 – Ecole Centrale Paris*. Paris, France (July 2007).

François, S.; Karg, C.; Haegeman, W. & Degrande, G. (2007b). A numerical model for vibration induced long-term foundation settlements due to accumulation of deformation in granular soils. *International Journal for Numerical Methods in Geomechanics*. submitted

Fretti, C.; Lo Presti, D. C. F. & Pedroni, S. (1995). A pluvial deposition method to reconstitute well-graded sand specimens. *Geotechnical Testing Journal, ASCE*. 18(2):292-298

Gidel, G.; Hornych, P.; Chauvin, J.-J.; Breysse, D. & Denis, A. (2001). A new approach for investigating the permanent deformation behaviour of unbound granular material using the repeated load triaxial apparatus. *Bulletin des Laboratoires des Ponts et Chaussées*. 233(4):5-21

Gotschol, A. & Kempfert, H.-G. (2004). Zyklisch viskoelastisch-viskoplastischer Stoffansatz nichtbindiger Böden und Schotter. *Bautechnik*.81(4):279-285

Gussmann, P. & Schanz, T. (1994). The influence of geometry and end restraint on the strength in triaxial compression in numerical

simulation. I. M. Smith, ed., *Proc. of the 5th International Conference on Numerical Methods in Geotechnical Engineering*. Manchester, UK. Balkema. 129-133

Hardin, B. O. & Black, W. L. (1966). Sand stiffness under various triaxial stresses. *Journal of the Soil Mechanics and Foundations Division, ASCE*. 92(SM2):27-42

Hardin, B. O. & Drnevich, V. P. (1972a). Shear modulus and damping in soils: measurement and parameter effects. *Journal of the Soil Mechanics and Foundations Division, ASCE*. 98(SM6):603-624

Hardin, B. O. & Drnevich, V. P. (1972b). Shear modulus and damping in soils: design equations and curves. *Journal of the Soil Mechanics and Foundations Division, ASCE*. 98(SM7):667-692

Head, K. H. (1998). Manual of soil laboratory testing – Volume 3: Effective stress tests. John Wiley & Sons, 2nd edition

Heeres, O. M. (2001). Modern strategies for the numerical modelling of the cyclic and transient behaviour of soils, Ph.D. thesis, Delft University of Technology

Heibrock, G.; Keßler, S. & Triantafyllidis, Th. (2006). On modelling vibro-compaction of dry sands. *Proc. of the international conference on numerical modelling of construction processes in geotechnical engineering for urban environment* . Bochum (March 2006). Balkema

Heller, H.-J. (1981). Bauwerkssetzungen bei sandigem Untergrund infolge von Erschütterungen durch Bahnverkehr. *Baumaschine und Bautechnik*. 35(2):56-61

Heller, H.-J. (1995). Setzungen von Kranbahnstützen infolge von Lastwechseln bei sandigem Untergrund. *Bautechnik*. 72(1):11-19

Hirt, C. W. (ed.) (2006). The Basics of Computational Fluid Dynamics Modeling – Implicit versus explicit methods. http://www.flow3d.com/Cfd-101/impvexp.htm

Hornych, P.; Corté, J.-F. & Paute, J.-L. (1993). Étude des déformations permanentes sous chargements répétés de trios graves non traitées. *Bulletin de liaison des Laboratoires des Ponts et Chausées*. 184(2):77-84

Hunaidi, O. & Tremblay, M. (1997). Traffic-induced building vibrations in Montréal. *Canadian Journal of Civil Engineering*. 24:736-753

Ishihara, K. (1993). Liquefaction and flow failure during earthquakes. The 33rd Rankine lecture. *Geotechnique* 43(3):351-415

Ishihara, K.; Tatsuoka, F. & Yasuda, S. (1975). Undrained deformation and liquefaction of sand under cyclic stresses. *Soils and Foundations* 15(1):29-44

Jamiolkowski, M.; Lo Presti, D. C. F. & Pallara, O. (1995). Role of in-situ testing in geotechnical earthquake engineering. *Proc. of the 3rd Int. Conf. on Recent Advances in Geotechnical Earthquake Engineering and Soil Dynamics*. St. Louis. Vol. 3: 1523-1546

Jefferies, M. & Been, K. (2006). Soil liquefaction. Spon Press. ISBN 0419161708

Kaggwa, W. S.; Booker, J. R. & Carter, J. P. (1991). Residual strains in calcareous sand due to irregular cyclic loading. *Journal of Geotechnical Engineering, ASCE*. 117(2):201-218

Karl, L. (2005). Dynamic soil properties out of SCPT and bender element tests with emphasis on material damping, Ph.D. Thesis, Ghent University

Kim, D.-S. & Lee, J.-S. (2000). Propagation and attenuation characteristics of various ground vibrations. *Soil Dynamics and Earthquake Engineering*. 19:115-126

Knödel, K.; Krummel, H. & Lange, G. (1997). Handbuch zur Erkundung des Untergrundes von Deponien und Altlasten, Band 3. Springer

Kogut, J. P.; Lombaert, G.; François, S.; Degrande, G.; Haegeman, W. & Karl, L. (2003). High speed train induced vibrations: in-situ measurements and numerical modelling. *Proc. of the 10th Int. Conf. on Sound and Vibration*. Stockholm, Sweden (July 2003)

Kramer, S. L. (1996). *Geotechnical earthquake engineering*. Prentice Hall.

Ladd, R. S. (1974). Specimen preparation and liquefaction of sands. *Journal of the Geotechnical Engineering Division, ASCE*. 100(GT10):1180-1184

Ladd, R. S. (1978). Preparing test specimen using undercompaction. *Geotechnical Testing Journal, ASCE.* 1(1):16-23

Lee, K. L. (1978). End restraint effects on undrained static triaxial strength of sand. *Journal of the Geotechnical Engineering Division, ASCE*. 104(4):687-704

Lehane, B. M.; Ismail, M. A. & Fahey, M. (2004). Seasonal dependence of in situ test parameters in sand above the water table. *Géotechnique.* 54(3):215-218

Levacher, D.; Garnier, J. & Chambon, P. (1994). Reconstitution d'éprouvettes de sable – Appareils de pluviation. *Revue Francais de Géotechnique*. 68(3):49-56

Li, D. & Selig, E. T. (1996). Cumulative plastic deformation for fine-grained subgrade soils. *Journal of Geotechnical Engineering, ASCE.* 122(12):1006-1013

Liyanapathirana, D. S.; Carter, J. P. & Airey, D. W. (2005). Numerical modeling of nonhomogeneous behavior of structured soils during triaxial tests. *International Journal of Geomechanics, ASCE*. 5(1):10-23

Lombaert, G. & Degrande, G. (2001). Experimental validation of a numerical prediction model for free field traffic induced vibrations by in situ experiments. *Soil Dynamics and Earthquake Engineering*. 21(6):485-497

Lombaert, G.; Degrande, G.; Kogut, J. & François, S. (2006). The experimental validation of a numerical model for the prediction of railway induced vibrations. *Journal of Sound and Vibration*. 297(3-5):512-535

Love, A. E. H. (1903). The propagation of wave-motion in an isotropic elastic solid medium. *Proc. Lond. Math. Soc.*. 2(1):291-344

Lucca, F. J. (2003). Tight construction blasting: ground vibration basics, monitoring, and prediction. *Terra Dinamica L.C.C. – Effective Blast Design Organization*

Luong, M. P. (1982). Mechanical aspects and thermal effects of cohesionless soils under cyclic and transient loading. *Proc. IUTAM Conf. on Deformation and Failure of Granular Materials*. Delft. pages 239-246

Marr, W. A. & Christian, J. T.(1981). Permanent displacement due to cyclic wave loading. *Journal of the Geotechnical Engineering Division, ASCE*. 107(GT8):1129-1149

Mengé, P. (1994). Gebruik van de akoestische emissie-techniek ter analyse van gedetailleerde grondparameters, Doctoral thesis, Ghent University

Monismith, C. L.; Ogawa, N. & Freeme, C. R. (1975). Permanent deformation characteristics of subgrade soils due to repeated loading. *Transp. Res. Rec. No. 537.* Transportation research board. Washington D.C.

Mulilis, J. P.; Seed, H. B.; Chan, C. K.; Mitchell, J. K. & Arulanandan, K. (1977). Effects of sample preparation on sand liquefaction. *Journal of the Geotechnical Engineering Division, ASCE*. 103(GT2):91-108

NF P 98-235-1. Unbound granular materials. Part 1: repeated load triaxial test.

Niemunis, A. & Wichtmann, T. (2005). Zuschrift zum Beitrag "Zyklisch visko-elastisch-viskoplastischer Stoffansatz nichtbindiger Böden und Schotter" von Gotschol, A. & Kempfert, H.-G.. *Bautechnik*, 82(1):57-59

Niemunis, A. (2003). Extended hypoplastic models for soils. State doctorate. *Veröffentlichungen des Instituts für Grundbau und Bodenmechanik*. Ruhr-Unversität Bochum. Heft 34 (available from www.pg.gda.pl/~aniem/an-liter.html)

Niemunis, A.; Wichtmann, T. & Triantafyllidis, Th. (2003). Compaction of freshly pluviated granulates under uniaxial and multiaxial cyclic loading. *13th European Conference On Soil Mechanics and Geotechnical Engineering: Geotechnical problems with man-made and man-influenced grounds*. Prag (August 2003). 855-860

Niemunis, A.; Wichtmann, T. & Triantafyllidis, Th. (2004). Explicit accumulation model for cyclic loading. *Proc. of the Int. Conf. on Cyclic Behaviour of Soils and Liquefaction Phenomena*. Bochum, Germany (March/April 2004). Balkema. 65-76

Niemunis, A.; Wichtmann, T. & Triantafyllidis, Th. (2005). A high-cycle accumulation model for sand. *Computers and Geotechnics*. 32(2005):245-263

Olszak, W. & Perzyna, P. (1969). On thermal effects in viscoplasticity. *J. Appl. Math. Phys.* 20:676-680

Papadimitriou, A.; Bouckovalas, G. & Dafalias Y. (1999). Use of elastoplasticity to simulate cyclic sand behaviour. *2nd Int. Conf. on Geotechnical Earthquake Engineering*. Lisbon, Portugal (June 1999)

Paute, J.-L.; Jouve, P.; Martinez, J. & Ragneau, E. (1988). Modèle de calcul pour le dimensionnement des chausses souples. *Bulletin de liaison des Laboratoires des Ponts et Chausées*. 156(4):21-36

Perzyna, P. (1966). Fundamental problems in viscoplasticity. *Rec. Adv. Appl. Mech.* 9:243-377

Piriyakul, K. & Haegeman, W. (2004). Determination of shear modulus using piezoelectric transducers. Ee-Pub – Online article database. www.ee-pub.com

Piriyakul, K. (2006). Anisotropic stress-strain behaviour of Belgian Boom clay in the small strain region, Ph.D. Thesis, Ghent University

Pyke, R.; Seed, H. B. & Chan, C. K. (1975). Settlements of sands under multidirectional shaking. *Journal of the Geotechnical Engineering Division, ASCE*. 101(GT4):379-398

Ravaska, O. (2006). Effect of testing conditions on the shear strength parameters – a numerical study. *Proceedings of the 6th Inernational Conference on Numerical Methods in Geotechnical Engineering*. Graz, Austria (September 2006). Taylor & Francis. 161-165

Rayleigh, D. (1885). On waves propagated along the plane surface of an elastic solid. *Proc. Lond. Math. Soc.*. 17:4-11

Sagaseta, G.; Cuellar, V. & Pastor, M. (1991). Cyclic loading. Deformation of soils and displacements of structures, Proceedings of the 10-th ECSMFE in Firenze, Italy 3: 981-999.

Santamarina, J. C. & Cho, G. C. (2004). Soil behaviour: The role of particle shape. *Proc. Skempton Conf.*. London

Sawicki, A. & Swidzinski, W. (1987). Compaction curve as one of basic characteristics of granular soils. In E. Flavigny and D. Cordary (ed.), *4th Colloque Franco-Polonais de Mechanique des Sols Appliquee*. Vol.1:103-115. Grenoble

Sawicki, A. & Swidzinski, W. (1989). Mechanics of a sandy subsoil subjected to cyclic loadings. *International Journal for Numerical and Analytical Methods in Geomechanics*. 13:511-529

Scawthorn, C.; Chen, W.-F. & Chen, C. (2002). Earthquake engineering handbook (new directions in civil engineering). CRC Press Inc

Schmidt, H.-G. & Wuttke, F. (2003). Seismische Feldmessungen zur Identifikation von Standortparametern. *6. Symposium "Bauwerkssanierung und Erschütterungsmessungen"*. EMPA Dübendorf-Zürich, Juni 2003

Seed, H. B. (1979). Soil liquefaction and cyclic mobility evaluation for level ground during earthquakes. *Journal of the Geotechnical Engineering Division, ASCE*. 105(GT2):201-255

Seed, H. B.; Lee, S. R. & Jong, H.-L. (1988). Penetration and liquefaction resistances: prior seismic history effects. *Journal of Geotechnical Engineering, ASCE*. 114(6):691-697

Seed, H. B.; Mori, K & Chan, C. K. (1977). Influence of seismic history on liquefaction of sands. *Journal of the Geotechnical Engineering Division, ASCE*. 103(GT4):257-270

Silver, L.; Chan, C. K.; Ladd, R. S.; Lee, K. L.; Tiedemann, D. A.; Townsend, F. C.; Valera, J. E. & Wilson, J. H. (1976). Cyclic triaxial strength of standard test sand. *Journal of the Geotechnical Engineering Division, ASCE*. 102(GT5):511-522

Silver, M. L. & See, H. B. (1971a). Deformation characteristics of sands under cyclic loading. *Journal of the Soil Mechanics and Foundations Division, ASCE*. 97(SM8):1081-1098

Silver, M. L. & See, H. B. (1971b). Volume changes in sands during cyclic loading. *Journal of the Soil Mechanics and Foundations Division, ASCE*. 97(SM8):1081-1098

Siskind, D. E. (2000). Vibrations from blasting. Int. Soc. of Expl. Eng.. Cleveland, OH (USA)

Skempton, A. W. (1954). The pore water coefficients A and B. *Geotechnique*. 4:143-147

SN 640312 a (1992). Erschütterungseinwirkungen auf Bauwerke. Schweizerische Normenvereini-gung SNV. Zürich

Stöcker, T. & Kempfert, H.-G. (2005). Numerische Modellierungen mit einem zyklisch-viskoplastischen Stoffansatz für granulare Böden. *Bautechnik*. 82(1):11-17

Stoneley, R. (1924). Elastic waves at the surface of separation of two solids. *Proc. R. Soc. London*. Ser. A, 106:416-428

Studer, J. A. & Koller, M. G. (1997). Bodendynamik – Grundlagen, Kennziffern, Probleme. Springer

Suiker, A. J. (2002). The mechanical behaviour of ballasted railway tracks. Doctoral thesis. Delft University of Technology

Sweeney, M. & Lambson, M. D. (1991). Long term settlements of storage tanks on sand. *X. ECSMFE, Florence*. Vol. 2, pages 587-591

Sweere, G. T. H. (1990). Unbound granular bases for roads. Doctoral thesis. Delft University of Technology

Thooft, K. (1991). Theoretisch-experimentele beschrijving van het spannings-verformingsgedrag van onsamenhangende gronden onder uitwendige dynamische belastingen, in het bijzonder bij grote verglijdingen, Doctoral thesis, Ghent University

Triantafyllidis, Th. (ed.). (2004). Cyclic behaviour of soils and liquefaction phenomena. Balkema

Triantafyllidis, Th.; Wichtmann, T. & Niemunis, A. (2003). Explicit accumulation model for granular materials under multiaxial cyclic loading. *Proc. of the 6th International Workshop on Mathematical Methods in Scattering Theory and Biomechanical Engineering*. Tsepelovo, Greece (September 2003). World Scientific. 394-405

Triantafyllidis, Th.; Wichtmann, T. & Niemunis, A. (2004). On the determination of cyclic strain history. *Proc. of the Int. Conf. on Cyclic Behaviour of Soils and Liquefaction Phenomena*. Bochum, Germany (March/April 2004). Balkema. 321-332

Van Impe, W. F. (1981). Studie van het verformingsgedrag van Molzand onder cyclisch wisselnde belastingen, Doctoral thesis, Ghent University

Vanden Berghe, J.-F. (2001). Sand strength degradation within the framework of vibratory pile driving. Ph.D. thesis, Katholieke Universiteit Leuven

Vermeer, P. A. (1980). Formulation and analysis of sand deformation problems. Doctoral thesis. Delft University of Technology

Werkmeister, S. (2003). Permanent deformation behaviour of unbound granular materials in pavement constructions. Doctoral thesis, Technical University Dresden

WFI (2005). Hardware Reference Manual – Cyclic Triaxial Test. Wykeham Farrance International.

Wichtmann, T. (2005). Explicit accumulation model for non-cohesive soils under cyclic loading, Doctoral thesis, Ruhr University Bochum

Wichtmann, T.; Niemunis, A. & Triantafyllidis, Th. (2004a). Strain accumulation in sand due to drained uniaxial cyclic loading. *Proc. of the Int. Conf. on Cyclic Behaviour of Soils and Liquefaction Phenomena*. Bochum, Germany (March/April 2004). Balkema. 233-246

Wichtmann, T.; Niemunis, A. & Triantafyllidis, Th. (2004b). The effect of volumetric and out-of-phase cyclic loading on strain accumulation. *Proc. of the Int. Conf. on Cyclic Behaviour of Soils and Liquefaction Phenomena*. Bochum, Germany (March/April 2004). Balkema. 247-256

Wichtmann, T.; Niemunis, A. & Triantafyllidis, Th. (2005a). Strain accumulation in sand due to cyclic loading: drained triaxial tests. *Soil Dynamics & Earthquake Engineering*. 25(12):967-979

Wichtmann, T.; Niemunis, A. & Triantafyllidis, Th. (2005b). Experimental evidence of a unique flow rule of non-cohesive soils under high-cyclic loading. *Acta Geotechnica*. 1(1):59-73

Wichtmann, T.; Niemunis, A. & Triantafyllidis, Th. (2007a). On the influence of the polarization and the shape of the strain loop on strain accumulation in sand under high-cyclic loading. *Soil Dynamics & Earthquake Engineering*. 27(1):14-28

Wichtmann, T.; Niemunis, A. & Triantafyllidis, Th. (2007b). Strain accumulation in sand due to cyclic loading: drained cyclic tests with triaxial extension. *Soil Dynamics & Earthquake Engineering*. 27(1):42-48

Witte, B. & Schmidt, H. (1995). Vermessungskunde und Grundlagen der Statistik für das Bauwesen. 3rd edition, Verlag Konrad Witwer.

Wolffersdorf, P.-A. von & Schwab, R. (2001). Schleuse Uelsen I – Hypoplastische Finite-Elemente-Analyse von zyklischen Vorgängen. *Bautechnik*. 78(11):711-782

Wuttke, F. (2005). Beitrag zur Standortidentifizierung mit Oberflächenwellen, Doctoral thesis, Bauhaus University Weimar

Yamada, Y. & Ishihara, K. (1982). Yielding of loose sand in three-dimensional stress conditions. *Soils and Foundations*. 22(3):15-31

Yang, Z. & Elgamal, A. (2002). Influence of permeability on liquefaction-induced shear deformation. *Journal of Engineering Mechanics* 128(7):720-729

Yang, Z.; Elgamal, A. & Parra, E. (2003). Computational model for cyclic mobility and associated shear deformation. *Journal of Geotechnical and Geoenvironmental Engineering* 129(12):1119-1127

Yoon, Y.-W. (1991). Static and dynamic behaviour of crushable and non-crushable sands – validation of stress-dilatancy theory, Ph.D. Thesis, Ghent University

Youd, T. L. (1972). Compaction of sands by repeated shear straining. *Journal of the Soil Mechanics and Foundations Division, ASCE*. 98(SM7):709-725

Yoshimi, Y.; Tokimatsu, K. & Ohara, J. (1994). In situ liquefaction resistance of clean sands over a wide density range. *Geotechnique* 44(3):479-494